INFORMATION TO USERS

This manuscript has been reproduced from the microfilm master. UMI films the text directly from the original or copy submitted. Thus, some thesis and dissertation copies are in typewriter face, while others may be from any type of computer printer.

The quality of this reproduction is dependent upon the quality of the copy submitted. Broken or indistinct print, colored or poor quality illustrations and photographs, print bleedthrough, substandard margins, and improper alignment can adversely affect reproduction.

In the unlikely event that the author did not send UMI a complete manuscript and there are missing pages, these will be noted. Also, if unauthorized copyright material had to be removed, a note will indicate the deletion.

Oversize materials (e.g., maps, drawings, charts) are reproduced by sectioning the original, beginning at the upper left-hand corner and continuing from left to right in equal sections with small overlaps. Each original is also photographed in one exposure and is included in reduced form at the back of the book.

Photographs included in the original manuscript have been reproduced xerographically in this copy. Higher quality 6" x 9" black and white photographic prints are available for any photographs or illustrations appearing in this copy for an additional charge. Contact UMI directly to order.

UMI

A Bell & Howell Information Company
300 North Zeeb Road, Ann Arbor MI 48106-1346 USA
313/761-4700 800/521-0600

UNIVERSITY OF OKLAHOMA

GRADUATE COLLEGE

INVESTIGATION INTO THE IN VIVO METABOLISM OF GLUTATHIONYL CONJUGATES OF DOPAMINE AND NOREPINEPHRINE — POSSIBLE INSIGHTS INTO NEURODEGENERATIVE DISEASES

A Dissertation

SUBMITTED TO THE GRADUATE FACULTY

in partial fulfillment of the requirements for the

degree of

Doctor of Philosophy

By

BING XIA

Norman, Oklahoma

1997

INVESTIGATION INTO THE IN VIVO METABOLISM OF GLUTATHIONYL CONJUGATES OF DOPAMINE AND NOREPINEPHRINE — POSSIBLE INSIGHTS INTO NEURODEGENERATIVE DISEASES

A Dissertation APPROVED FOR THE
DEPARTMENT OF CHEMISTRY AND BIOCHEMISTRY

BY

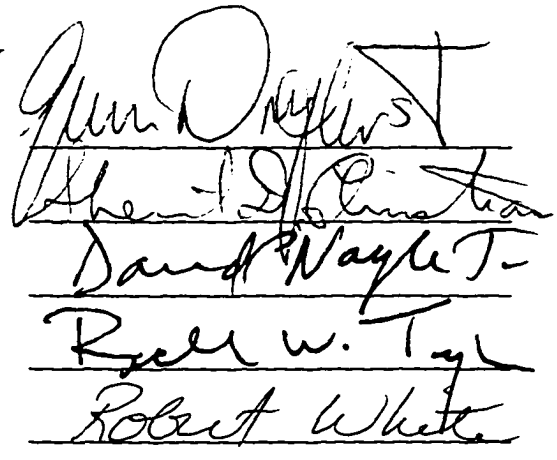

ACKNOWLEDGEMENTS

I would like to express my sincere appreciation and gratitude to my advisor Dr. Glenn Dryhurst for the opportunity to work on this project and for his guidance, encouragement, and patience during the course of this study.

I would like to thank the members of my graduate advisory committee Drs. Sherril D. Christian, David P. Nagle, Jr., Richard W. Taylor, and Robert L. White. Their valuable advice and suggestions are gratefully appreciated.

Many thanks are due to the members of Dr. Dryhurst's group, past and present, for their assistance and friendship. Special thanks are due to Drs. Monika Wrona, Fa Zhang, Qingping Han, Xue-Ming Shen, and Zhaoliang Yang for their valuable discussions.

Finally, I am indebted to my family for their endless love and support. To my parents: thank you for the faith you have in me and all the things you have done for me. To my brothers Tian and Di, and my sister Xue: your charm, intelligence and support have made my life more joyful and complete. To my beloved wife Shanyan: thank you for your love, support and endurance. Without you, I would not be able to make it.

TABLE OF CONTENTS

FIGURE LIST

Abstract

Parkinson's disease (PD) and Alzheimer's disease (AD) are the two major neurodegenerative diseases. There is a significant clinical and neuropathological overlap between PD and AD. A selective degeneration of pigmented dopaminergic neurons on the substantia nigra occurs in PD, while neurofibrilary tangles, senile plaques and loss of populations of neurons are the three hallmarks of AD.

Based on the *in vitro* study of catecholamine neurotransmitters, it was hypothesized that the chronic exposure to environmental toxicants or other factors could trigger the aberrant oxidation of neurotransmitters like dopamine (DA) and norepinephrine (NE). The oxidative intermediate *o*-quinone would be attacked by glutathione (GSH), a common antioxidant in the tissue, to form a series of glutathionyl conjugates. The latter may be hydrolyzed by peptidase enzymes to give rise to cysteinyl conjugates. These metabolites are more readily oxidized than DA and NE. Therefore, more complicated metabolites may be formed. Preliminary study showed that some compounds derived from the oxidation of dopamine and norepinephrine in the presence of cysteine were toxic when administered in mice. These toxic metabolites may ultimately contribute to the neuronal degeneration.

In this study, the oxidation of NE in the presence of GSH at physiological pH was investigated. Under electrochemical conditions, four glutathionyl conjugates of NE were formed: 2-*S*-glutathionylnorepinephrine (2-*S*-Glu-NE), 5-*S*-glutathionylnorepinephrine (5-*S*-Glu-NE), 2,5-bis-*S*-glutathionylnorepinephrine (2,5-bis-*S*-Glu-NE), and 2,5,6-tris-*S*-glutathionylnorepinephrine (2,5,6-tris-*S*-Glu-NE). These reaction products were isolated by preparative HPLC methods and structurally identified by spectroscopic methods,

including NMR, MS, and UV-Vis. Other oxidation conditions investigated include autoxidation, hydroxyl radical (HO•)-mediated and superoxide anion radical (O_2^{-1}•)-mediated oxidation of NE in the presence of glutathione at physiological pH.

The *in vitro* and *in vivo* hydrolyses of 5-*S*-Glu-NE were investigated in rat brain homogenates and by intracerebroventricular (icv) administration in rat brains. Under *in vitro* conditions, 5-*S*-Glu-NE was hydrolyzed to give rise to 5-*S*-cysteinylnorepinephrine (5-*S*-Cys-NE). Under *in vivo* conditions, 5-*S*-Cys-NE was further metabolized into 5-*S*-*N*-acetylcysteinylnorepinephrine (5-*S*-NAc-Cys-NE).

The effects of the icv administration of 5-*S*-Glu-NE on the neurotransmitter levels of serotonergic system, dopaminergic system and noradrenergic system were investigated. The levels of 5-HT and 5-HIAA were increased in all brain areas studied 30 min or 120 min after the icv administration of 5-*S*-Glu-NE. The levels of NE were increased in midbrain (30 min) and striatum (120 min) after the icv administration of 5-*S*-Glu-NE. The levels of DA were decreased at hippocampus (120 min) and increased at cortex (120 min) after the icv administration of 5-*S*-Glu-NE. The level of HVA, a metabolite of DA, was decreased at midbrain 120 min after the icv administration of 5-*S*-Glu-NE.

The *in vitro* hydrolyses of 5-*S*-glutationyldopamine (5-*S*-Glu-DA) and 2,5-bis-*S*-glutathionyldopamine (2,5-bis-*S*-Glu-DA) were investigated in rat brain homogenates. The *in vivo* hydrolysis of 5-*S*-Glu-DA in rat brains was studied by the icv administration of 5-*S*-Glu-DA, 5-*S*-cysteinyldopamine (5-*S*-Cys-DA) and 5-*S*-cysteinylglycinyl-dopamine (5-*S*-Cys-Gly-DA). Under *in vitro* condition, 5-*S*-Glu-DA and 2,5-bis-*S*-Glu-DA were hydrolyzed to their corresponding cysteinyl conjugates of DA. Under *in vivo*

condition, 5-*S*-Glu-DA was metabolized to 5-*S*-Cys-DA, and further metabolized into 5-*S*-*N*-acetylcysteinyldopamine (5-*S*-NAc-Cys-DA). 5-*S*-NAc-Cys-DA was formed after the icv administration of 5-*S*-Cys-DA. 5-*S*-Glu-DA, 5-*S*-Cys-DA and 5-*S*-NAc-Cys-DA were observed after the icv administration of 5-*S*-Cys-Gly-DA.

Chapter 1 Introduction

1.1 Neurodegenerative Diseases

Parkinson's disease (PD) and Alzheimer's disease (AD) are the two major neuro-degenerative diseases. There is a significant clinical and neuropathological overlap between PD and AD. Therefore, there might be similar but yet unknown etiological factors in PD and AD[1].

PD is an idiopathic, chronic neurologic disorder. PD was first described by an English physician named James Parkinson in 1817[2]. Although almost 180 years have passed, the cause or causes of PD still remain unknown. PD afflicts approximately 10% of people over the age of 65[3], while another study showed an annual incidence of 15-20/100,000[4]. PD is clinically defined as a progressive neuronal disorder with characteristic symptoms of tremor, rigidity, and bradykinesia. Pathologically, PD can be defined as the selective degeneration of pigmented dopaminergic neurons in the substantia nigra (SN) with the presence of Lewy bodies[5]. The distribution of dopaminergic cell loss is different between PD and normal aging. The ventral tier of the SN pars compacta is affected most in PD, while the primary neuronal cell loss affects the dorsal tier of SN in normal aging[6,7]. Other neuronal systems affected in PD include the noradrenergic locus ceruleus (LC), the serotonergic raphe nucleus (RN), and the cholinergic nucleus basalis of Meynert (NBM)[8]. The SN supplies DA to the striatum and DA is needed for normal motor function. When DA is depleted in the striatum, the result is disastrous.

AD is the other major neurodegenerative brain disorder. It was first described by a German physician named Alois Alzheimer in 1907[9]. It has an insidious onset and an inexorable progression. Like PD, the etiopathogenesis of AD remains unknown. By an arbitrary dividing line of age of 65, the disease is termed as Alzheimer's disease if it begins before 65 or dementia of the Alzheimer type (DAT) if after 65. DAT affects about 5-11%

of the population over the age of 65 and as much as 47% of population over the age of 85[10]. It is the fourth major cause of death after heart attack, cancer and stroke in developed countries[11]. Symptoms include loss of memory, impaired thought processes, and abnormal behavior. Eventually, patients become profoundly demented and bedridden, and frequently die of the intercurrent infection.

Pathological characteristics of AD include neurofibrillary tangles (NFTs), senile plaques (SPs), and loss of populations of nerve cells. SPs are the principal histological hallmark of AD and are located within the cortex, amygdala, and hippocampus. Noticeably, SPs frequently appear to be associated with blood capillaries[12]. SPs consist of a central core of radiating deposition of extracellular aggregates of the ß-amyloid peptide (ßAP), a 39-43 amino acid peptide, surrounded by dystrophic neurites (axons and synaptic terminals) with non-neuronal reactive microglia and astrocytes.

NFTs consist of paired helical filaments (PHFs)[13], ubiquitin and amyloid protein; and are found inside the cell bodies of dying neurons in certain areas of the temporal cortex, hippocampus and amygdala[14], as well as in four subcortical groups of cell bodies: the cholinergic NBM, the noradrenergic LC, the serotonergic RN[15] and the dopaminergic ventral tegmentum (VT)[16]. PHFs are composed of highly phosphorylated forms of the microtubule-associated protein tau. The noradrenergic neurons in the rostral LC are degenerated in patients with AD[17,18]. This LC neuronal loss leads to norepinephrine (NE) deficiency and contributes to the depressive symptoms in AD. The concentration of choline acetyltransferase is decreased in hippocampus and neocortex[19]. Cholinergic neurons originating in NBM are degenerated. Degeneration of cholinergic neurons and concomitant impairment of cortical and hippocampal neurotransmission may lead to cognitive and memory deficits[20].

1.2. Hypotheses

1.2.1 Genetic factors

Molecular genetics can provide information on the biochemical basis of diseases and eventually lead to therapies for their cure and/or prevention. It is the primary aim in molecular genetics to identify the genes that are responsible for or contribute to the expression of diseases. Once such a gene is identified, its normal and/or abnormal functions can be studied and effective therapies may be developed.

Genetic causes are considered in both PD and AD. Lewy bodies are found in a great majority of PD patients by postmortem examination. The analysis of familial PD cases has provided information on the inheritance patterns of PD, phenotypic heterogeneity of familial parkinsonism. A systematic genomic search has begun but there are no positive results so far[21].

In contrast to the genetic study of PD, four genes that enhance ßAP production or deposition (or both) have been associated with familial AD[22]. It is known that all individuals with Down's syndrome, for which trisomy of chromosome 21 is responsible[23,24], eventually develop AD in middle age. ßAP accumulation in cerebral cortex in patients with AD or Down's is an early and invariant event years or decades before other brain lesions and clinical symptoms. Two forms of ßAP are deposited in the brain in AD: a 40-amino acid peptide ($Aß_{40}$) and a 42-amino acid peptide ($ßA_{42}$). Although $Aß_{40}$ accounts 90% of all ßAP released from nerve cells, it is $ßA_{42}$ that sets the stage for amyloid deposition[25]. ßAPs are clipped from ß-amyloid precursor protein (ßAPP) by enzymes dubbed ß-secretase and γ-secretase. ßAPP is encoded in chromosome 21 and its mutations cause the increase of ßAP secretion, particularly $ßA_{42}$[26,27]. Therefore, AD is caused by ßAPP mutations through enhanced generation of ßAP and amyloidogenesis.

Recently, apolipoprotein E (ApoE) in cerebrospinal fluid (CSF) has been found to

bind to ßAP with high affinity[28]. The ε4 allele of Apo-E (APOE-ε4) is associated with sporadic and late-onset familial forms of AD[29]. The APOE gene has three common alleles, ε2, ε3, and ε4, and is located on chromosome 19[30]. Apo-E is expressed in different tissues including brain and functions in lipid transport. The overexpressed ApoE4 isoform of ApoE binds more readily to ßAP and might make ßAP insoluble and prone to deposition[31].

The third and fourth familial AD genes are presenilin (PS) 1 and 2 discovered on chromosomes 14 and 1, respectively[32,33]. The production of $ßA_{42}$ is increased in plasma and in the media from cultured skin fibroblasts in Alzheimer's patients who inherited mutant PS 1 or PS 2 genes[34]. The increased levels of $ßA_{42}$ were observed in brains of transgenic mice expressing human PS 1[35,36].

Direct neurotoxicity of ßAP can injure local neurons and their processes, causing profound metabolic changes — likely including PHF formation through altered protein tau phosphorylation in some plaque-associated neurites. ßAP accumulation may cause oxidative injury from free radical formation as well.

1.2.2. Environmental factors

Genetic studies can provide only limited information on neurodegenerative diseases at the present time. Environmental factors are considered to be responsible for triggering the diseases by themselves or to act synergistically with the patient genotypes[37,38].

There might be a link between the incidence of PD and industrialization. A PD study in China indicated a higher incidence of PD in the urban industrialized areas than in rural regions[39]. There seems to be a lower incidence of PD in recently industrialized countries than in those with a longer industrialization history[40]. However, a study in the U. S. A. showed no significant increase of incidence of PD over the period of 1955-1979[41].

1-Methyl-4-phenyl-1,2,3,6-tetrahydropyridine (MPTP) was found as a toxic contaminant of illicit meperidine synthesis[42,43]. People who injected MPTP-contaminated drugs developed severe parkinsonism with selective degeneration in the SN[42-44]. MPTP is taken up into cerebral astrocytes where it is oxidized to 1-methyl-4-phenylpyridinium ion (MPP^+)[45] by monoamine oxidase-B (MAO-B)[46]. MPP^+ is actively taken up into dopaminergic nerve terminals through the dopamine transporter leading to a marked concentration within dopaminergic neurons[47,48]. Dopamine transporters are expressed only in dopamingergic neurons and therefore the concentration of MPP^+ occurs only in dopaminergic neurons. Within nigral neurons, MPP^+ is further concentrated in mitochondria. MPP^+ inhibits complex I of the mitochondrial respiratory chain[49] and finally causes nigral neuronal death[50,51]. However, the search for organic toxins structurally similar to MPTP has not yet given any conclusive results[38].

Aluminum (Al) has been found in increased concentrations in AD affected brains[52] and aluminosilicates have been found at the cores of SPs and within neurons with NFTs[53,54]. Chronic exposure to Al is a controversial possible cause of sporadic forms of AD[55]. The role of Al in AD is supported by a) toxicological studies of the learning and memory of animals, b) increased incidence of the disease correlated with the exposure of aluminum in drinking water, and c) progress of AD is slowed down by a drug which selectively removes aluminum from the body. However, a conclusive case that exposure to Al initiates the pathological process in AD remains to be established[55].

1.2.3. Oxidative stress and free radicals

The oxidative properties of oxygen play a vital role in a wide range of biological processes, including electron transport to produce ATP[56,57]. However, oxygen can also evoke oxidative damage by being transformed into more reactive forms, like superoxide

anion radical, hydrogen peroxide, and hydroxyl radical. These reactive oxygen species (ROS) can damage DNA, essential enzymes and structural proteins, and have been linked to neurodegenerative diseases such as PD and AD[58]. Normally, the cells balance these oxidative events through reducing agents such as ascorbic acid (AA), glutathione (GSH), and α-tocopherol (vitamin E). Oxidative stress occurs when the balance between the production of ROS and the reducing protection ability is lost. In this situation, either ROS production increases or the concentrations of reducing agents and/or activities of related protective enzymes decrease, or both.

One source of ROS is from leakage of the respiratory chain of mitochondria where oxygen is ultimately reduced to water, as shown in equation 1.1:

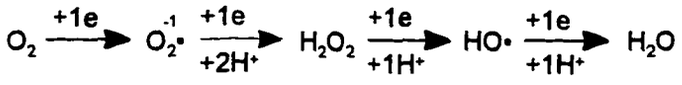

(1.1)

During the catabolic process, catecholamines can be oxidatively deaminated by monoamine oxidase (MAO). MAO is a mitochondrial enzyme and is located exclusively on the surface of mitochondria. There are two forms of MAO, MAO-A and MAO-B. In the SN and striatum, for example, DA is oxidized by MAO (77% by MAO-B, 23% by MAO-A)[59]. Hydrogen peroxide is produced when DA is oxidized by MAO, as shown in equation 1.2:

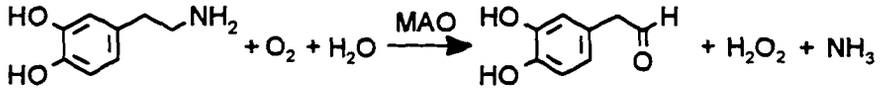

(1.2)

In the SN, when DA is autoxidized to form neuromelanin, ROS are produced, as shown in equations1.3 and 1.4:

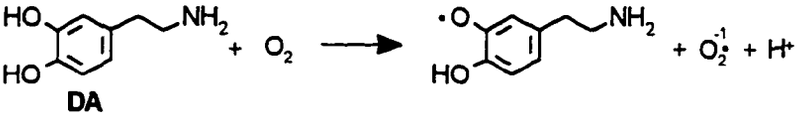

DA

(1.3)

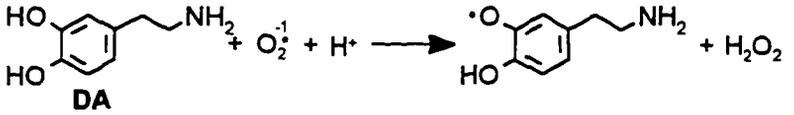

DA

(1.4)

Generally, superoxide dismutase (SOD) catalyzes the conversion of superoxide anion radical (O_2^{-1}) into H_2O_2 (equation 1.5)[60]. Catalase (CAT) and glutathione peroxidase (GSH-Px) catalyze the conversion of H_2O_2 into H_2O. These reactions prevent the accumulation of free hydroxyl radicals[61], as shown in equation 1.6 and 1.7. GSH is a substrate of GSH-Px and is oxidized to form oxidized GSH (GSSG)(equation 1.7). GSH is regenerated by the action of GSH reductase (GSH-Red) coupled with reduced nicotinamide adenine dinucleotide phosphate (NADPH) (equation 1.8).

$$2O_2^{-1\bullet} + 2H^+ \xrightarrow{SOD} H_2O_2 + O_2 \quad (1.5)$$

$$2H_2O_2 \xrightarrow{CAT} O_2 + 2H_2O \quad (1.6)$$

$$2GSH + H_2O_2 \xrightarrow{GSH\text{-}Px} GSSG + 2H_2O \quad (1.7)$$

$$GSSG + NADPH + H^+ \xrightarrow{GSH\text{-}Red} 2GSH + NADP^+ \quad (1.8)$$

In the brain, the GSH system is the most important defense mechanism for detoxification of H_2O_2 into H_2O. However, the GSH system is saturable, and an increased production of H_2O_2 can lead to the formation of hydroxyl free radicals with subsequent tissue damage[62]. Hydroxyl radicals may be generated through the Fenton reaction with the presence of trace transition metal ions, such as ferrous (Fe^{2+}) and cuprous ions (Cu^+), as shown in equation 1.9:

$$H_2O_2 + Fe^{2+} \longrightarrow \bullet OH + OH^- + Fe^{3+} \quad (1.9)$$

Fe^{2+} is a catalyst and is regenerated by reducing agents such as AA, vitamin E, and GSH. Ferric ions (Fe^{3+}) can also be reduced into Fe^{2+} in the presence of superoxide anion radicals, as shown in equation 1.10:

$$Fe^{3+} + O_2^{-1} \longrightarrow O_2 + Fe^{2+} \quad (1.10)$$

The result of combining equation 1.9 and 1.10 is called the Haber-Weiss reaction[63], as shown in equation 1.11:

$$H_2O_2 + O_2^{-1}\cdot \longrightarrow O_2 + \cdot OH + OH^- \qquad (1.11)$$

Several lines of evidence support the oxidative stress hypothesis in PD. First, a high concentration of DA in nigral neurons predisposes those neurons to oxidative stress. When DA is oxidized by MAO, hydrogen peroxide is formed. Second, SOD activities appear to be increased in the SN[64,65]. As a result of free radicals, increased lipid peroxidation in the SN of PD patients was reported[66]. Thirdly, iron is increased in the SN of PD patients. Though most tissue iron exists in the form of Fe^{3+}, Fe^{3+} may be reduced to Fe^{2+} in the presence of neuromelanin[67]. In the presence of Fe^{3+}/Fe^{2+}, both the Fenton reaction (equation 1.9) and Haber-Weiss (equation 1.11) reaction may proceed to form hydroxyl radicals, which do the most of the damage from ROS. Finally, the level of GSH is reduced in PD[68,69]. As discussed earlier, people who injected MPTP-contaminated meperidine developed parkinsonism with selective neuronal degeneration in the SN. MPTP is oxidized to MPP^+, which inhibits complex I of the mitochondrial respiratory chain and ultimately causes cell death. Excessive hydroxyl radicals produced at this situation can react and damage virtually any biomolecules nearby, including DNA, proteins and membrane lipids[70,72] and finally cause cell death. To the extent that PD is caused by MPTP or MPTP-like protoxins, oxidation reactions may be crucial to the development of PD. The MPTP model has been considered the best model of PD available.

Recently, evidence has been obtained that free radicals play an important role in the development of AD. A major pathological feature in the brains of AD patients is the presence of SPs, insoluble plaques with high-density amyloid deposits, of which ßAP is a major component. The neurotoxicity of ßAP may be related to its promotion of hydroxyl radical formation. ßAPs can cause ROS generation and calcium homeostasis destablization in rat hippocampal cultures[73] and increased levels of H_2O_2 and lipid peroxides to accumulate in a PC 12 cell line, a clonal CNS cell line and cultured rat cortical neurons[74]. While the free radical production is linked to the exposure of $ßA_{25-30}$, a biologically active fragment of ßAP, in rat cortical neurons[75], antioxidant drugs can prevent the calcium

elevation and cytotoxic actions of βA_{25-30} from PC 12 cell lines[76]. Iron is frequently a potent facilitator of the free radical production due to its ability to mediate the conversion of H_2O_2 to hydroxyl radicals via the Fenton reaction. It is not surprising that the iron increase is observed within or close to the plaques and in NFTs in AD[77,78].

In summary, evidence supports the hypothesis that free radicals contribute to the pathogenesis of neurodegenerative diseases such as PD and AD.

1.3. Experimental Design

1.3.1 Hypothesis

One of the major neuropathological changes in PD is the degeneration of the nigrostriatal DA pathway[79,80]. This causes the depigmentation of SN and a severe deficiency of DA in striatum. There are some characteristic chemical and biochemical changes in the Parkinsonian SN. These changes include the decrease of nigral concentrations of GSH without an accompanying increase of GSSG concentration[81,82], a significant increase of the of 5-*S*-cysteinyldopamine (5-*S*-Cys-DA) to DA concentration ratio[83], upregulation of γ-glutamyl transpeptidase (γ-GT), and progressive depigmentation of the SN[84-87]. In the SN, DA is autooxidized to form DA-*o*-quinone, and the further oxidation of DA-*o*-quinone leads to the formation of black neuromelanin (Scheme I)[88].

However, DA-*o*-quinone possesses an electron deficient ring and is an easy target for nucleophilic agents. L-Cysteine and GSH are among the strongest endogenous nucleophiles. Indeed, experiments done in our lab show that *in vitro* the neuromelanin pathway is blocked by both cysteine and GSH[89-91]. When DA is oxidized at physiological pH in the presence of cysteine or GSH, a number of soluble cysteinyl and glutathionyl conjugates are formed, including 5-*S*-Cys-DA, 5-*S*-glutathionyldopamine (5-*S*-Glu-DA),

2-*S*-cysteinyldopamine (2-*S*-Cys-DA), 2-*S*-glutathionyldopamine (2-*S*-Glu-DA), 2,5-bis-*S*-cysteinyldopamine (2,5-bis-*S*-Cys-DA) and 2,5-bis-*S*-glutathionyldopamine (2,5-bis-*S*-

Scheme I

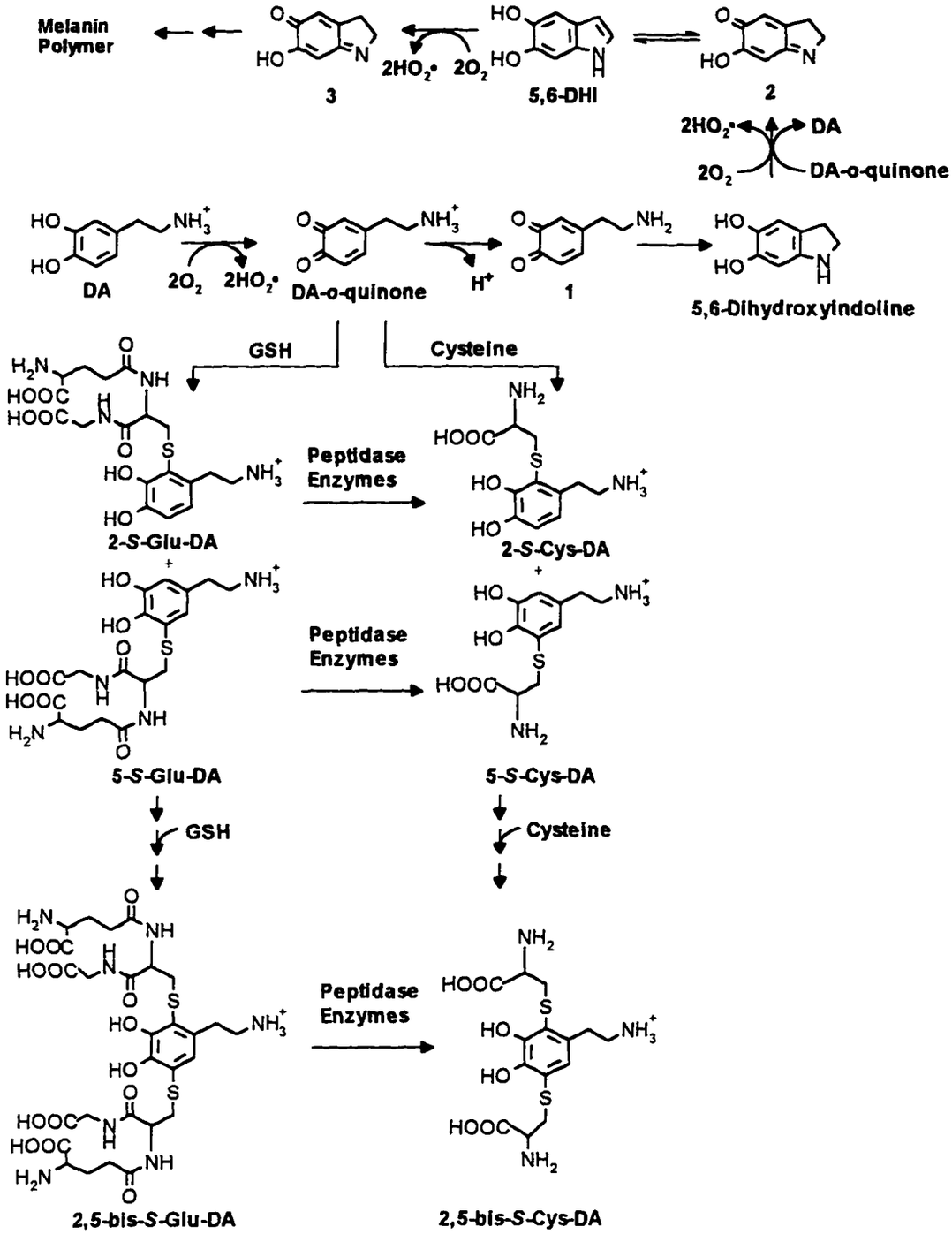

Glu-DA). Based on these results, a new hypothesis has been recently advanced[89,90]. Basically, this hypothesis proposes that chronic exposure to environmental toxicants may evoke elevated biosynthesis of cysteine and GSH in glial cells and upregulation of γ-GT. This leads to elevated translocation of GSH and/or cysteine into pigmented DA neurons and subsequent diversion of the neuromelanin pathway, causing the loss of GSH without accompanying GSSG formation, increased 5-*S*-Cys-DA to DA concentration ratio, and the depigmentation of DA neurons. Owing to the larger concentration of GSH in brain, GSH is postulated *in vivo* as the nucleophilic agent to attack the DA-*o*-quinone to give rise to glutathionyl conjugates of DA. Glutathionyl conjugates are then hydrolyzed by peptidase enzymes to give rise to cysteinyl conjugates of DA[83]. Under conditions that DA is oxidized, cysteinyl conjugates of DA are even more easily oxidized than DA itself. For example, 5-*S*-Cys-DA is oxidized to give rise to a dihydrobenzothiazine (DHBT) compound, 7-(2-aminoethyl)-3,4-dihydro-5-hydroxy-2*H*-1,4-benzothiazine-3-carboxylic

Scheme II

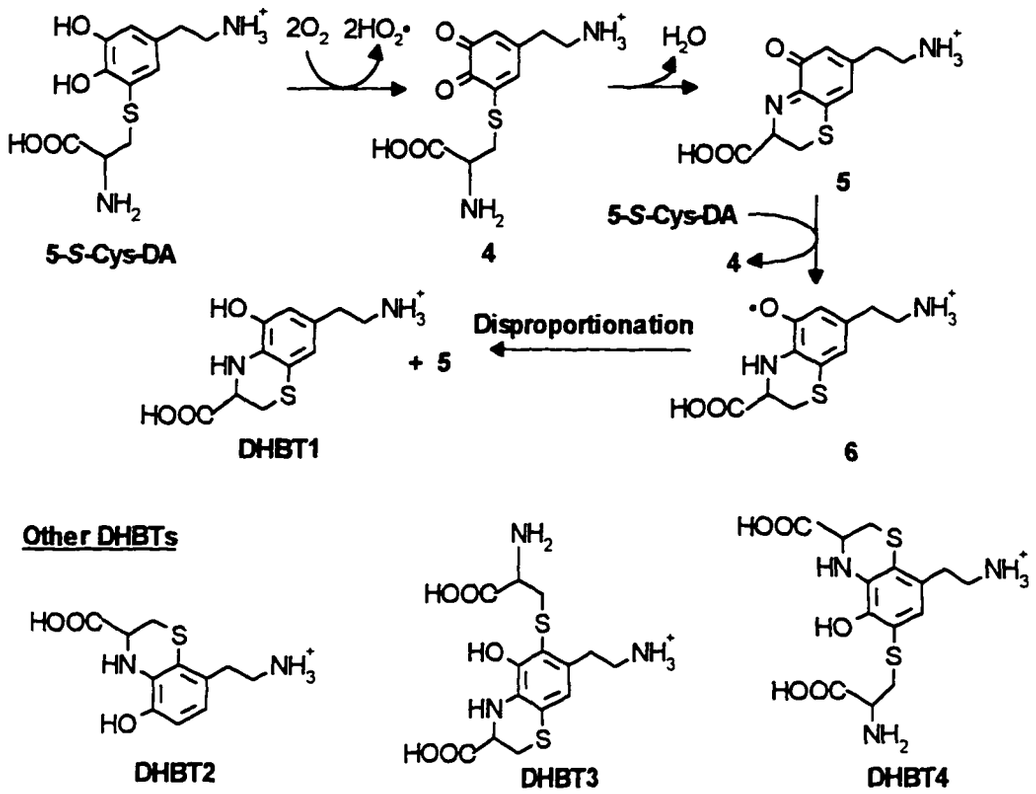

acid (DHBT1) (Scheme II). Other DHBT compounds are also shown in Scheme II. At least one of the cysteinyl conjugates of DA and several DHBTs derived from cysteinyl conjugates are toxic when administered into the brains of mice and rats[89,90].

The pigmented cell bodies of noradrenergic LC neurons degenerate in PD[92]. Moreover, noradrenergic neurons that project from the LC to the cortex and hippocampus also degenerate in AD. These neurons are degenerated in their terminal regions[93] in contrast to SN and LC cell bodies[94] in PD. Similar to DA, NE is easily oxidized to NE-*o*-quinone, which should be readily attacked by GSH and/or cysteine to give rise to glutathionyl and/or cysteinyl conjugates. The further oxidation products of glutathionyl and/or cysteinyl conjugates of NE may yield endotoxins which might contribute to the degeneration of noradrenergic neurons. It is clearly of interest to explore the influence of GSH on the oxidation chemistry of NE at physiological pH.

It is conceivable that DA and NE in neurons are oxidized under oxidative stress to form *o*-quinone intermediates, which are attacked by nucleophiles like GSH and/or cysteine. However, the level of GSH is much higher than that of cysteine. GSH is synthesized in glial cells and then transferred into nerve cells. It is reported that the concentrations of GSH are 2.41 mM in the whole brain and 3.49 mM in the striatum in rats[95]. It is reasonable to assume that the *o*-quinones formed from the oxidation of DA and NE will first be attacked by GSH. The glutathionyl conjugates are then hydrolyzed to form cysteinyl conjugates via peptidase enzymes. Recently, it has been reported that α-methyldopamine (α-MeDA), a metabolite of the serotonergic neurotoxicants 3,4-(±)-(methylenedioxy)amphetamine (MDA) and 3,4-(±)-(methylenedioxy)methamphetamine (MDMA), is readily oxidized in the presence of GSH to form 5-*S*-glutathionyl-α-methyldopamine (5-*S*-Glu-α-MeDA). 5-*S*-Glu-α-MeDA is rapidly transformed into 5-*S*-cysteinyl-α-methyldopaime (5-*S*-Cys-α-MeDA) mediated by γ-GT in rat brains. 5-*S*-Cys-α-MeDA is *N*-acetylated to form 5-*S*-(*N*-acetyl-*S*-cysteinyl)-α-MeDA (5-*S*-NAc-Cys-α-MeDA), which may contribute the long-term neurotoxicity of MDA and MDMA[96]. These

observation suggest that glutathionyl conjugates of DA and NE may also be hydrolyzed in reactions mediated by γ-GT. Similar to the mechanism of MPTP, these cysteinyl and conjugates of DA and NE, in addition to their further metabolites DHBTs, might be taken up into the mitochondria and inhibit the respiratory chain complex I and ultimately cause cell death. At least one cysteinyl conjugate of DA and several DHBTs from DA and NE are toxic when administered in to the brains of mice and rats[89,90,97]. This project includes the study of the *in vitro* oxidation chemistry of NE in the presence of GSH at physiological pH, and both the *in vitro* and *in vivo* hydrolysis of glutathionyl conjugates of DA and NE in rat brain homogenates and rat brains.

1.3.2. Project description

The following work was carried out:

(1) The oxidation chemistry of NE in the presence of GSH at physiological pH

A) Cyclic voltammetric methods were employed to study the reduction-oxidation properties of NE in the presence of GSH and of the glutathionyl conjugates of NE.

B) Controlled potential electrolysis was employed to electrochemically synthesize the oxidation products of NE in the presence of GSH. Preparative HPLC techniques were employed to isolate and purify the reaction products.

C) Spectroscopic methods, such as UV-visible spectroscopy (UV-Vis), nuclear magnetic resonance spectroscopy (NMR), and mass spectroscopy (MS), were employed to elucidate the chemical structures of glutathionyl conjugates of NE.

D) Autoxidation and oxygen radical-mediated oxidation of NE in the presence

of GSH at submicromolar concentrations and physiological pH were studied.

(2) *In vitro* and *in vivo* metabolism of glutathionyl conjugates of NE

A) Cysteinyl, glutathionyl, cysteinylglycinyl and *N*-acetylcysteinyl conjugates of NE were prepared by employing electrochemical synthesis and preparative HPLC techniques.

B) HPLC-EC systems were optimized to monitor the *in vitro* and *in vivo* metabolism of 5-*S*-glutathionylnorepinephrine (5-*S*-Glu-NE).

C) *In vitro* metabolism of 5-*S*-Glu-NE in rat brain homogenates was studied at physiological pH. The metabolite 5-*S*-Cys-NE was confirmed by spectroscopic methods in addition to comparison of the retention time using HPLC methods.

D) *In vivo* metabolism of 5-*S*-Glu-NE was studied by intracerebroventricular (icv) administration of 5-*S*-Glu-NE in rat brains. The effects of icv administration of 5-*S*-Glu-NE on levels of electroactive neurotransmitters and their metabolites in rat brains were also studied.

(3) *In vitro* and *in vivo* metabolisms of glutathionyl conjugates of DA

A) Cysteinyl, glutathionyl, and *N*-acetyl-cysteinyl conjugates of DA were prepared by employing electrochemical synthesis and preparative HPLC techniques.

B) An HPLC-EC system was optimized to monitor the 5-*S*-Glu-DA metabolism.

C) *In vitro* metabolism of cysteinyl conjugates in rat brain homogenate was studied at physiological pH and 37 °C.

D) *In vivo* metabolism of 5-*S*-Glu-DA was studied by icv administration of 5-*S*-Glu-DA, 5-*S*-Cys-DA, and 5-*S*-cysteinylglycinyl dopamine (5-*S*-Cys-Gly-DA) into rat brains.

Chapter 2 Oxidation Reaction of Norepinephrine in the Presence of Glutathione

2.1 Introduction

In the LC, noradrenergic pigmented cell bodies neurons degenerate in patients with PD. The pigmentation of these neurons is due to the autoxidation of NE to NE-*o*-quinone that polymerizes to neuromelanin. Noradrenergic neurons that project from the LC to the cortex and hippocampus also degenerate in their terminal regions in patients with AD.

Similar to DA, NE can easily be oxidized under physiological conditions. Oxidative stress can produce excessive ROS, which may oxidize NE to NE-*o*-quinone. It is reasonable to assume that the oxidation intermediate, NE-*o*-quinone, may be attacked by nucleophiles in the neurons such as GSH and cysteine. Since the concentration of GSH is much larger than that of cysteine in the cells, GSH would attack NE-*o*-quinone to form glutathionyl conjugates. The resulting glutathionyl conjugates, in turn, may be hydrolyzed to cysteinyl conjugates by peptidase enzymes. The oxidation of NE in the presence of cysteine was studied in this laboratory recently[97]. Cysteinyl conjugates were formed by the electrochemical oxidation of NE in the presence of cysteine at physiological pH. These cysteinyl conjugates have more negative redox potential than NE and thus are easily oxidized to give rise to further oxidation products. Two products caused animal behavioral responses and were found lethal when administered into the brains of laboratory mice. The current study focused on the oxidation chemistry of NE in the presence of GSH at physiological pH by means of electrooxidation, autoxidation and hydroxyl radical oxidation.

2.2 Experimental

2.2.1 Chemicals

Norepinephrine hydrochloride (NE•HCl), glutathione (GSH, reduced form, free base), N_{ω}-methyl-5-hydoxytryptamine (N-MET), trifluoroacetic acid (TFA), $Na_2EDTA•2H_2O$, and sodium ascorbate (AA) were obtained from Sigma (St. Louis, MO). Ammonium hydroxide, sodium phosphate (monobasic), sodium phosphate (dibasic), acetonitrile (MeCN, HPLC grade) were obtained from Fisher Scientific Company (Springfield, NJ). Hydrogen peroxide (H_2O_2) and ferrous ammonium sulfate [$Fe(NH_4)_2•6H_2O$] were obtained from Mallinckrodt (Paris, KY). All chemicals were used without further purification. All solutions were prepared with deionized water obtained from a Milli-Q system (Continental Water System, El Paso, TX). Phosphate buffer solution (PBS) of μ = 1.0 and pH = 7.4 were prepared according to Christian and Purdy[98]. All reaction solutions were filtered through a membrane (type HA, pore size 0.45 nm, Millipore Corporation, Bedford, MA) before the injection into an HPLC system.

2.2.2 Instrumentation

Cyclic voltammograms were obtained at a pyrolytic graphite electrode (PGE; Pfizer Minerals, Pigments and Metals Division, Easton, PA) having an approximate surface area of 12 mm^2, using a BAS model 100A electrochemical analyzer (Bioanalytical Systems, West Lafayette, IN). The PGE was resurfaced before recording each voltammogram as described[99]. All voltammograms were corrected for iR drop. Controlled

potential electrolyses employed a Princeton Applied Research Corporation (Princeton, NJ) model 173 potentiostat. The working electrode consisted of several plates of pyrolytic graphite having a total surface area of ca. 150 cm^2. These electrodes were suspended into the solution containing the appropriate supporting electrolyte and compound of interest contained in the working electrode compartment of the electrochemical cell. A conventional three-compartment electrochemical cell was employed in which the three compartments were separated with Nafion® membranes (Type 117, DuPont Co., Wilmington, DE). The working electrode compartment had a capacity of 50 mL. The counter electrode employed was platinum gauze. A saturated calomel electrode (SCE) was used as reference electrode. All controlled potential electrolyses were carried out with the solution into the working electrode compartment stirred with Teflon-coated magnetic stirring bar and nitrogen (N_2) gas bubbling vigorously through the solution. All potentials are referenced to the SCE at ambient temperature (22 ± 2°C).

HPLC employed a Gilson (Middleton, WI) binary gradient system equipped with two Gilson model 302 pumps, a Gilson model 112 UV detector set at 254 nm and a Rheodyne model 7125 loop injector with a 10 mL sample loop. Larger sample volumes (10-30 mL) were pumped directly onto the column through one of the HPLC pumps. A preparative reversed-phase column (J. T. Baker, Phillipsburg, NJ; Bakerbond C18, 10 μm, 25 × 2.1 cm) protected by a short guard column (Brownlee Laboratories, Santa Clara, CA, RP-18, 5 × 1 cm) was used. Six mobile phase solvents were used. Solvent A was prepared by adding 30.0 mL concentrated ammonium hydroxide to 4.0 L of deionized water and its pH was adjusted to 3.0 by adding TFA. Solvent B was prepared by adding 2.0 L methanol (MeOH) and 30.0 mL concentrated ammonium hydroxide to 2.0 L deionized water. The pH of this solution was adjusted to 2.5 by adding TFA. Solvent C was prepared by adjusting the pH of 4.0 L deionized water to 2.5 by adding TFA. Solvent

D was prepared by adjusting the pH of 2.0 L deionized water and 2.0 L MeCN to 2.5 by adding TFA. Deionized water and MeCN were used as solvent E and F, respectively.

^{1}H NMR (one- and two-dimensional correlated spectroscopy (COSY) experiments) were recorded on a Varian (Palo Alto, CA) XL-300 spectrometer. Low- and high resolution fast atom bombardment-mass spectrometry (FAB-MS) employed a VG Instruments (Manchester, U. K.) ZAB-E mass spectrometer. Ultraviolet-visible (UV-Vis) spectra were recorded on a Hewlett-Packard 8452 diode array spectrophotometer using 0.5-cm pathlength quartz cuvettes.

HPLC method I was used to monitor the oxidation of NE in the presence of GSH and to separate and isolate the products from the reaction mixture. HPLC method I employed solvents A and B and the following gradient: 0-2 min, 0% solvent B; 2-7 min, linear gradient to 10% solvent B; 7-40 min, linear gradient to 30% B; 40-48 min, linear gradient to 100% solvent B; 48-55 min, 100% solvent B; 55-55.01 min, linear gradient to 0% solvent B; 55.01-60 min, 0% solvent B. The flow rate was constant at 7.0 mL/min.

HPLC method II was used to further purify (desalting) the products obtained from HPLC method I. It employed solvents C and D and the following gradient profile: 0-2 min, 0% solvent D; 2-7 min, linear gradient to 5% solvent D; 7-25 min, linear gradient to 15% D; 25-37.5 min, linear gradient to 30% solvent D; 38-48 min, linear gradient to 100% solvent D; 48-58 min, 100% solvent D; 58-59 min, linear gradient to 0% solvent D; 59-65 min, 0% solvent D. The flow rate was constant at 7.0 mL/min.

HPLC method III was used to study the oxidation of NE in the presence of GSH at various conditions. It was an HPLC system with electrochemical detection (HPLC-EC). The method employed a Bio-Rad (Hercules, CA) Model 1300 pump, a Rheodyne 7125 injector with a 5.0 μL sample loop, and a BAS (West Lafayette, IN) LC-4C electrochemical detector equipped with a glass carbon detector electrode set at 800 mV

vs. a Ag/AgCl reference electrode. The detector was set the full-scale at 10 nA. A reversed phase column (BAS, Phase-II ODS, 3 μm, 100×3.2 mm) was employed. The mobile phase consisted of 0.085% diethylamine (v/v), 0.057 mM ethylenediamine-tetraacetic acid (EDTA), 0.50 mM sodium octyl sulfate (SOS), and 0.10 M citric acid in 9.3% MECN/deionized water at pH = 2.37. The flow rate was constant at 0.6 mL/min.

2.3 Electrochemical Oxidation Reaction of NE

2.3.1 Cyclic voltammetric study of the oxidation of NE in the presence of GSH

A cyclic voltammogram of NE (1.0 mM) at a PGE in pH 7.4 (μ = 1.0) PBS at a sweep rate (ν) of 200 mVs^{-1} is shown in Figure 2.1A. On the initial anodic sweep, peak I_a appears at a peak potential (E_p) of 179 mV and corresponds to the oxidation (2*e*, $2H^+$) of NE to NE-*o*-quinone (Scheme III[100,101]). Following scan reversal, peak I_c appears at E_p of 113 mV and corresponds to the quasi-reversible reduction of NE-*o*-quinone to NE.

Scheme III

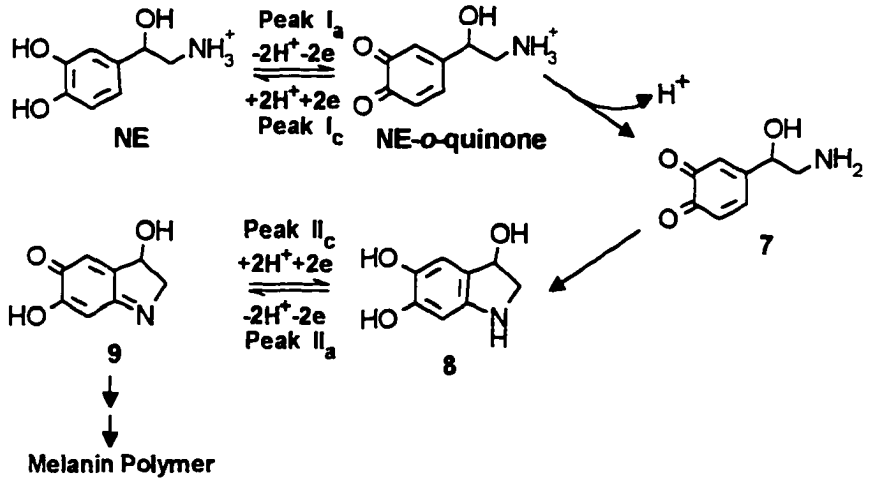

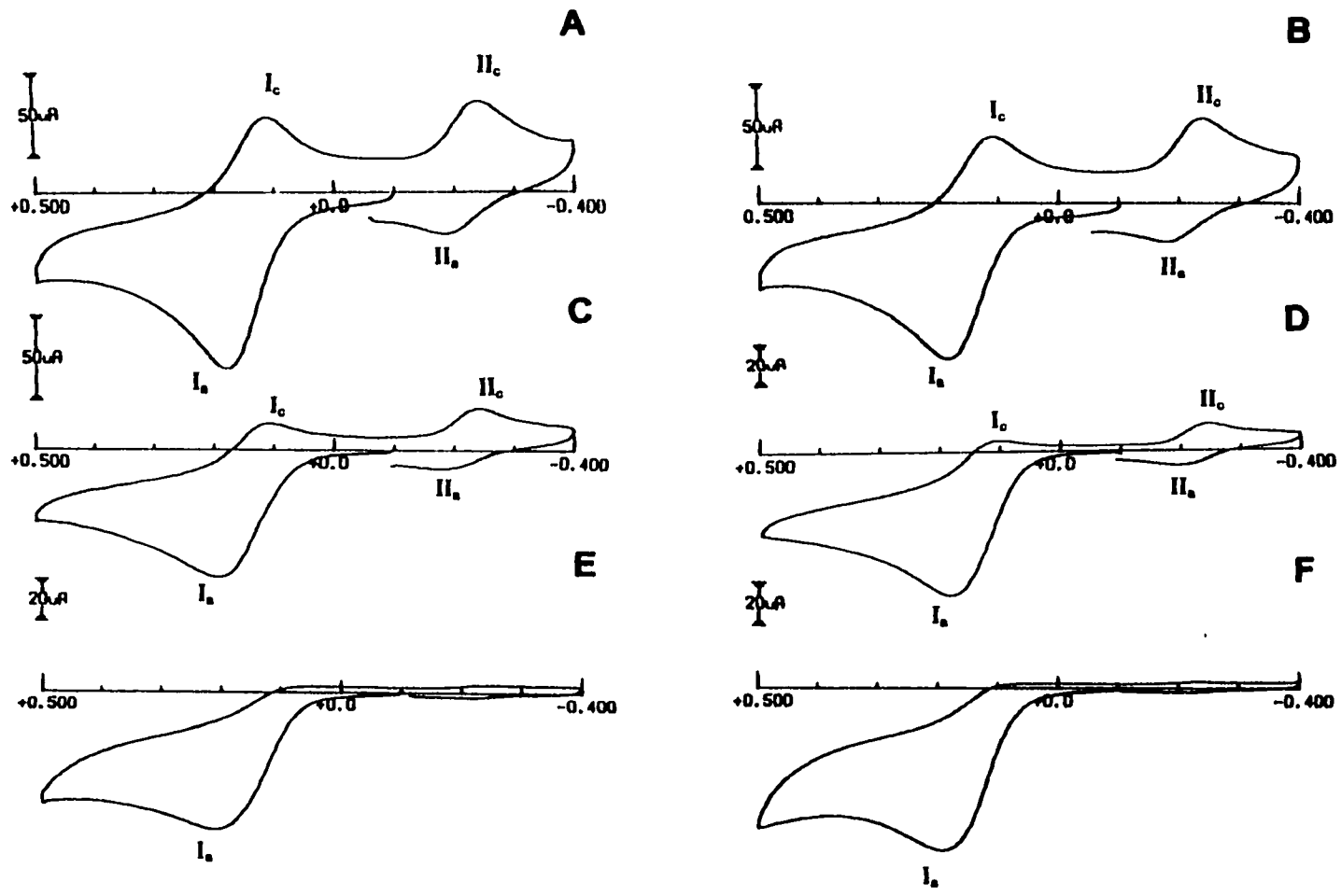

Figure 2.1 Cyclic voltamograms of 1.0 mM NE at PGE in the presence of (A) 0 mM, (B) 0.1 mM, (C) 0.4 mM, (D) 1.0 mM, (E) 5.0 mM and (F) 10.0 mM GSH in PBS (pH = 7.4, μ = 1.0). Sweep rate: 200 mVs^{-1}.

Previous studies[100,101] showed that at pH 7.4, NE-*o*-quinone deprotonates to **7** and the latter cyclizes to yield 3, 5, 6-trihydroxyindoline (**8**). Compound **8** is then further oxidized ($2e$, $2H^+$) by NE-*o*-quinone to yield the aminochrome **9** and NE. Aminochrome **9**, formed at the surface of the electrode, is the species that is responsible for peak II_c (E_p = -241 mV) on the reversal cathodic scan. Peak II_p observed on the second anodic sweep appears at E_p = -178 mV and corresponds to the oxidation of **8** to **9**. Peak I_c virtually disappears at $\nu = 20\ mVs^{-1}$ owing to the relatively rapid redox reaction between NE-*o*-quinone and **8**.

Cyclic voltammograms ($\nu = 200\ mVs^{-1}$) of 1.0 mM NE in the presence of GSH (0.1 mM — 10 mM) in PBS (pH = 7.4, μ = 1.0) are shown in Figure 2.1B-F. The addition of GSH changes the cyclic voltammetric behavior of NE. With increasing amounts of GSH, the peak height of reduction peak I_c and the peak II_a/peak II_c couple decrease. In the presence of 5.0 mM GSH (molar ratio of NE:GSH = 1:5) peak I_c disappears. When GSH reaches a concentration of 10 mM (molar ratio of NE:GSH = 1:10), the peak II_a/peak II_c couple almost completely disappears. The role of GSH in the electrooxidation of NE is to scavenge the intermediate NE-*o*-quinone and thus to block the formation of **8** and **9**. The reason that the peak II_a/peak II_c couple still appears might be due to the possibility that the glutathionyl conjugates of NE, if formed during the cyclic voltammetric process, can still be oxidized to give an NE-*o*-quinone product which undergoes a similar process to that of NE itself.

2.3.2 Isolation, purification and identification of oxidation reaction products

The oxidation reaction mixture was obtained by the electrooxidation of NE in the presence of GSH. In a typical electrooxidation reaction, NE•HCl (4.9 mg, 24 mmol) and

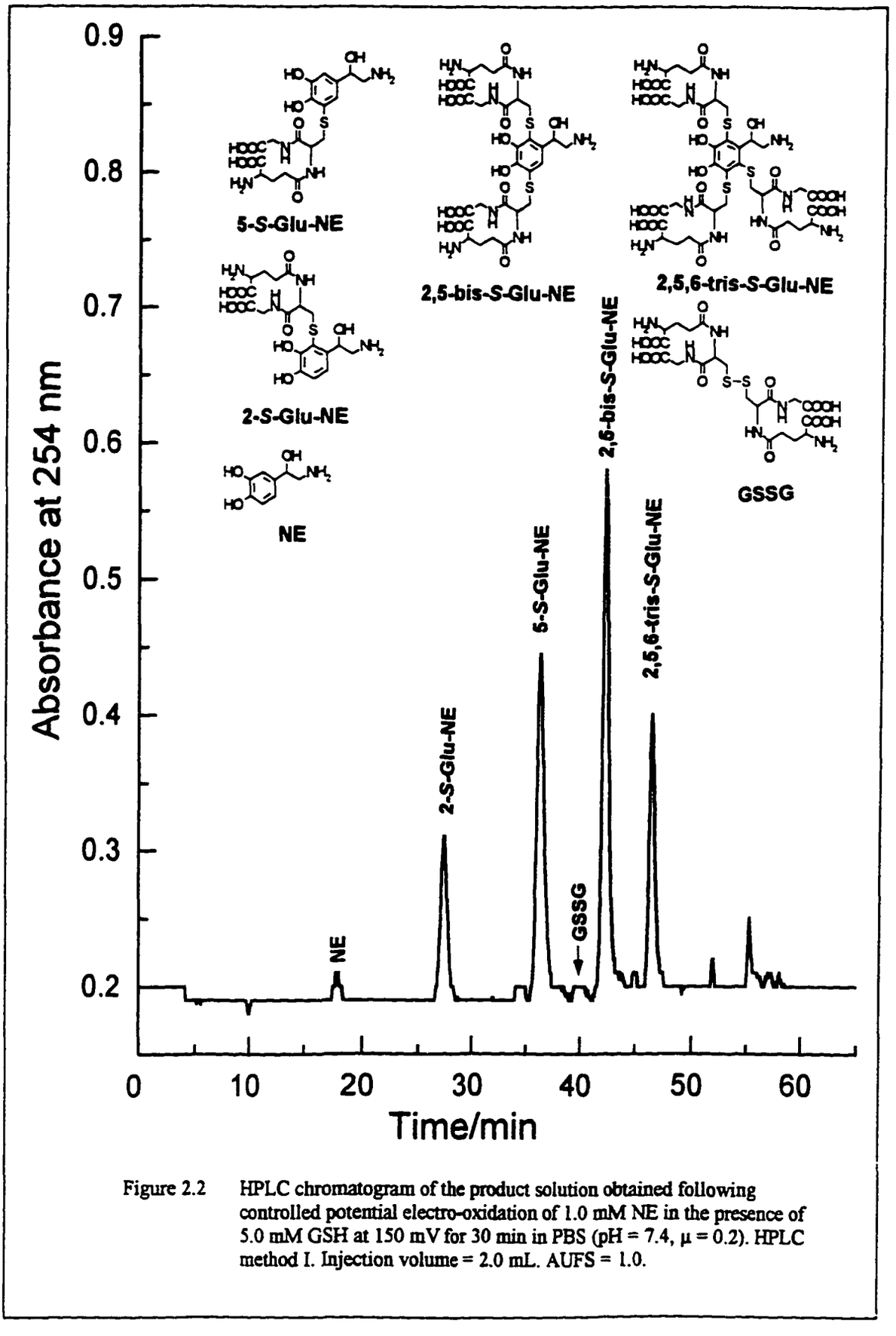

Figure 2.2 HPLC chromatogram of the product solution obtained following controlled potential electro-oxidation of 1.0 mM NE in the presence of 5.0 mM GSH at 150 mV for 30 min in PBS (pH = 7.4, μ = 0.2). HPLC method I. Injection volume = 2.0 mL. AUFS = 1.0.

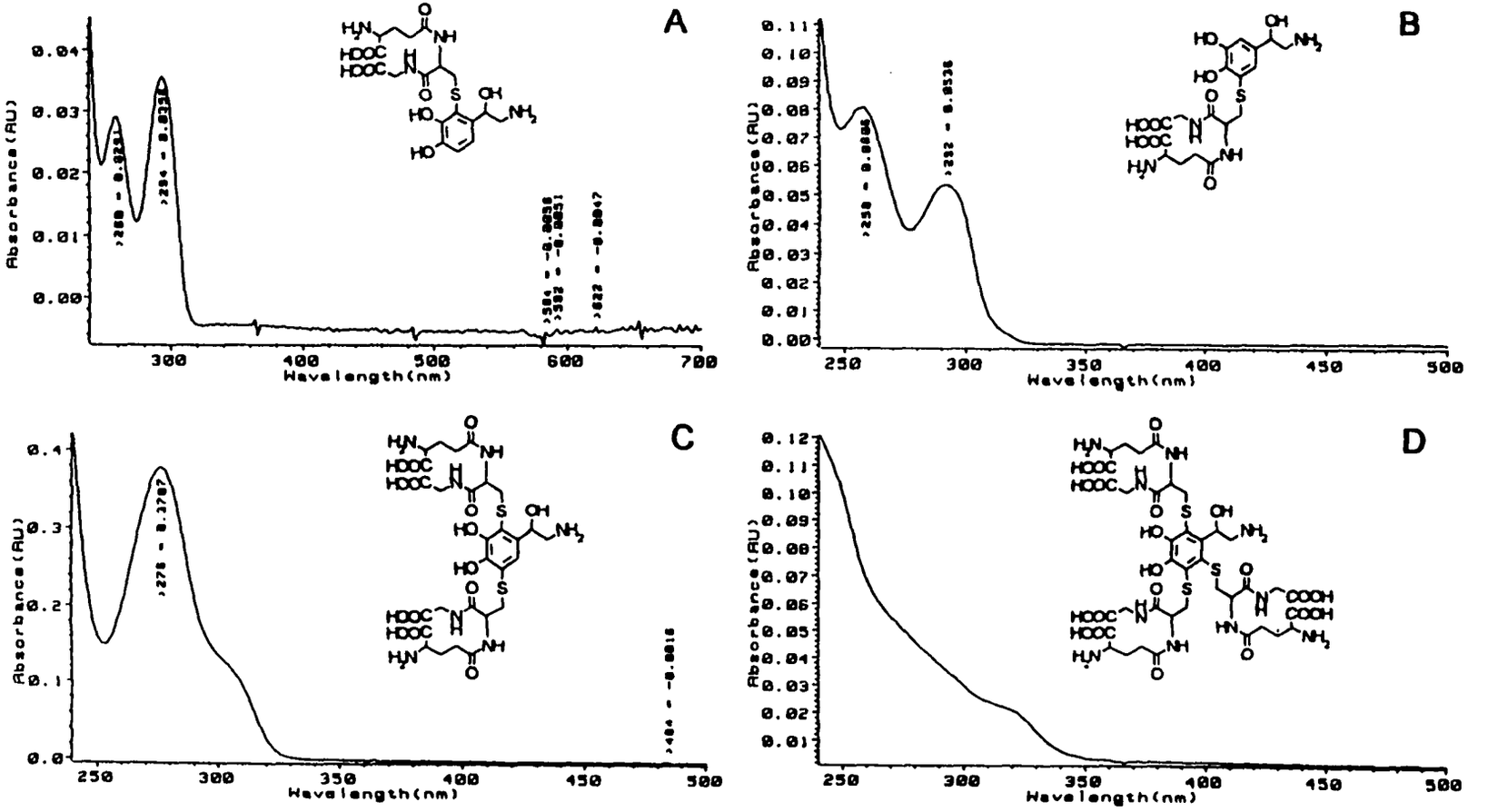

Figure 2.3 UV-Vis spectra of (A) 2-*S*-Glu-NE, (B) 5-*S*-Glu-NE, (C) 2,5-bis-*S*-Glu-NE and (D) 2,5,6-tris-*S*-Glu-NE as collected in mobile phase eluted under HPLC method II.

GSH (37 mg, 120 mmol) were dissolved in 25 mL of pH 7.4 PBS (μ = 0.2). The resulting solution was electrolyzed at 150 mV for 30 min under the flow of N_2. Upon termination of the reaction the entire pale yellow solution was adjusted to pH < 3 with dilute HCl and filtered. Then, 10 mL aliquots of the reaction solution were repeatedly injected into the preparative HPLC system and the components separated using HPLC method I. A typical chromatogram is shown in Figure 2.2. Four major components, which were later identified as 2-*S*-glutathionyl norepinephrine (2-*S*-Glu-NE), 5-*S*-Glu-NE, 2,5-bis-*S*-glutathionyl norepinephrine (2,5-bis-*S*-Glu-NE), and 2,5,6-tris-*S*-glutathionyl norepinephrine (2,5,6-tris-*S*-Glu-NE), respectively, were eluted under these conditions. Each component showed a unique UV-Vis spectrum in the mobile phase (Figure 2.3). These UV-Vis spectra were used to assist the collection of each component for verification purposes during the initial isolation and purification (desalting) processes.

Controlled potential electrooxidation of NE at the PGE in PBS (pH = 7.4, μ = 0.2) at 150 mV for 30 minute with different molar ratios of GSH showed similar product patterns (Figure 2.4). 5-*S*-Glu-NE is the major product and the 2,5-bis-*S*-Glu-NE is the second major one. The yield of 2,5,6-tris-*S*-Glu-NE is the lowest. Overall, the product yields reached maximum at ratios of GSH:NE between 2 and 4. When the molar ratio of GSH:NE was greater than 5, the relative yield of each product did not change very much.

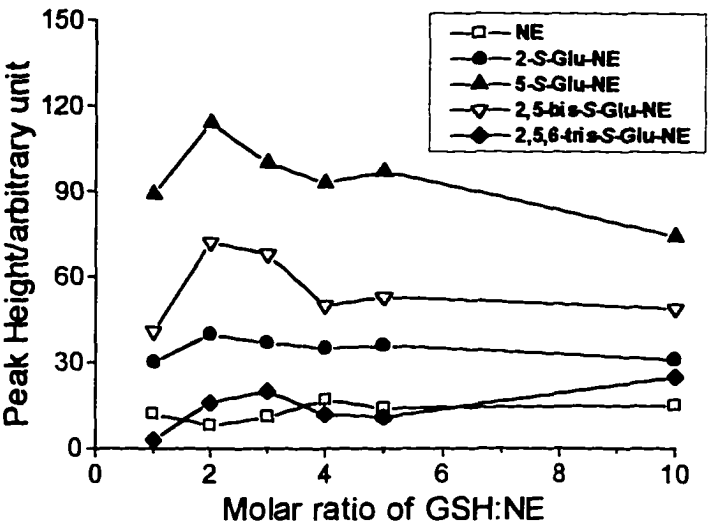

Figure 2.4 Product yields vs. molar ratio of GSH:NE at controlled potential electrooxidation of 1mM NE in PBS (pH = 7.4, μ = 0.2) at 150 mV for 30 min.

Therefore, a molar ratio of GSH:NE = 5 was chosen for the rest of the experiment. At a fixed GSH:NE molar ratio of 5, the relative yields of each major product are shown in Figure 2.5. During the first 40 min, the yield of each product grew very quickly, while after 60 – 90 min, the yields of each product remained relatively unchanged (except the

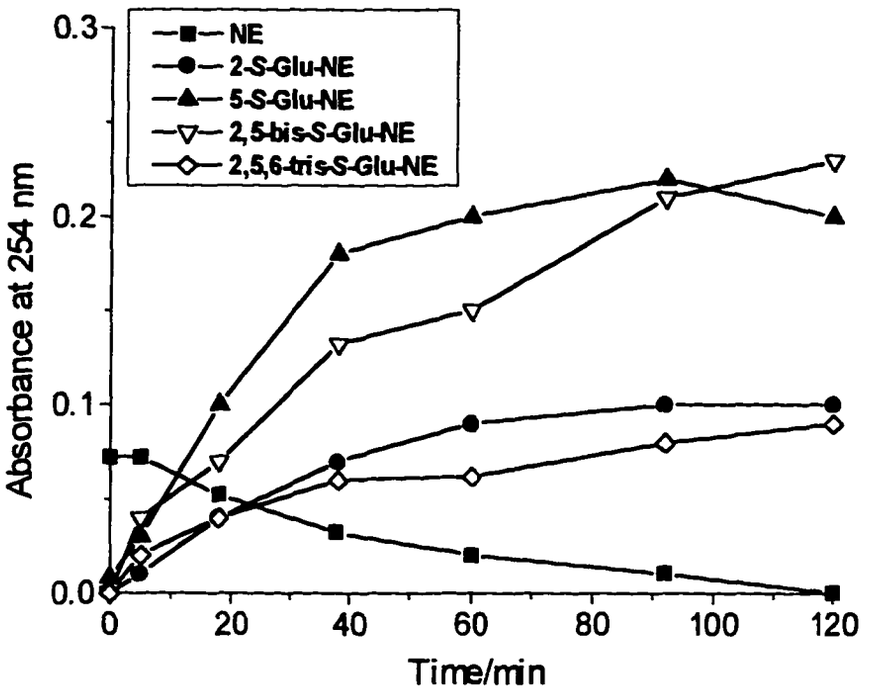

Figure 2.5 Time dependence of relative yields of the products formed after the controlled potential electrooxidation of 1mM NE and 5 mM GSH at PGE in PBS (pH = 7.4, μ = 0.2) at 150 mV.

yield of 2,5-bis-*S*-Glu-NE which continued to form). The electrolysis time of 60 min was employed in the following procedures to prepare the reaction mixture for HPLC separation.

The four major components were collected separately. Each component was immediately frozen on dry ice and subsequently freeze-dried. The resulting white solid materials, which contained TFA from the HPLC mobile phase (HPLC method I), were dissolved in minimum volume of deionized water and purified using HPLC method II (desalting). Assignments of ^{1}H NMR resonance to structures of reaction products, 2-*S*-

GLu-NE, 5-*S*-Glu-NE, 2,5-bis-*S*-Glu-NE, and 2,5,6-tris-*S*-Glu-NE, were based on the comparison with ^{1}H NMR spectra of NE (Figure B.1 in Appendix B) and GSH (Figure B.2 and B.3 in Appendix B), and were confirmed using two-dimensional COSY NMR experiments. NMR data for glutathionyl conjugates dopamine[91] and cysteinyl conjugates of norepinephrine[97] were also used as comparison with those of the reaction products.

2-*S*-glutathionylnorepinephrine (2-*S*-Glu-NE)

2-*S*-GLu-NE eluted at t_R = 27.5 min and its UV-Vis spectrum showed bands at λ_{max} = 258 nm and 292 nm (A_{258}/A_{292} = 0.88) in mobile phase at pH = 2.5. It was isolated as a white solid. In PBS (pH = 7.4, μ = 1.0), it exhibited UV bands at λ_{max}/nm (log $\varepsilon_{max}/M^{-1}cm^{-1}$): 256 (3.65) and 294 (3.62) (Figure B.4 in Appendix B). FAB-MS (glycerol matrix) gave *m/e* = 475.1491 (MH^+, 23%, $C_{18}H_{27}N_4O_9S$; calculated *m/e* = 475.1499) (Figure B.5 in Appendix B). ^{1}H NMR (CD_3OD) gave δ: 7.00 (d, $J_{5,6}$ = 8.1 Hz, 1H, C(5)-H), 6.87 (d, $J_{2,6}$ = 8.1 Hz, 1H, C(6)-H), 5.48 (dd, $J_{5,6}$ = 9.7, 2.9 Hz, 1H, C(α)-H), 4.51 (t, J = 6.3 Hz, 1H, C(d)-H), 3.91 (t, J = 6.5 Hz, 1H, C(a)-H), 3.84 (d, J = 4.2 Hz, 2H, C(f)-H_2), 3.19-3.08 (m, 2H, C(e)-H_2), 2.93-2.85 (m, 2H, C(β)-H_2), 2.62-2.44 (m, 2H, C(c)-H_2), 2.17-2.10 (m, 2H, C(b)-H_2) (Figure B.6 and B.7 in Appendix B). These data reveal the structure of the first peak, is 2-*S*-glutathionylnorepinephrine (2-*S*-Glu-NE), $C_{18}H_{26}N_4O_9S$, M = 474.14.

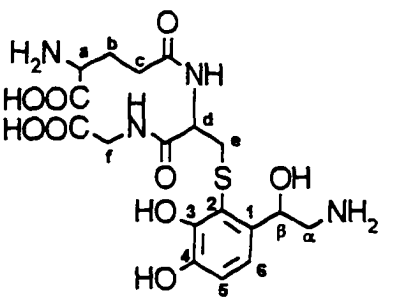

2-S-Glu-NE

5-*S*-glutathionylnorepinephrine (5-*S*-Glu-NE)

The second component, 5-*S*-Glu-NE, eluted at t_R = 37 min and showed UV-Vis spectrum bands at λ_{max} = 256 nm and 292 nm (A_{258}/A_{292} = 1.4) in mobile phase at pH =

2.5. It is a white solid compound and in PBS (pH = 7.4, μ = 1.0), it exhibited UV bands at λ_{max}/nm (log ε_{max}/M^{-1} cm^{-1}): 254 (3.77) and 294 (3.57) (Figure B.8 in Appendix B). FAB-MS (thioglycerol/glycerol matrix) gave *m/e* = 475.2 (MH^+, 100%, $C_{18}H_{27}N_4O_9S$; calculated *m/e* = 475.1499) (Figure B.9 in Appendix B). ^1H NMR (D_2O) gave δ: 6.84 (d, $J_{2,6}$ = 2.1 Hz, 1H, C(2)-H), 6.74 (d, $J_{2,6}$ = 2.1 Hz, 1H, C(6)-H), 4.69-4.65(m, 1H, C(α)-H), 4.23 (dd, J = 4.8, 8.4 Hz, 1H, C(d')-H), 3.63 (s, 3H, C(f')-H, C(a')-H), 3.84 (dd, J = 14.7, 4.8 Hz, 1H, C(e')-H), 3.09-2.94 (m, 3H, C(e')-H, C(β)-H_2), 2.26 (t, J = 7.5 Hz, 2H, C(c')-H_2), 1.93 (m, 1.88-1.92, 2H, C(b')-H_2) (Figure B.9 and B.10 in Appendix B). These data reveal the structure of the second component is 5-*S*-glutathionylnorepinephrine (5-*S*-Glu-NE), $C_{18}H_{26}N_4O_9S$, M = 474.14.

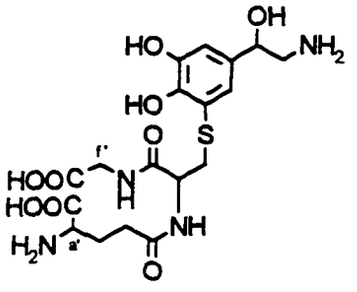

5-S-Glu-NE

2, 5-Bis-*S*-glutathionylnorepinephrine (2,5-bis-*S*-Glu-NE)

The third component, 2,5-bis-*S*-Glu-NE, eluted at t_R = 42.5 min and showed an UV-Vis band at λ_{max} = 276 nm with a shoulder band at 305 nm (A_{276}/A_{305} = 3) in mobile phase at pH = 2.5. It was isolated as a white solid. In PBS (pH = 7.4, μ = 1.0), it exhibited UV bands at λ_{max}/nm (log ε_{max}/M^{-1} cm^{-1}): 274 (4.17) and 310 (3.73) (Figure B.12 in Appendix B). FAB-MS (thioglycerol/glycerol matrix) gave *m/e* = 780.2192 (MH^+, 95%, $C_{28}H_{42}N_7O_{15}S_2$; calculated *m/e* = 780.2180) (Figure B.13 in Appendix B). ^1H NMR (D_2O) gave δ: 7.02 (s, 1H, C(6)-H), 5.31 (dd, J = 3.0, 9.0 Hz, 1H, C(α)-H), 4.27-4.20 (m, 2H, C(d)-H, C(d')-H), 3.77 (m, 4H, C(f)-H, C(f')-H), 3.77-3.64 (m, 4H, C(f)-H_2, C(f')-H_2), 3.25 (dd, J = 14.4, 4.8 Hz, 1H,

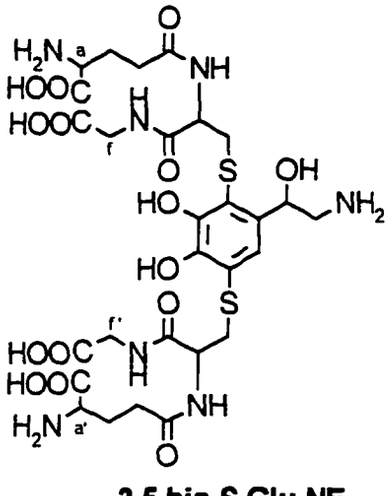

2,5-bis-S-Glu-NE

C(e)-H), 3.14-2.73 (m, 3H, C(e')-H, C(β)-H_2), 2.33-2.26 (m, 4H, C(c)-H_2, C(c')-H_2), 2.04-1.93 (m, 4H, C(b)-H_2, C(b')-H_2) (Figure B.14 and B.15 in Appendix B). These data reveal the structure of the third component is 2, 5-bis-*S*-glutathionyl-norepinephrine (2,5-bis-*S*-Glu-NE), $C_{28}H_{41}N_7O_{15}S_2$, M = 779.21.

2, 5, 6-Tris-*S*-glutathionylnorepinephrine (2,5,6-tris-*S*-Glu-NE)

The fourth component, 2,5,6-tris-*S*-Glu-NE, eluted at t_R = 47 min and showed no specific UV-Vis bands but with a wide shoulder at λ_{max} = 320 nm in mobile phase at pH = 2.5. It was isolated as a white solid compound. In PBS (pH = 7.4, μ = 1.0), it exhibited UV bands at λ_{max}/nm (log ε_{max} /$M^{-1}cm^{-1}$): 266 (4.43) and 328 (3.86) (Figure B.16 in Appendix B). FAB-MS (Thioglycerol/ glycerol/1000 PEG matrix) gave *m/e* = 1085.2784 (MH^+, 5.2%, $C_{38}H_{57}N_{10}O_{21}S_3$; calculated *m/e* = 1085.2862) (Figure B.17 in Appendix B). ^1H NMR (D_2O) gave δ: 6.02 (dd, J = 10.8, 3.6 Hz, 1H, C(α)-H), 4.45-4.39 (m, 2H, C(d')-H, C(d")-H), 4.04 (dd, J = 9.0, 3.0 Hz, 1H, C(d)-H), 3.77 (m, 3H, C(a)-H, C(a')-H, C(a")-H), 3.77-3.64 (m, 6H, C(f)-H_2, C(f')-H_2, C(f")-H_2), 3.25 (dd, J = 14.4, 4.8 Hz, 1H, C(e)-H), 3.14-2.73 (m, 3H, C(e')-H_2, C(β)-H_2), 2.33-2.26(m, 6H, C(c)-H_2, C(c')-H_2, C(c")-H_2), 2.04-1.93 (m, 6H, C(b)-H_2, C(b')-H_2, C(b")-H_2) (Figure B.18 and B.19 in Appendix B). This component can be structurally identified as 2, 5, 6-tris-*S*-glutathionylnorepinephrine (2,5,6-tris-*S*-Glu-NE), $C_{38}H_{56}N_{10}O_{21}S_3$; M = 1084.28.

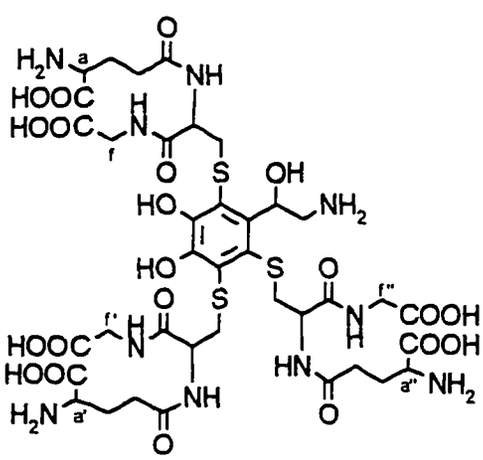

2,5,6-tri-S-Glu-NE

2.3.3 Cyclic voltammetric study of glutathionyl conjugates of NE

Cyclic voltammograms at ν = 200 mVs^{-1} of 2-*S*-Glu-NE, 5-*S*-Glu-NE, 2,5-bis-*S*-Glu-NE and 2,5,6-tris-*S*-Glu-NE in PBS (pH = 7.4, μ = 1.0) are shown in Figure 2.6. On the initial anodic sweep, there are two oxidation peaks (peak I_a, and peak III_a) for 5-*S*-Glu-NE, 2,5-bis-*S*-Glu-NE and 2,5,6-tris-*S*-Glu-NE; there is one oxidation peak for 2-*S*-Glu-NE (peak I_a). After scan reversal, all conjugates showed reduction peaks (peak I_c) which were quasi-reversibly coupled with oxidation peaks I_a. The E_p values for peaks I_a of 2-*S*-Glu-NE, 5-*S*-Glu-NE, 2,5-bis-*S*-Glu-NE and 2,5,6-tris-*S*-Glu-NE were 160 mV, 134 mV, 140 mV and 184 mV, respectively. Except for peak I_a of 2,5,6-tris-*S*-Glu-NE, all E_p values were smaller than that of NE (E_p = 179 mV). This means that glutathionyl conjugates of NE (except 2,5,6-tris-*S*-Glu-NE) are more easily oxidized than NE. The E_p values for the reversible peak III_a / peak III_c couples of 2-*S*-Glu-NE, 5-*S*-Glu-NE, 2,5-bis-*S*-Glu-NE and 2,5,6-tris-*S*-Glu-NE appeared at $E_{p,a}/E_{p,c}$ = -196/-234 mV, -216/-250 mV, -192/-250 mV and -192/-242 mV, respectively, which were very close to that of NE, -178/-241 mV. Glutathionyl conjugates may be oxidized to *o*-quinone intermediates, which may deprotonate at the side chain of the NE moiety. The subsequent cyclization of the side chain may yield a trihydroxyindoline which is then oxidized by the *o*-quinone of glutathionyl conjugate of NE to yield an aminochrome. The trihydroxy-indolines/aminochromes are presumably responsible for the peak III_a/peak III_c couples. This may explain the fact that the peak III_a/peak III_c couple did not completely disappear when NE was electroxidized in the presence of GSH. Peaks II_a might be attributed to the further oxidation of the glutathionyl conjugates of NE.

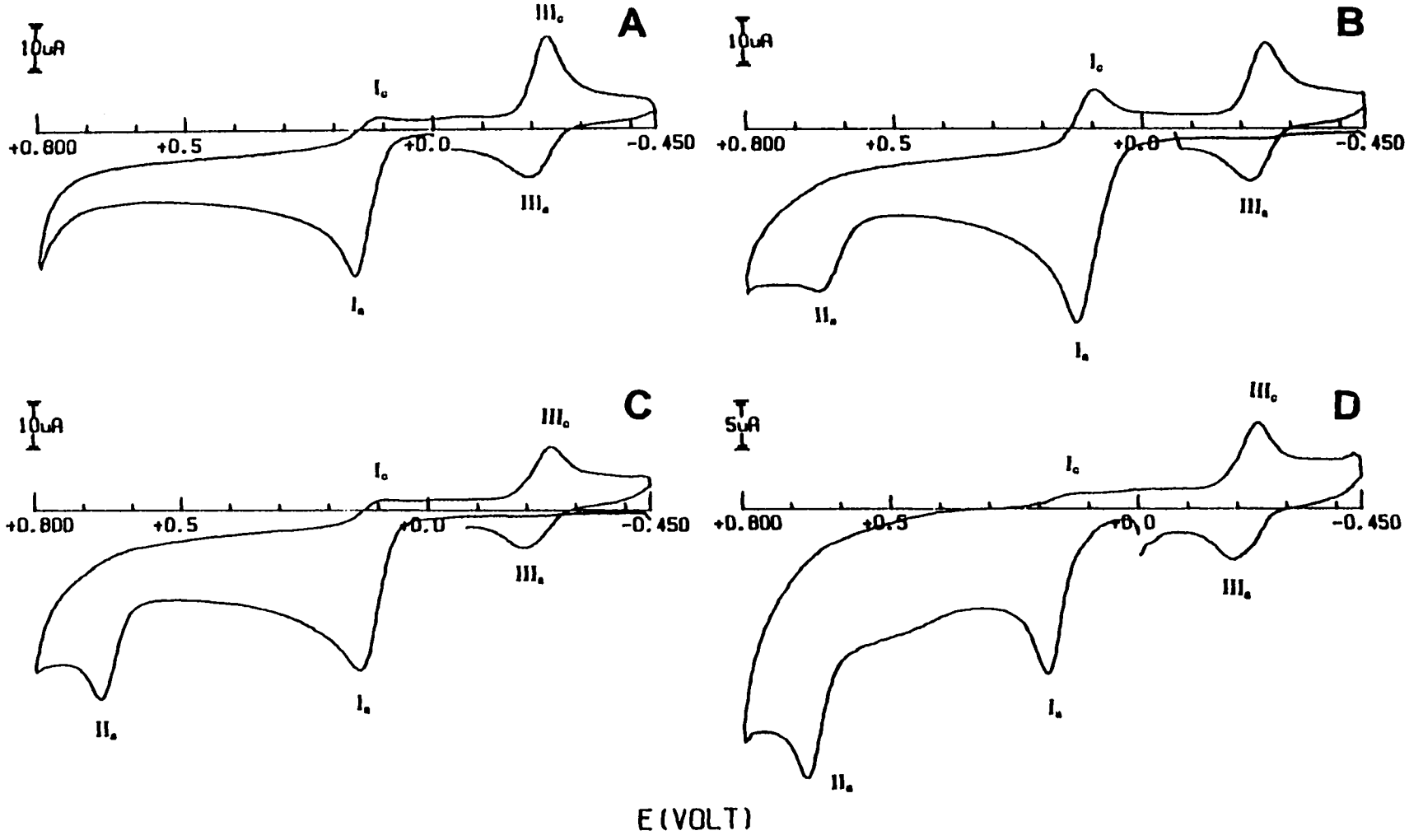

Figure 2.6 Cyclic voltammograms at the PGE of 0.1 mM (A) 2-*S*-Glu-NE, (B) 5-*S*-Glu-NE, (C) 2,5-bis-*S*-Glu-NE, (D) 2,5,6-tris-*S*-Glu-NE in PBS (pH = 7.4, μ = 1.0). Sweep rate: 200 mVs^{-1}.

2.3.4 Reaction Pathways

The results of cyclic voltammetric experiments indicate that GSH scavenges NE-*o*-quinone, the proximate oxidation product of NE (Figure 2.1). In controlled potential electrolyses of NE in the presence of GSH (molar ratio of GSH:NE = 5) 5-*S*-Glu-NE was the major product along with minor yield of 2-*S*-GLu-NE at the initial stages of the oxidation reaction. Therefore, the nucleophilic attack of GSH on NE-*o*-quinone, 5-*S*-Glu-NE is the most favored product. Addition of GSH to the C-2 position of NE-*o*-quinone is relatively unfavorable than that of C-5 position. At the potentials corresponding to the foot of peak I_a of NE, the initial oxidation product of NE, NE-*o*-quinone, is rapidly attacked by GSH to yield 2-*S*-Glu-NE and 5-*S*-Glu-NE. Thus the concentration of NE-*o*-quinone at the electrode surface is momentarily depleted. More NE must therefore be oxidized to achieve Nernstian equilibrium. Thus, instead of protecting NE from oxidation, GSH actually facilitates the reaction.

After prolonged controlled potential electrolyses of NE in the presence of GSH, 2,5-bis-*S*-Glu-NE and 2,5,6-tris-*S*-Glu-NE became the major products. The primary products from the oxidation of NE at the presence of GSH are mono-glutathionyl conjugates of NE, 2-*S*-Glu-NE and 5-*S*-Glu-NE. At the potential that NE is oxidized, 2-*S*-Glu-NE and 5-*S*-Glu-NE can also be oxidized to form the corresponding *o*-quinone intermediates, which are attacked by GSH to form 2,5-bis-*S*-Glu-NE. Finally, 2,5-bis-*S*-Glu-NE can again be oxidized to form 2,5-bis-*S*-Glu-NE *o*-quinone, which is attacked by GSH to form 2,5,6-tris-*S*-Glu-NE. These processes are summarized in Scheme IV.

Scheme IV

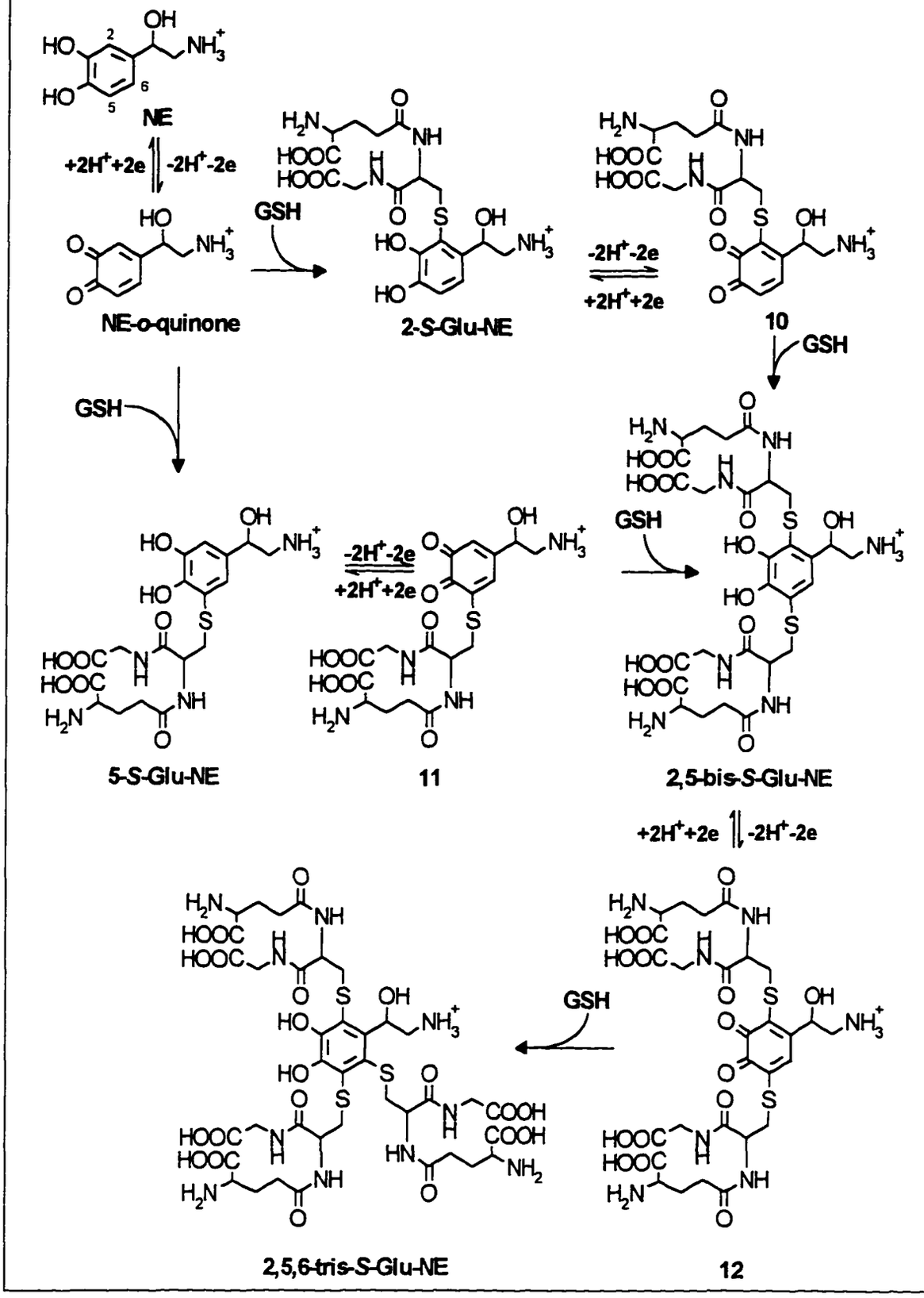
NE
+2H+ +2e
-2H+ -2e
NE-o-quinone
GSH
2-S-Glu-NE
-2H+ -2e
+2H+ +2e
10
GSH
GSH
5-S-Glu-NE
-2H+ -2e
+2H+ +2e
11
GSH
2,5-bis-S-Glu-NE
+2H+ +2e
-2H+ -2e
GSH
2,5,6-tris-S-Glu-NE
12

2.4. Autoxidation, Hydroxyl Radical-Mediated and Superoxide Anion Radical-Mediated Oxidation of NE in the Presence of GSH

2.4.1 Autoxidation of NE in the presence of GSH

To study the possible oxidation of NE by molecular oxygen, 0.5 mM NE was incubated in the presence of 5 mM GSH in PBS (pH = 7.4, μ = 0.2) at 37 °C in a reaction vessel that was exposed to the air. The temperature was chosen to be close to human body temperature. After about 2 h, HPLC showed trace amounts of 2-*S*-Glu-NE (t_R = 27.4 min) and 5-*S*-Glu-NE (t_R = 33.5 min), along with significant yields of GSSG (t_R = 39.5 min), in addition to unreacted NE (t_R = 18.4 min) and several unidentified peaks (t_R = 10.0, 24.1, 32.1, 34.1 and 55.8 min) (Figure 2.7 A). After 34 h of incubation at 37 °C, the GSSG peak was increased dramatically (Figure 2.7 B). GSSG may be formed from the oxidation of GSH by the oxygen dissolved in the incubation solution. During the incubation period between 2 h and 34 h, the concentration (measured by peak heights) of NE was reduced by 38%. Moreover, after 34 h of incubation, significant amounts of 2-*S*-Glu-NE and 5-*S*-Glu-NE were observed. Without the presence of GSH under the same conditions, NE formed black insoluble polymers. Therefore, at the present experiment conditions, NE is oxidized to NE-*o*-quinone, which is subsequently attacked by GSH to form the glutathionyl conjugates of NE.

When 0.5 mM NE was incubated in the presence of 5 mM GSH in PBS (pH = 7.4, μ = 0.2) along with 0.2 mM Fe^{2+} (ferrous ammonium sulfate) at 37 °C, the oxidation reaction was accelerated. After just 10 min, the amounts of mono-glutathionyl conjugates 2-*S*-Glu-NE and 5-*S*-Glu-NE formed was noticeably larger than the same incubation in the absence of Fe^{2+} for 2 h (Figure 2.8 A). After 17 h, the concentration of NE was reduced

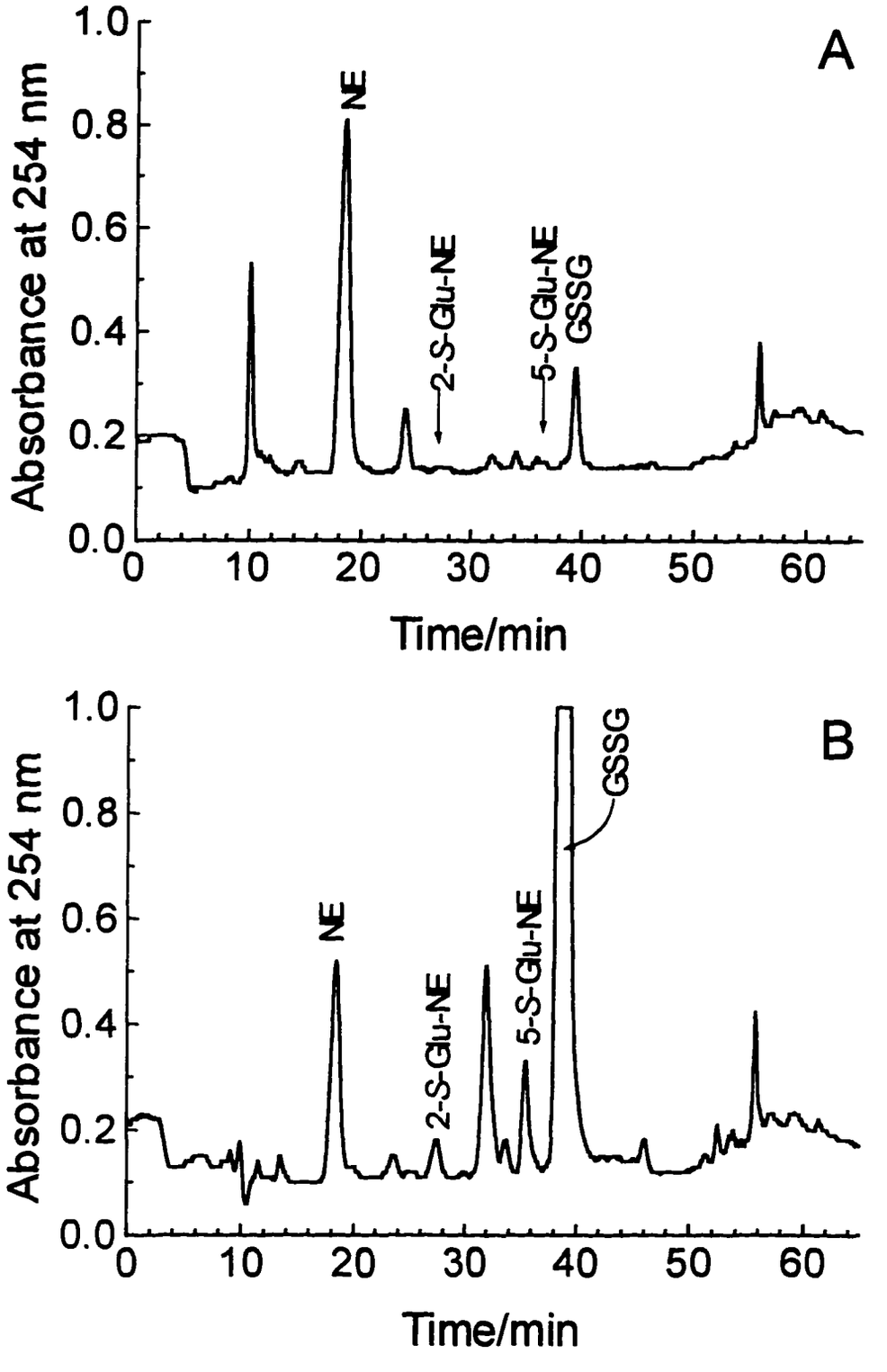

Figure 2.7 Autoxidation of 0.5 mM NE in the presence of 5.0 mM GSH in PBS (pH = 7.4, μ = 0.2) at 37 °C for (A) 2 h and (B) 34 h. HPLC method I. Injection volume = 3.0 mL. AUFS = 0.1.

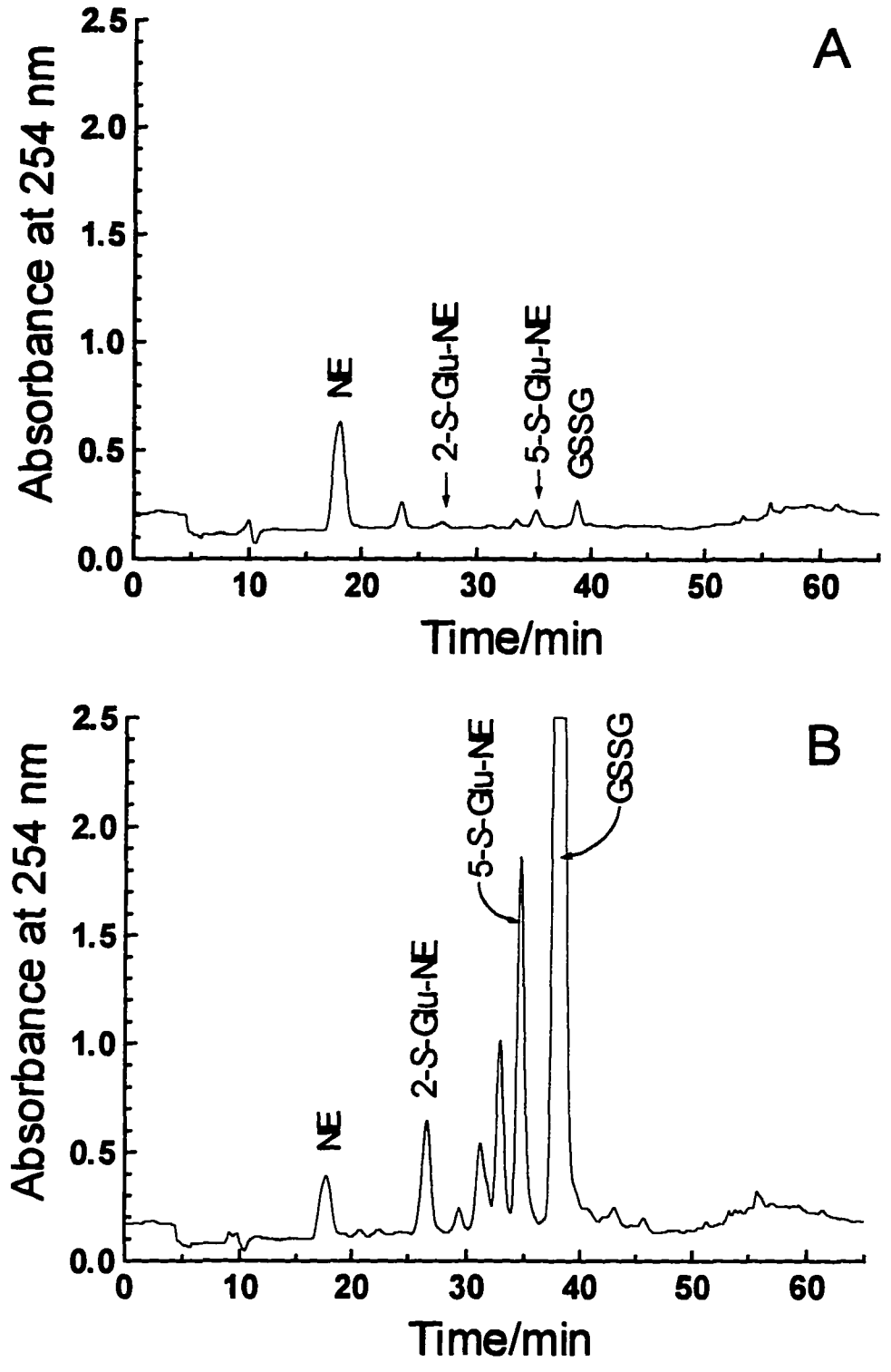

Figure 2.8 Autoxidation of 0.5 mM NE in the presence of 5.0 mM GSH and 0.2 mM Fe^{2+} in PBS (pH = 7.4, μ = 0.2) at 37 °C for (A) 10 min and (B) 17 h. HPLC method I. Injection volume = 3.0 mL. AUFS = 0.1.

by 42%, while the concentrations of 2-*S*-Glu-NE and 5-*S*-Glu-NE were increased by 1200% and 1800%, respectively. Again, a very large GSSG peak was recorded after 17 h. As discussed in the Chapter 1, DA may produce hydrogen peroxide during the course of its autoxidation. The accelerated reaction by Fe^{2+} implied the involvement of hydroxyl radicals in the autoxidation of NE. NE is oxidized in the similar way as is DA (equations 1.3 and 1.4 in Chap. 1) to give rise to the hydrogen peroxide byproduct. Fe^{2+} will catalyze the conversion of hydrogen peroxide into hydroxyl radical through Fenton reaction (equation 1.9 in Chap. 1). Actually, iron exists as a trace contaminant in chemical reagents and is very difficult to get rid of. It is this trace amount of Fe^{2+}/Fe^{3+} that catalyzes the hydroxyl radical formation via Fenton reaction and Haber-Weiss reaction (equation 1.11 in Chap. 1).

2.4.2 Effects of AA and GSH concentrations on autoxidation of NE

Since the possible leakage of the capillary blood vessels in the brain could release hemoglobin[102] and trace amounts of low molecular weight iron[103] from erythrocytes, iron could be responsible for the free radical reactions *in vivo*. It is reported[104] recently that the loosely bound iron was found significantly higher in the brains of AD patients than in the control samples.

Because chemical reagents always contain trace amount of iron, the autoxidation reaction of NE may be catalyzed through HO•-mediated oxidation, as the demonstration reaction accelerating by adding Fe^{2+} in the reaction media. In this section the study was focused on the effect of antioxidants, AA and GSH, on the oxidation of NE. Submicromolar concentrations of the reaction components were employed to mimic

concentration levels in the tissue. HPLC-EC (HPLC method III) was employed for sample assay. *N*-methyl-5-hydroxytryptamine (N-MET) was used as an internal standard for quantitative measurement. The ratios of peak height of reaction components to that of N-MET were used to calculate the concentrations of reaction components using the following equation:

$$C_{sample} = C_{standand} \times \frac{R_{sample}}{R_{standand}} \quad (2.1)$$

where R_{sample} is the ratio of the peak height of the product to that of N-MET; $R_{standard}$ is the ratio of peak height of the standard compound for the product to that of N-MET; $C_{standard}$.is the concentration of the standard compound for the product; C_{sample} is the concentration of the product in the reaction mixture.

No concentration changes of NE were observed as there were no changes of peak height ratio of NE to N-MET. Typical concentrations of the reaction products were about 1-5% of that of NE. The peak height ratios of 5-*S*-Glu-NE, 2-*S*-Glu-NE and 2,5-bis-*S*-Glu-NE to N-MET were linear in a range up to 1.0 μM. HPLC conditions were optimized to monitor the reaction products.

NE (3.0 μM) was incubated with 2.0 μM Fe^{2+}, 24 μM EDTA in PBS (pH = 7.4, μ = 0.2) and various amounts of AA and GSH. The reaction mixtures were kept at 37 °C in a water bath for 1 h. Effects of AA on reaction product yields at different concentrations of GSH are shown in Figure 2.10. Only mono-glutathionyl conjugates of NE were observed under these conditions. The molar ratio of the 2-*S*-Glu-NE to 5-*S*-Glu-NE was approximately 1:2 under these conditions. When the GSH:NE molar ratio was 1, a high concentration of 45 μM AA virtually blocked the formation of 2-*S*-Glu-NE. In general, an increase of the AA concentration decreased the yields of glutathionyl conjugates of NE. In contrast to the autoxidation of NE in phosphate buffer solution, AA may prevent NE from oxidation by limiting the formation of NE-*o*-quinone, which is the target of the nucleophile

GSH. There must be a competition between the GSH and AA for the oxidation intermediate NE-*o*-quinone. GSH tends to nucleophilically attack on the o-quinone intermediate, while AA tends to reduce the *o*-quinone intermediate back to NE.

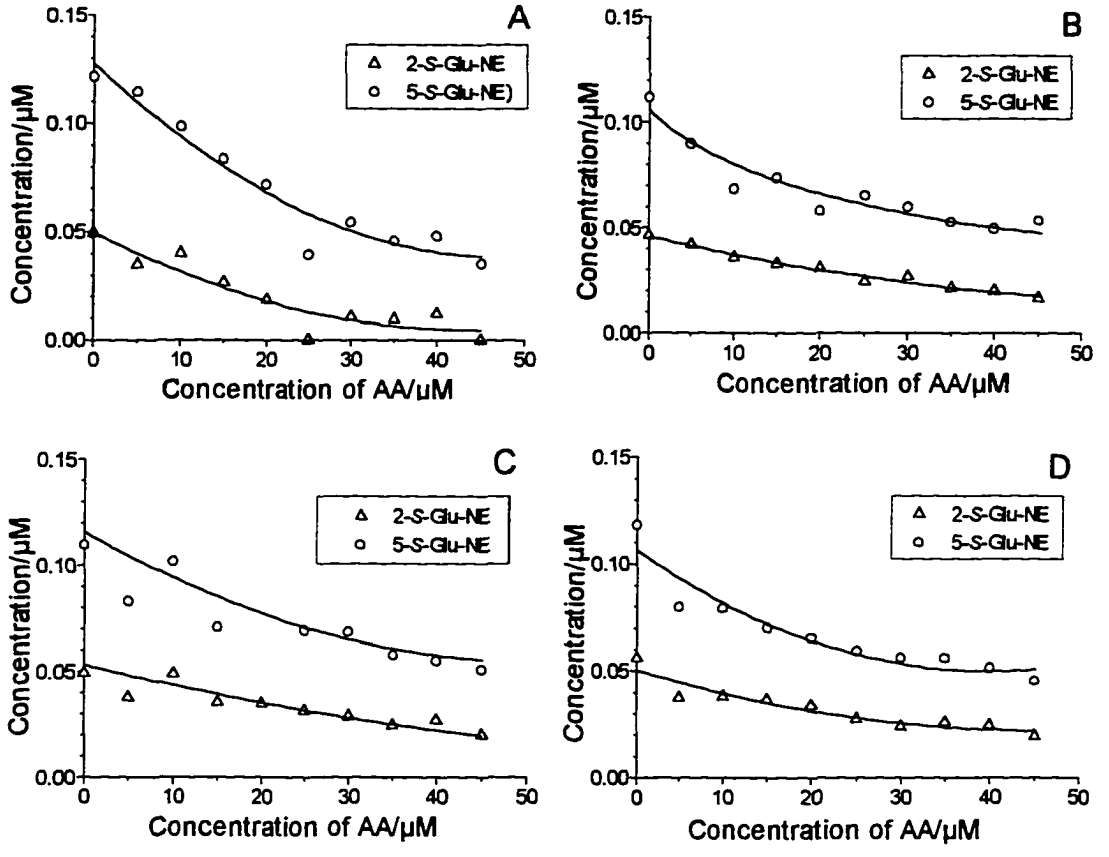

Figure 2.9 Effect of concentration of AA on the autoxidation of 3.0 μM NE with 2.0 μM Fe^{2+}, 24 μM EDTA in PBS (pH = 7.4, μ = 0.2) at 37°C for 1 h in the presence of GSH of A) 1.0 μM, B) 3.0 μM, C) 5.0 μM and D) 10.0 μM. Data shown are the average of two independent experiments.

The effects of GSH:NE molar ratio on the autoxidation of NE at various concentrations of AA are shown in Figure 2.10. When concentrations of AA were at 0 and 15 μM, yields of 2-*S*-Glu-NE and 5-*S*-Glu-NE were almost unaffected by different GSH:NE molar ratios. When AA were at 30 and 45 μM, yields of 2-*S*-Glu-NE and 5-*S*-Glu-NE were increased when molar ratio of GSH:NE increased from 1 to 3. The yields of the reaction products were virtually unchanged by the GSH:NE molar ratio. Overall, the

yields of 2-*S*-Glu-NE and 5-*S*-Glu-NE at 45 μM AA were about the 50% of those at 0 μM AA. When the concentration of AA was 45 μM, the autoxidation reaction reached a minimum level among the experimental conditions employed. Under these conditions,

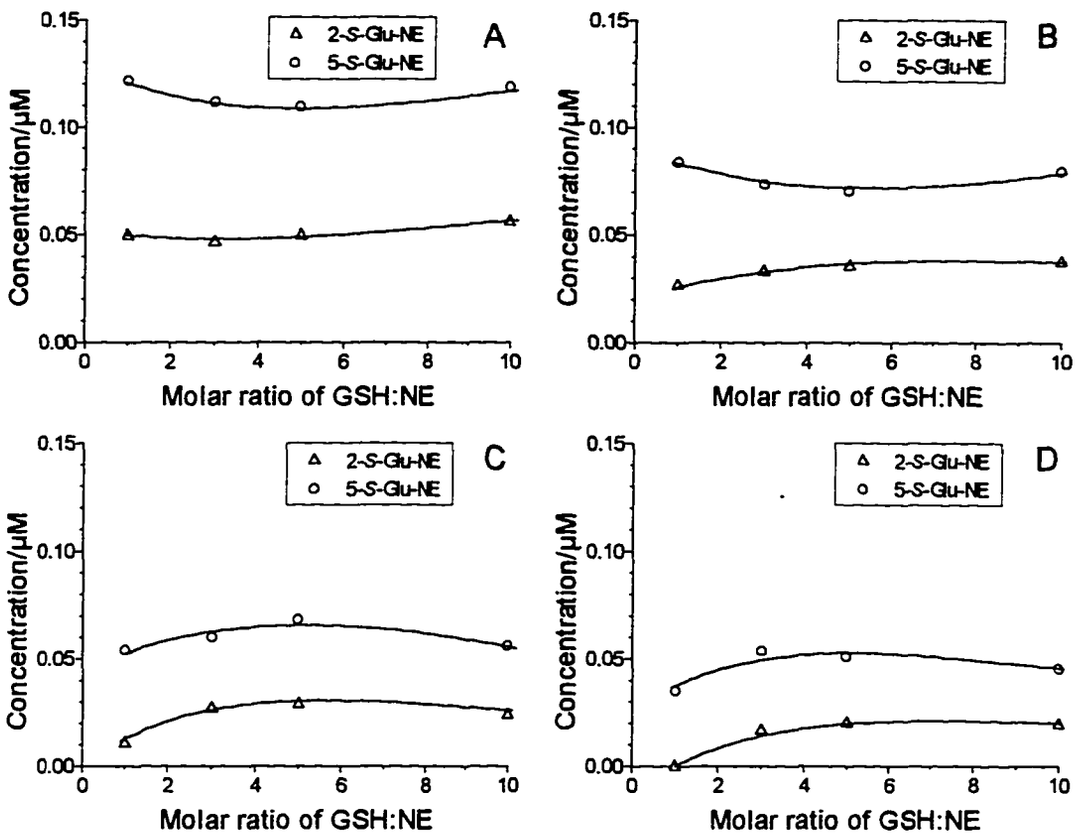

Figure 2.10 Effect of molar ratio of GSH:NE on autoxidation of 3.0 μM NE with 2.0 μM Fe^{2+} and 24 μM EDTA in PBS (pH = 7.4, μ = 0.2) at concentrations of AA = A) 0 μM, B) 15, C) 30 μM, and D) 45 μM.

2-*S*-Glu-NE was not formed if the concentration of GSH (low molar ratio of GSH:NE) was low at the same time. Generally, roughly two moles of 5-*S*-Glu-NE were produced for one mole of 2-*S*-Glu-NE. 2-*S*-Glu-NE and 5-*S*-Glu-NE were formed in 1:2 molar ratio. This revealed that the C-5 position is favored twice as much as the C-2 position of NE-*o*-quinone intermediate during nucleophilic attack by GSH. This may partly be attributed to the fact that there is less steric hindrance effect at the C-5 position than at the C-2 position on NE-*o*-quinone.

2.4.3 Hydroxyl radical (HO•)-mediated oxidation of NE in the presence of GSH

Hydroxyl radical (HO•) was generated by the procedure adapted from the literature[105]. Stock solutions of 10 mM ascorbic acid (AA), 24 mM Na_2EDTA, 10 mM Fe^{2+}, 176 mM H_2O_2 10 mM NE, and 10 mM GSH were prepared fresh daily. An oxidation reaction was started by adding: 1.0 mL AA, 0.1 mL EDTA, 0.2 mL Fe^{2+}, 1.0 mL NE, 5.0 mL GSH, 2.0 mL PBS (pH = 7.4, μ = 1.0) and 0.7 mL H_2O_2. Reaction timing began from the moment of adding H_2O_2. The reaction mixtures were kept at ambient temperature (22 ± 2°C).

The reaction was very rapid. Thus, after 10 min incubation HPLC chromatograms clearly showed the formation of 2-*S*-Glu-NE, 5-*S*-Glu-NE and 2,5-bis-*S*-Glu-NE (Figure 2.9 A). It was noticed that bis-glutathionyl conjugate of NE was formed, while only mono-glutathionyl conjugates of NE were observed in the autoxidation experiments. After 75 min, even tris-glutathionyl conjugate (2,5,6-tris-*S*-Glu-NE) began to appear (Figure 2.9 B). Besides the difference in the glutathionyl conjugate products, there was a much lower amount of oxidized GSH (GSSG) produced in HO•-mediated oxidation of NE in the presence of GSH. The oxidation reaction incurred by HO• is much faster than that of oxygen dissolved in the solution. HO• was generated by Fenton chemistry, equation 2.2, as shown below:

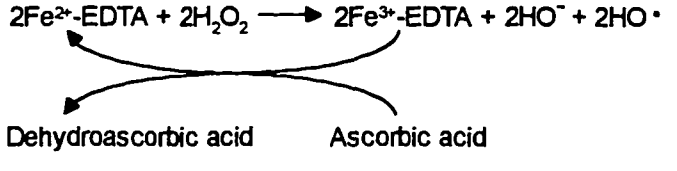

(2.2)

HO• is formed by decomposition of H_2O_2 by Fe^{2+}, and the resulting Fe^{3+} is then regenerated back to Fe^{2+} by ascorbic acid. Ascorbic acid itself is oxidized into dehydroascorbic acid[105]. In the reaction mixture, H_2O_2 is the limiting reagent. Therefore, the reaction stopped when no H_2O_2 remained. The reaction mechanism is similar to that of

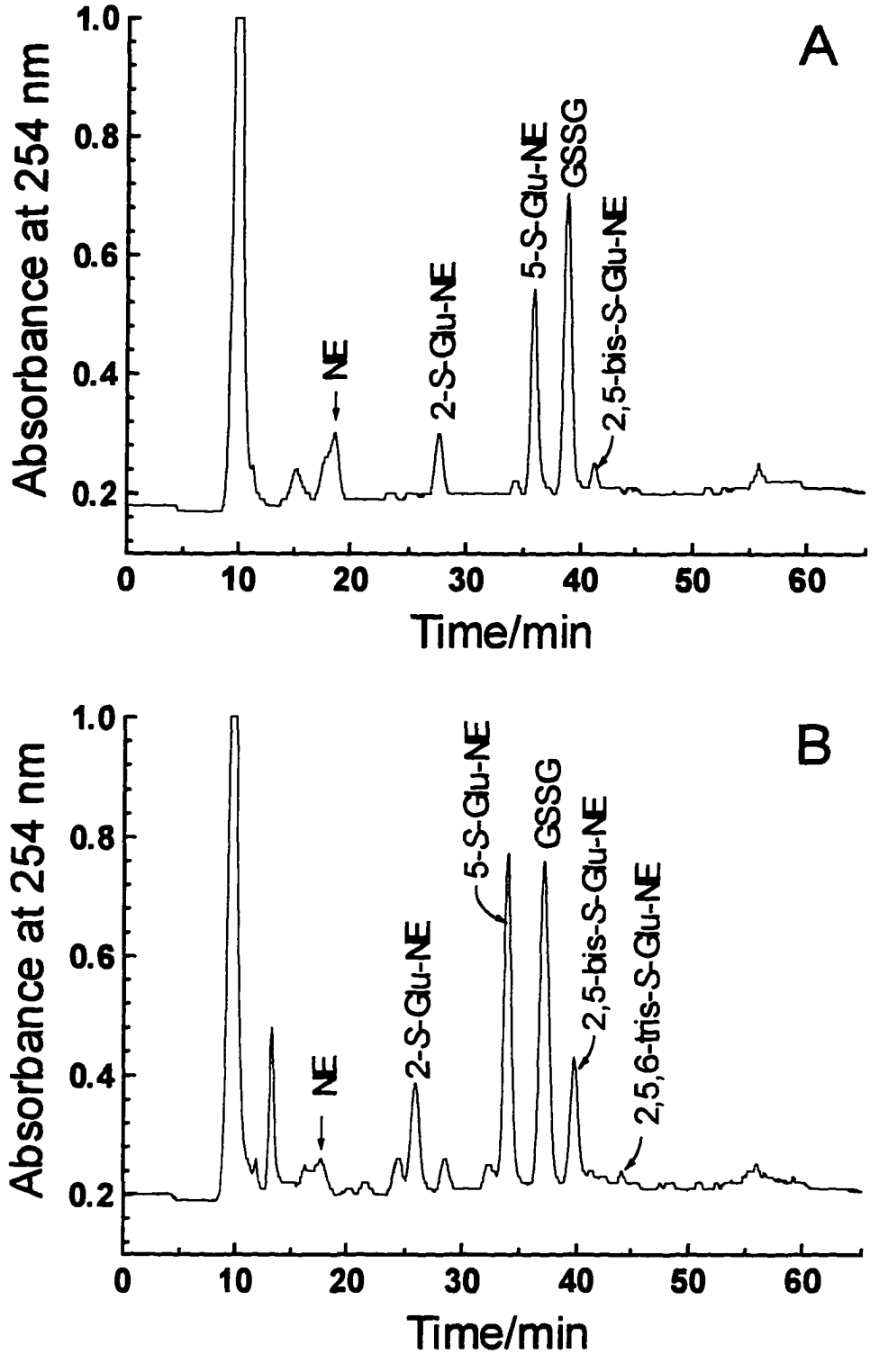

Figure 2.11 Hydroxyl radical oxidation of 1.0 mM NE in the presence of 5.0 mM GSH, 0.2 mM Fe^{2+}, and 12 mM H_2O_2 in PBS (pH = 7.4, μ = 0.2) at 22 °C for (A) 10 min, and (B) 75 min. HPLC method I. Injection volume = 4.0 mL. AUFS = 1.0.

the electrochemical oxidation of NE in the presence of GSH except that the oxidation condition was originated from HO• instead of electrochemical means. The much lower GSSG yield compared to that of the autoxidation may come from the shorter reaction time and the presence of AA in the reaction media.

2.4.4 Superoxide anion radical-mediated oxidation of NE in the presence of GSH

Superoxide anion radical ($O_2^{-}\bullet$) was generated by the procedure adapted from the literature[106]. NE (4 μM) was incubated with 20 μM GSH, 400 μM xanthine and 47 mU/mL xanthine oxidase in 10 mL PBS (pH = 7.4, μ = 0.2) at 37 °C. The reaction was monitored by HPLC method III. A 5.0 μL aliquot of the reaction mixture was injected into the HPLC system at the different time periods. The concentration of NE decreased rapidly during the first 10 min and remained almost constant after 10 min (Figure 2.12). 2-*S*-Glu-NE and 5-*S*-Glu-NE were detected as products. However, the product peaks were very small and could not be measured quantitatively.

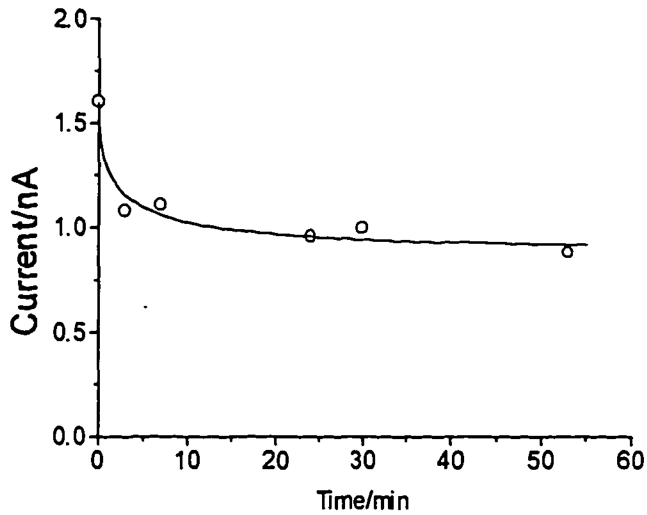

Figure 2.12 NE peak height vs. time when 4 μM NE was oxidized in the presence of 20 μM GSH in xanthine/xanthine oxidase superoxide anion radical generation system in PBS (pH = 7.4, μ = 0.2) at 37 °C.

To optimize the chromatograms for the reaction mixture, another reaction with NE (10 μM) was incubated with 50 μM GSH, 100 μM xanthine and 0.047 Unit/mL xanthine oxidase in 10 mL PBS (pH = 7.4, μ = 0.2) at 37 °C. HPLC-EC Chromatograms of the reaction solution formed after incubation for 3 min, 36 min, and 91 min are shown in Figure 2.13. After 3 min incubation, 2-*S*-Glu-NE, 5-*S*-Glu-NE and 2,5-bis-*S*-Glu-NE were recorded at t_R = 6.4, 9.4 and 18.8 min, respectively. Unlike under the previous conditions, the yields of glutathionyl conjugates of NE decreased as the superoxide anion radical-mediated reaction continued. After 91 min incubation, peak heights of all three glutathionyl conjugates decreased significantly. Among them, the chromatographic peak of 2,5-bis-*S*-Glu-NE almost disappeared. Over the 91 min incubation period an unknown peak at a retention time of t_R = 17.0 increased intensively. The retention time of this unknown peak was compared with the samples available in this laboratory, including 2,5,6-tris-*S*-Glu-NE, but this unknown product remains to be identified.

During the incubation, the concentration of 2-*S*-Glu-NE was relatively unchanged, while concentration of 5-*S*-Glu-NE already reached its maximum at or before 3 min and declined thereafter. 2,5-bis-*S*-Glu-NE was formed in the early incubation time and its concentration declined as the incubation continued. In the mean time, there was an unidentified component at t_R = 17.0 min with a continuously increased peak height, in addition to other unknown peaks. The superoxide anion radical-mediated oxidation reaction of NE in the presence of GSH was different from electrochemical oxidation, autoxidation and HO•-mediated oxidation.

Under the experimental conditions, the Haber-Weiss reaction might contribute to the generation of hydroxyl radical. The buffer solution and reagents used could contain enough trace amounts of transition metals[107] to catalyze the HO• formation in the presence of hydrogen peroxide and superoxide anion radicals. Hydroxyl radical will oxidize NE in

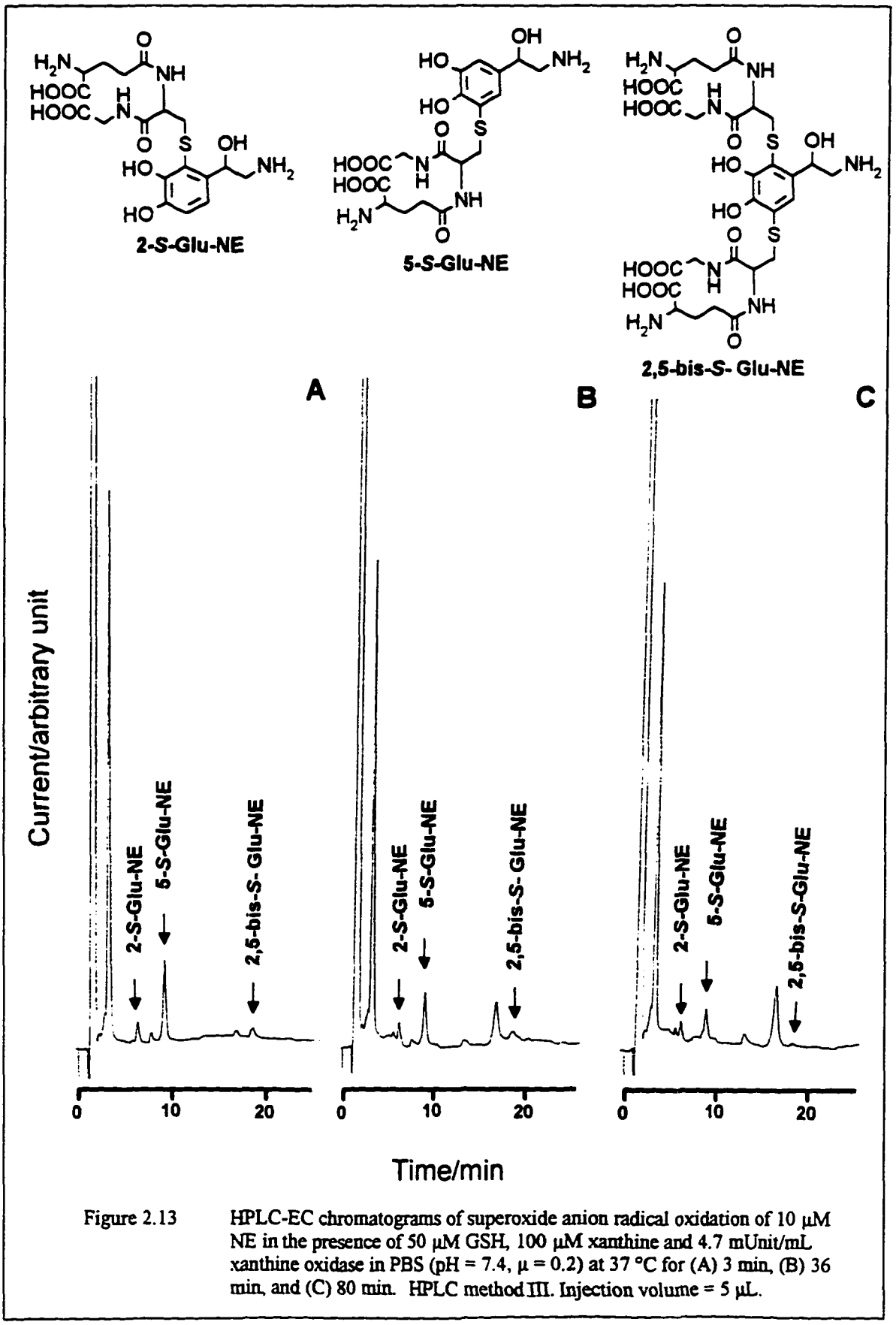

Figure 2.13 HPLC-EC chromatograms of superoxide anion radical oxidation of 10 μM NE in the presence of 50 μM GSH, 100 μM xanthine and 4.7 mUnit/mL xanthine oxidase in PBS (pH = 7.4, μ = 0.2) at 37 °C for (A) 3 min, (B) 36 min, and (C) 80 min. HPLC method III. Injection volume = 5 μL.

the presence of GSH the similar way as it would in autoxidation and Fenton reaction-generated hydroxyl radical oxidation reactions. This would lead to the production of mono- and bis-glutathionyl conjugated NE at early incubation stage. It seemed that the oxidation condition generated by xanthine/xanthine oxidase system is stronger than that of autoxidation and HO•-mediated reaction. Therefore the glutathionyl conjugates of NE produced at early stage of incubation were soon be oxidized to secondary products. The identification of the reaction product which had a retention time of t_R = 17.0 min may shed some light on the reaction mechanism. However, under the current conditions, it was difficult to collect enough to do the spectral analysis as was done on the glutathionyl conjugates of NE.

2.5 Discussion

In this chapter, the oxidation of NE in the presence of GSH yielded a series of glutathionyl conjugates of NE and thus diverted the melanin pathway. The reaction was carried out by means of electrooxidation, autoxidation, HO•-mediated oxidation and superoxide anion radical-mediated oxidation in physiological pH (pH = 7.4). Apparently, the electrooxidation and HO•-mediated oxidation provided the most proper conditions, which favored the formation of all four glutathionyl conjugates of NE. When NE was oxidized, the NE-*o*-quinone intermediate was nucleophilically attacked by GSH to form 2-*S*-Glu-NE and 5-*S*-Glu-NE. 2-*S*-Glu-NE and 5-*S*-Glu-NE were more easily be oxidized than NE as indicated by the cyclic voltammetric study of the glutathionyl conjugates. Therefore, mono-glutathionyl conjugates of NE were oxidized under the same conditions as NE was oxidized and formed glutathionyl conjugate *o*-quinones. Subsequent

nucleophilic attack by GSH yielded bis- and eventually tris-*S*-glutathionyl conjugates of NE. When NE was auto-oxidized by the oxygen in the atmosphere, only mono-glutathionyl conjugates 2-*S*-Glu-NE and 5-*S*-Glu-NE were formed in a molar ratio of about 1:2 (2-*S*-Glu-NE to 5-*S*-Glu-NE). The superoxide anion radical-mediated reaction was different from other oxidation conditions. The yields of the glutathionyl conjugates of NE did not increase during the course of the reaction. The unknown products were precluded from any known glutathionyl conjugates of NE.

In recent years, increasing evidence implicates oxygen-derived free radicals with pathological conditions that occur in neurodegenerative diseases[108]. Superoxide radical is the most abundant oxygen radical generated *in vivo*, from sources that include activated leukocytes[109], the mitochondrial electron transport chain [110], and tissue oxidases. The most notable oxidase is xanthine oxidase[111,112]. Xanthine oxidase catalyzes the oxidation of hypoxanthine and xanthine by oxygen to produce hydrogen peroxide, superoxide anion radical and uric acid. The xanthine oxidase is reduced by the hypoxanthine and/or xanthine; and the reduced xanthine oxidase then passes the electrons to molecular oxygen. There are two distinct pathways to pass the electrons to oxygen: monovalently (equation 2.3) and divalently (equation 2.4), giving rise to superoxide anion radical and hydrogen peroxide, respectively[113].

$$\text{Enzyme-}H_2 + 2O_2 \longrightarrow \text{Enzyme} + 2H^+ + 2O_2^{-1}\bullet \qquad (2.3)$$

$$\text{Enzyme-}H_2 + O_2 \longrightarrow O_2 + H_2O_2 \qquad (2.4)$$

The monovalent pathway is favored with an increased ratio of oxidized to reduced enzyme, such as the conditions of high concentrations of oxygen, low concentrations of substrate, and high pH[113]. To participate in electron transport, four redox centers in the active site are present in xanthine oxidase: one molybdenum, two iron-sulfur clusters and

one flavin adenine dinucleotide center (FAD). The molybdenum and FAD can hold up to two electrons, while iron-sulfur clusters can only hold one electron[114]. Fully reduced xanthine oxidase bears six transferable electrons and reacts with excess oxygen to form a sequence of products in the order of H_2O_2, H_2O_2, $O_2^{\cdot -}$, and $O_2^{\cdot -}$[115,116]. Therefore, conditions favoring a high steady state of reduction of xanthine oxidase (high xanthine concentration) will favor the formation of H_2O_2. In contrast, conditions favoring partial reduction of xanthine oxidase (high concentration of oxygen or high pH) favor the formation of superoxide anion radical.

Superoxide dismutase, AA and α-tocopherol are the main scavengers of superoxide anion radicals[117]. Cysteine, GSH and other sulfhydryl donors are also radical scavengers and may act as anti-oxidants *in vivo*[118,119]. GSH is an important substrate of the GSH-Red to convert hydrogen peroxide to water.

Superoxide anion radical and hydrogen peroxide generated from the xanthine/xanthine oxidase system react in the presence of certain transition metal ions, metal chelates, or heme proteins through the Fenton (equation 1.9) and/or Haber-Weiss reactions (equation 1.11) to yield hydroxyl radical. Iron is an essential species for several normal brain functions and trace levels of low molecular weight iron can be found in brain tissue[120]. Hydroxyl radicals will attack the nearby proteins, nucleic acids and lipids in the cell and may eventually cause cell death. In aqueous solution, superoxide anion radical can also auto-dismutate into singlet oxygen ($^1O_2$)[121], as shown in the equation 2.5:

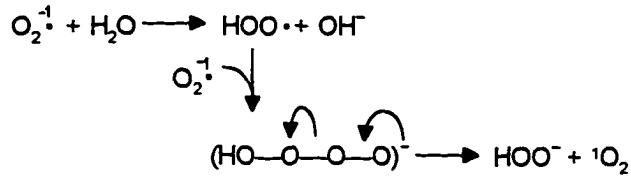

(2.5)

The scavengers for superoxide anion radical are more protective than the scavengers for hydroxyl radical and singlet oxygen. This may imply that both hydroxyl radical and singlet

oxygen are produced secondary to the generation of superoxide anion radical[122]. The involvement of $^1O_2$ in addition to HO• might contribute to the different oxidation pattern of the superoxide anion radical-mediated oxidation of NE in the presence of GSH at physiological pH.

Chapter 3 *In Vivo* Metabolism of 5-*S*-Glu-NE in Rat Brain

3.1 Introduction

In this chapter, both the *in vitro* and *in vivo* metabolisms of 5-*S*-Glu-NE were studied. The aberrant metabolites of NE were thought to be involved in the pathogenesis of neurodegenerative diseases like PD and AD. *In vitro* study has shown that a series of cysteinyl and glutathionyl conjugates of NE were formed when NE was oxidized in the presence of cysteine and GSH. Among those reaction products, at least two compounds from the further oxidation of the cysteinyl conjugates of NE were toxic and led to animal behavior changes when administered into the brains of laboratory mice[97]. Since the concentration of GSH is larger than that of cysteine in neurons, it is conceivable that GSH would nucleophilically attack the NE-*o*-quinone when NE is oxidized under the conditions of oxidative stress, which is thought to be responsible for neurodegenerative diseases including PD and AD. The hydrolysis of 5-*S*-Glu-NE was studied to investigate the possible link between the glutathionyl conjugate of NE and cysteinyl conjugate of NE.

3.2 Experimental

3.2.1 Chemicals

L-Cysteine, L-cysteinylglycine, 3,4-dihydroxyphenylacetic acid (DOPAC), 5-hydroxyindole-3-acetic acid (5-HIAA), 5-hydroxytryptamine (5-HT), homovanillic acid

(HVA), and 3,4-dihydroxybenzylamine (DHBA•HBr), and 5-hydroxytryptophan (5-HT) were obtained from Sigma (St. Louis, MO). *N*-Acetyl-L-cysteine (NAc-Cys) was obtained from Aldrich (Milwaukee, WI). Sodium meta-bisulfate ($Na_2S_2O_5$) was obtained from Fisher Scientific Company Springfield, NJ. Other chemicals have been described in Chapter 2. All other chemicals were of highest commercially available grade and used without further purification.

5-*S*-Cysteinylnorepinephrine (5-5-*S*-Cys-NE) was synthesized according to the literature[97]. 5-*S*-*N*-acetylcysteinylnorepinephrine (5-*S*-NAc-Cys-NE) and 5-*S*-cysteinyl-glycinylnoripinephrine (5-*S*-Cys-Gly-NE) were synthesized as described in Appendix A.

3.2.2 Instrumentation

Instruments for controlled potential electrolysis, preparative HPLC system and HPLC-EC system have been described in Chapter 2. A pHBOY-P2 FET pH meter (Shindengen Electric Mfg. Co., Ltd, Japan) was employed to monitor the pH values when preparing drugs for animal experiments. A CMA/100 Microinjection Pump (CMA/Microdialysis AB, Stockholm, Sweden) was used for intracerebroventricular (icv) administration. Rat brain tissues were homogenized with a Polytron PT 1200 (Kinematica Ag, Switzerland) tissue homogenizer. Rat brain tissue homogenates were centrifuged before injection into the HPLC-EC system using a Beckman GS-15R Centrifuge (Beckman, Palo Alto, CA).

The preparative HPLC system and solvents (A and B) employed for HPLC methods IV, V, and VII were described in Chap. 2. HPLC method IV was used to isolate 5-*S*-NAc-Cys-NE. It employed solvents A and B and the following gradient profile: 0-2

min, 0% solvent B; 2-25 min, linear gradient to 45% solvent B; 25-25.5 min, linear gradient to 100% B; 25.5-45 min, 100% solvent B; 45-45.01 min, linear gradient to 0% solvent B; 45.01-55 min, 0% solvent B. The flow rate was constant at 7.0 mL/min.

HPLC method V was used to isolate 5-*S*-Cys-Gly-NE. It employed solvents A and B and the following gradient profile: 0-2 min, 0% solvent B; 2-25 min, linear gradient to 45% solvent B; 25-25.5 min, linear gradient to 100% B; 25.5-40 min, 100% solvent B; 40-40.01 min, linear gradient to 0% solvent B; 40.01-50 min, 0% solvent B. The flow rate was constant at 7.0 mL/min.

5-*S*-NAc-Cys-NE and 5-*S*-Cys-Gly-NE were further purified by a desalting process through HPLC method VII. HPLC method VI employed Solvent E (deionized water) and F (100% MeCN) and the following gradient profile: 0-5 min, 0% solvent F; 5-45 min, linear gradient to 40% solvent F; 45-45.01 min, linear gradient to 0% solvent F; 45.01-55 min, 0% solvent F. The flow rate was constant at 7.0 mL/min.

HPLC method VII was used to verify the hydrolysis process and collect the hydrolysis products for spectroscopic verification purposes. It employed the following gradient profile: 0-2 min, linear gradient to 1% solvent B; 2-25 min, linear gradient to 5% solvent B; 25-36 min, linear gradient to 100% B; 36-46 min, 100% solvent B; 46-47 min, linear gradient to 0% solvent B; 47-55 min, 0% solvent B. The flow rate was constant at 7.0 mL/min.

HPLC-EC system and the column for HPLC methods VIII and IX were the same as described in Chap. 2. In addition, ChromGraph® CONTROL 1.30 (Bioanalytical Systems, Inc., West Lafayette, IN) was used to control the system and collect the chromatograms. HPLC method VIII was used to monitor the *in vitro* hydrolysis process. The mobile phase consisted of 0.087% diethylamine (v/v), 0.050 mM EDTA, 0.48 mM SOS, and 0.025 M citric acid in 3.1% Methanol/deionized water. The pH value was

adjusted to 2.37 by concentrated HCl and NaOH. The flow rate was constant at 0.6 mL/min. HPLC method IX was used to monitor the *in vivo* hydrolysis process. The mobile phase was the same as used in HPLC method VIII. The flow rate was constant at 0.9 mL/min.

The concentrations of 5-*S*-Glu-NE, 5-*S*-Cys-NE, and 5-*S*-NAc-Cys-NE were calculated by the equation:

$$C_{sample}(\text{nmol/g}) = \frac{R_{sample}}{R_{standard}} \times 5 \times C_{standard} \qquad (3.1)$$

where R_{sample} is the ratio of the peak area of the analyte to that internal standard (N-MET or DHBA); $R_{standard}$ is the ratio of peak area of the standard compound to that of internal standard; $C_{standand}$ (μmol/L) is the concentration of the standard compound; C_{sample} is the concentration of the analyte in the homogenate. Constant 5 in equation 3.1 comes from the procedure in which the homogenate was prepared by adding 5.0 μL homogenization solution to each milligram (mg) of rat brain tissue.

The concentrations of 5-*S*-Glu-NE, 5-*S*-Cys-NE, 5-*S*-NAc-Cys-NE were calculated by equation 3.1. Each sample was assayed by HPLC-EC system twice and the mean was taken for final calculation.

3.2.3 Animals

Male Sprague-Dawley rats weighing 307 to 418 g were used. Some of the rats (Zivic-Miller Laboratories, Inc., Zelienople, PA) were purchased with cannulas pre-installed into their left lateral ventricles. The animals were housed 3 in each cage, while the pre-cannulated ones were housed individually. Rats were allowed to access to Purina rat

chow and water *ad libitum*, and maintained on a 12 h light/dark cycle with lights on at 7:00 am. Rats were not used in experiments until two weeks after receipt from the supplier. All animal procedures were approved by the Institutional Animal Use and Care Committee at the University of Oklahoma.

3.2.4 Preparation of rat brain homogenates

Rats were sacrificed by guillotine. Brains were removed and the whole brain was homogenized in PBS (pH = 7.4, μ = 0.2) (1 mg brain tissue in 5 μL PBS) using a Polytron PT 1200 tissue homogenizer (Kinematica Ag, Switzerland) for 30 s at the scale of 3 (maximum scale = 5). 5-*S*-Glu-NE was added into the homogenate and then incubated at 37 °C in a water bath. At different time period, 0.3 mL homogenate sample was taken from the incubation and was centrifuged at 14,000 rpm and 4 °C for 40 min. 80 μL supernatant was combined with 20 μL 5.0 μM N-MET. A 5 μL aliquot of the mixture solution (with 1.0 μM N-MET as internal standard) were injected into the HPLC-EC system using HPLC method VIII.

3.2.5 Drug intracerebroventricular (icv) administration

44 nmol (21 μg) of 5-*S*-Glu-NE was dissolved in 5.0 μL of artificial cerebrospinal fluid (CSF) consisting of 147 mM NaCl, 4 mM KCl, 1.2 mM $CaCl_2$, and 1.2 mM $MgSO_4$ in deionized water. The pH of the drug solution was adjusted to neutral (pH = 7.0 ± 0.5) by NaOH solution.

For pilot experiments, rats were anesthetized with a mixture of ketamine (50 mg/kg) and xylasine (4 mg/kg) administered intraperitoneally (ip) and were then placed in a stereotaxic apparatus with the incisor bar positioned 3.3 mm below the interaural line. A small hole was made with a hand-held drill on the leveled skull using the coordinates: AP – 0.8 mm and L + 1.4 mm relative to bregma. Drugs were injected by means of a 10 μL Hamilton microsyringe equipped with a 31 gauge needle, the tip of which was lowered 3.6 mm ventral to bregma. A 5.0 μL injection was made over a period of 2 min, the needle being maintained in place for an additional 1 minute before withdrawal. Timing was started upon the completion of the drug injection.

For the rest of the experiments, guide cannulas were pre-installed into the left lateral ventricles of rats. Drugs prepared as described above were infused into left lateral ventricles through the cannulas. A CMA/100 Microinjection Pump coupled with a 50 μL Hamilton microsyringe was used to deliver the drugs. 5.0 μL aliquots of drug solution were infused over a period of 2 min and timing was started at the end of this time. Meanwhile, the infusion tube remained in place for an additional 2 min before withdrawal.

5, 15, 30, 60, and 120 min after icv administration of 5-*S*-Glu-NE rats were sacrificed by guillotine decapitation. Brains were removed and dissected into striatum, midbrain, hippocampus, medulla/pons and cortex on an ice-chilled glass plate. Each brain part was immediately wrapped in aluminum foil and frozen in liquid nitrogen (– 78 °C). Brain tissues were then store at – 80 °C in a refrigerator until assayed.

Immediately prior to HPLC-EC analysis, brain tissues were weighed and homogenized in a homogenization solution (0.1 M $HClO_4$, 134 μM Na_2EDTA, 263 μM $Na_2S_2O_5$, and 1.0 μM DHBA). DHBA was added into the homogenization solution as an internal standard. 5.0 μL homogenization solution was added to 1 mg brain tissue. Brain tissues were homogenized with a Polytron PT-1200 tissue homogenizer with a speed scale

adjustable from 1 to 6. Tissues were first blended at the lowest speed (for about 10 s) and then at speed scale of 3 (5 for cortex tissue) for an additional 20 s. The resulting homogenates were centrifuged at 14,000 rpm for 60 min at 4 °C and kept at 0 °C on ice. A 5 μL aliquot of supernatant was injected directly into HPLC-EC system for analysis.

The concentrations of 5-*S*-Glu-NE, 5-*S*-Cys-NE, 5-*S*-NAc-Cys-NE were calculated by equation 3.1. Each sample was assayed by HPLC-EC system twice and the mean was taken for final calculation.

3.3 *In Vitro* Metabolism of 5-*S*-Glu-NE

3.3.1 Hydrolysis of 5-*S*-Glu-NE in rat brain homogenate

The *in vitro* hydrolysis of 5-*S*-Glu-NE was first studied by adding 30 nmol of 5-*S*-Glu-NE into 5 mL rat brain homogenate (sample A). A 5 mL rat brain homogenate was used as a control (sample B). Two samples were incubated at 37 °C in a water bath. An HPLC peak appeared at retention time t_R = 18.5 min, (Figure 3.1 1A) before the incubation started. After 1 h incubation, a new HPLC peak appeared at retention time t_R = 13.5 min. During the 6 h incubation, peak at t_R = 18.5 min decreased and disappeared at the end of the incubation, while peak at t_R = 13.5 min increased and reached maximum at the end of 6 h incubation (Figure 3.1 5A). Comparing the retention times of the two peaks with standard sample, the peak at t_R = 18.5 min corresponded to 5-*S*-Glu-NE and the peak at t_R = 13.5 min was corresponded to 5-*S*-Cys-NE. In contrast, there were no peaks observed at retention times of t_R = 13.5 and 18.5 min throughout the incubation period (Figure 3.1 1B to 5B). However, there was an HPLC peak at t_R = 13.3 min, close to 5-*S*-

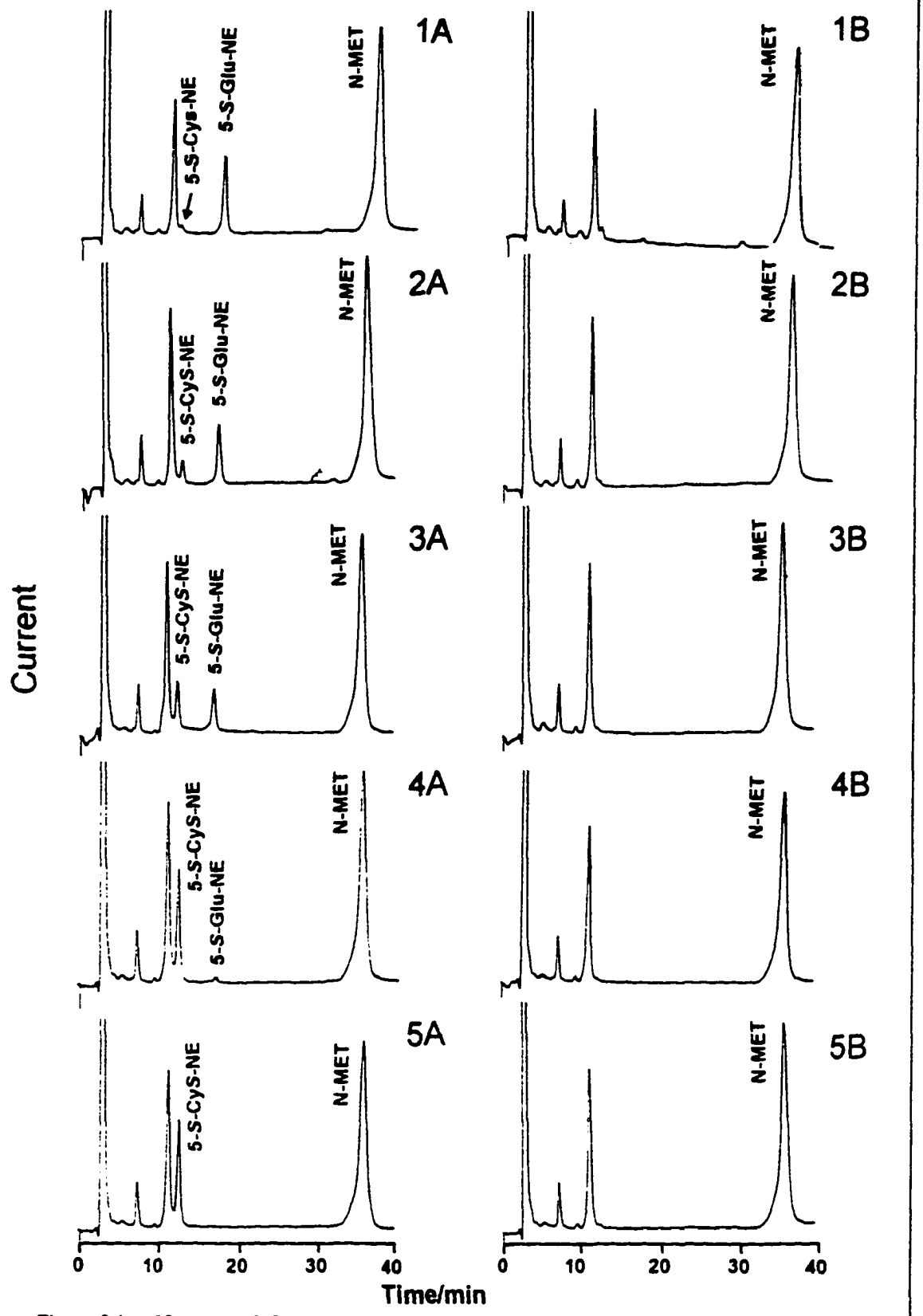

Figure 3.1 30 nmol 5-*S*-Glu-NE incubated in 5 mL rat brain homogenate at 37 °C for 1A) 0 h, 2A) 1 h, 3A) 2 h, 4A) 3 h, and 5A) 6 h. 5 mL rat brain homogenate at 37 °C for 1B) 0 h, 2B) 1 h, 3B) 2 h, 4B) 3 h, and 5B) 6 h. HPLC method VII. Injection volume = 5 µL.

Cys-NE peak, at the beginning of the incubation in both sample A and B. It disappeared during the incubation period and its identity remained unknown. Other peaks were presumably electroactive neurotransmitters and their metabolites. The current conditions were only optimized to separate the NE conjugates from other components in the rat brain homogenates.

The above incubation was repeated with 50 nmol 5-*S*-Glu-NE in 5 mL rat brain homogenate. The results are summarized in Figure 3.2. It took a longer time to convert all the 5-*S*-Glu-NE into the 5-*S*-Cys-NE in the second incubation as expected.

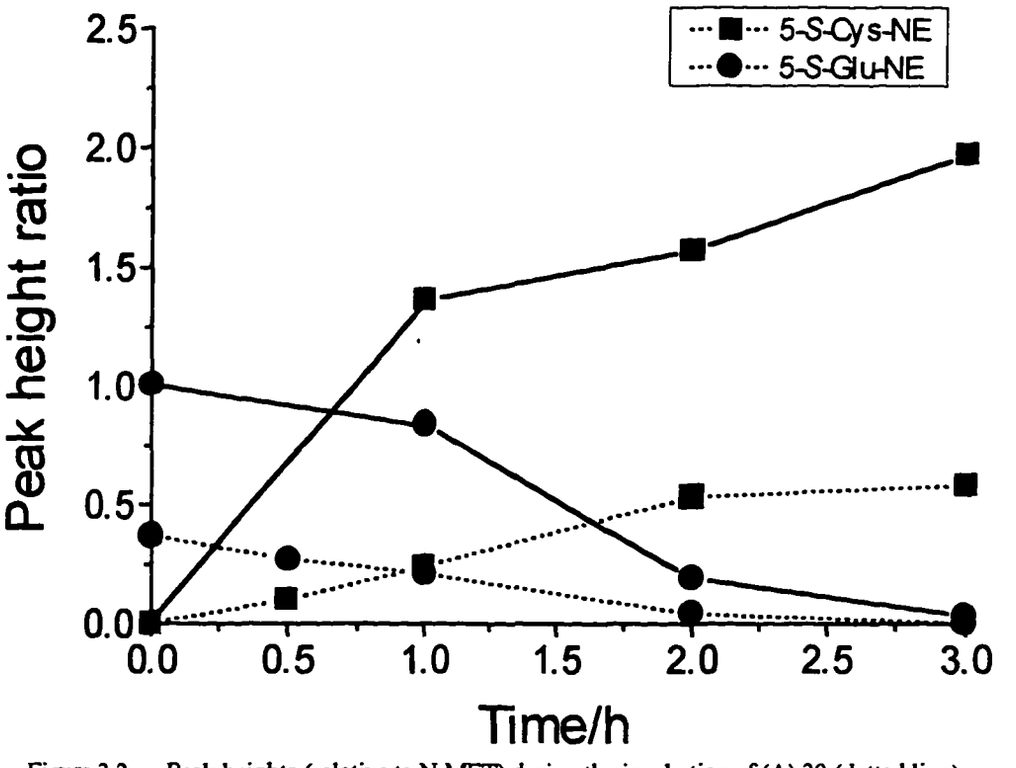

Figure 3.2 Peak heights (relative to N-MET) during the incubation of (A) 30 (dotted line) and (B) 50 (solid line) nmol 5-*S*-Glu-NE in 5 mL rat brain homogenate in PBS (pH = 7.4, μ = 0.1) at 37 °C.

3.3.2 Structural confirmation of 5-*S*-Cys-NE

To further confirm the formation of 5-*S*-Cys-NE from the *in vitro* hydrolysis of 5-*S*-Glu-NE, 2.7 mg 5-*S*-Glu-NE was added to 20 mL rat brain homogenate (ca. 3.3 g brain whole brain tissue, pH = 7.4) and incubated at 37 °C. The hydrolysis was completed in 8 h. After centrifugation, the supernatant obtained from the homogenate was injected directly into a preparative HPLC system using HPLC method VII. The HPLC peak at retention time t_R = 13.3 min (Figure 3.3) was confirmed to be 5-*S*-Cys-NE by comparing its retention time and UV-Vis spectrum (Figure 3.4) with those of the authentic sample. Other HPLC peaks under the same condition were not identified. They might be proteins in the homogenates, since a UV detector was used in the HPLC system. The eluent

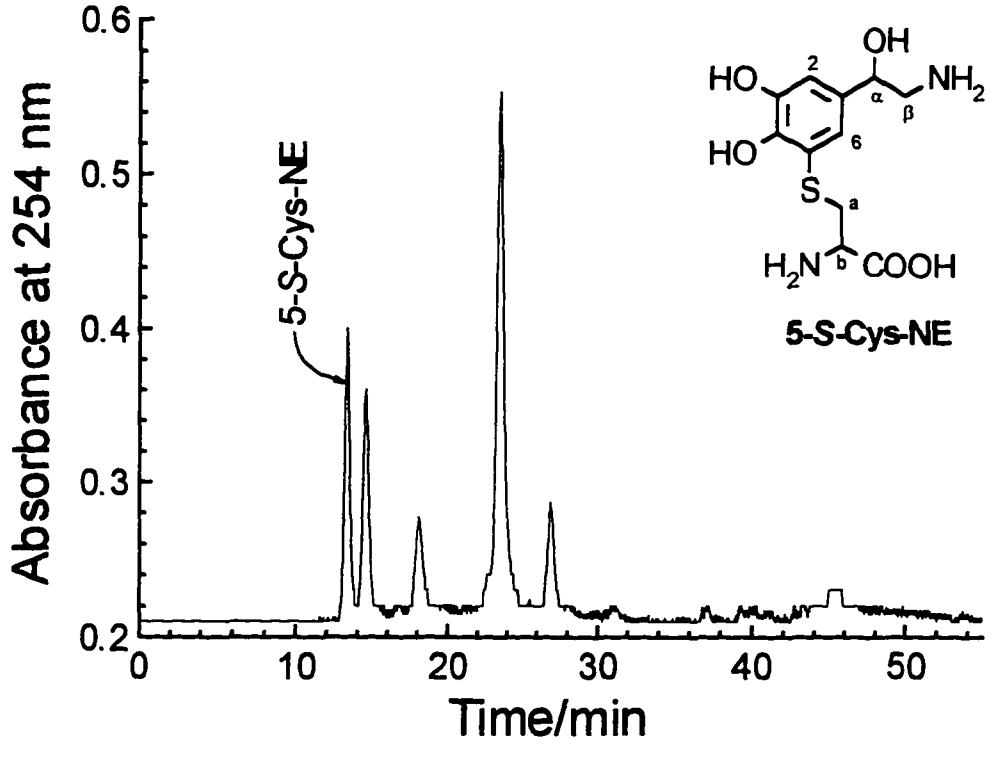

Figure 3.3 Preparative HPLC chromatogram of 20 mL rat brain homogenate incubated with 2.7 mg 5-*S*-Glu-NE in PBS (pH = 7.4, μ = 0.1) at 37 °C for 8 h. HPLC method VII. Injection volume 1.0 mL. AUFS = 1.0.

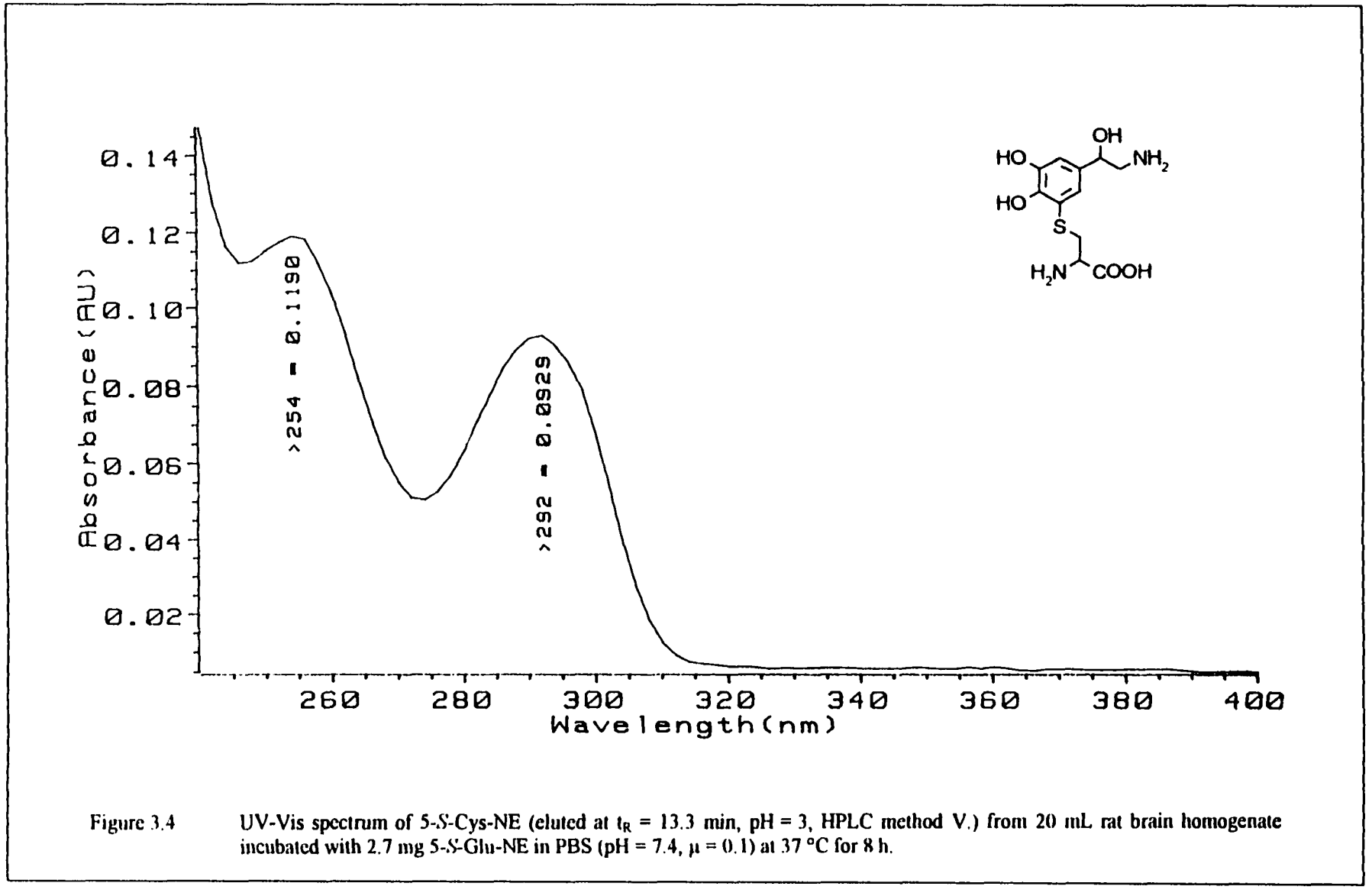

Figure 3.4 UV-Vis spectrum of 5-*S*-Cys-NE (eluted at t_R = 13.3 min, pH = 3, HPLC method V.) from 20 mL rat brain homogenate incubated with 2.7 mg 5-*S*-Glu-NE in PBS (pH = 7.4, μ = 0.1) at 37 °C for 8 h.

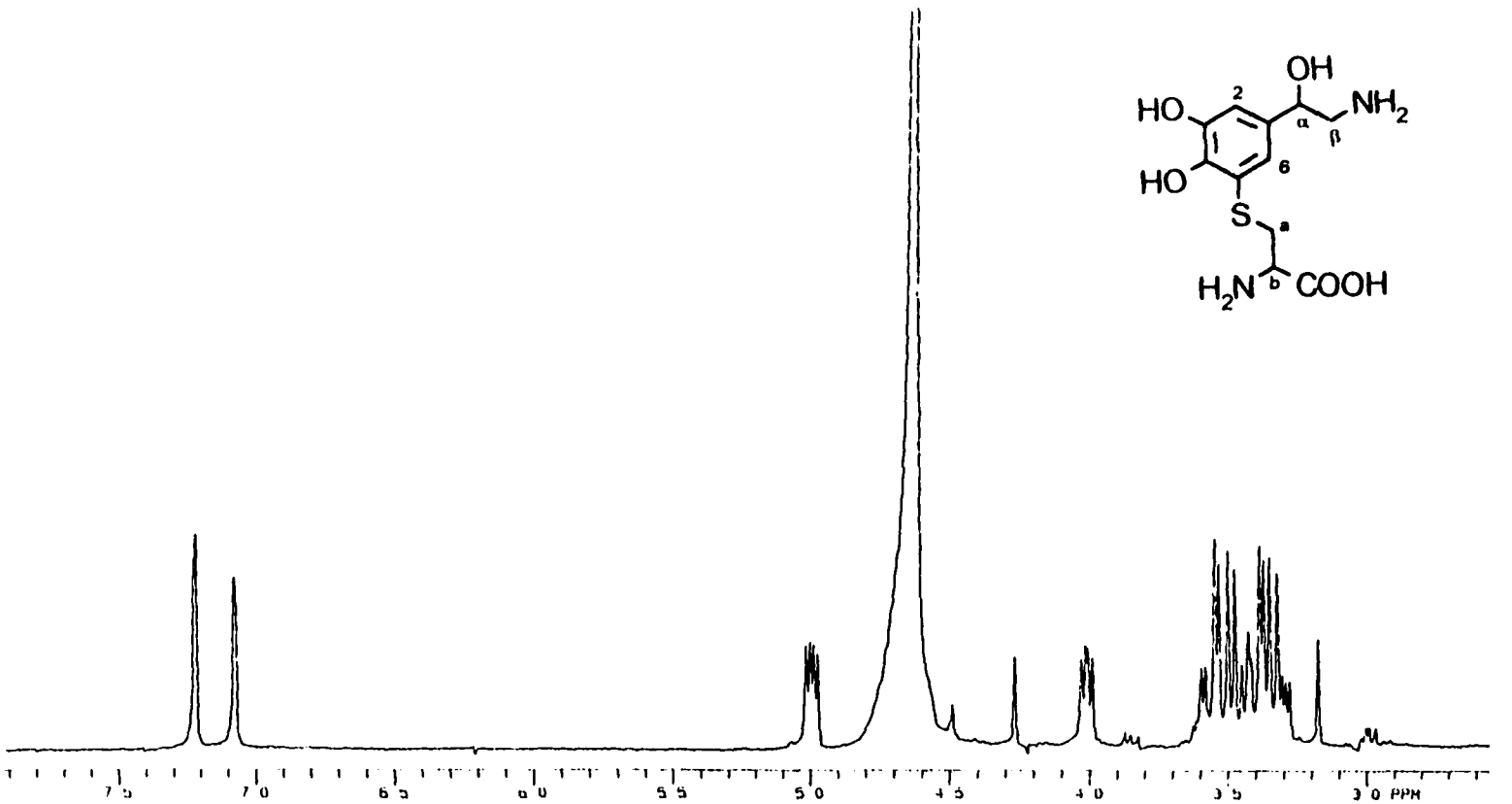

Figure 3.5 ^{1}H NMR spectrum (in D_2O) of 5-*S*-Cys-NE isolated from rat brain homogenate incubated with 5-*S*-Glu-NE in PBS (pH = 7.4, μ = 0.1) at 37 °C.

collected under the HPLC peak at t_R = 13.3 min was frozen on dry ice. The sample was later freeze-dried. ^{1}H NMR spectrum was obtained from the white solid isolated from the homogenate without further purification. ^{1}H NMR (D_2O) gave δ 7.23 (s, 1H, C(2)-H), 7.09 (s, 1H, C(6)-H), 5.01 (dd, J = 8.0, 4.0 Hz, 1H, C(α)-H), 4.02 (dd, J = 7.3, 4.9 Hz, 1H, C(b)-H), 3.60 – 3.28 (m, 4H, C(β)-H_2, C(a)-H_2) (Figure 3.5).

It is concluded that 5-*S*-Glu-NE was hydrolyzed into 5-*S*-Cys-NE in rat brain homogenate at physiological pH. However, the search for other possible metabolites, for example, 5-*S*-Cys-Gly-NE and 5-*S*-NAc-NE was unsuccessful.

3.4 *In vivo* metabolism of 5-*S*-Glu-NE

3.4.1 Icv administration of 5-*S*-Glu-NE in rat brain

5 rats were used in each group at different periods of time. 44 nmol (21 μg) of 5-*S*-Glu-NE dissolved in 5 μL artificial CSF was administered into the left lateral ventricle of the rats through pre-installed cannulas. The rats were sacrificed 5, 15, 30, 60 and 120 min after icv administration. 5 rats were used in each experimental group, while 4 rats were used as the control group. The rats of control groups were sacrificed 30 and 120 min after the infusion of the artificial CSF. HPLC method IX was employed for the sample assay. In addition, one-way analysis of variance (ANOVA) was used to calculate the statistical significance (P value) at 95% confidence limit.

Typical HPLC-EC chromatograms from the striatum, midbrain, hippocampus, cortex and medulla/pons 15 min after icv administration of 44 nmol 5-*S*-Glu-NE are shown in Figure 3.6. After icv administration of 5-*S*-Glu-NE, 5-*S*-Cys-NE and 5-*S*-NAc-

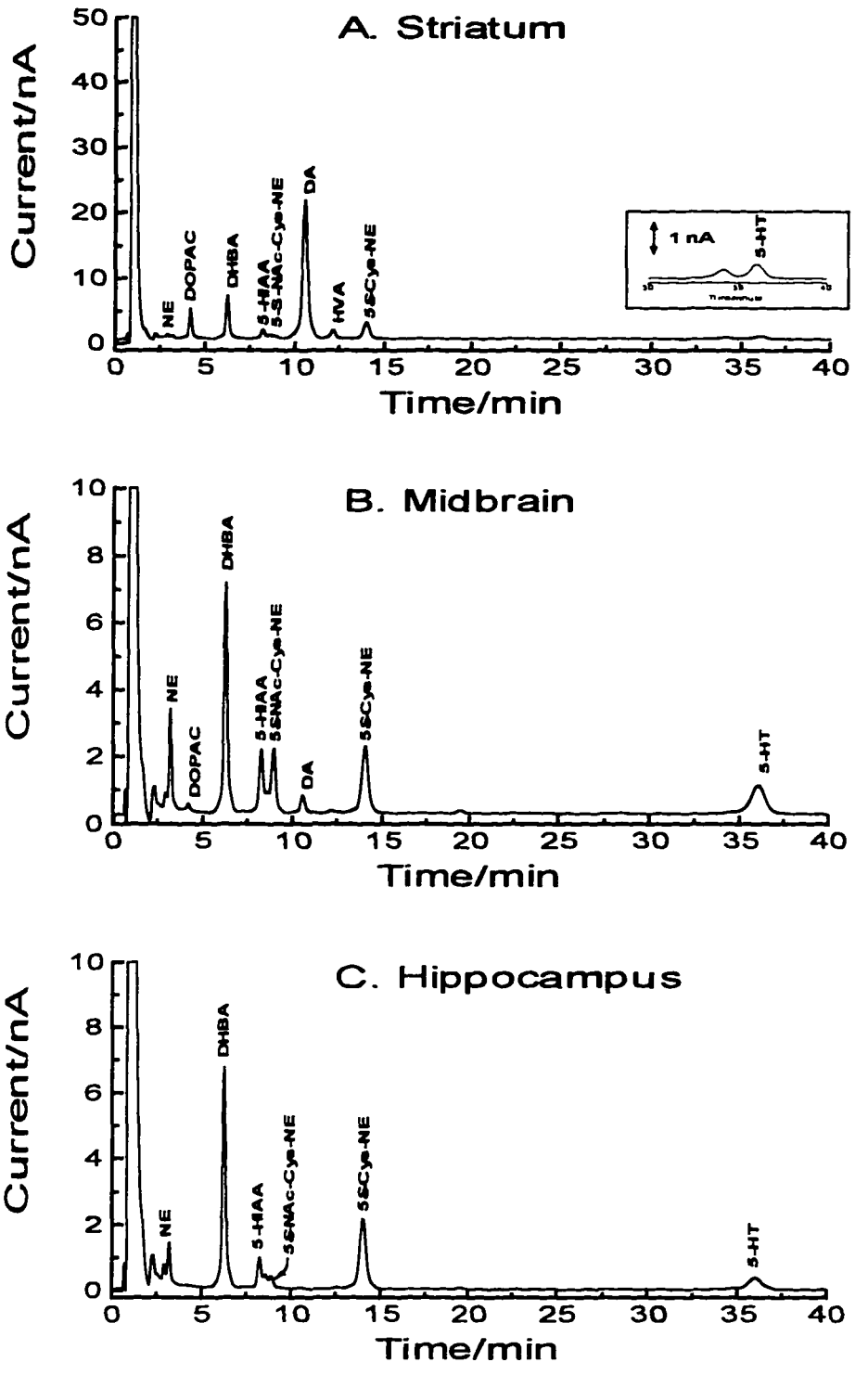

Figure 3.6 15 min after icv administration of 44 nmol 5-*S*-Glu-NE to rat. (A) striatum, (B) midbrain, (C) hippocampus, (D cortex, (E) medulla/pons, and (F) standards. HPLC method IX. Injection volume = 5 µL. (Continued on next page).

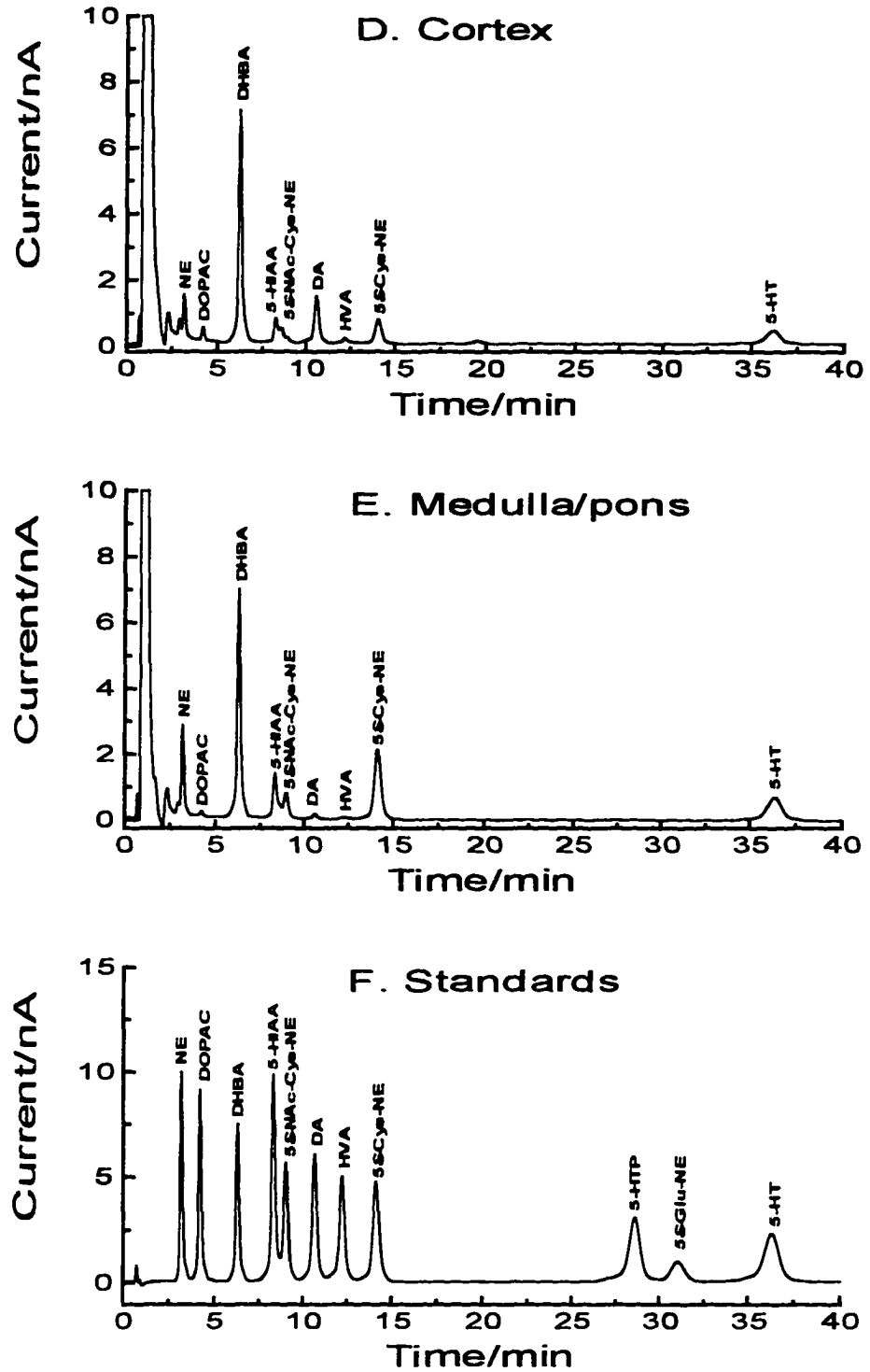

Figure 3.6 (Continued from previous page)
15 min after icv administration of 44 nmol 5-*S*-Glu-NE to rat. (A) striatum, (B) midbrain, (C) hippocampus, (D) cortex, (E) medulla/pons, and (F) standard. HPLC method IX. Injection volume = 5 μL.

Cys-NE were detected as metabolites of 5-*S*-Glu-NE. The retention times of each HPLC peak are summarized in Table 3.1.

Table 3.1 Summary of Retention Time of Rat Brain Tissue after Icv Administration of 5-*S*-Glu-NE

Component	Retention time (min)
5-*S*-NAc-Cys-NE	9.0
5-*S*-Cys-NE	14.0
5-*S*-Glu-NE	33.8
DHBA	6.2
NE	3.0
DOPAC	4.2
5-HIAA	8.2
DA	10.6
HVA	12.2
5-HT	36.5

3.4.2 *In vivo* metabolism of 5-*S*-Glu-NE in rat brain.

The quantitative results of metabolism of 5-*S*-Glu-NE in striatum, midbrain, hippocampus, cortex and medulla/pons of the rat brain are summarized in Figures 3.7 — 3.11, respectively. Data are represented as mean ± standard error (SE).

In all brain regions except the cortex, 5-*S*-Glu-NE was cleared within 15 min, However, it took about 1 h to clear the 5-*S*-Glu-NE in the cortex. The concentrations 5-*S*-Glu-NE were found highest at 5 min after icv administration in the brain regions in the order of medulla/pons (1.52 nmol/g), midbrain (1.31 nmol/g), striatum (1.14 nmol/g), hippocampus (1.02 nmol/g) and cortex (0.80 nmol/g).

5-*S*-Cys-NE was formed as a metabolite as expected. The maximum concentrations of 5-*S*-Cys-NE in striatum and midbrain were 7.54 nmol/g and 5.78 nmol/g, respectively, which were reached 15 min after icv administration of 5-*S*-Glu-NE and declined by 60% and 85% (compared to the maximum level) 120 min after icv

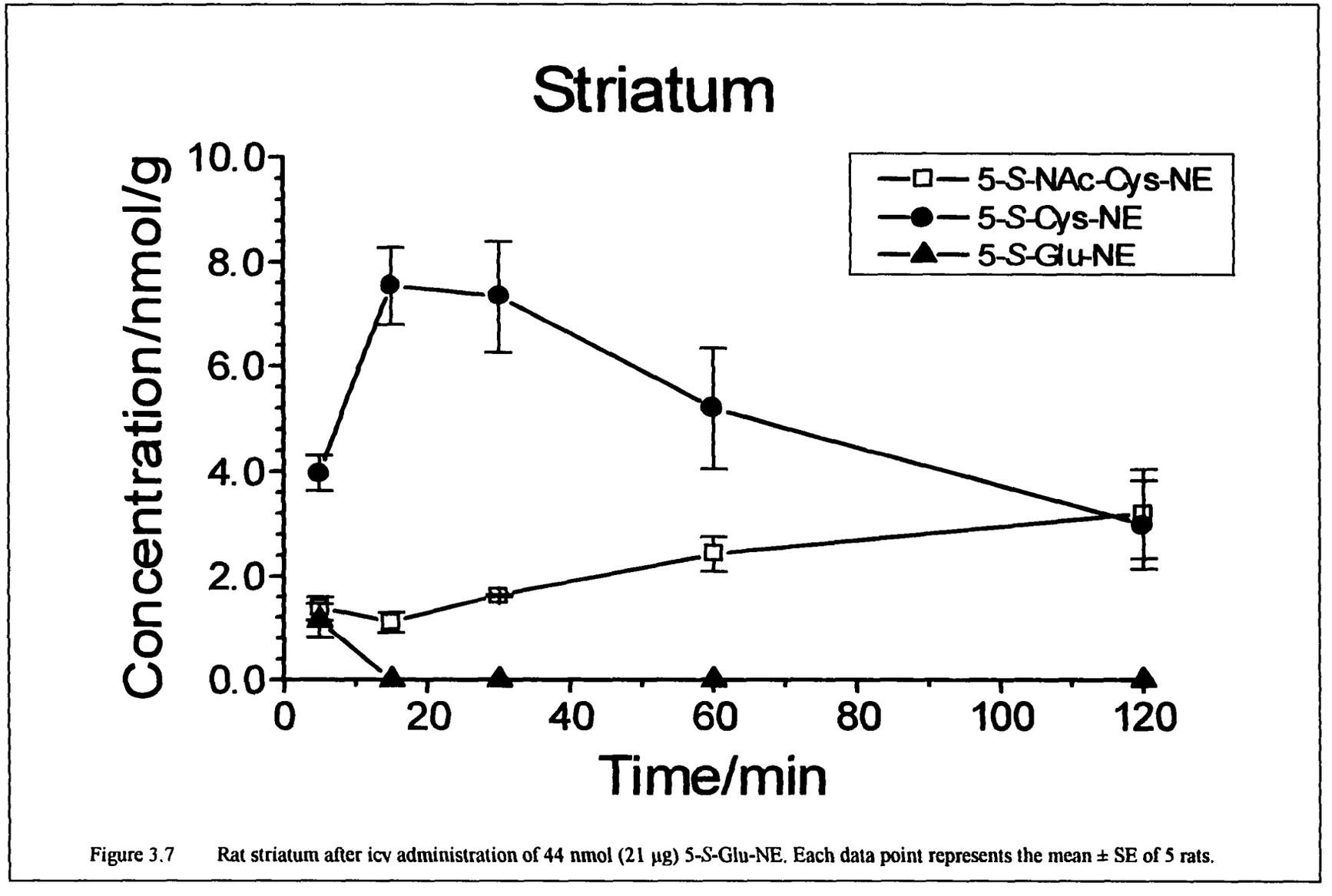

Figure 3.7 Rat striatum after icv administration of 44 nmol (21 μg) 5-*S*-Glu-NE. Each data point represents the mean ± SE of 5 rats.

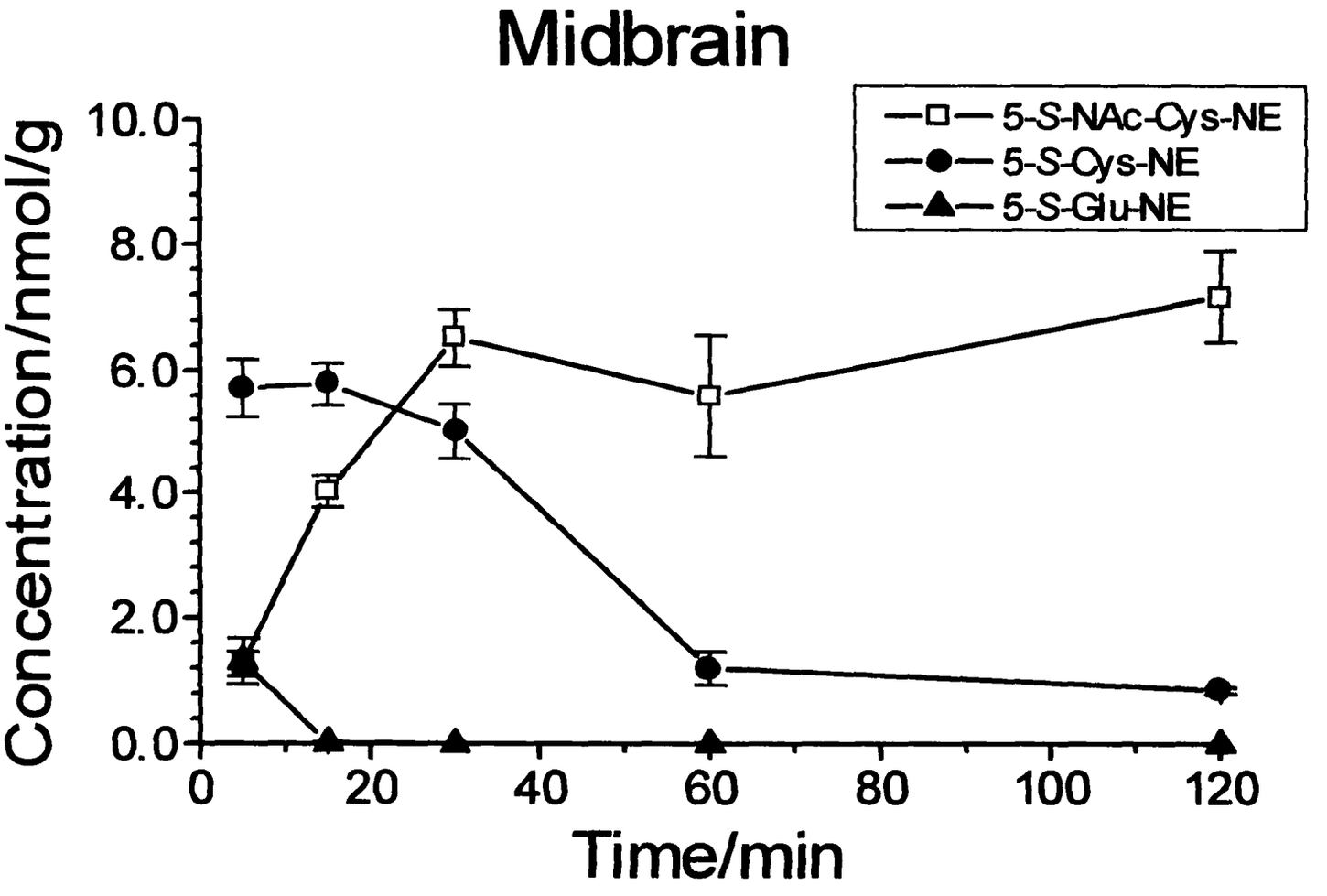

Figure 3.8 Rat midbrain after icv administration of 44 nmol (21 μg) 5-*S*-Glu-NE. Each data point represents the mean ± SE of 5 rats.

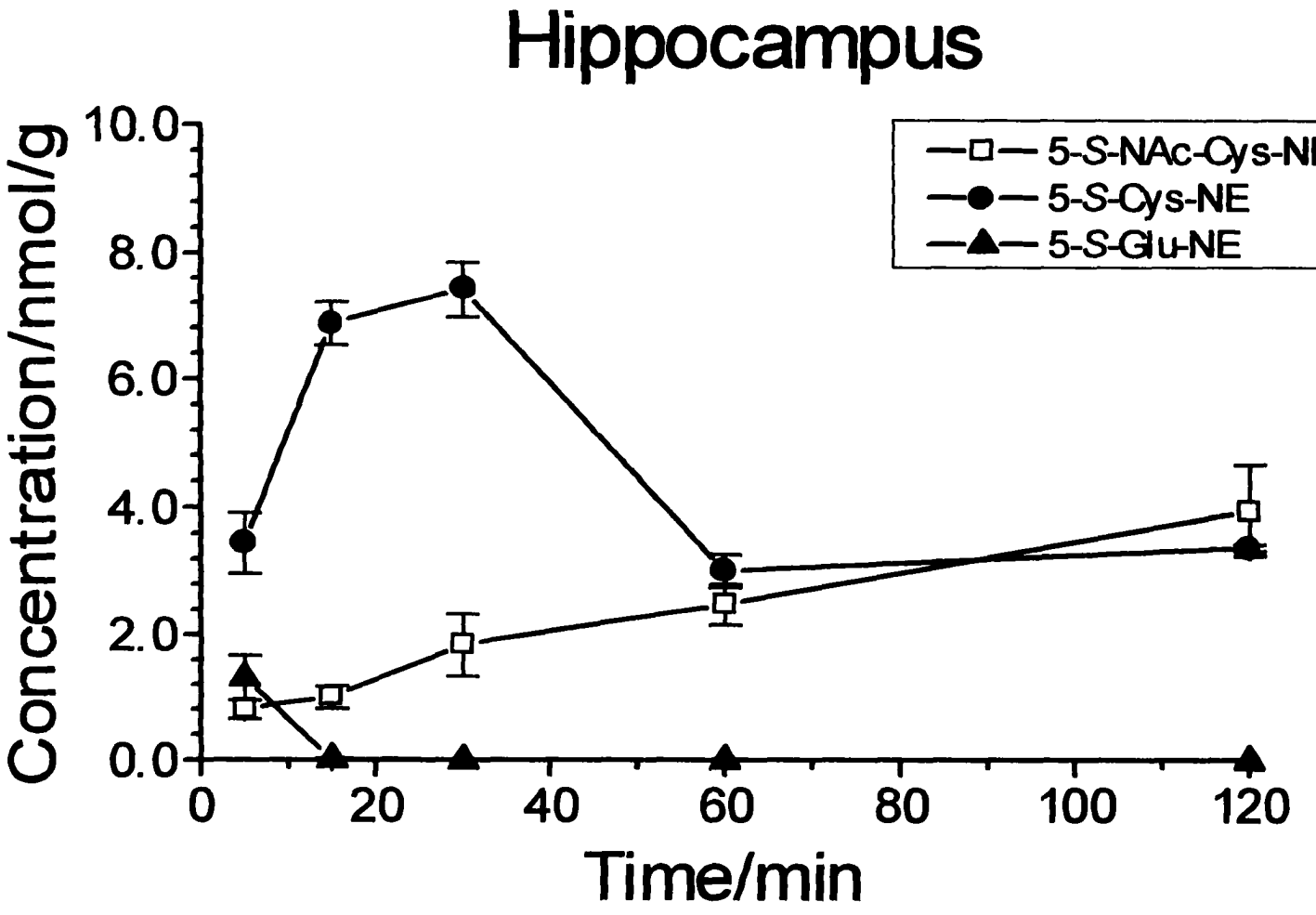

Figure 3.9 Rat hippocampus after icv administration of 44 nmol (21 μg) 5-*S*-Glu-NE. Each data point represents the mean ± SE of 5 rats.

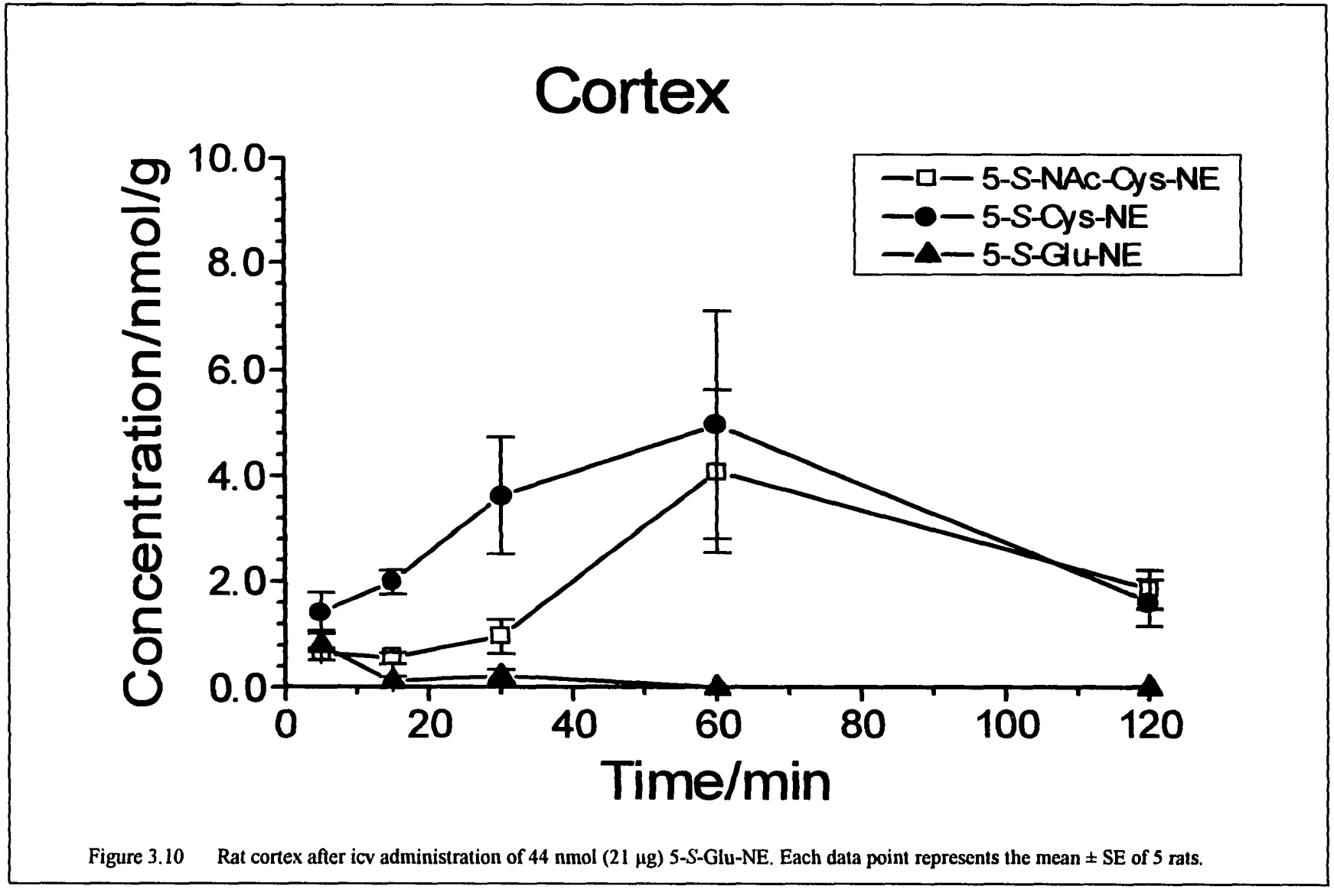

Figure 3.10 Rat cortex after icv administration of 44 nmol (21 μg) 5-*S*-Glu-NE. Each data point represents the mean ± SE of 5 rats.

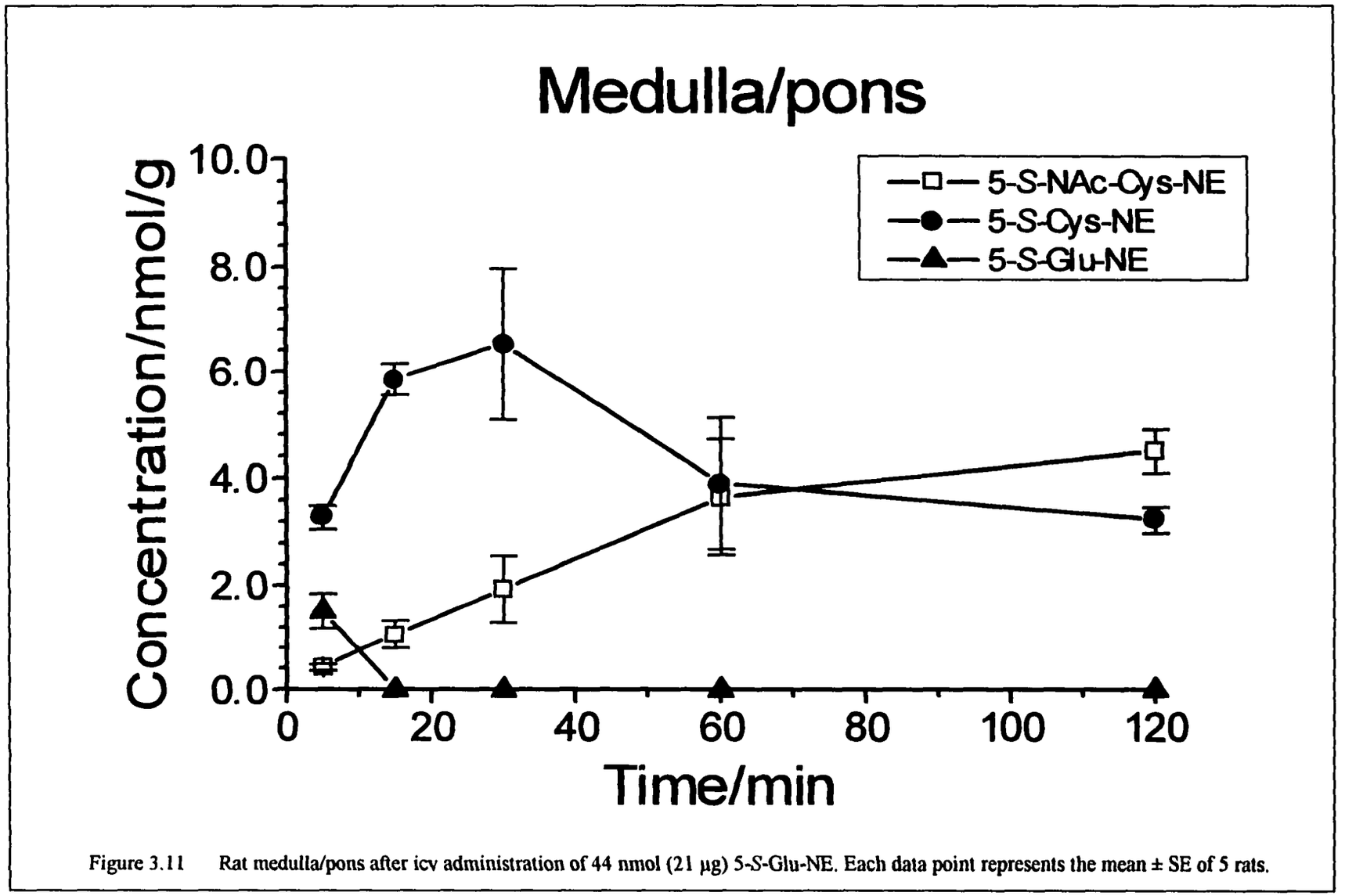

Figure 3.11 Rat medulla/pons after icv administration of 44 nmol (21 μg) 5-*S*-Glu-NE. Each data point represents the mean ± SE of 5 rats.

administration of 5-*S*-Glu-NE. In the hippocampus and medulla/pons the maximum concentrations of 5-*S*-Cys-NE, 7.41 nmol/g and 6.53 nmol/g, were reached 30 min after icv administration of 5-*S*-Glu-NE. The concentrations of 5-*S*-Cys-NE declined from the maximum levels by 54% and 50%, respectively, 120 min after icv administration of 5-*S*-Glu-NE. The maximum concentration of 5-*S*-Cys-NE in the cortex, 4.95 nmol/g, was reached at 60 min, the slowest among all areas of the brain in terms of the time required to reach the maximum concentration. In the next 1 h, 5-*S*-Cys-NE decline 68% in the cortex.

The last hydrolysis intermediate detected in the current experimental condition was 5-*S*-NAc-Cys-NE. It was formed in all brain regions at the shortest icv administration time (i.e., 5 min). The concentrations in these areas were, from the highest concentration to the lowest, 1.37 nmol/g (striatum), 1.28 nmol/g (midbrain), 0.81 nmol/g (hippocampus), 0.64 nmol/g (cortex) and 0.43 nmol/g (medulla/pons). In cortex, the concentration of 5-*S*-NAc-Cys-NE reached its maximum at 4.08 nmol/g and then reduced by 55% 1 h later. Contrarily, the concentration of 5-*S*-NAc-Cys-NE continued to grow, except the concentration momentarily went down at 15 min in striatum and 60 min in midbrain. The final concentrations of 5-*S*-NAc-Cys-NE were increased (compared to the initial value at 5 min) by 1.64 times in striatum, 5.65 times in midbrain, 4.89 times in hippocampus and 10.5 times in medulla/pons. Even in the cortex, the final concentration of 5-*S*-NAc-Cys-NE was still 2.89 times the initial level.

3.4.3 Effect of icv administration of 5-*S*-Glu-NE on neurotransmitter levels

A. Dopaminergic system

DOPAC and HVA are the metabolites of DA. The concentrations of DA,

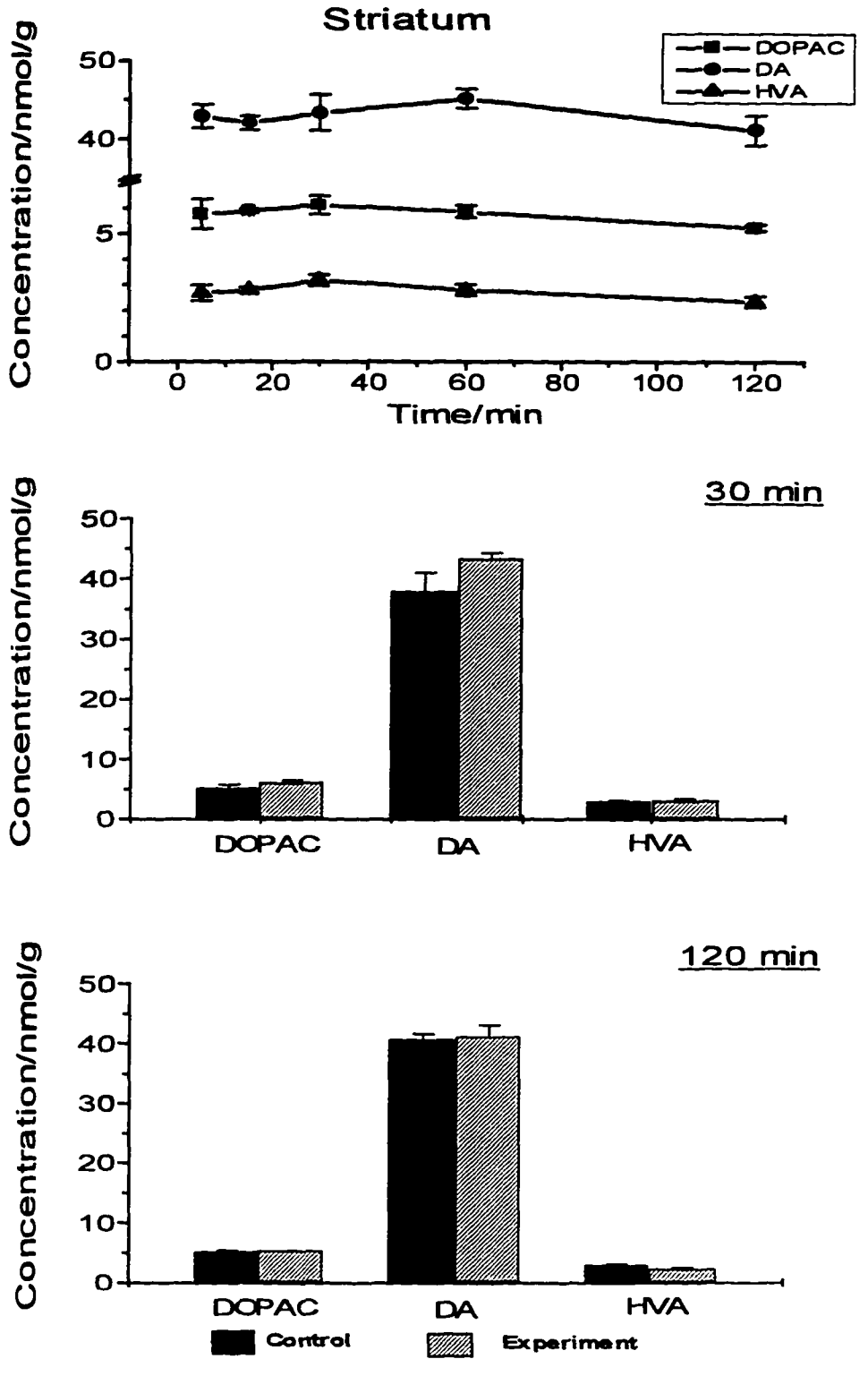

Figure 3.12 Effect of icv administration of 44 nmol (21 μg) 5-*S*-Glu-NE on the concentrations of DA, DOPAC and HVA in rat striatum (top). Comparison with controls at 30 min (middle) and 120 min (bottom). Each data point represents the mean ± SE of 4-5 rats.

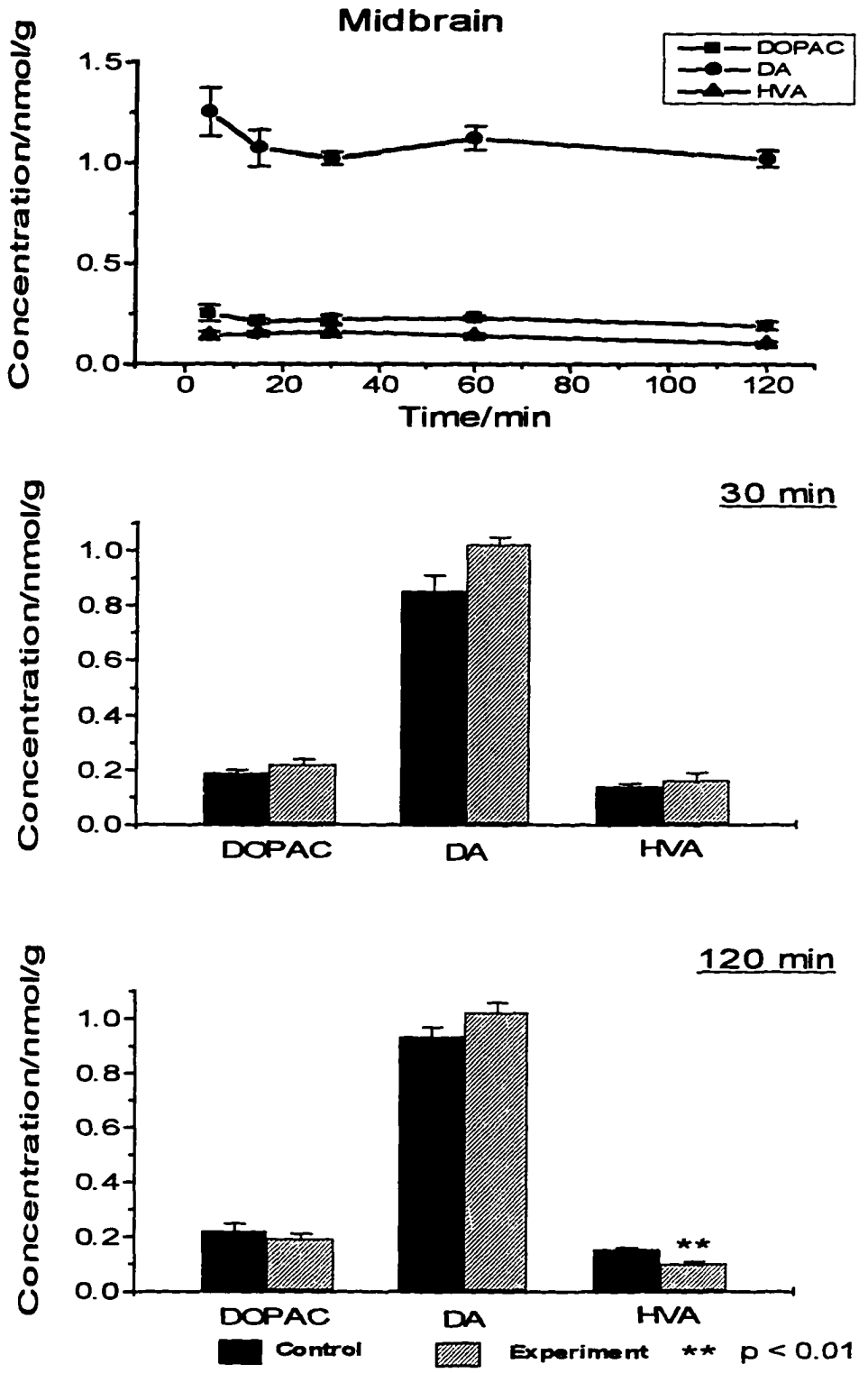

Figure 3.13 Effect of icv administration of 44 nmol (21 μg) 5-*S*-Glu-NE on the concentrations of DA, DOPAC and HVA in rat midbrain (top). Comparison with controls at 30 min (middle) and 120 min (bottom). Each data point represents the mean ± SE of 4-5 rats.

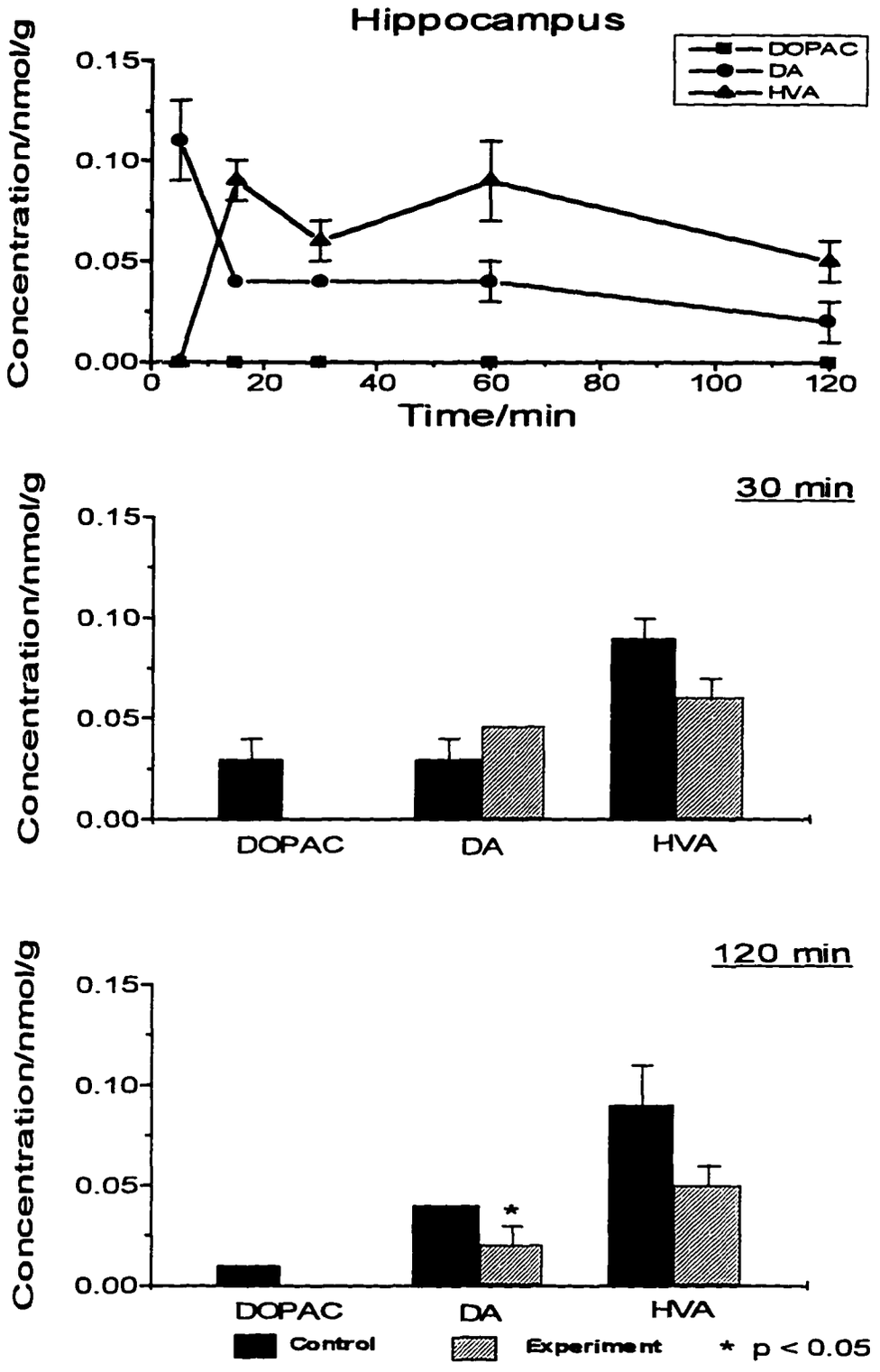

Figure 3.14 Effect of icv administration of 44 nmol (21 μg) 5-*S*-Glu-NE on the concentrations of DA, DOPAC and HVA in rat hippocampus (top). Comparison with controls at 30 min (middle) and 120 min (bottom). Each data point represents the mean ± SE of 4-5 rats.

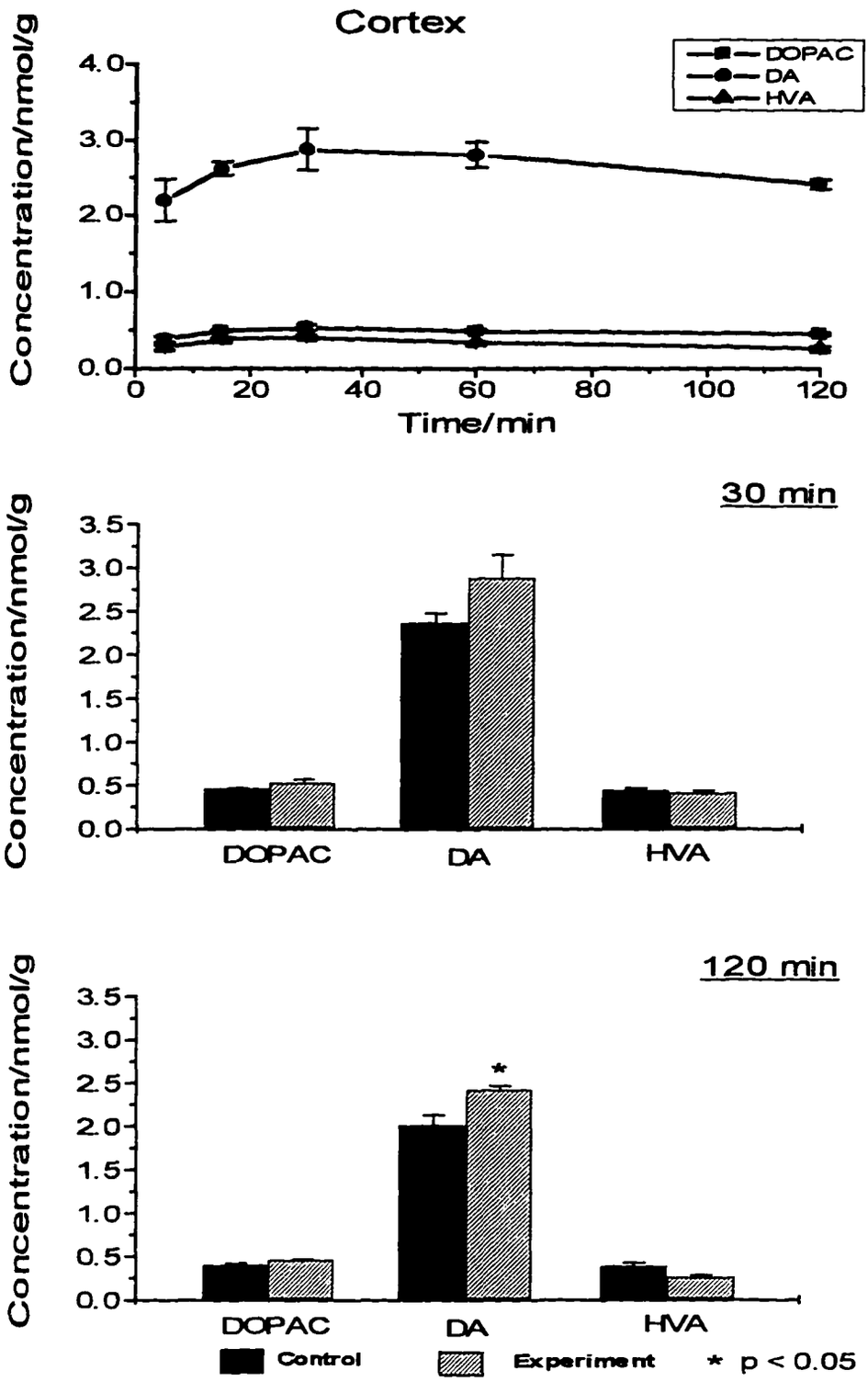

Figure 3.15 Effect of icv administration of 44 nmol (21 µg) 5-*S*-Glu-NE on the concentrations of DA, DOPAC and HVA in rat cortex (top). Comparison with controls at 30 min (middle) and 120 min (bottom). Each data point represents the mean ± SE of 4-5 rats.

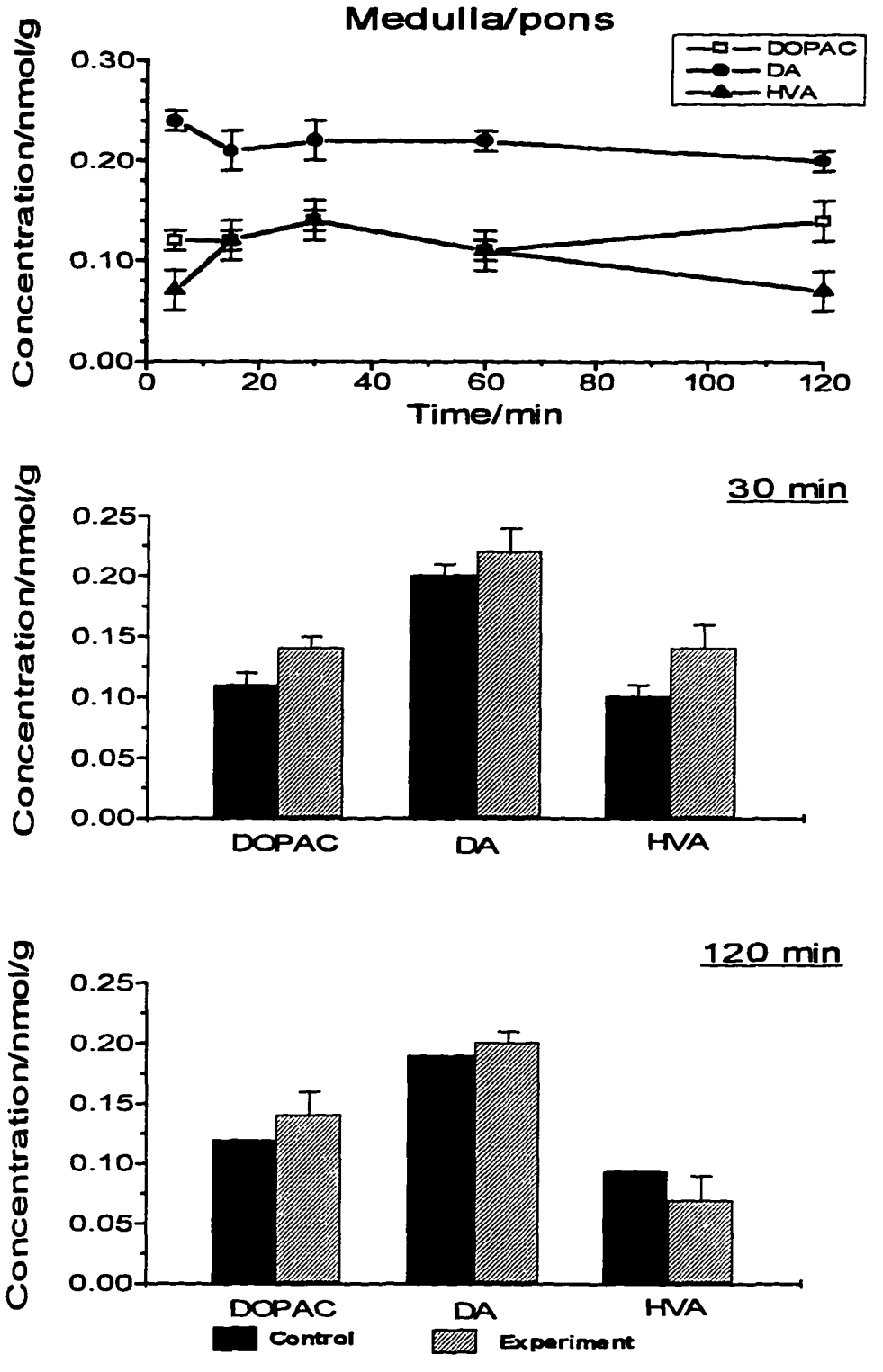

Figure 3.16 Effect of icv administration of 44 nmol (21 μg) 5-*S*-Glu-NE on the concentrations of DA, DOPAC and HVA in rat medulla/pons (top). Comparison with controls at 30 min (middle) and 120 min (bottom). Each data point represents the mean ± SE of 4-5 rats.

DOPAC and HVA in all five brain regions following icv administration of 5-*S*-Glu-NE are shown in Figures 3.12 – Figure 3.16.

In the striatum and medulla/pons, there were no significant changes in the concentrations of DA, DOPAC and HVA and (Figure 3.12 and 3.16).

In the midbrain the concentration of HVA was decreased by 33% ($p < 0.01$) compared with controls 120 min after icv administration of 5-*S*-Glu-NE, with no significant changes on the concentrations of DA and DOPAC (Figure 3.13).

In the hippocampus the concentration of DA was decreased by 50% ($p < 0.05$) after 120 min icv administration. No significant changes for DOPAC and HVA were observed in this brain region (Figure 3.14).

Last, in the cortex, the concentration of DA was increased by 20% ($p < 0.05$) after 120 min icv administration. No significant changes were observed on DOPAC and HVA (Figure 3.15).

B. Serotonergic system

5-HT is also called serotonin. In neurons, L-tryptophan is oxidized through tryptophan hydroxylase to L-5-hydroxytryptophan, which metabolizes to 5-HT through 5-hytroxytryptophan decarboxylase. 5-HT is oxidized by MAO to form 5-hydroxyindoleacetaldehyde, which converts to 5-hydroxyindoleacetic acid (5-HIAA) by aldehyde dehydrogenase.

The concentration changes of 5-HT and 5-HIAA during icv administration of 44 nmol 5-*S*-Glu-NE are shown in Figures 3.17 - Figure 3.21. In all brain regions, the concentrations of both 5-HT and 5-HIAA were increased 30 min after icv administration of 5-*S*-Glu-NE, except that 5-HT was decreased in the hippocampus in the same time period (Table 3.2).

Table 3.2 Concentration Changes (%) in Rat Brain during the First 30 min after Icv Administration of 44 nmol 5-*S*-Glu-NE.

Area	5-HT	5-HIAA
Striatum	44	65
Midbrain	4	37
Hippocampus	-10	127
Cortex	30	59
Medulla/pons	13	54

The levels of 5-HT and 5-HIAA were significantly increased in all brain regions compared to those of the controls 30 min and 120 min after icv administration 5-*S*-Glu-NE.

In the striatum the concentration of 5-HIAA increased by 40% ($p < 0.05$) 30 min after icv administration 5-*S*-Glu-NE, while the concentration of 5-HT increased by 51% ($p < 0.005$) 30 min after icv administration of 5-*S*-Glu-NE and 48% ($p < 0.05$) at 120 min after icv administration 5-*S*-Glu-NE (Figure 3.17).

In the midbrain, the level of 5-HIAA increased 38% ($p < 0.05$) and 33% ($p < 0.05$), separately, 30 min and 120 min after icv administration of 5-*S*-Glu-NE. 5-HT increased 38% ($p < 0.01$) 30 min after icv administration of 5-*S*-Glu-NE (Figure 3.18).

In the hippocampus, levels of 5-HIAA and 5-HT increased 35% and 30%, respectively, 30 min after icv administration 5-*S*-Glu-NE, while no significant change was seen after 120 min (Figure 3.19).

In the cortex, the level of 5-HIAA increased 29% ($p < 0.01$) after 30 min and 33% ($p < 0.05$) after 120 min. The level of 5-HT increased 65% ($p < 0.05$) at 30 min while the change at 120 min without significant difference (Figure 3.20).

Finally, in the medulla/pons, the level of 5-HIAA increased 50% ($p < 0.05$) at 30 min and 35% ($p < 0.01$) at 120 min. The level of 5-HT increased 38% ($p < 0.005$) at 30 min and 32% ($p < 0.05$) at 120 min (Figure 3.21).

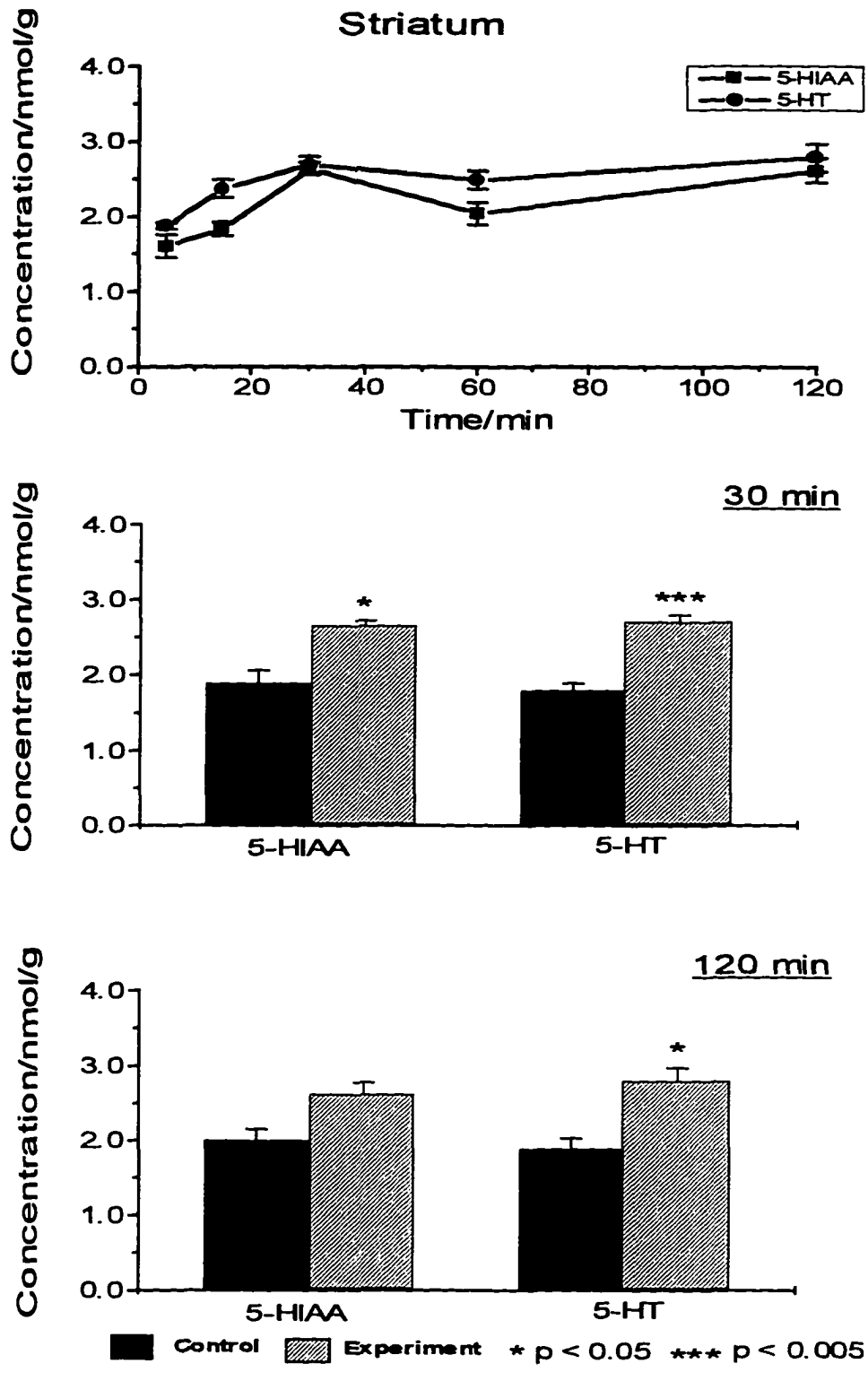

Figure 3.17 Effect of icv administration of 44 nmol (21 µg) 5-*S*-Glu-NE on the concentrations of 5-HIAA and 5-HT in rat striatum (top). Comparison with controls at 30 min (middle) and 120 min (bottom). Each data point represents the mean ± SE of 4-5 rats.

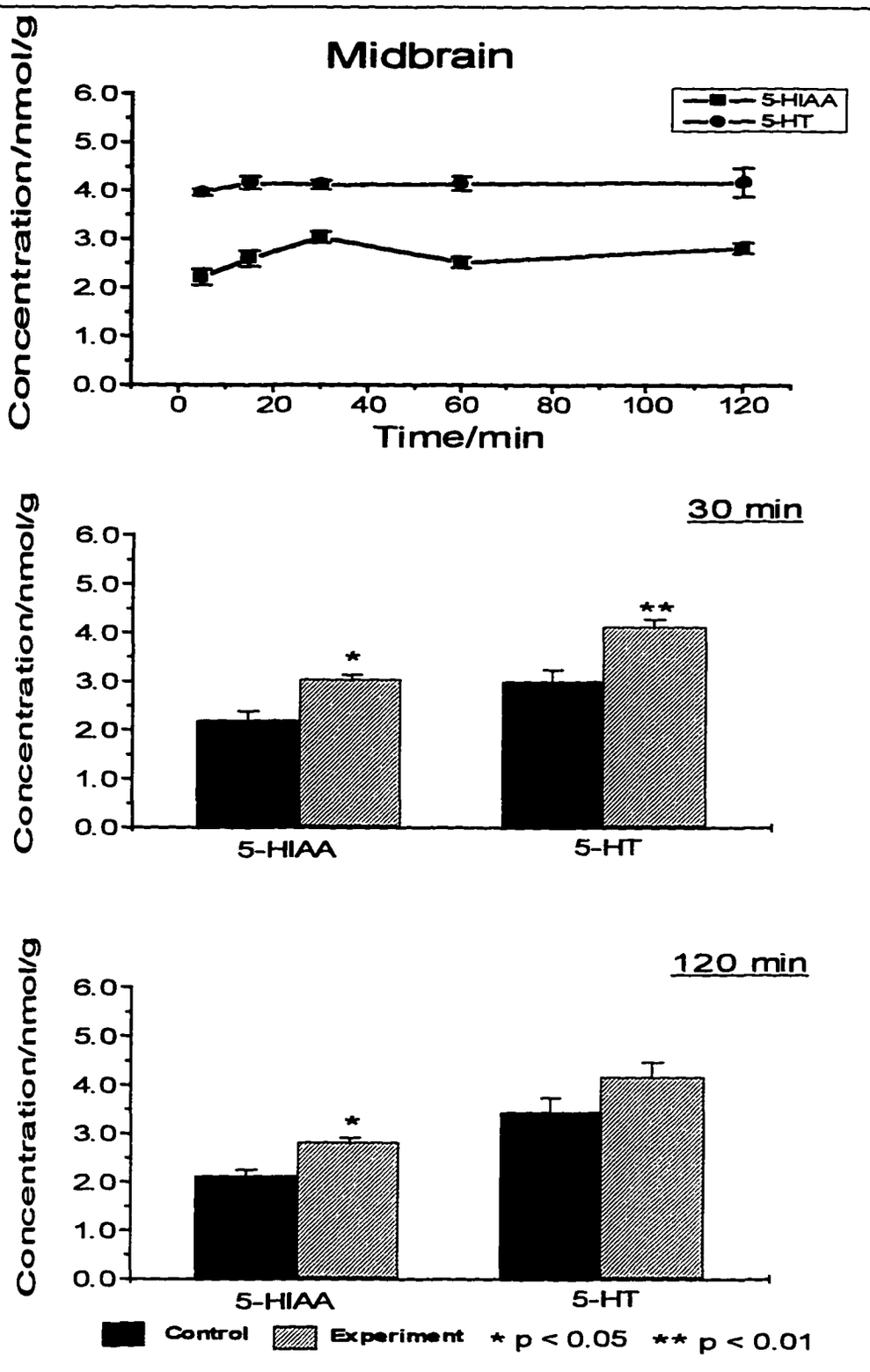

Figure 3.18 Effect of icv administration of 44 nmol (21 μg) 5-*S*-Glu-NE on the concentrations of 5-HIAA and 5-HT in rat midbrain (top). Comparison with controls at 30 min (middle) and 120 min (bottom). Each data point represents the mean ± SE of 4-5 rats.

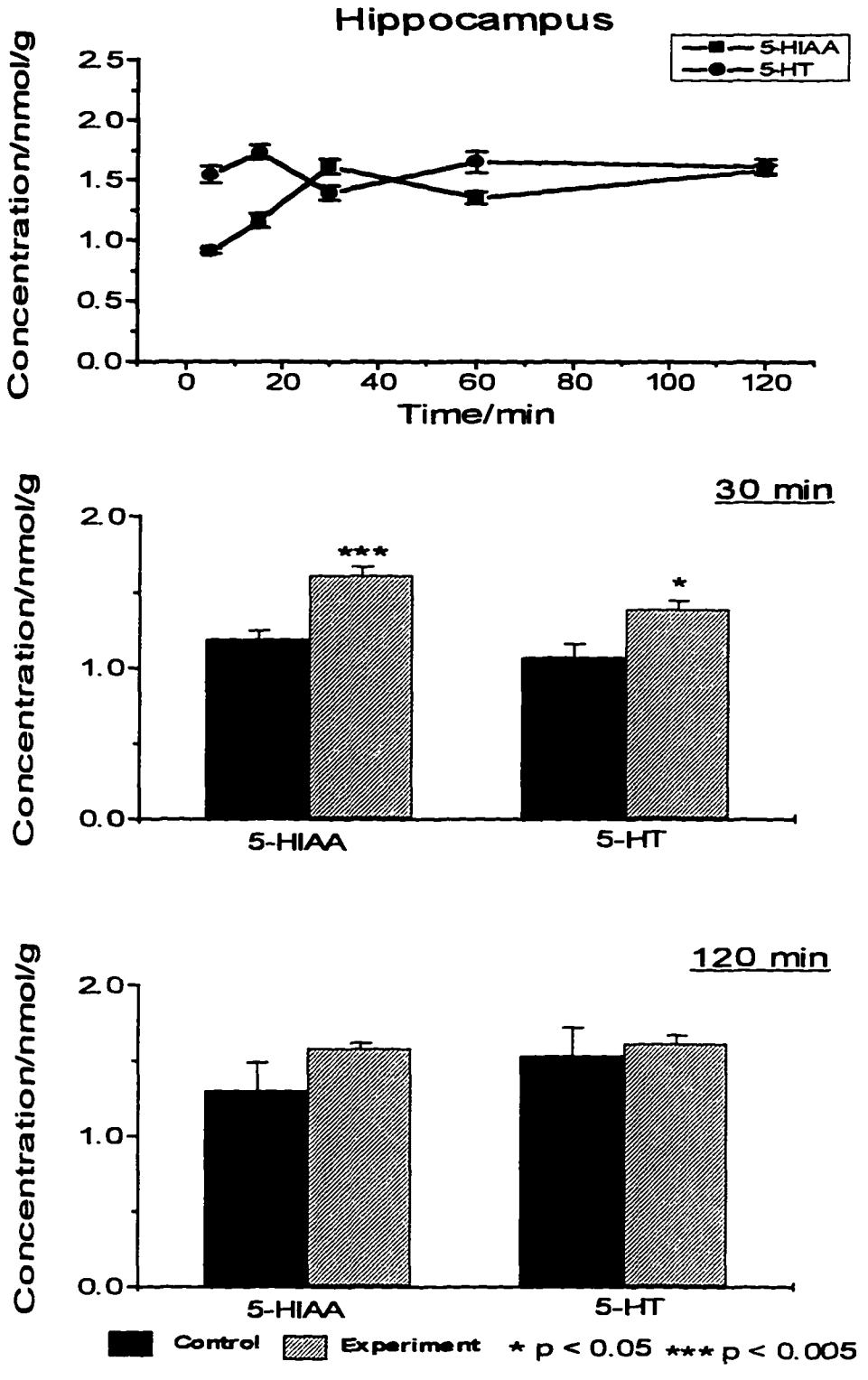

Figure 3.19 Effect of icv administration of 44 nmol (21 μg) 5-*S*-Glu-NE on the concentrations of 5-HIAA and 5-HT in rat hippocampus (top). Comparison with controls at 30 min (middle) and 120 min (bottom). Each data point represents the mean ± SE of 4-5 rats.

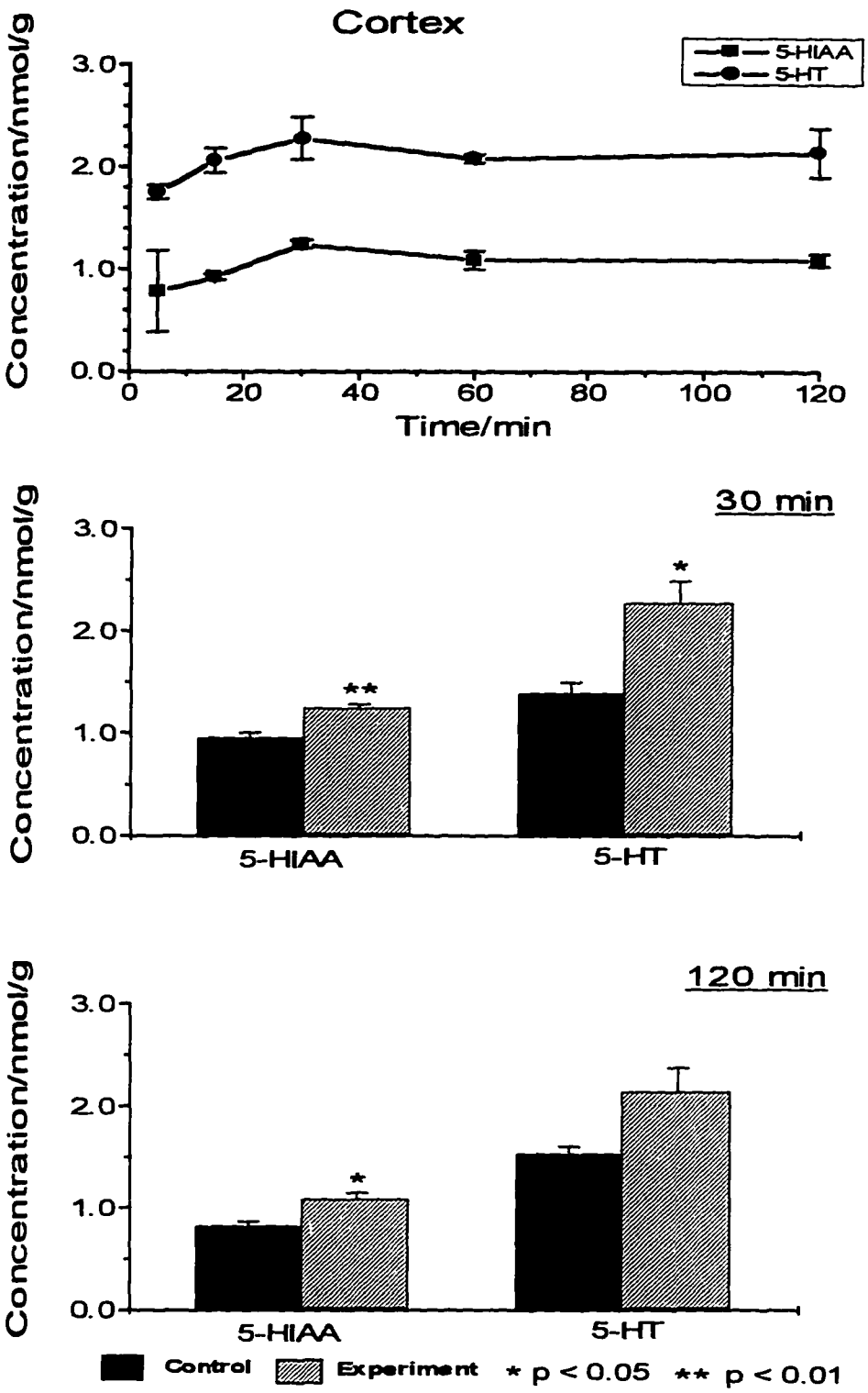

Figure 3.20 Effect of icv administration of 44 nmol (21 μg) 5-*S*-Glu-NE on the concentrations of 5-HIAA and 5-HT in rat cortex (top). Comparison with controls at 30 min (middle) and 120 min (bottom). Each data point represents the mean ± SE of 4-5 rats.

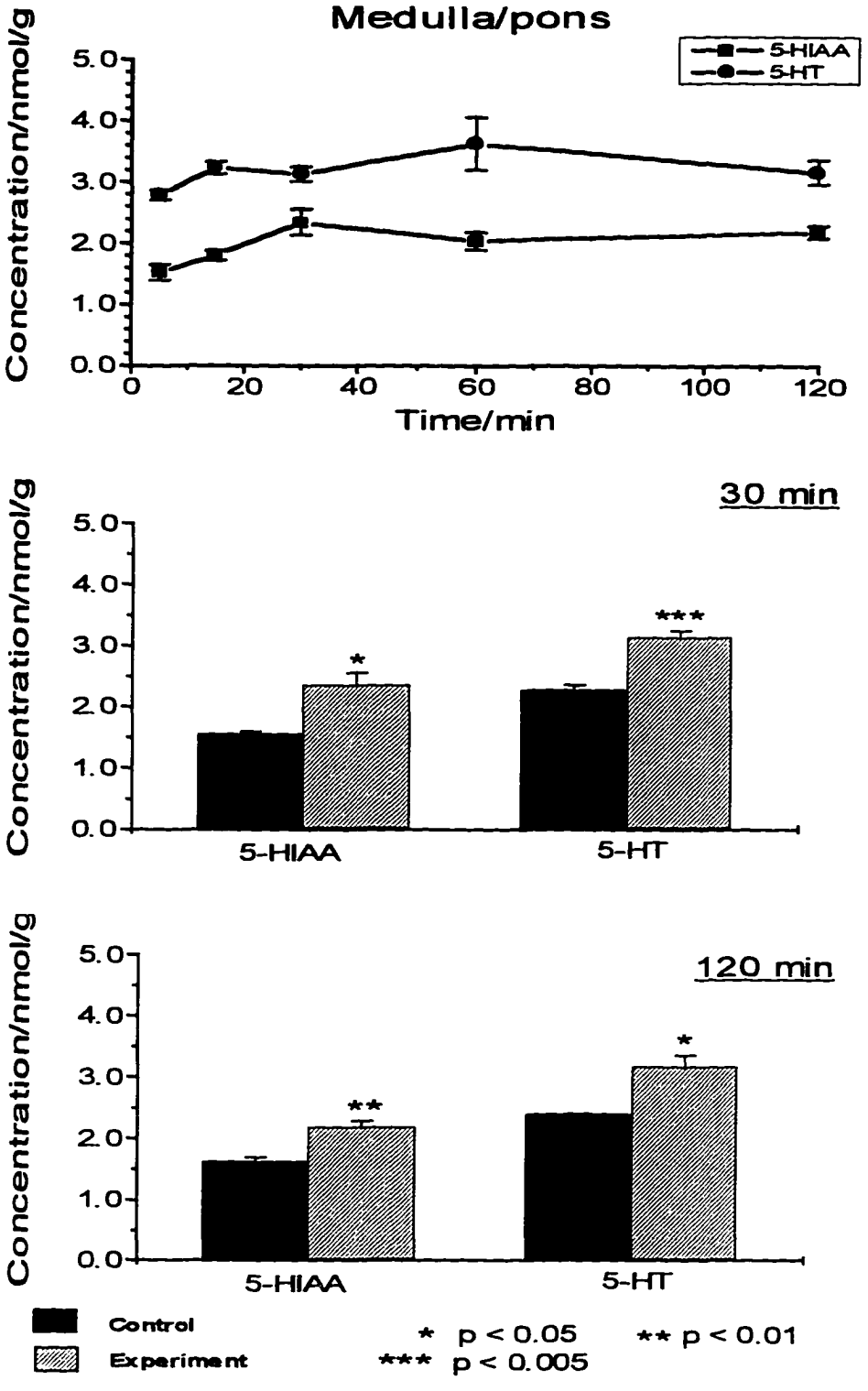

Figure 3.21 Effect of icv administration of 44 nmol (21 µg) 5-*S*-Glu-NE on the concentrations of 5-HIAA and 5-HT in rat medulla/pons (top). Comparison with controls at 30 min (middle) and 120 min (bottom). Each data point represents the mean ± SE of 4-5 rats.

C. Noradrenergic system

NE is synthesized in the cell body or in the synaptic terminal from DA through the catalysis of dopamine-ß-hydroxylase. NE is also oxidized by MAO. In the current experimental condition, only NE itself was detectable.

Concentrations of NE in various brain regions following icv administration of 5-*S*-Glu-NE are shown in Figure 3.22. The only significant changes observed were a 35% increase ($p < 0.05$) in the striatum 120 min and a 14% increase ($p < 0.05$) in the midbrain 30 min after icv administration of 5-*S*-Glu-NE.

3.5 Discussion

The experimental results in this chapter demonstrate that 5-*S*-Glu-NE can be metabolized to form 5-*S*-Cys-NE *in vitro* and metabolized to 5-*S*-Cys-NE and 5-*S*-NAc-Cys-NE *in vivo*. The formation of 5-*S*-Cys-NE and 5-*S*-NAc-Cys-NE was confirmed by comparing the brain tissue homogenate with the authentic samples on HPLC systems. The formation of the metabolite 5-*S*-Cys-NE was further structurally confirmed by spectroscopic methods, i.e., UV-Vis and ^{1}H NMR.

The first step in the metabolism of glutathionyl conjugate of NE is the removal of the γ-glutamyl group by γ-glutamyl transpeptidase (γ-GT). γ-GT is a membrane bound enzyme with its active site directed toward outside of the cell. Therefore the cleavage of the γ-glutamyl group occurred extracellulary. The cysteinylglycinyl conjugate of NE is converted to the cysteinyl conjugates of NE by dipeptidase(s). *S*-Cysteinylglycinyl conjugates may serve as substrates for several different peptidases. Aminopeptidase M and a dipeptidase have been suggested as the primary enzymes responsible for the metabolism

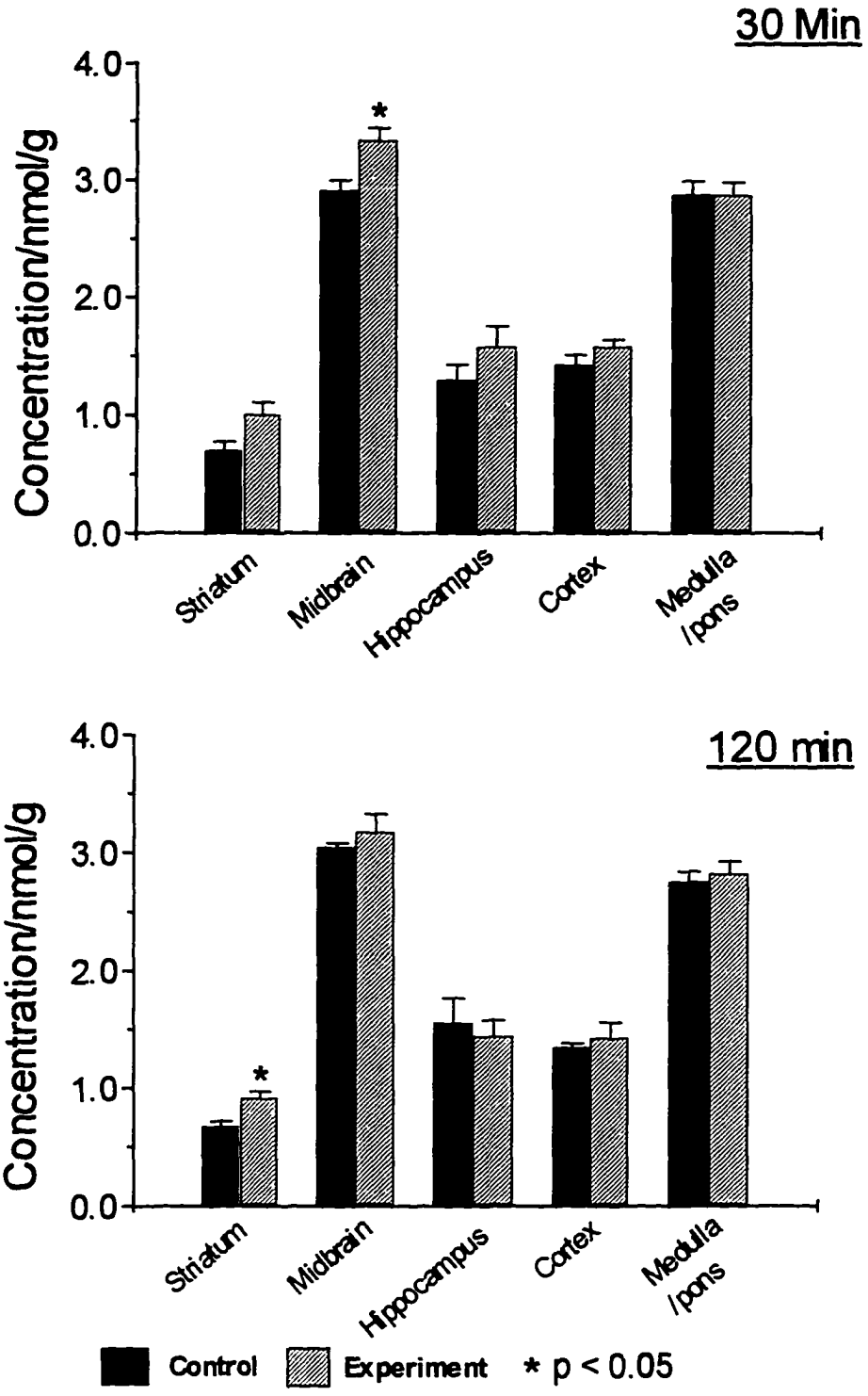

Figure 3.22 Effect of icv administration of 44 nmol (21 μg) 5-*S*-Glu-NE on the concentrations of NE in rat brains: 30 min (top) and 120 min (bottom). Each data point represents the mean ± SE of 4-5 rats.

of *S*-cysteinylglycinyl conjugates[123,124]. Finally, the formation of 5-*S*-NAc-Cys-NE is mediated by cysteine conjugate *N*-acetyltransferase and *N*-acetyl-cysteine conjugate *N*-deacetylase. The metabolism of 5-*S*-Glu-NE is summarized in Scheme V.

Scheme V

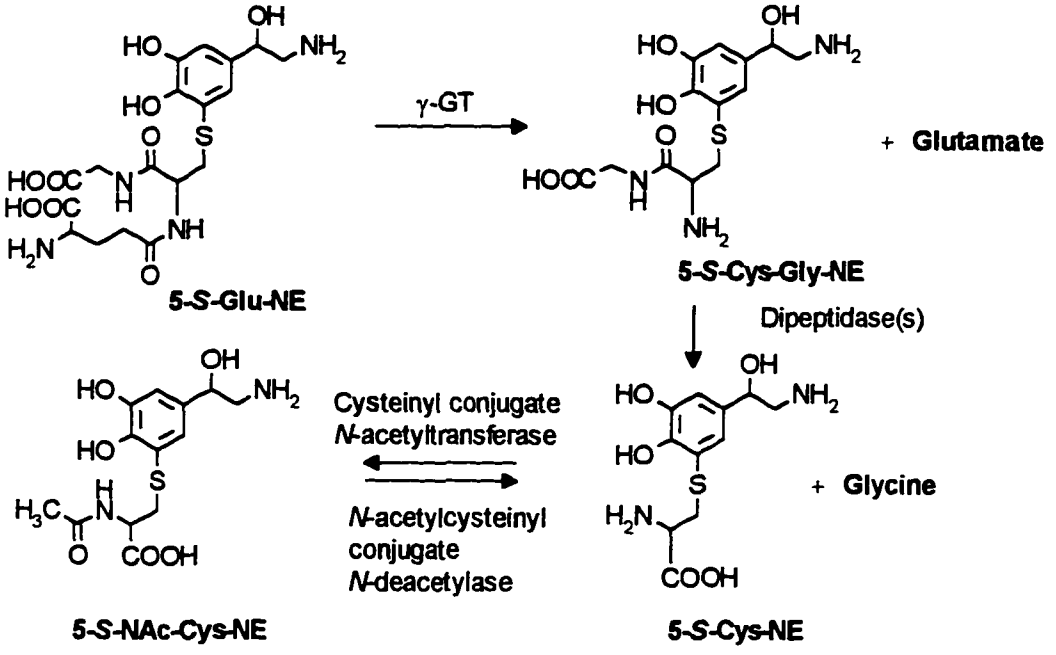

Under *in vitro* conditions, however, the hydrolysis metabolite 5-*S*-NAc-Cys-NE was not found as a metabolite of 5-*S*-Glu-NE. The reason may be attributed to the loss of activities of the related enzymes and their cofactors during homogenate preparation.

The effect of icv administration of 5-*S*-Glu-NE on neurotransmitter levels varies. For the dopaminergic system, 120 min after icv administration of 5-*S*-Glu-NE, DA levels were significantly decreased by 50% ($p < 0.05$) in the hippocampus and increased by 20% ($p < 0.05$) in the cortex. Levels of DA metabolite HVA were significantly decreased by 33% ($p < 0.01$) 120 min after icv administration of 5-*S*-Glu-NE.

Levels of 5-HIAA or 5-HT or both were significantly increased (from $p < 0.05$ to $p < 0.005$) in all brain regions either 30 min or 120 min after icv administration of 5-*S*-Glu-NE.

Levels of NE were significantly increased by 14% ($p < 0.05$) in midbrain 30 min after icv administration of 5-*S*-Glu-NE and by 35% ($p < 0.05$) in striatum 120 min after icv administration of 5-*S*-Glu-NE.

These observations suggest a general increase in noradrenergic and serotonergic activity in rat brain and various changes of dopaminergic activities in different rat brain regions.

Chapter 4 *In Vivo* Metabolism of 5-*S*-Glu-DA in Rat Brain

4.1 Introduction

In this chapter the investigation was focused on the metabolism of glutathionyl conjugates of DA under *in vitro* and *in vivo* conditions. A key step in the hypothesis is that the elevated influx of GSH or cysteine into SN neurons would divert the neuromelanin pathway causing depigmentation of the SN. GSH (or cysteine) attacks the oxidation intermediate, DA-*o*-quinone, to yield glutathionyl (or cysteinyl) conjugates. It is most likely that GSH would attack the DA-*o*-quinone first, since GSH has a larger concentration than cysteine in neurons. The subsequent glutathionyl conjugates of DA would be hydrolyzed to give rise to cysteinyl conjugates of DA. *In vitro* studies showed that the oxidation potentials of cysteinyl conjugates of DA are more negative than that of DA. Therefore, it is reasonable to assume that, in the same location where DA is auto-oxidized to neuromelanin, cysteinyl conjugates of DA, if formed, would likely be oxidized to give rise to further oxidative metabolites. Electrochemical studies show that cysteinyl conjugates of DA are easily oxidized to form a series of dihydrobenzothiazines (DHBTs) at physiological pH (Scheme II in Chap. 2). Preliminary biological studies show that DHBTs are lethal to laboratory mice and caused neurobehavioral effects as well[90]. Both the *in vitro* and *in vivo* metabolism of glutathionyl conjugates of DA were studied.

4.2 Experimental

4.2.1 Chemicals

Dopamine hydrochloride (DA•HCl) was obtained from Sigma (St. Louis, MO). 5-*S*-Cysteinylglycine-DA (5-*S*-Cys-Gly-DA) was provided by Dr. Xueming Shen from this laboratory. 5-*S*-Cysteinyldopamine (5-*S*-Cys-DA), 5-*S*-glutathionyldopamine (5-*S*-Glu-DA), 5-*N*-acetyl-cysteinyldopamine (5-*S*-NAc-Cys-DA) were prepared according to literature procedures[89,91,125]. In brief, 1 mM DA in 0.1 M HCl was electrolyzed at 1.0 V for 60 min resulting a bright yellow solution. The solution became a pale yellow in color immediately when GSH (molar GSH:DA = 5:1) was added. The reaction mixture was injected into HPLC system using HPLC method X. 5-*S*-Glu-DA was collected, frozen on dry ice and freeze-dried. The same procedure was repeated by substituting GSH with L-cysteine and *N*-acetyl-L-cysteine separately to produce the corresponding conjugates of DA. HPLC method XI and XII were employed for the isolation of cysteinyl, and *N*-acetylcysteinyl conjugates of DA. Each white solid was dissolved in a minimum amount of deionized water and purified (desalting) by HPLC method VI. Other chemicals have been described in Chap. 2 and 3. All other chemicals were of highest commercially available grade and used without further purification.

4.2.2 Instrumentation

Instruments for controlled potential electrolysis, preparative HPLC system, and HPLC-EC system have been described in Chap. 2 and 3.

Preparative HPLC system and solvents (A and B) employed for HPLC methods X, XI, and XII were described in Chap. 2. HPLC method X was used to isolate 5-*S*-GSH-DA. It employed the following gradient profile: 0-2 min, 0% solvent B; 2-20 min, linear gradient to 30% solvent B; 20-35 min, linear gradient to 100% B; 35-45 min, 100%

solvent B; 45-46 min, linear gradient to 0% solvent B; 46-50 min, 0% solvent B. The flow rate was constant at 7.0 mL/min.

HPLC method XI was used to isolate 5-*S*-Cys-DA. It employed the following gradient profile: 0-2 min, 0% solvent B; 2-25 min, linear gradient to 28% solvent B; 25-25.5 min, linear gradient to 100% B; 25.5-35 min, 100% solvent B; 35-35.01 min, linear gradient to 0% solvent B; 35.01-45 min, 0% solvent B. The flow rate was constant at 7.0 mL/min.

HPLC method XII was used to isolate 5-*S*-NAc-Cys-DA. It employed the following gradient profile: 0-2 min, 0% solvent B; 2-25 min, linear gradient to 45% solvent B; 25-25.5 min, linear gradient to 100% B; 25.5-40 min, 100% solvent B; 40-40.01 min, linear gradient to 0% solvent B; 40.01-50 min, 0% solvent B. The flow rate of was constant at 7.0 mL/min.

HPLC method XIII employed an HPLC-EC system as described in Chap. 2 and 3. The mobile phase consisted of 0.084% diethylamine (v/v), 0.055 mM EDTA, 0.46 mM SOS, and 0.10 M citric acid in 6.2% ACN/deionized water. pH was adjusted to 2.37 by concentrated HCl and NaOH. The flow rate was constant at 0.6 mL/min.

Data treatment and the calculation of concentrations of 5-*S*-Glu-DA, 5-*S*-Cys-DA, 5-*S*-NAc-Cys-DA and 5-*S*-Cys-Gly-DA were described in Chap. 3.

4.2.3 Animals

Male Sprague-Dawley rats weighing from 300 — 386 g were used. Other conditions were described in Chap. 3. All animal procedures were approved by the Institutional Animal Use and Care Committee at the University of Oklahoma.

4.2.4 Preparation of rat brain homogenates

The preparation of rat brain homogenates was described in Chap. 3. HPLC-EC system using HPLC method XIII was employed for sample assay.

4.2.5 Icv administration of DA conjugates

44 nmol of drug (i.e., 20 μg 5-*S*-Glu-DA, 11.8 μg 5-*S*-Cys-DA, and 4.8 μg 5-*S*-Cys-Gly-DA, separately) was dissolved in 5.0 μL of artificial CSF. Rats were sacrificed 5, 15, 30, 60, and 120 min after icv administration of 5-*S*-Glu-DA; 15, 30, 60 and 120 min after icv administration of 5-*S*-Cys-DA; and 5, 30, and 60 min after icv administration of 5-*S*-Cys-Gly-DA. Three rats were used at each time period for icv administration of 5-*S*-Glu-DA and 5-*S*-Cys-DA, while one rat was used for each time period for icv administration of 5-*S*-Cys-Gly-DA. Other procedures were the same as described in Chap. 3.

4.3 *In Vitro* Metabolism of Glutathionyl Conjugates of DA in Rat Brain Homogenates

4.3.1 Hydrolysis of 5-*S*-Glu-DA in rat brain homogenates

10 μL of 1.0 mM 5-*S*-Glu-DA was added into 10 mL (ca. 1.7 g whole brain tissue) rat brain homogenate and then incubated at 37 °C on a water bath. Immediately after

adding 5-*S*-Glu-DA to the homogenate a 0.5 mL aliquot of sample was taken and centrifuged at 14,000 rpm and 4 °C for 40 min. A 5 μL aliquot of the supernatant was injected into HPLC-EC system using HPLC method XIII. The chromatogram of the supernatant showed two peaks at retention times of t_R = 9.1 and 13.2 min (Figure 4.1 A), identical to the retention times obtained with authentic samples of 5-*S*-Cys-DA and 5-*S*-Glu-DA under the same conditions. After 30 min incubation, almost all 5-*S*-Glu-DA was converted to 5-*S*-Cys-DA with little 5-*S*-Glu-DA remaining (Figure 4.1 B). After 60 min incubation, HPLC-EC chromatogram showed only the peak of 5-*S*-Cys-DA.

These chromatograms demonstrate the hydrolysis process of 5-*S*-Glu-DA at physiological pH in rat brain homogenate. The hydrolysis may involve γ-glutamyl transpeptidase to clip the glutamyl residue from the GSH moiety to give rise to 5-*S*-Cys-Gly-DA which may be further metabolized by a dipeptidase enzyme to remove the glycinyl residue to form 5-*S*-Cys-DA. The hydrolysis of 5-*S*-Glu-DA must have occurred very fast. Since there was no special treatment to stop the activities of enzymes in the homogenate, the enzymes responsible for the hydrolysis may still be active at 4 °C during the centrifugation. The real hydrolysis process may be slightly slower than that shown in Figure 4.1, if the extra 40 min at 4 °C were taken into account. These results demonstrate for the first time that glutathionyl DA could be hydrolyzed *in vitro* into cysteinyl DA. However, the effort trying to identify other possible intermediates, e.g., 5-*S*-NAc-Cys-DA and DHBT1 (Scheme II in Chap. 1), failed to obtain any positive results.

The experiment in this section concludes that 5-*S*-Glu-DA can be hydrolyzed into 5-*S*-Cys-DA *in vitro* at rat brain homogenate at physiological pH 7.4 and 37 °C and 5-*S*-Cys-DA is the only confirmed product in this process.

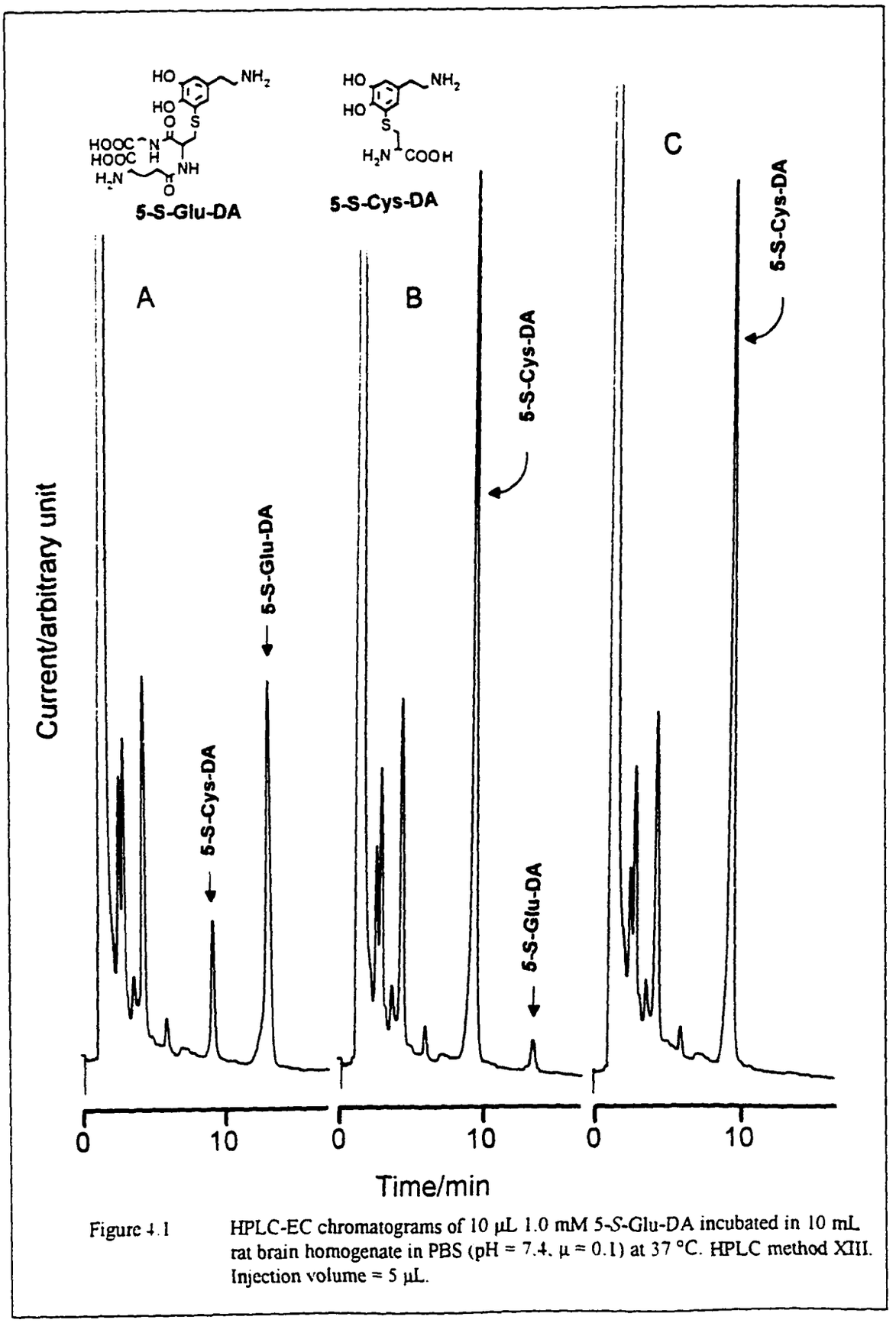

Figure 4.1 HPLC-EC chromatograms of 10 µL 1.0 mM 5-*S*-Glu-DA incubated in 10 mL rat brain homogenate in PBS (pH = 7.4, µ = 0.1) at 37 °C. HPLC method XIII. Injection volume = 5 µL.

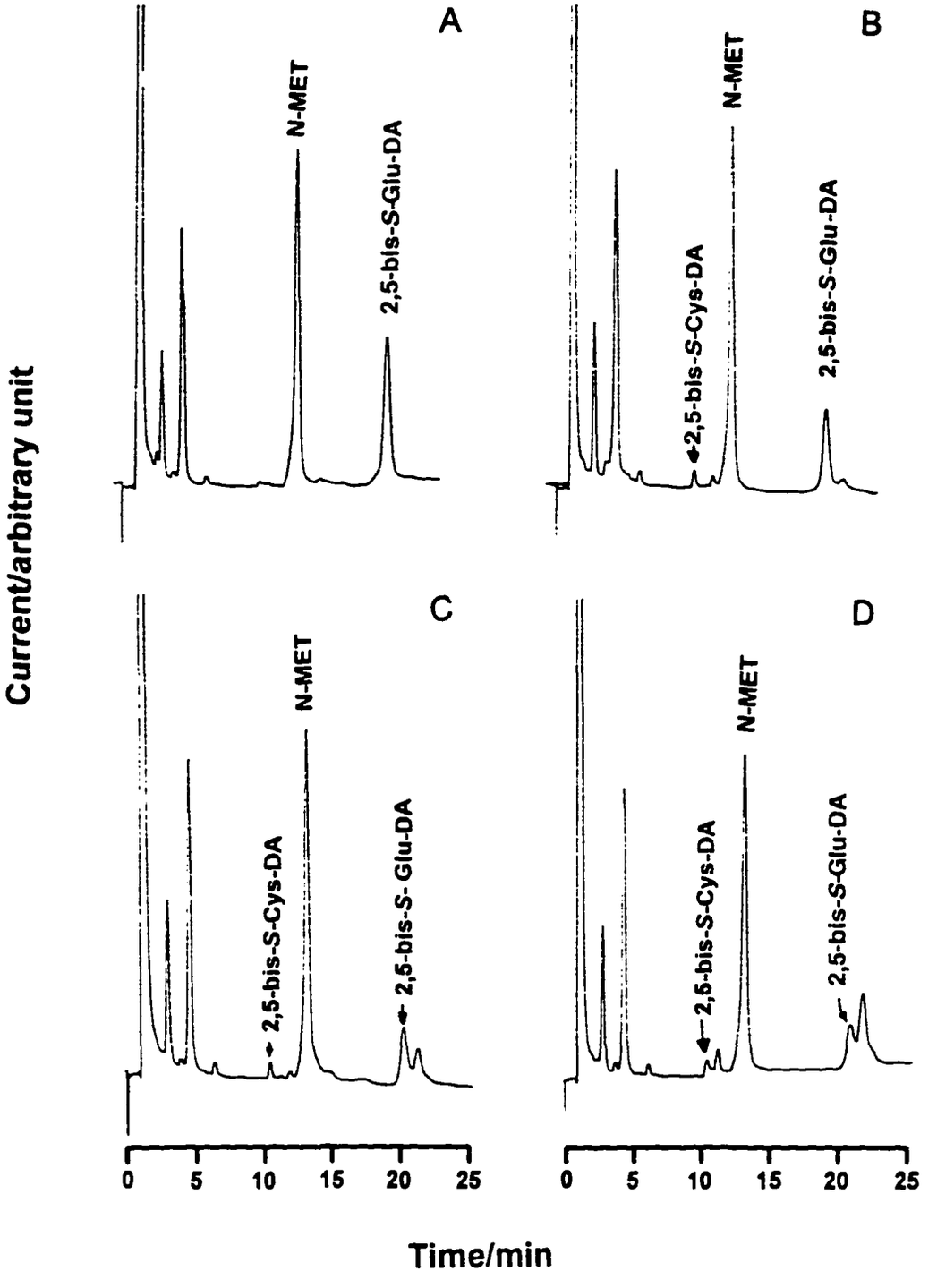

Figure 4.2 20 nmol 2,5-bis-*S*-Glu-DA incubated in 5.0 mL rat brain homogenate with PBS (pH = 7.4, μ = 0.1) at 37 °C for (A) 0.5, (B) 1, (C) 3, and (D) 6 h. HPLC method XIII. Injection volume = 5 µL.

4.3.2 *In vitro* metabolism of 2,5-bis-*S*-Glu-DA in rat brain homogenate.

2,5-bis-*S*-Glu-DA is one of the major products, along with 5-*S*-Glu-DA and *2,5,6-tris*-*S*-Glu-DA, at the initial stage of electro-oxidation of DA in the presence of the GSH at physiological pH[91].

20 μL of 1.0 mM 2,5-bis-*S*-Glu-DA was added to 5.0 mL rat brain homogenate and incubated at 37 °C in a water bath. A piece of parafilm was used to seal the vial to prevent the homogenate from evaporating during the incubation. 2,5-bis-*S*-Glu-DA was eluted at retention time t_R = 20.7 min. N-MET was added into the homogenate as an internal standard and eluted at retention time t_R = 13.3 min. The expected metabolite, 2,5-bis-*S*-Cys-DA, did not appear (Figure 4.3 A and B) until after 3 h incubation and was eluted at retention time t_R = 11.5 min (Figure 4.3 C). The changes of peak heights of 2,5-bis-*S*-Cys-DA and 2,5-bis-*S*-Glu-DA relative to N-MET (internal standard) are summarized in Figure 4.4.

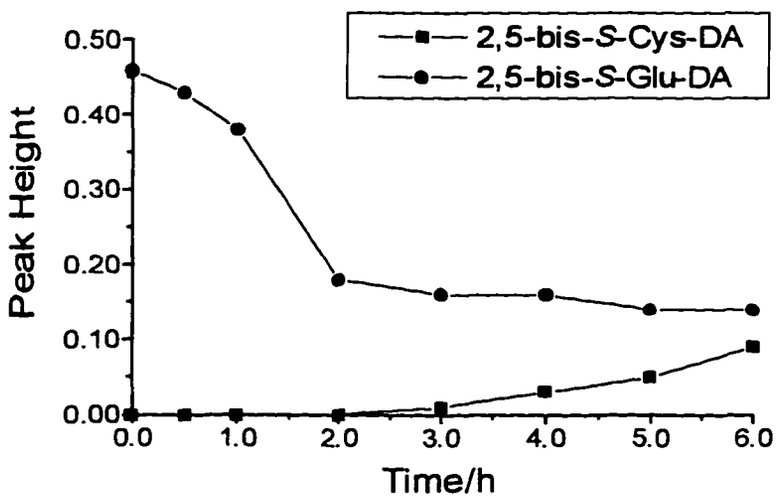

Figure 4.3 Changes of peak heights (relative to N-MET) of 2,5-bis-*S*-Cys-DA and 2,5-bis-*S*-Glu-DA during incubation of 20 nmol of 2,5-bis-*S*-Glu-DA with 5.0 mL rat brain homogenate in PBS (pH = 7.4, μ = 0.1) at 37 °C.

During the first 2 h incubation, the concentration of 2,5-bis-*S*-Glu-DA decreased

rapidly without a concomitant increase in the yield of 2,5-bis-*S*-Cys-DA. After 2 h incubation, the decrease of the concentration of 2,5-bis-*S*-Glu-DA slowed down and 2,5-bis-*S*-Cys-DA began to form. There were 3 peaks which remained unidentified. One of the unknowns appeared at a retention time t_R = 12.1 min momentarily (Figure 4.2 B and C) and disappeared later (Figure 4.2 D). The second unknown peak eluted at a retention time t_R = 10.7 min and stayed at a constant level. The third unknown peak eluted at a retention time t_R = 21.8 and grew steadily with the incubation time (Figure 4.2).

It is also possible that the unknown peaks might be one of the products from the further oxidation of the hydrolysis product 2,5-bis-*S*-Cys-DA (Scheme II). Therefore, the retention times of those unknown peaks were compared to those of DHBTs. Unfortunately, none of the retention time of the unknown peaks matched those of DHBTs. The retention times are listed in Table 4.1.

Table 4.1 Retention Times for the Peaks during *in vitro* Metabolism of 2,5-bis-*S*-Glu-DA in Rat Brain Homogenate.

Compound Name	Retention Time/min
2,5-bis-*S*-Glu-DA	20.7
2,5-bis-*S*-Cys-DA	11.5
N-MET (internal standard)	13.3
Unknown peak 1	10.7
Unknown peak 2	12.1
Unknown peak 3	21.8
DHBT2	27.0
DHBT3	16.5

To conclude, the *in vitro* metabolism of 2,5-bis-*S*-Glu-DA in rat brain homogenate at physiological pH 7.4 and 37 °C yielded the 2,5-bis-*S*-Cys-DA together with other unidentified metabolites.

4.4 *In Vivo* Metabolism of 5-*S*-Glu-DA in Rat Brain

4.4.1 Icv administration of 5-*S*-Glu-DA

44 nmol (20 μg) of 5-*S*-Glu-DA was infused into the left lateral ventricles through cannulas pre-installed on rats as described in Chap. 3. The rats were sacrificed 5, 15, 30, 60 and 120 min after icv administration. 3-4 rats were used as a group for each of the different periods of time. HPLC-EC method XIII was employed to monitor the hydrolysis process. Each sample was injected into the HPLC-EC system twice and the average was taken. The concentration was calculated by equation 3.1 (Chap. 3). The mean and standard error (SE) of a group of animal were calculated.

Typical HPLC chromatograms shown in Figure 4.4 were obtained from tissues of the striatum, midbrain, hippocampus, cortex and medulla/pons of a rat brain 15 min after icv administration of 44 nmol 5-*S*-Glu-DA. Data of the complete *in vivo* experiment are summarized in Figure 4.5 to 4.9.

5 min after icv administration the concentration of 5-*S*-Glu-DA was found highest in the striatum (4.08 nmol/g), followed by hippocampus (3.13 nmol/g), medulla/pons (2.47 nmol/g), midbrain (2.44 nmol/g) and cortex (1.62 nmol/g). 5-*S*-Glu-DA disappeared from striatum within 30 and all other areas within 60 min.

Unlike the *in vitro* metabolism of 5-*S*-Glu-DA, the dipeptidyl metabolite 5-*S*-Cys-Gly-DA was detected during the *in vivo* metabolism of 5-*S*-Glu-DA. It appeared during roughly the same time window as 5-*S*-Glu-DA could be detected. Therefore, 5-*S*-Cys-Gly-DA appeared at highest levels 5 min after icv administration with concentrations in each brain area in the order hippocampus (0.77 nmol/g) > striatum (0.72 nmol/g) > midbrain (0.67 nmol/g) > medulla/pons (0.46 nmol/g) > cortex (0.39 nmol/g). 5-*S*-Cys-Gly-DA

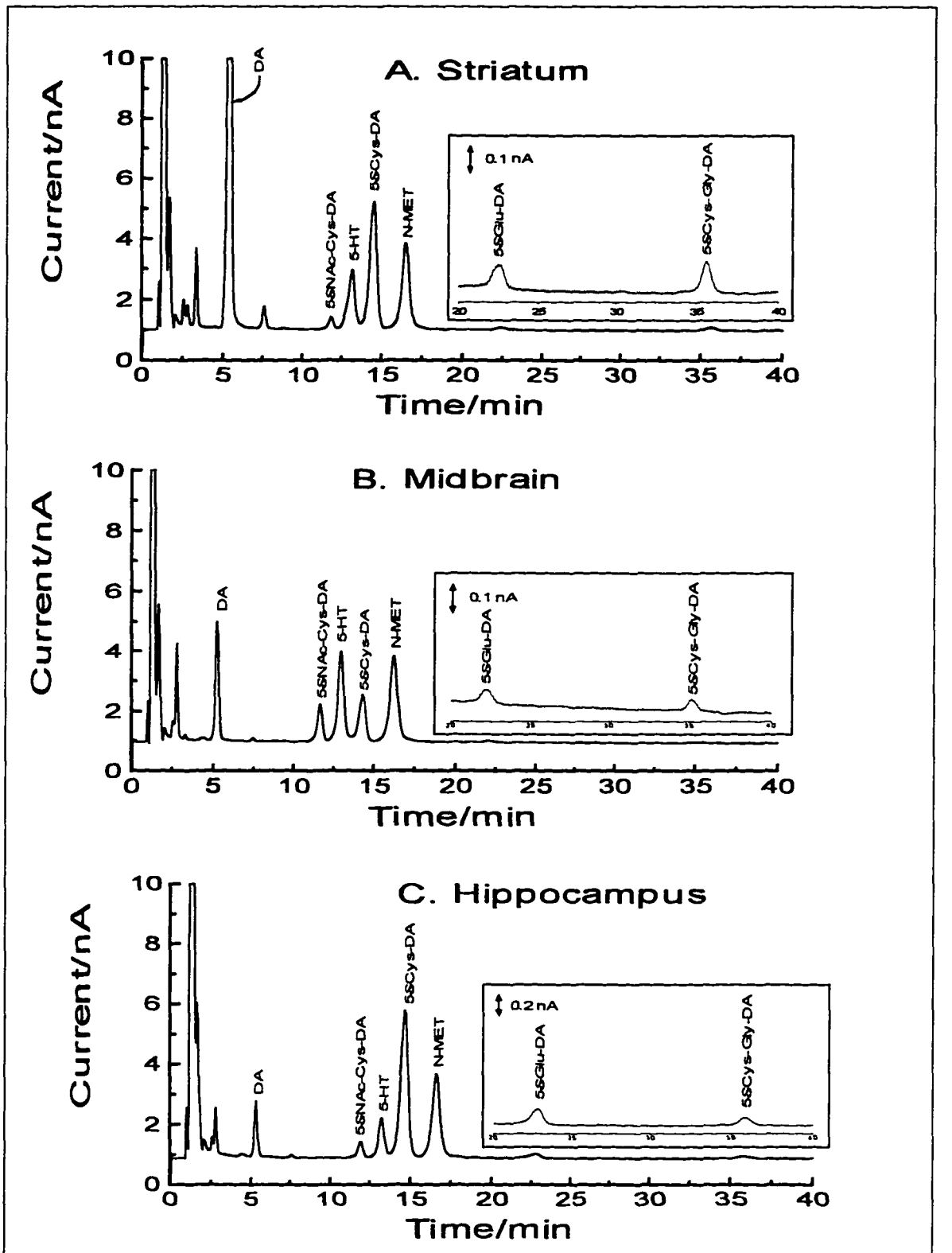

Figure 4.4 15 min after icv administration of 44 nmol 5-*S*-Glu-DA to rat. (A) striatum, (B) midbrain, (C) hippocampus, (D) cortex and (E) medulla/pons. HPLC method XIII. Injection volume = 5 µL. Insets in (A) and (E) show peaks of 5-*S*-Glu-DA and 5-*S*-Cys-Gly-DA in details. (Continued on the next page)

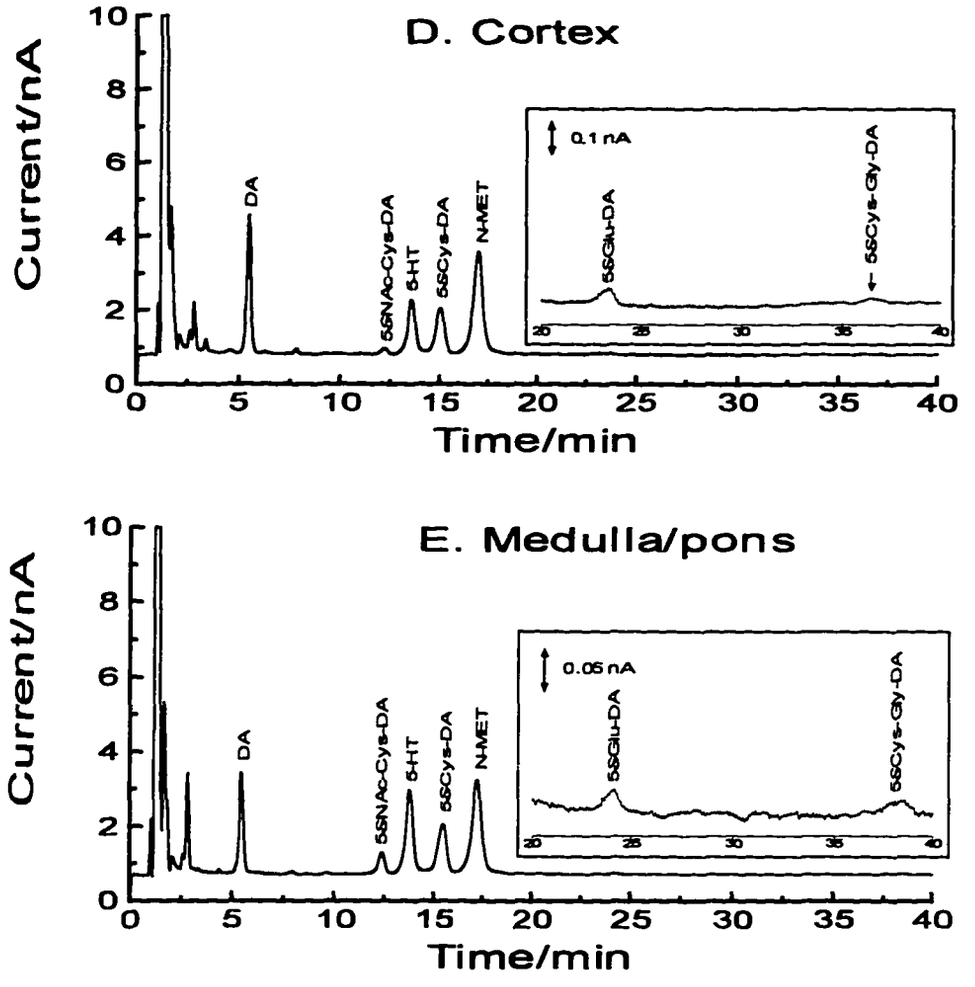

Figure 4.4 (Continue from the previous page)

15 min after icv administration of 44 nmol (20 μg) 5-*S*-Glu-DA to rat. (A) striatum, (B) midbrain, (C) hippocampus, (D) cortex and (E) medulla/pons. HPLC method XIII. Injection volume = 5 μL. Insets in (A) and (E) show peaks of 5-*S*-Glu-DA and 5-*S*-Cys-Gly-DA in details.

disappeared from the medulla/pons 15 min after icv administration of 5-*S*-Glu-DA. 5-*S*-Cys-Gly-DA disappeared from striatum and midbrain 30 min after icv administration, and from hippocampus and cortex within 60 min after icv administration of 5-*S*-Glu-DA. The first step of hydrolysis of 5-*S*-Glu-DA is the conversion of 5-*S*-Glu-DA itself into 5-*S*-Cys-Gly-DA and this step seemed to be the rate limiting step. The concentration of 5-*S*-Cys-Gly-DA was just high enough to be detected under the current conditions. Once 5-*S*-Glu-

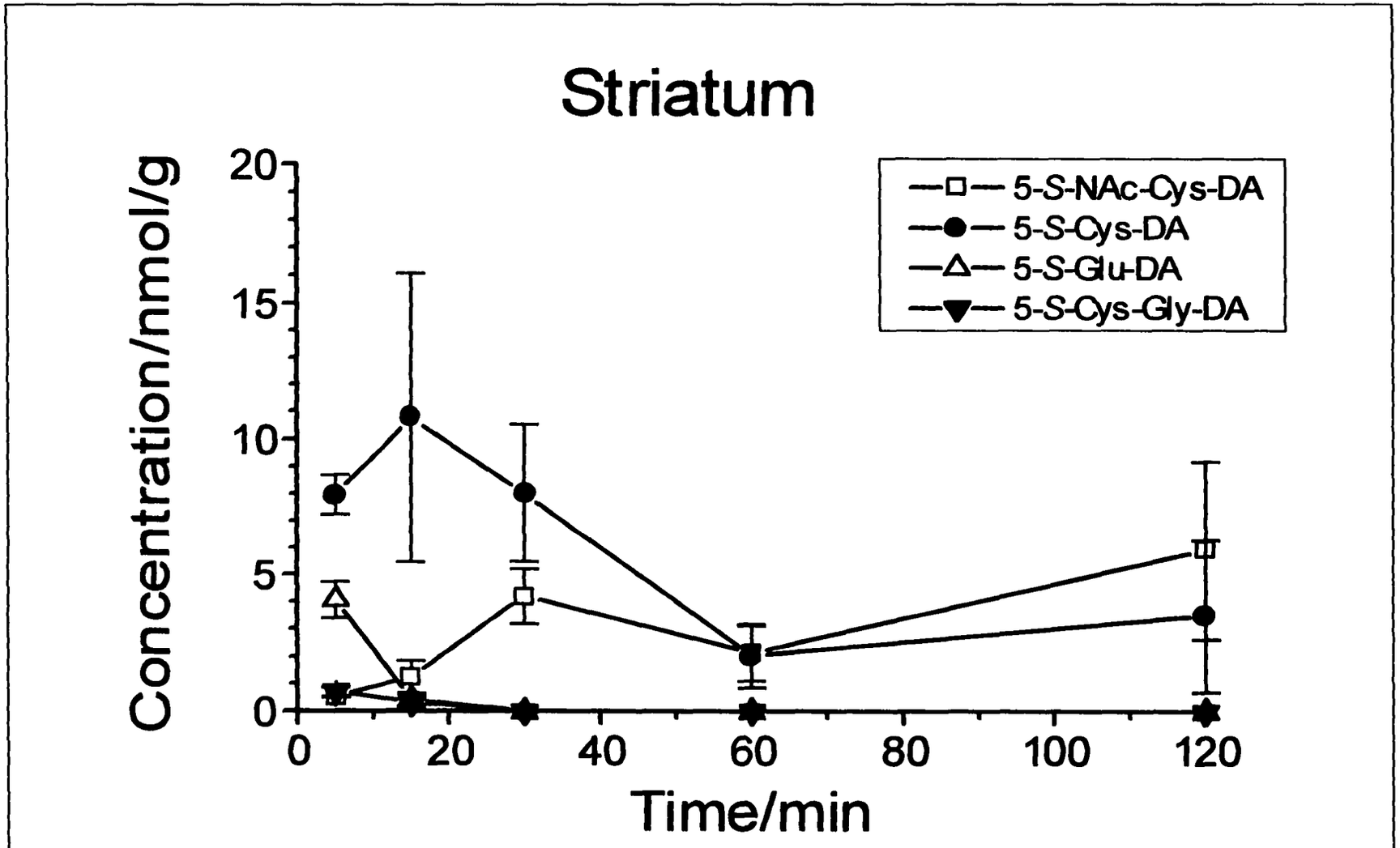

Figure 4.5 Striatum of rats after icv administration of 44 nmol (20 μg) 5-*S*-Glu-DA. Each data point represents the mean ± SE of 3-4 rats.

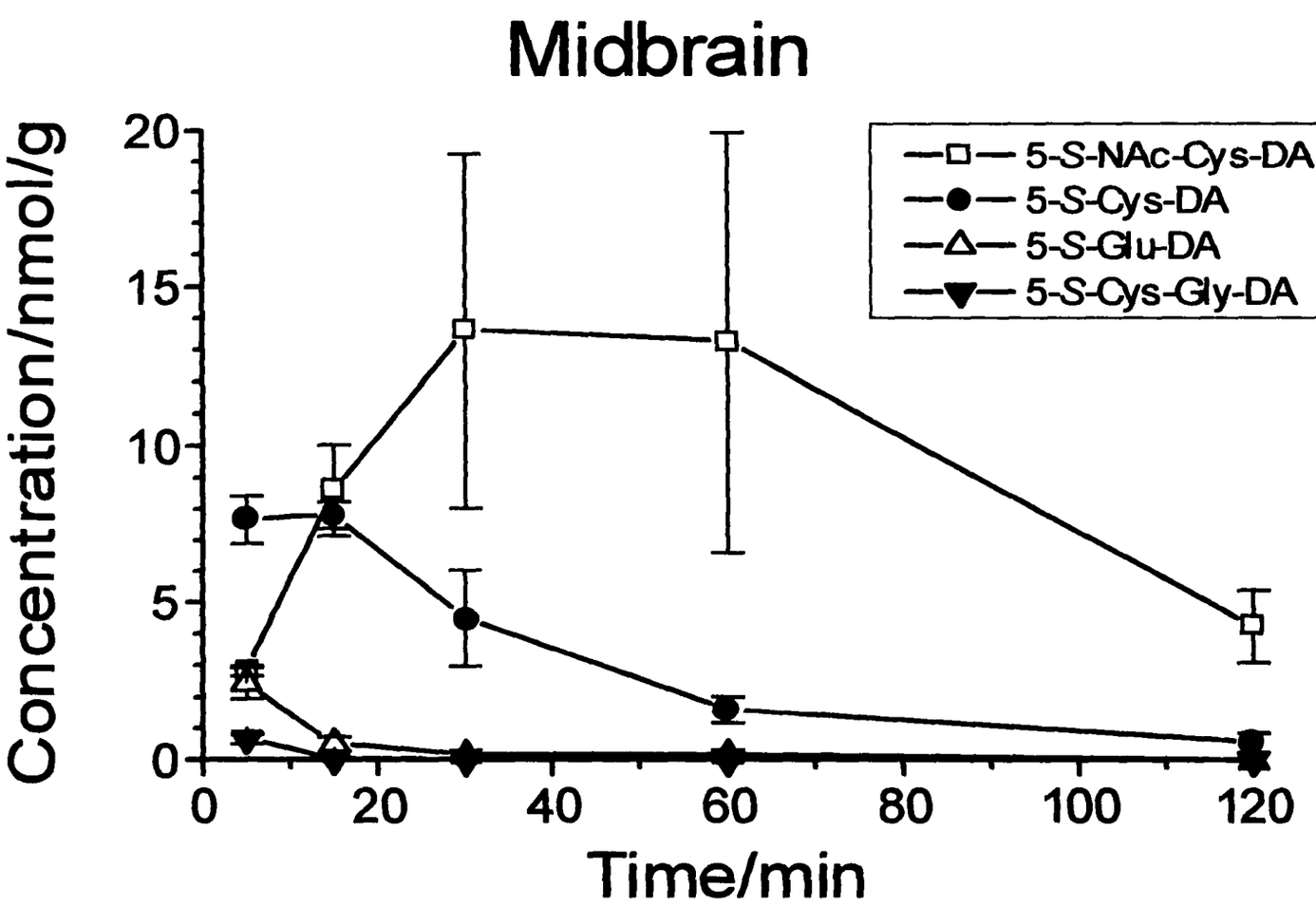

Figure 4.6 Midbrain of rats after icv administration of 44 nmol (20 μg) 5-*S*-Glu-DA. Each data point represents the mean ± SE of 3-4 rats.

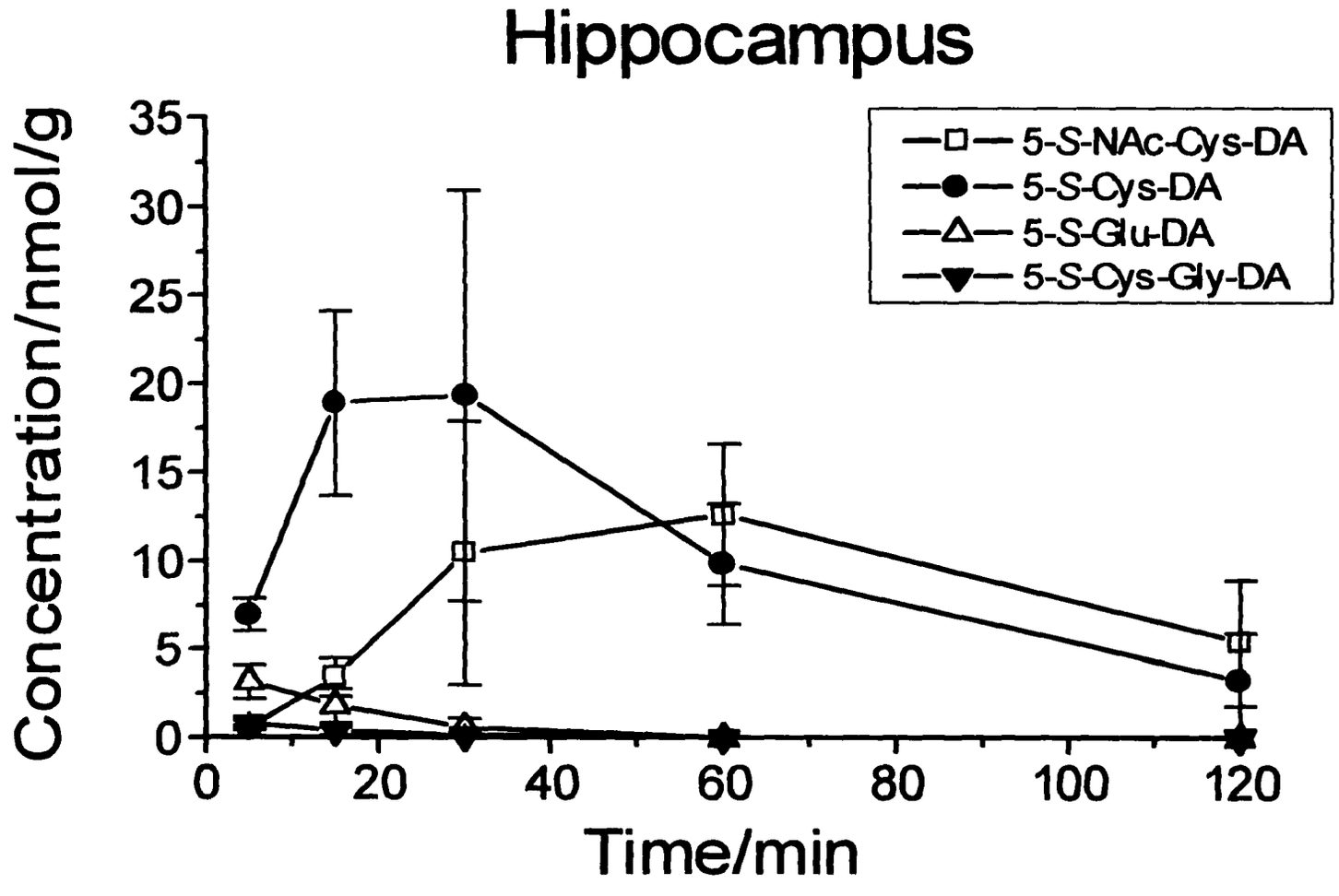

Figure 4.7 Hippocampus of rats after icv administration of 44 nmol (20 μg) 5-*S*-Glu-DA. Each data point represents the mean ± SE of 3-4 rats.

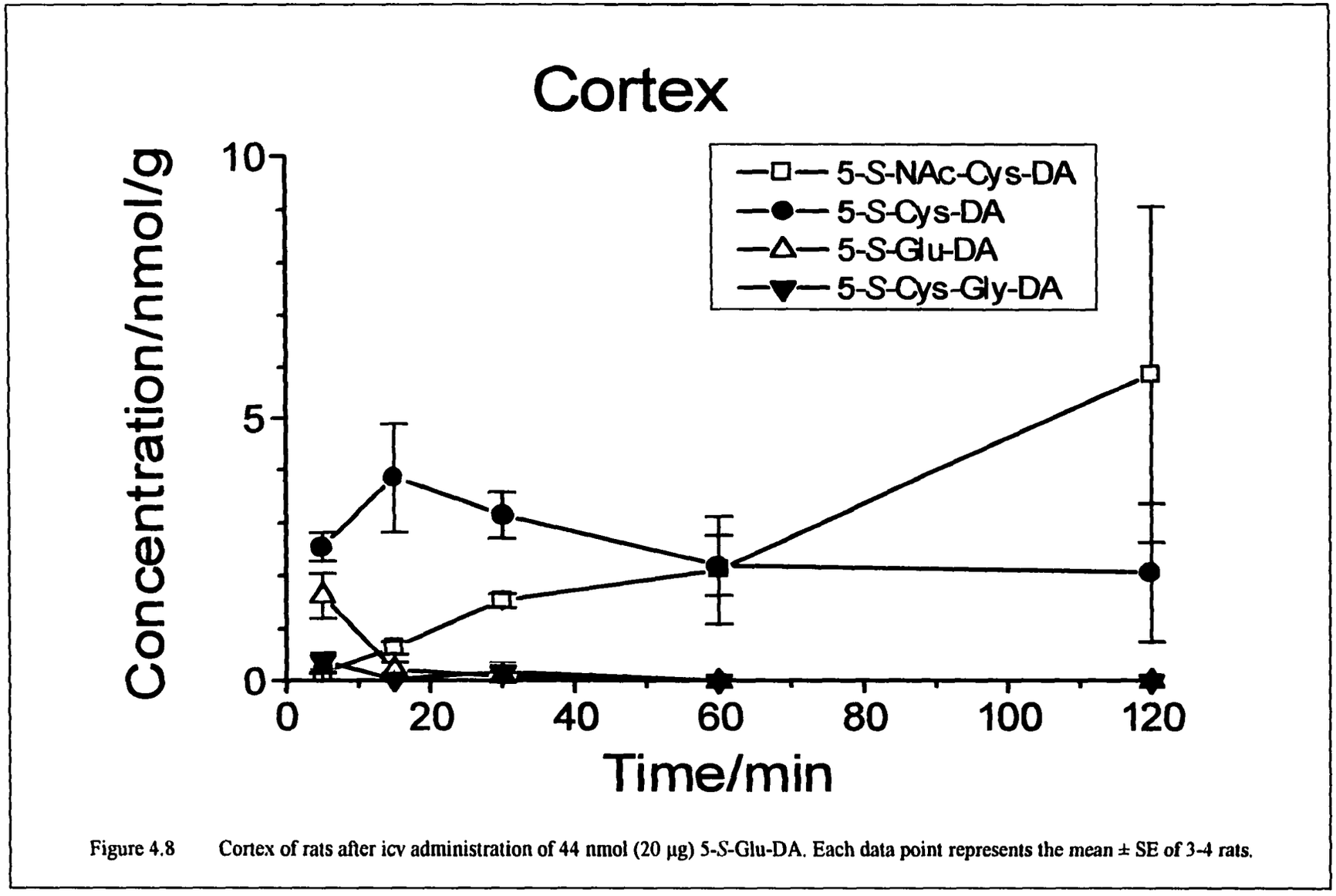

Figure 4.8 Cortex of rats after icv administration of 44 nmol (20 μg) 5-*S*-Glu-DA. Each data point represents the mean ± SE of 3-4 rats.

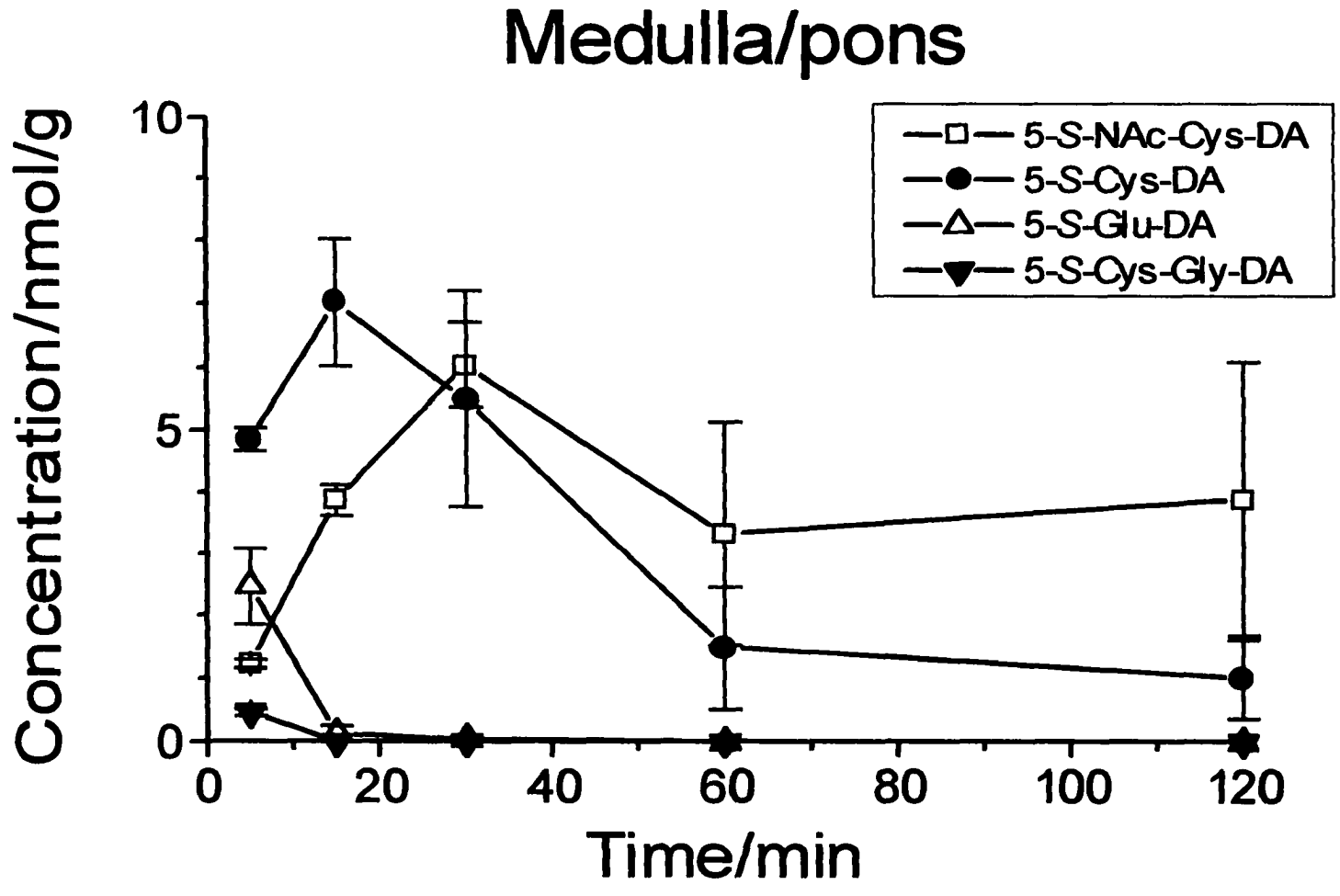

Figure 4.9 Medulla/pons of rats after icv administration of 44 nmol (20 μg) 5-*S*-Glu-DA. Each data point represents the mean ± SE of 3-4 rats.

DA is gone, 5-*S*-Cys-Gly-DA can no be longer detected.

As in the *in vitro* metabolism of 5-*S*-Glu-DA, 5-*S*-Cys-DA is also a major metabolite of the *in vivo* metabolism of 5-*S*-Glu-DA. The concentration of 5-*S*-Cys-DA reached a maximum level 15 min after icv administration of 5-*S*-Glu-DA in the order striatum (10.8 nmol/g) > midbrain (7.8 nmol/g) > cortex (3.9 nmol/g) > medulla/pons (7.0 nmol/g); and 30 min after icv administration in the hippocampus (19.3 nmol/g). In the midbrain, only 5 min after icv administration, the concentration of 5-*S*-Cys-DA was of 98% of the maximum level (Figure 4.6). 15 min after icv administration of 5-*S*-Glu-DA, the concentration of 5-*S*-Cys-DA reached 98% of its maximum in the hippocampus (Figure 4.7). However, at the end of the experiment, the relative level of 5-*S*-Cys-DA was the lowest in midbrain, with a concentration of only 7% of the maximum value. The midbrain, therefore, is the region having the highest turnover rate for 5-*S*-Cys-DA. The clearance of 5-*S*-Cys-DA in other brain areas is as follows (% of the maximum level remaining): medulla/pons (14%), hippocampus (16%), striatum (32%) and cortex (54%).

Another major metabolite detected in the *in vivo* metabolism of 5-*S*-Glu-DA was 5-*S*-NAc-Cys-DA, which did not appear *in vitro*. This may be attributed to the loss of activity of the enzyme — cysteinyl conjugate *N*-acetyltransferase. It is still unclear why this particular enzyme loses its activity during the preparation of the brain homogenate, but among other things its substrate may be lost. Under *in vivo* conditions, 5-*S*-NAc-Cys-DA was formed in all brain areas studied. The patterns of the concentration change of 5-*S*-NAc-Cys-DA were quite different than that of 5-*S*-Cys-DA. Thus, the concentrations of 5-*S*-Cys-DA in all areas of the brain first reached their maximum levels and then decreased as the experiment continued. In contrast, the concentration of 5-*S*-NAc-Cys-DA first increased to a maximum level, then decreased to a minimum, and then increased again to a level even higher than the maximum at the end of the experiment in striatum (Figure 4.5).

The concentration of 5-*S*-NAc-Cys-DA behaved in this manner only in the midbrain and hippocampus (Figure 4.6 and 4.7). In the cortex, the concentration of 5-*S*-NAc-Cys-DA steadily increased without reaching a maximum at the end of the experiment (Figure 4.8). In medulla/pons, the concentration of 5-*S*-NAc-Cys-DA first increased to a maximum level then decreased to a minimum, and then slightly increased again at the end of the experiment (Figure 4.9). The concentration of 5-*S*-NAc-Cys-DA was found in brain areas in the order from the highest concentration to the lowest: midbrain (13.6 nmol/g, 30 min), hippocampus (12.6 nmol/g, 60 min), medulla/pons (6.03 nmol/g), striatum (5.91 nmol/g, 120 min), and cortex (5.86 nmol/g, 120 min).

4.4.2 Icv administration of 5-*S*-Cys-DA

44 nmol 5-*S*-Cys-DA was icv administered into the left lateral ventricles through pre-installed cannulas as described in Chap. 3. 3 rats were used in each group that were sacrificed 15, 30, 60 and 120 min after icv administration of 5-*S*-Cys-DA. Typical HPLC-EC chromatograms from different brain areas 15 min after icv administration of 5-*S*-Cys-DA are shown in Figure 4.10. The changes of 5-*S*-Cys-DA levels and its metabolite 5-*S*-NAc-Cys-DA in different brain areas are shown in Figure 4.11 to 4.15.

In the striatum the concentration of 5-*S*-Cys-DA steadily decreased from the initial value of 9.92 nmol/g to 4.38 nmol/g, a 56% decrease within 2 h. Correspondingly, the concentration of 5-*S*-NAc-Cys-DA increased from 0.68 nmol/g to 2.49 nmol/g (Figure 4.11).

In the midbrain the concentration of 5-*S*-Cys-DA also steadily decreased from 8.67 nmol/g to 1.92 nmol/g (78%) in 2 h (Figure 4.12).

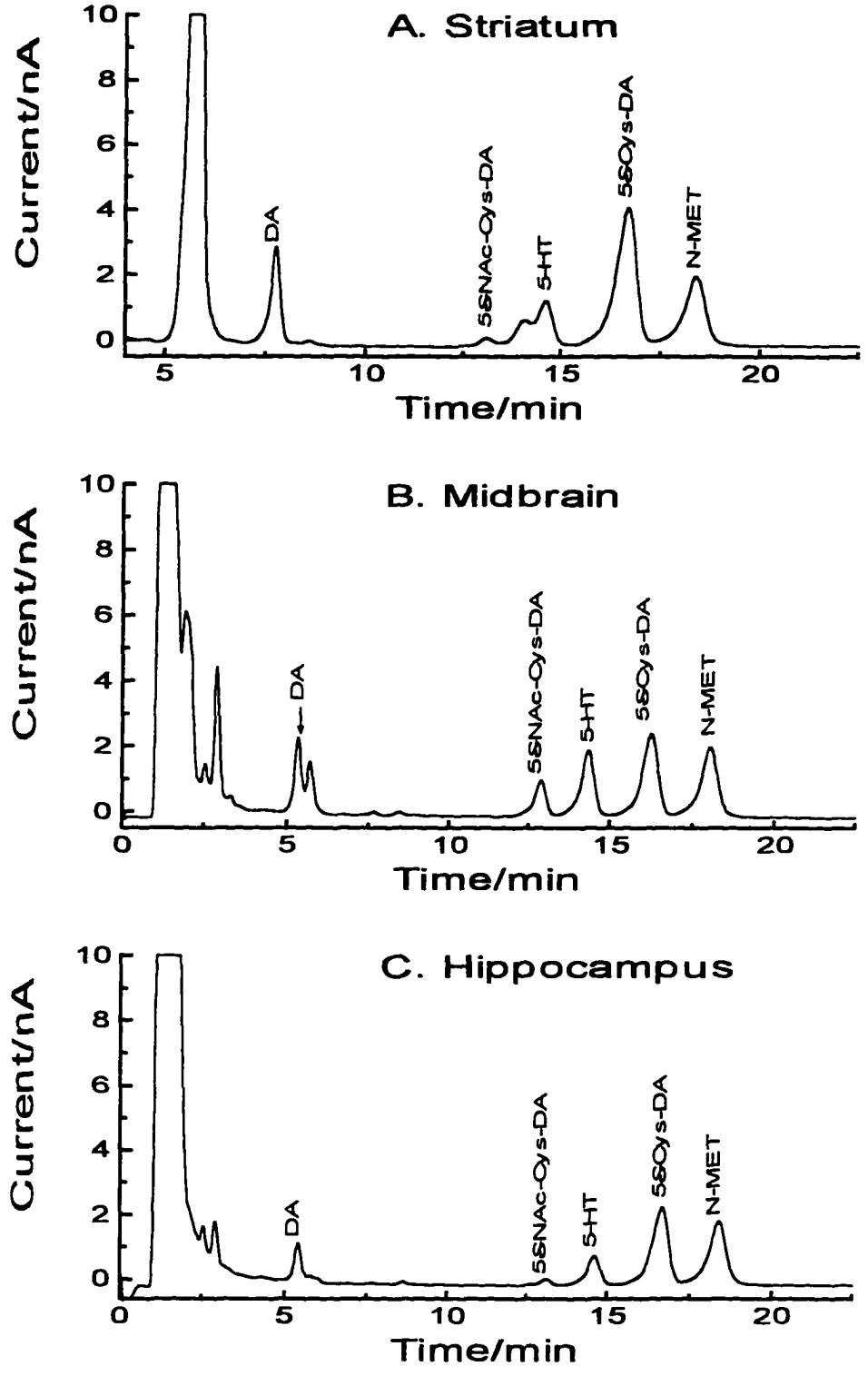

Figure 4.10 15 min after icv administration of 44 nmol 5-*S*-Cys-DA to rat. (A) striatum, (B) midbrain, (C) hippocampus, (D) cortex and (E) medulla/pons. HPLC method XIII. Injection volume = 5 μL. (Continued on the next page.)

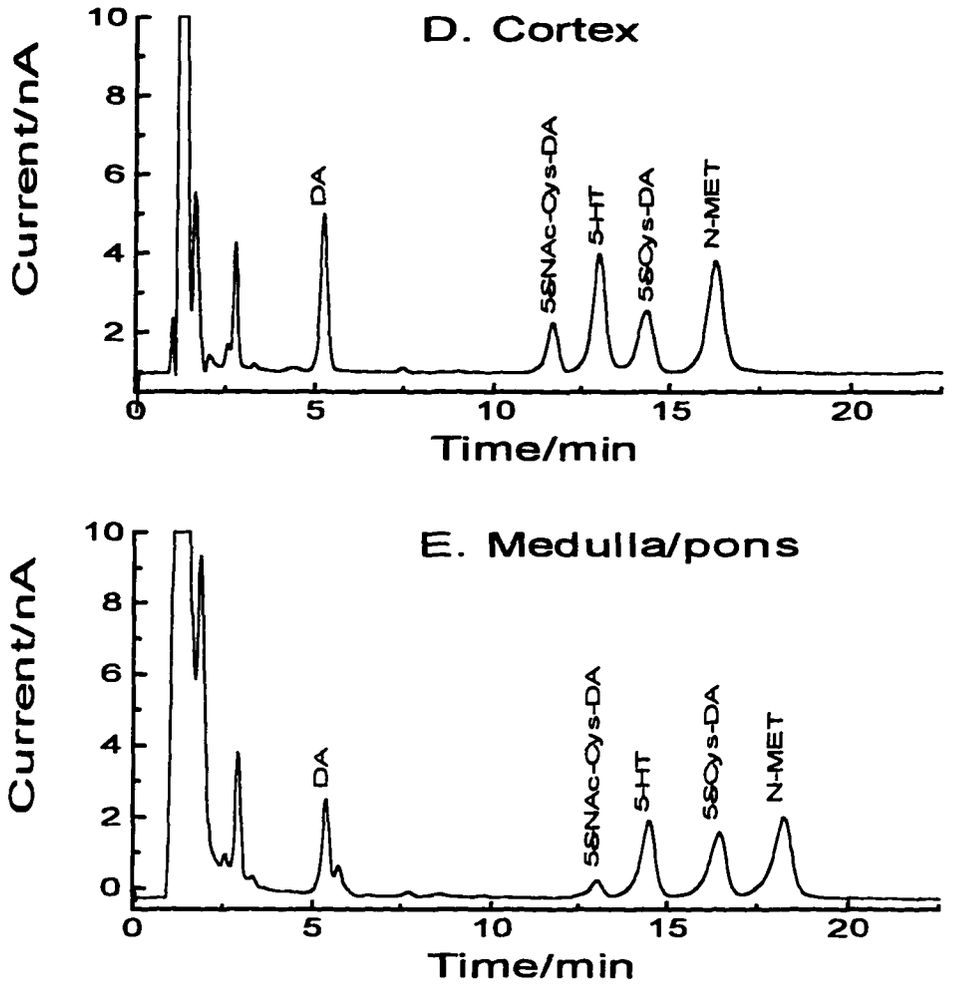

Figure 4.10 (Continued from previous page)
15 min after icv administration of 44 nmol 5-*S*-Cys-DA to rat. (A) striatum, (B) midbrain, (C) hippocampus, (D) cortex and (E) medulla/pons. HPLC method XIII. Injection volume = 5 μL.

In the hippocampus, the concentration of 5-*S*-Cys-DA decreased from 10.6 nmol/g 15 min after icv administration to 5.55 nmol/g after 30 min. The concentration of 5-*S*-Cys-DA then increased slightly and decreased again. The concentration of 5-*S*-NAc-Cys-DA was about linearly increased with respect to the incubation time (Figure 4.13).

The concentration of 5-*S*-Cys-DA in the cortex was first increased to a maximum of 4.27 nmol/g 30 min after icv administration of 5-*S*-Cys-DA and then decreased to

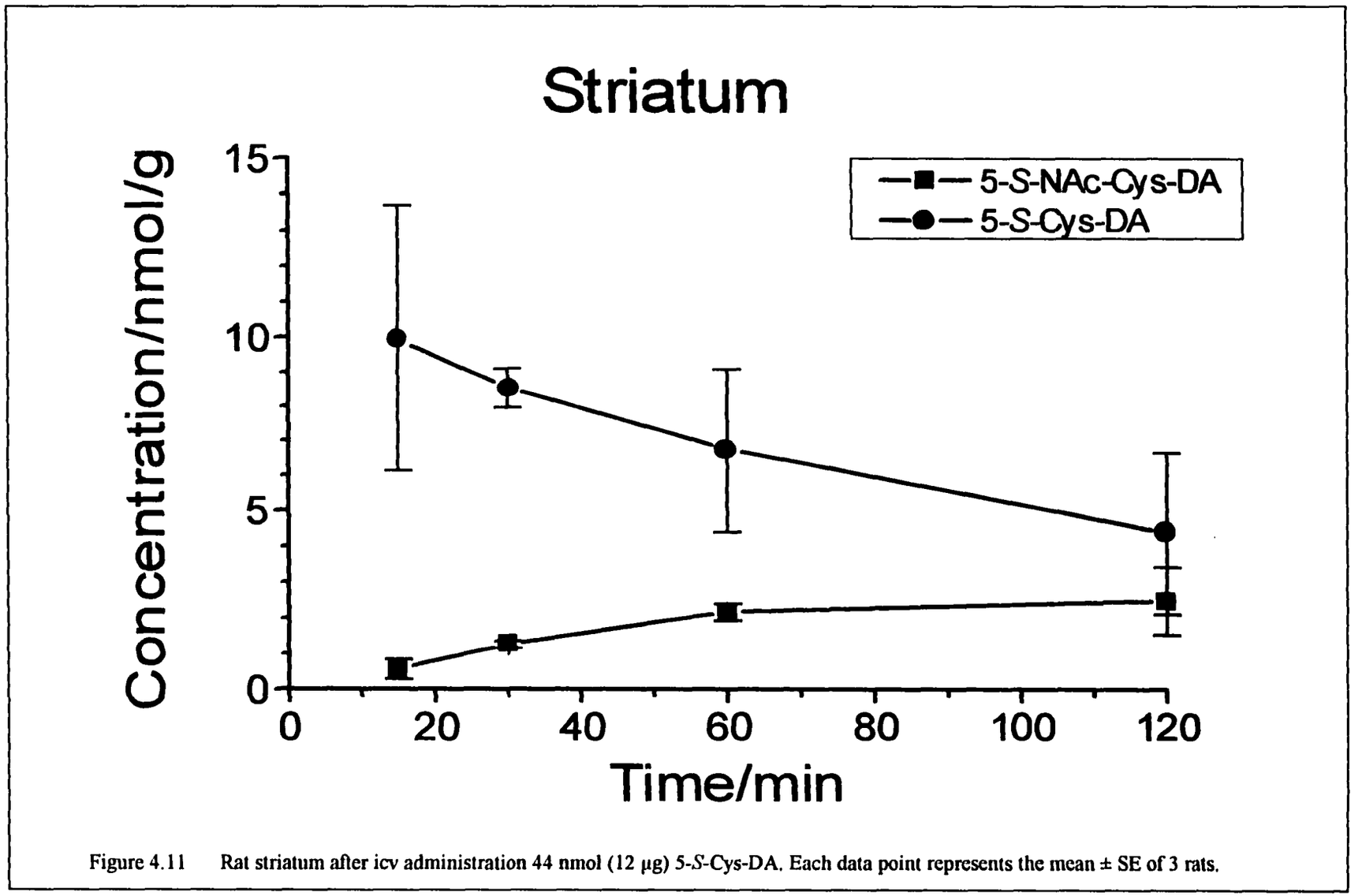

Figure 4.11 Rat striatum after icv administration 44 nmol (12 μg) 5-*S*-Cys-DA. Each data point represents the mean ± SE of 3 rats.

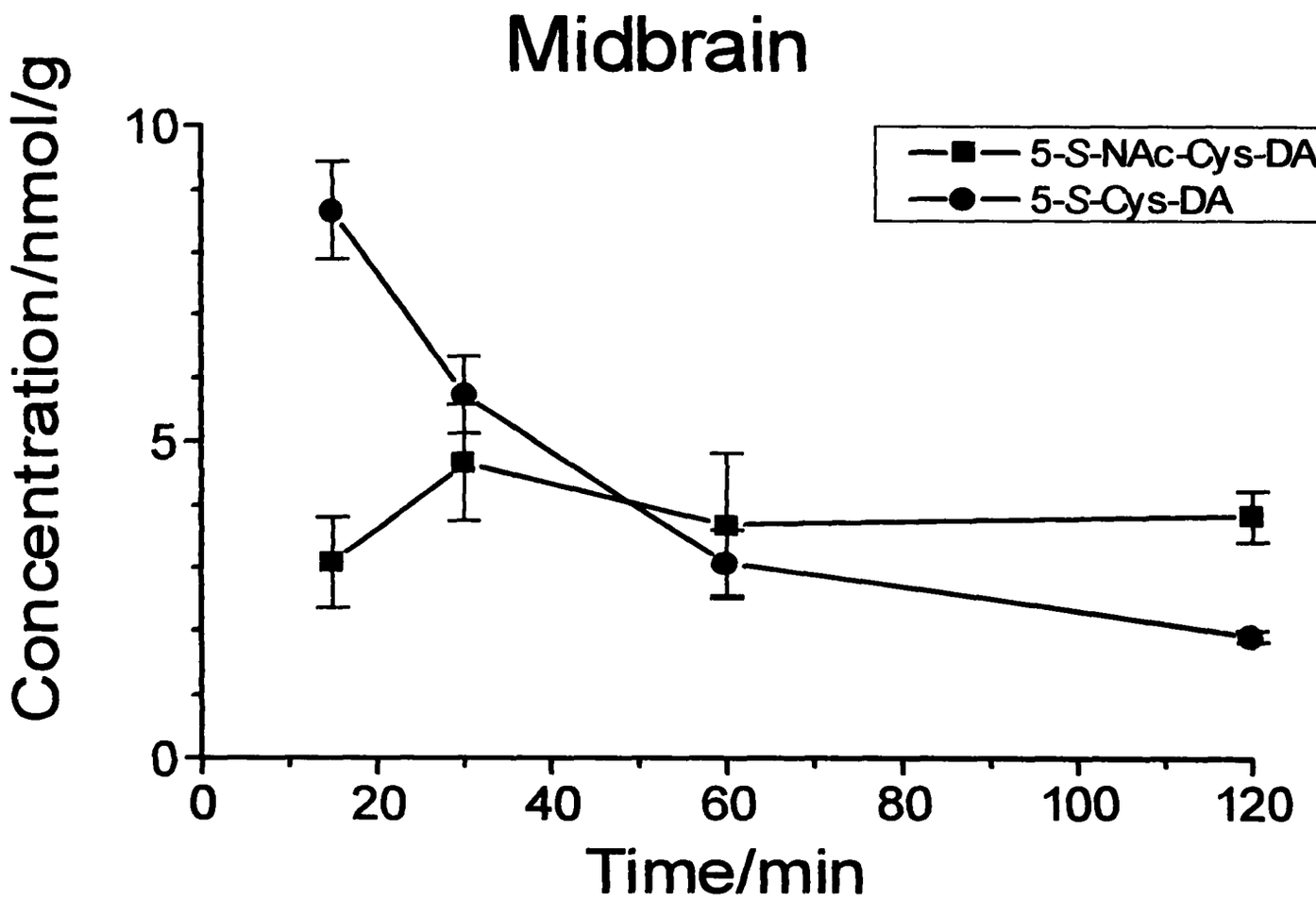

Figure 4.12 Rat midbrain after icv administration of 44 nmol (12 μg) 5-*S*-Cys-DA. Each data point represents the mean ± SE of 3 rats.

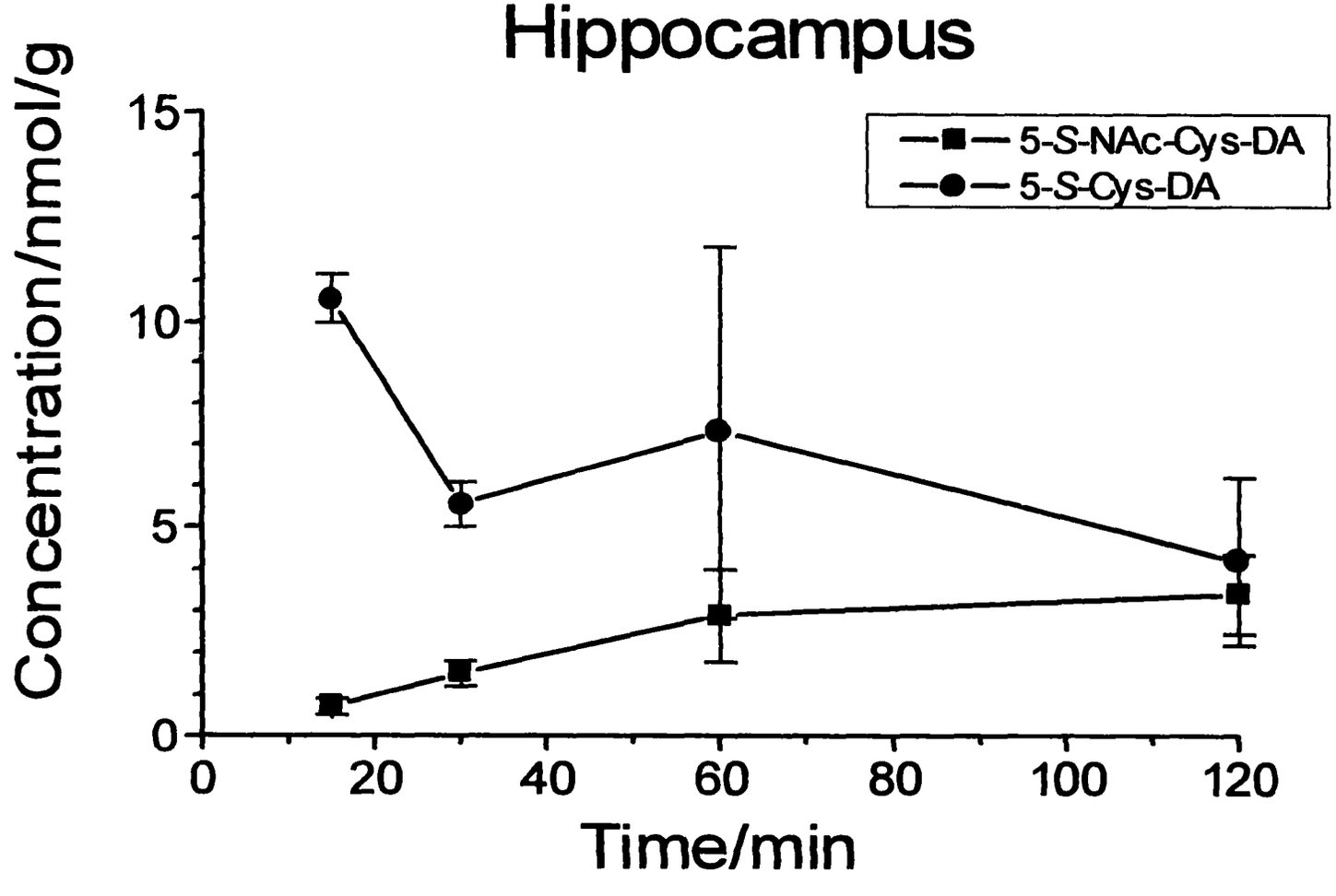

Figure 4.13 Rat hippocampus after icv administration of 44 nmol (12 μg) 5-*S*-Cys-DA. Each data point represents the mean ± SE of 3 rats.

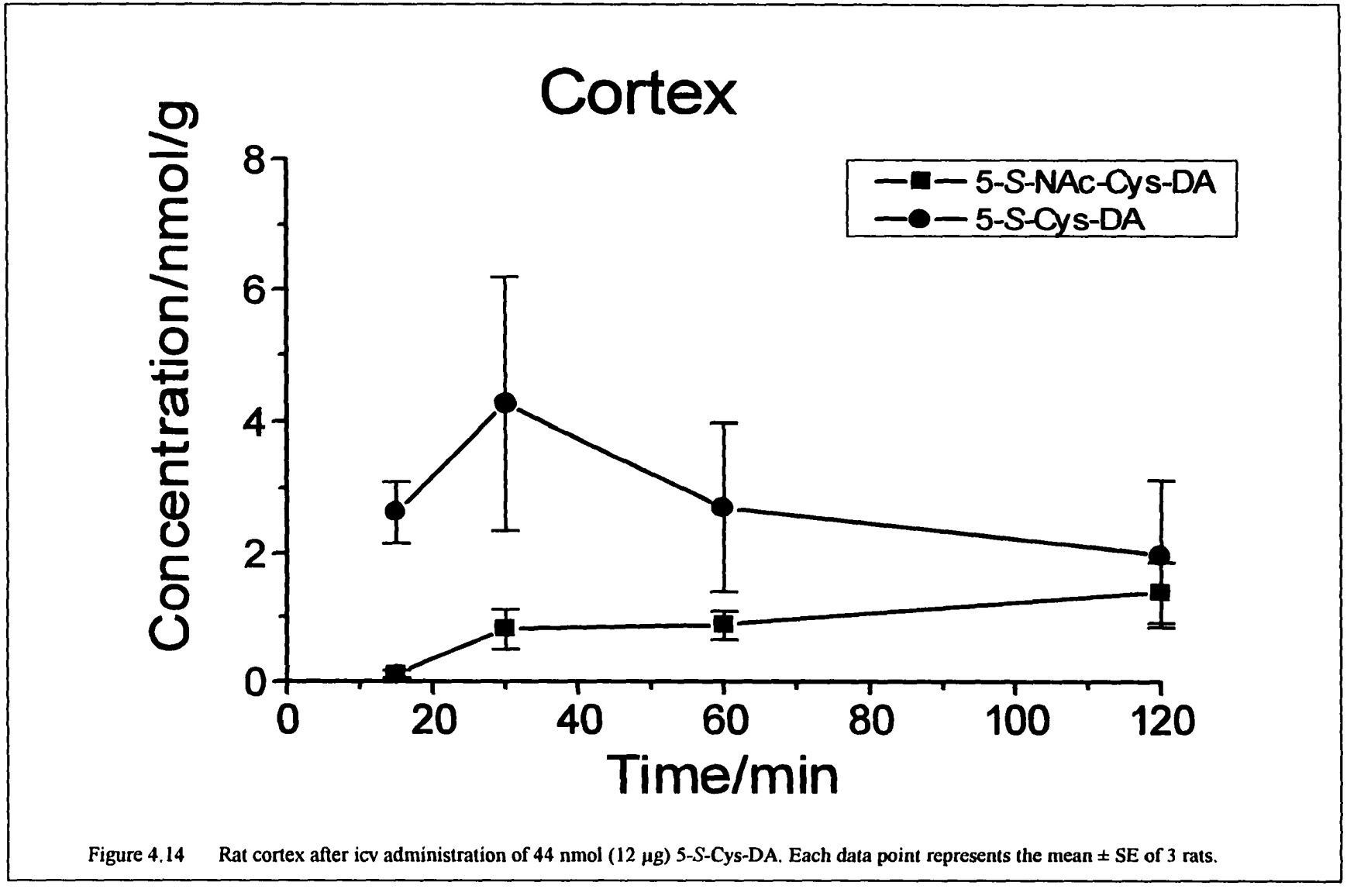

Figure 4.14 Rat cortex after icv administration of 44 nmol (12 μg) 5-*S*-Cys-DA. Each data point represents the mean ± SE of 3 rats.

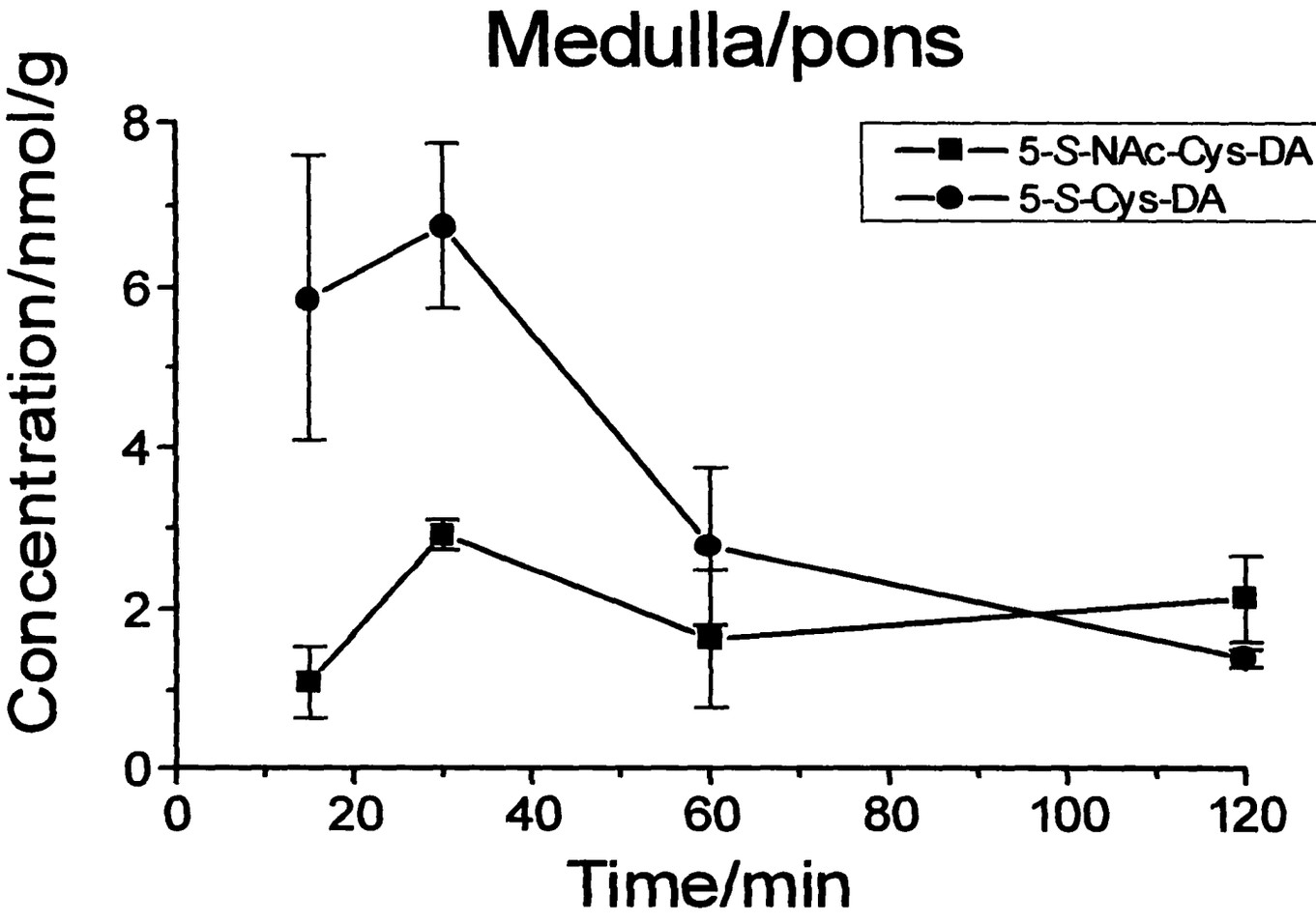

Figure 4.15 Rat medulla/pons after icv administration of 44 nmol (12 μg) 5-*S*-Cys-DA. Each data point represents the mean ± SE of 3 rats.

1.98 nmol/g after 2 h. The concentration of 5-*S*-NAc-Cys-DA increased from barely nothing (0.12 nmol/g) 5 min after icv administration of 5-*S*-Cys-DA to 1.39 nmol/g after 2 h (Figure 4.14).

The concentrations of 5-*S*-Cys-DA and 5-*S*-NAc-Cys-DA in medulla/pons increased to a maximum at 6.75 nmol/g and 2.92 nmol/g, respectively, 30 min after icv administration of 5-*S*-Cys-DA.

The highest concentrations of 5-*S*-Cys-DA were found as 10.6 nmol/g in the hippocampus (15 min), 9.92 nmol/g in the striatum (15 min), 8.67 nmol/g in the midbrain (15 min), 6.75 nmol/g in the medulla/pons (30 min), and 4.27 nmol/g in the cortex (30 min) respectively. The highest concentrations of 5-*S*-NAc-Cys-DA were found as 4.67 nmol/g in the midbrain (30 min), 3.42 nmol/g in the hippocampus (120 min), 2.92 nmol/g in the medulla/pons (30 min), 2.49 nmol/g in the striatum (120 min), and 1.39 nmol/g in the cortex (120 min), respectively.

The concentrations of 5-*S*-Cys-DA in each brain area should be decreased after icv administration of 5-*S*-Cys-DA, while the concentrations of 5-*S*-NAc-Cys-DA should be increased after icv administration. However, on certain occasions the concentration did not change in this way. Further statistical treatment (one-way ANOVA applied to two adjacent data points) showed no significant differences in those changes. Those abnormal changes can thus be attributed to the differences of individual rats.

4.4.3 Icv administration of 5-*S*-Cys-Gly-DA

5-*S*-Cys-Gly-DA was dissolved in artificial CSF and the pH was adjusted to neutral (pH = 7.0 ± 0.5) as described in Chap. 3. 44 nmol 5-*S*-Cys-Gly-DA (24 μg 5-*S*-Cys-Gly-

DA•2TFA) was icv administered into the left lateral ventricle through pre-installed cannulas on rats as described previously. 5, 30 and 60 min after icv administration of the drug, rats were sacrificed. One rat was used for each time period. The HPLC-EC chromatograms of brain sample obtained 5 min after icv administration of 5-*S*-Cys-Gly-DA are shown in Figure 4.16. Data are summarized in Table 4.2.

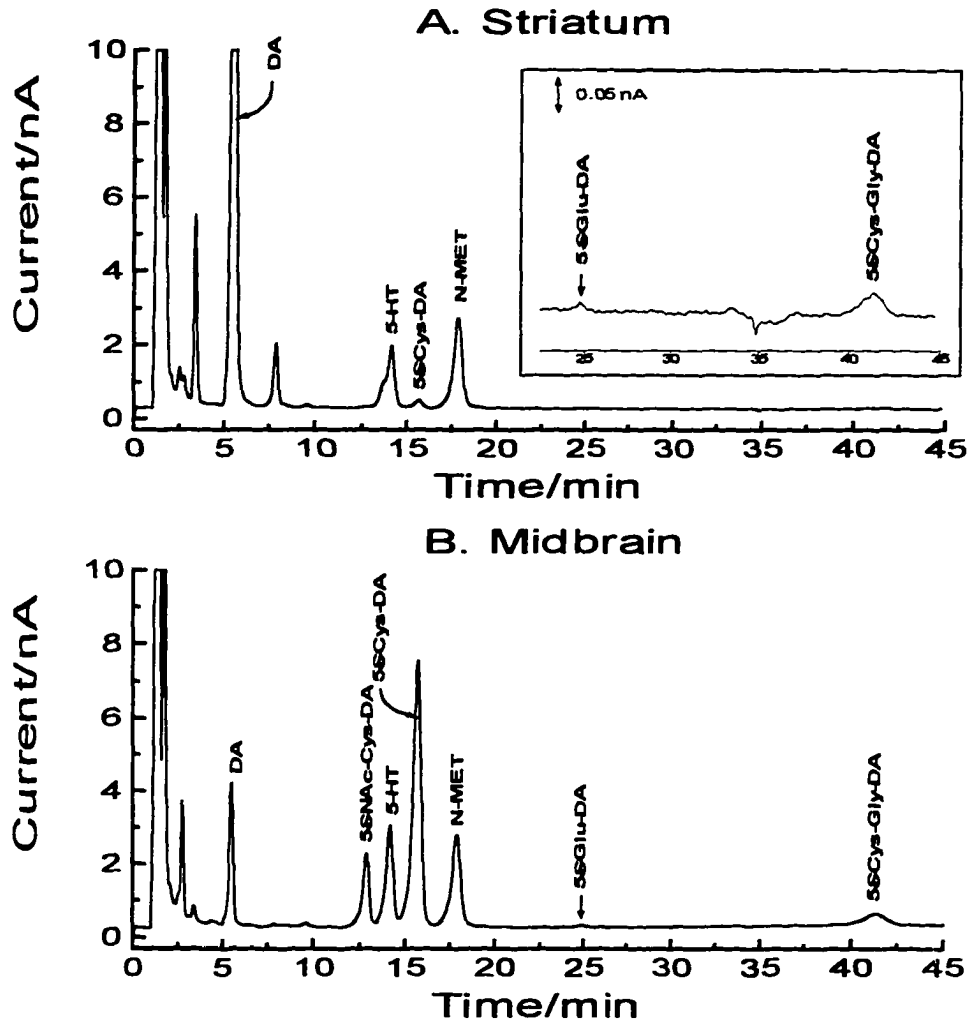

Figure 4.16 5 min after icv administration of 44 nmol (24 μg) 5-*S*-Cys-Gly-DA to rat. (A) striatum, (B) midbrain, (C) hippocampus, (D) cortex and (E) medulla/pons. HPLC method XIII. Injection volume = 5 μL.
(Continued on the next page)

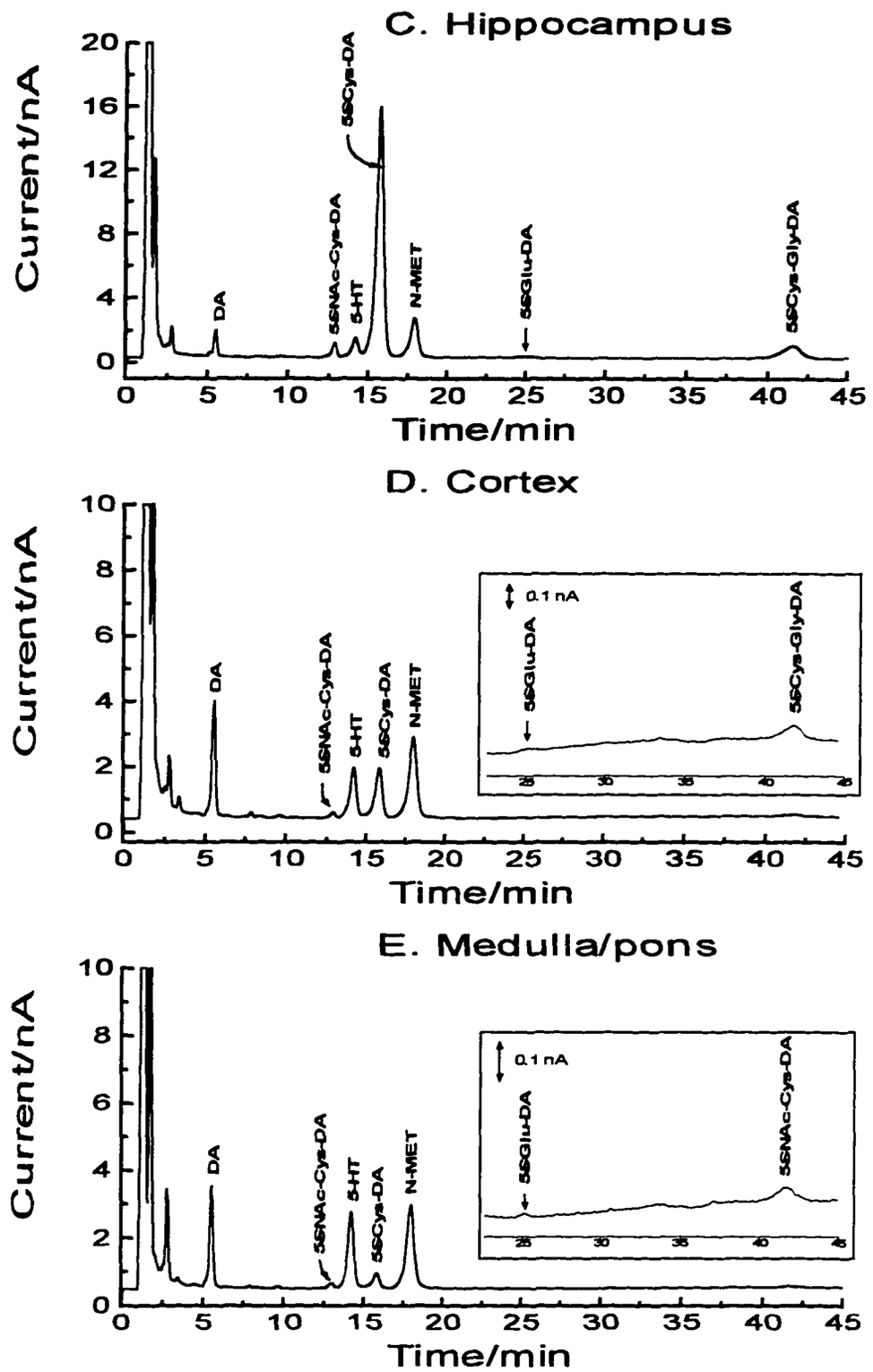

Figure 4.16 (Continued from previous page)
5 min after icv administration of 44 nmol (24 μg) 5-*S*-Cys-Gly-DA to rat. (A) striatum, (B) midbrain, (C) hippocampus, (D) cortex and (E) medulla/pons. HPLC method XIII. Injection volume = 5 μL.

Table 4.2 DA Conjugates (nmol/g) Detected after Icv Administration of 5-*S*-Cys-Gly-DA

	Time/min	5-*S*-NAc-Cys-DA	5-*S*-Cys-Gly-DA	5-*S*-Cys-DA	5-*S*-Glu-DA
Striatum	5	0.00	0.11	0.80	0.00
	30	4.11	0.00	14.88	0.00
	60	4.08	0.00	3.15	0.00
Midbrain	5	7.00	1.55	28.30	4.03
	30	3.50	0.00	2.79	0.00
	60	11.30	0.00	1.25	0.00
Hippocampus	5	3.37	4.01	63.90	0.84
	30	8.58	0.00	32.44	0.00
	60	1.82	0.00	0.16	0.00
Cortex	5	0.58	0.26	6.34	0.04
	30	0.93	0.00	5.61	0.00
	60	0.95	0.00	0.67	0.00
Medulla/pons	5	0.67	0.19	1.88	0.00
	30	1.78	0.00	0.85	0.00
	60	12.36	0.00	5.75	0.00

As expected, 5-*S*-Cys-Gly-DA was metabolized to 5-*S*-Cys-DA and 5-*S*-NAc-Cys-DA through peptidase(s) and cysteinyl conjugate *N*-acetyltransferase. The highest concentration of 5-*S*-Cys-DA was found in the hippocampus (63.9 nmol/g), followed by midbrain (28.3 nmol/g), cortex (6.3 nmol/g), medulla/pons (1.88 nmol/g) and striatum (0.8 nmol/g). 60 min after icv administration of 5-*S*-Cys-Gly-DA, the concentration of 5-*S*-NAc-Cys-DA was found highest in the medulla/pons (12.4 nmol/g), followed by midbrain (11.3 nmol/g), striatum (4.1 nmol/g), hippocampus (1.82 nmol/g) and cortex (0.9 nmol/g).

5-*S*-Glu-DA was detected shortly (5 min) after icv administration of 5-*S*-Cys-Gly-DA in the midbrain, hippocampus and cortex and disappeared with 5-*S*-Cys-Gly-DA.

4.6 Discussion

The experimental results in this chapter demonstrate that 5-*S*-Glu-DA and 2,5-bis-

S-Glu-DA are hydrolyzed to their corresponding cysteinyl conjugates, 5-*S*-Cys-DA and 2,5-bis-*S*-Cys-DA, respectively, in rat brain homogenate at physiological pH (pH = 7.4).

The hydrolysis of glutathionyl conjugates into cysteinyl conjugates involves the removal of the γ-glutamyl group from glutathionyl substituent by γ-glutamyl transpeptidase, followed by the cleavage of glycinyl group from cysteinylglycinyl conjugates of DA by a dipeptidase. The cysteinyl conjugates of DA were *N*-acetylized by cysteine conjugates *N*-acetyltransferase to form *N*-acetylcysteinyl conjugates of DA. The process is illustrated by the hydrolysis of 5-*S*-Glu-DA in Scheme VI below.

Scheme VI

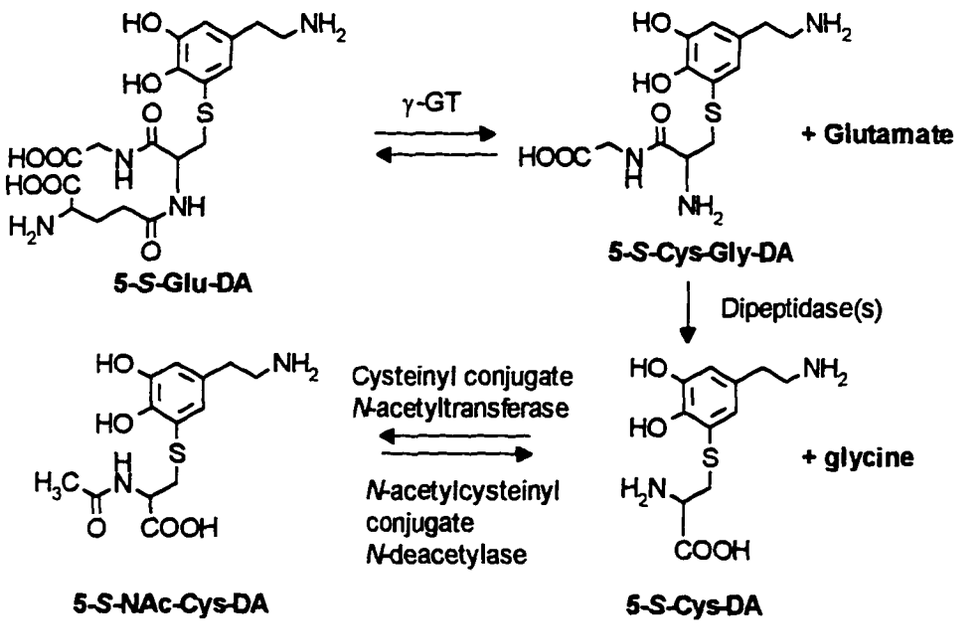

The *in vitro* hydrolysis of 2,5-bis-*S*-Glu-DA had a more complicated process with several metabolites remaining unidentified. Possible metabolites during the hydrolysis of 2,5-bis-*S*-Glu-DA are sketched in Scheme VII, supposing that the first amino acid group to be removed is a glutamyl group. The unidentified chromatographic peaks might have structures among those in Scheme VII.

Scheme VII

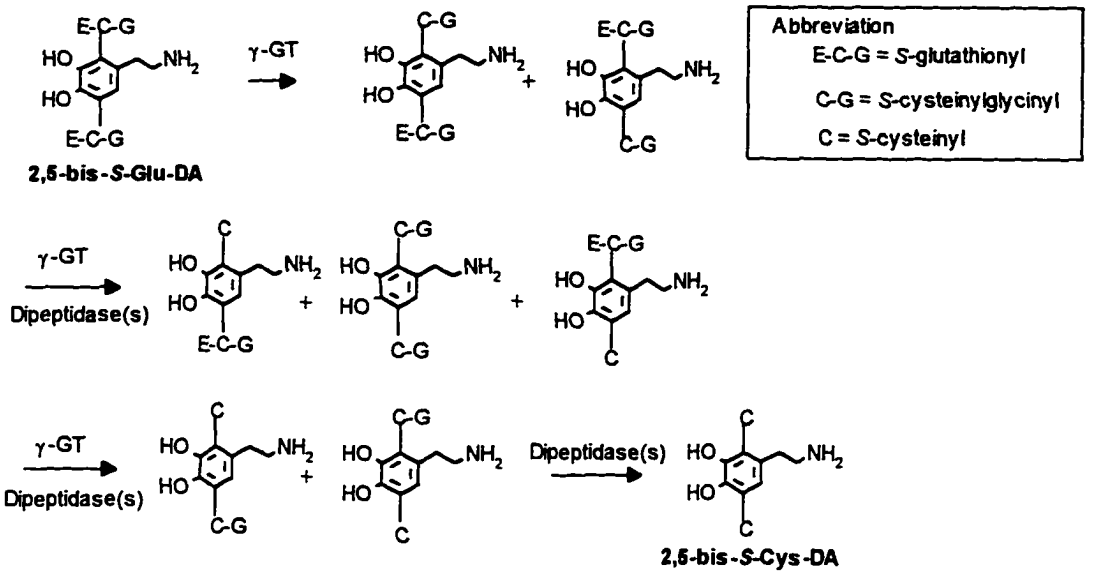

The first step in the metabolism of glutathionyl conjugates of DA is to remove the glutamyl group catalyzed by γ-GT, followed by the removal of a glycinyl moiety from the resulting cysteinylglycinyl conjugate by a dipeptidase[123,124].

When 5-*S*-Cys-Gly-DA was administered into rat brain for 5 min, 5-*S*-Glu-DA was observed in all brain areas, though the concentrations of 5-*S*-Glu-DA were below the quantitative range in some areas (i.e., striatum and cortex). This might be due to the activity of γ-GT. γ-GT is a membrane-bound protein that catalyzes the transfer of the γ-glutamyl group of glutathione and glutathionyl conjugates and other γ-glutamyl peptides to an acceptor molecule. The acceptor molecules may be an animo acids, dipeptides, glutathione itself and water[126]. When 5-*S*-Cys-Gly-DA was administered into the rat brain the local concentration of 5-*S*-Cys-Gly-DA is much higher than the concentration experienced during the hydrolysis of 5-*S*-Glu-DA. Therefore, 5-*S*-Cys-Gly-DA might act as an acceptor of glutamyl group. Finally, the cysteinyl conjugates of DA is *N*-acetylated by cysteinyl conjugates *N*-acetyltransferase.

Other enzymes involved in the hydrolysis of glutathionyl conjugates are cysteinyl conjugate *N*-acetyltransferase and *N*-acetylcysteinyl conjugate deacetylase. However, the activities of these two enzymes were only observed *in vivo* in this study. 5-*S*-Glu-DA was cleared from all brain regions within 60 min. Correspondingly, the concentrations of 5-*S*-Cys-DA reached maximum within 15 min. 5-*S*-Cys-DA was then acetylated to give rise 5-*S*-NAc-Cys-DA. The maximum concentration of 5-*S*-NAc-Cys-DA occurred to be about 15 to 30 min after that of 5-*S*-Cys-DA. The dipeptidyl conjugate of DA, 5-*S*-Cys-Gly-DA was momentarily detected before 5-*S*-Glu-DA was cleared from the brain.

The hydrolysis 5-*S*-Glu-DA into 5-*S*-Cys-DA was confirmed experimentally the first time in this experiment. The only similar experiment carried out in rat brain was the hydrolysis of 5-Glu-α-methyldopamine[96], which is a putative metabolite of 3, 4-(±)-(methylenedioxy)-amphetamine (MDA) and 3,4-(±)-(methylenedioxy)-methamphetamine (MDMA) that do not exit in brain.

The metabolism of glutathionyl conjugates of DA to *N*-acetylcysteinyl conjugates of DA is called the mercapturic acid pathway. This pathway usually occurs at locations with relatively high activities of γ-GT, cysteinylglycine dipeptidase(s), and *N*-acetyl transferases, such as the kidney. The normal function of this pathway is to form the water-soluble metabolites that can be excreted from the body and therefore to detoxify potential toxicants. Whether this is a detoxification process, however, depends on the properties of the metabolites thus formed. In the MDA and MDMA study, the final *N*-acetylcysteinyl conjugates were considered as the reason for the neurotoxic properties of MDA and MDMA. Instead of *N*-acetylation, cysteinyl conjugates of DA may form benzothiazines via the intramolecular cyclization of the cysteinyl conjugates. This is also believed to be a general detoxification process[96]. However, in the case of DA, both the *N*-acetylcysteinyl conjugates and dihydrobenzothiazines are toxic when administered in mouse brain.

Therefore, if the glutathionyl conjugate of DA is formed in brain under certain conditions, it might undergo the hydrolysis process described in this chapter. The further metabolism the cysteinyl conjugate of DA may form toxic metabolites and eventually contribute to the neurodegeneration.

Conclusions

Dopaminergic neurons degenerate in their pigmented cell bodies in the SN of PD patients[80]. The pigmentation occurs as a result of the autoxidation of cytoplasmic DA to DA-*o*-quinone which polymerizes to black neuromelanin[88]. The characteristic biochemical changes include: 1) a massive loss of GSH without a corresponding increase in GSSG (oxidized GSH)[127,128], 2) increased 5-*S*-Cys-DA/DA concentration ratio[83], 3) increased γ-GT activity[129], and 4) the depigmentation of the SN cells. A new hypothesis[89] based on these observations suggests that an elevated γ-GT-mediated translocation of GSH or cysteine into the SN cell bodies is an early step in the pathogenesis of PD. *In vitro* study[89] suggests that cysteine would divert the neuromelanin pathway by scavenging DA-*o*-quinone to form soluble cysteinyl conjugates of DA, causing the depigmentation of the SN cells and an increase of the 5-*S*-Cys-DA/DA concentration ratio. The subsequent autoxidation of cysteinyldopamines would lead to the toxic products which might lead to nigral cell death and PD.

The noradrenergic neurons degenerate in the cell bodies in the LC in PD patients. The noradrenergic neurons that project from LC to the cortex and hippocampus also degenerate in AD patients[130]. The neurodegenerative processes occur in noradrenergic cell bodies in PD but in terminal regions in AD. There is a significant concentration of GSH in terminal regions of noradrenergic neurons. *In vitro* study[97] shows that cysteine would divert the melanin pathway by scavenging NE-*o*-quinone to form soluble cysteinyl conjugates of NE, which are further oxidized to form DHBTs. Among them, DHBT1 and DHBT2 are lethal when administered into the mouse brain[89,90].

Due to the facile oxidation of NE and DA under cytoplasmic autoxidation conditions, the *o*-quinones of NE and DA may be nucleophilically attacked by GSH to give glutathionyl conjugates, which are subsequently hydrolyzed to form cysteinyl conjugates. The cysteinyl conjugates of NE and DA are more easily be oxidized than NE and DA themselves in physiological conditions *in vitro*. Therefore, under the conditions where NE and DA are oxidized, the cysteinyl conjugates of NE and DA would also be oxidized and lead to the formation of a series of toxic products contributing to cell death.

This project studied the *in vitro* oxidation of NE in the presence of GSH at physiological pH. The oxidation conditions included electro-oxidation, autoxidation, hydroxyl radical-mediated oxidation, and superoxide anion radical-mediated oxidation. 2-*S*-Glu-NE and 5-*S*-Glu-NE were formed under all these conditions. In addition, 2,5-bis-*S*-Glu-NE and 2,5,6-tris-*S*-Glu-NE were formed under electro-oxidation and hydroxyl radical-mediated oxidation conditions. All these products were purified and structurally identified.

The metabolisms of glutathionyl conjugates of NE and DA were studied under both *in vitro* and *in vivo* conditions. Glutathionyl conjugates of NE and DA were converted to cysteinyl conjugates *in vitro* in whole rat brain homogenates at physiological pH. Cysteinyl conjugates of NE and DA were metabolized to cysteinylglycinyl conjugate, cysteinyl conjugates and *N*-acetylcysteinyl conjugates of NE and DA *in vivo* after icv administration of glutathionyl conjugates to rats. The formation of glutathionyl conjugates and the subsequent conversion of glutathionyl conjugates to cysteinyl conjugates and finally to *N*-acetylcysteinyl conjugates is called mercapturic acid pathway[126]. It is considered as a detoxification process. However, recent study[125] showed

that *N*-acetylcysteinyl conjugates of DA were toxic when administered into mouse brain.

In summary, the autoxidation of NE and DA in noradrenergic and dopaminergic neurons might be diverted by the nucleophilic attack of GSH and/or cysteine to form glutathionyl and/or cysteinyl conjugates of NE and DA, respectively. If glutathionyl conjugates of NE and DA could be formed under certain abnormal conditions such as oxidative stress, they may be metabolized to form the corresponding cysteinyl conjugates. Further metabolism of the cysteinyl conjugates may form *N*-acetylcysteinyl conjugates through enzyme-mediated reactions and might form DHBTs through cytoplasmic autoxidation. These metabolites together might represent endotoxins that contribute to the degeneration of noradrenergic and dopaminergic neurons in AD and PD patients.

References

1 J. D. Adams, Jr., L. K. Klaidman, I. N. Odunze, H. C. Shen and C. A. Miller. *Mol. Chem. Neuropathol.*, **14**, 213-226, (1991).

2 J. Parkinson. In: An Essay on the Shaking Palsy. London, Sherwood, Neely & Jones, p66, (1817).

3 J. D. Adams and N. Odunze. *Free Radical Biol. Med.*, **10**, 161-169, (1991).

4 A. H. V. Schapira. *Neuropathol. Appl. Neurobiol.*, **21**, 3-9, (1995).

5 L. S. Forno. *J. Neuropathol. Exp. Neurol.*, **55**, 259-272, (1996).

6 W. A. G. Gibb and A. J. Lees. *J. Neurol. Neurosurg. Psych.*, **54**, 388-96, (1991).

7 J. M. Fearnley and A. J. Lees. *Brain*, **114**, 2283-301, (1991).

8 Y. Agid, F. Jayoy-Agid, and M. Ruberg. In: C. D. Marsden and S. Fahn, Eds. London: Butterworths, 199-230, (1987).

9 A. Alzheimer. *Allg. Z. Psychiat.*, **64**, 146-148, (1907).

10 B. A. Yankner and M. -M. Mesulam. *New Engl. J. Med.*, **325**, 1849-1857, (1991).

11 A. Dresse, D. Marechal, J. Scuvee-Moreau, and V. Seutin. *Life Sci.*, **55**, 2179-2187, (1994).

12 T. Miyakawa, A. Shimoji, R. Kuramoto, and Y. Higuchi. *Virchows Arch.*, **B40**, 121-129, (1982).

13 M. Kidd, *Nature*, **197**, 192-193, (1963).

14 D. M. A. Mann. In: Psychopharmacology of the Aging Nervous System. L. L. Iversen and S. H. Snyder. Eds., Plenum Press, New York, p1-67, (1988).

15 D. C. German, C. L. White, and D. R. Sparkman. *Neurosci.*, **21**, 305-312, (1987).

16 D. M. A. Mann, P. O. Yates, and B. Marcyniuk. *J. Neurol. Neurosurg. Psych.*, **50**, 341-344, (1987).

17 D. M. A. Mann, J. Lincoln, P. O. Yates, J. E. Stamp, and S. Toper. *Br. J. Psychiatry*, **136**, 533-541, (1980).

18 W. Bondareff, C. Q. Mountjoy, and M. Roth. *Neurology*, **32**, 164-168, (1982).

19 P. Davies and A. J. F. Maloney. *Lancet*, **2**, 1403, (1976).

20 M. Schorderet. *Experientia*, **51**, 99-105, (1995).

21 R. C. Duviosin. *Adv. Neurol.*, **69**, 33-40, (1996).

22 D. J. Selkoe. *Science*, **275**, 630-631, (1997).

23 D. E. Wisniewski, A. J. Dalton, D. R. Crapper-Mclachlan, G. Y. Wen, and H. M. Wisniewski. *Neurology*, **35**, 957-961, (1985).

24 D. A. M. Mann. *Mech. Age Dev.*, **43**, 99-136, (1988).

25 J. T. Jarrett, E. P. Berger, and P. T. Lansbury Jr.. *Biochemistry*, **32**, 4693, (1993).

26 M. Citron et. al., *Nature*, **360**, 672, (1992).

27 X.-D. Cai, T.E. Golde, and S. G. Younkin. *Science*, **259**, 514, (1993).

28 W. J. Strittmatter, A. M. Saunders, D. Schmechel, M. Pericak-Vance, J. Enghild, G. S. Slvesen, and A. D. Roses. *Proc. Natl. Acad. Sci. U. S. A.*, **90**, 1977-1981, (1993).

29 G. Uterman. *Curr. Biol.*, **4**, 362-365, (1994).

30 M. A. Pericak-Vance, J. L. Bebout, P. C. Gaskell, Jr., L. H. Yamaoka, W. Y. Hung, M. J. Alberts, A. P. Walker, R. J. Bartlett, C. A. Haynes, K. A. Welsh, N. L. Earl, A. Heyman, C. M. Clark, and A. D. Roses. *Am J. Hum. Genet.*, **49**, 1034-1050, (1991).

31 T. Wisnieski and B. Frangione. *Neurosci. Lett.*, **135**, 235-238, (1992).

32 R. Sherrngton, et al, *Nature*, **375**, 754, (1995).

33 E. Levy-Lahad, et al, *Science*, **269**, 973, (1995).

34 D. Scheuner, et al., *Nature Med.*, **2**, 864, (1996).

35 G. Thinakaran, et al., *Neuron*, **17**, 181, (1996).

36 K. Duff, et al., *Nature*, **383**, 710, (1996).

37 M. C. Royston, N. J. Rothwell and G. W. Roberts. *Trends pharmac. Sci.*, **13**, 131-133, (1993).

38 K. F. Tipton. *Environmental Biochem.*, **23**, 429-435, (1995).

39 C. M. Tanner. *Trends Neurosci.*, **12**, 49-54, (1989).

40 B. S. Schoenberg, B. O. Osuntokun, A. O. G. Adeuja, O. Bademosi, V. Nottidge, D. W. Anderson, and A. F. Haerer. *Neurology*, **38**, 645-646, (1988).

41 A. H. Rajput, K. P. Offord, C. M. Beard, and L. T. Kurtland. *Ann. Neurol.*, **16**, 278-282, (1984).

42 G. C. Davis, A. C. Williams, S. P. Markey, M. H. Ebert, E. D. Caine, C. M. Reichert, and I. J. Kopin. *Psychiatry Res.*, **1**, 249-254, (1979).

43 J. W. Langston, P. Ballard, J. W. Tetrud, and I. Irwin. *Science*, **219**, 979, (1983).

44 P. A. Ballard, J. W. Tetrud, and J. W. Langston. *Neurology*, **35**, 949, (1985).

45 R. S. Burns, C. C. Chiueh, S. P. Markey, M. H. Ebert, D. M. Jacobowits, and I. J. Kopin. *Proc. Natl. Acad. Sci. U.S.A.*, **80**, 4546-4550, (1983).

46 K. Chiba, A. J. Trevor, and N. Castagnoli Jr.. *Biochem. Biophys. Res. Commun.*, **120**, 547, (1984).

47 J. A. Javitch, R. J. D'Amato, S. M. Strittmatter, and S. H. Snyder. *Proc Natl*

Acad. Sci. U.S.A., **82**, 2173, (1985).

48 I. Irwin and J. W. Langston. *Life Sci.*, **36**, 207, (1985).

49 A. H. V. Schapira, V. M. Mann, J. M. Cooper, D. Dexter, S. E. Daniel, P. Jenner, J. B. Clark, and C. D. Marsden. *J. Neurochem.*, **55**, 2142-2145, (1990).

50 W. J. Nicklas, I. Vyas, and R. E. Heikkila. *Life Sci.*, **36**, 2503, (1985).

51 R. R. Ramsay, J. I. Salach, J. Dadgar, and T. P. Singer. *Biochem. Biophys. Res. Commun.*, **135**, 269, (1986).

52 S. S. Krisnan, D. R. McLachlan, B. Krisnan, et al. *Sci. Total Environ.*, **71**, 59-64, (1988).

53 D. P. Wills and A. R. Brody. *Science*, **208**, 297-299, (1980).

54 J. D. Birchall and J. S. Chappell. *Lancet*, **2**, 1008-1010, (1988).

55 R. A. Armstrong, S. J., Winsper. and J. A. Blair, *Dementia*, 7, 1-9, (1996).

56 A. C. Bowling and M. F. Beal. *Life Sci.*, **56**, 1151-1171, (1995).

57 C. W. Olanow. *Ann. Neurol.*, **32 Suppl.**, S2-9, (1992).

58 N. A. Simonian and J. T. Coyle. *Annu. Rev. Pharmacol. Toxicol.*, **36**, 83-106, (1996).

59 L. Oreland. *Acta Neurol. Scand.*, **81(Suppl 136)**, 60-65, (1991).

60 J. M. McCord and I. Fridovich. *J. Biol. Chem.*, **244**, 6049-6055, (1969).

61 G. Cohen, In: Handbook of Neurochemistry, A. Lajtha, Ed., Plenum Press, New York, pp315-330, (1985).

62 M. B. Spina, and G. Cohen. *Proc. Natl. Acad. Sci. U.S.A.*, **86**, 1398-1400, (1989).

63 F. Harber and J. Weiss. *Proc. R. Soc. Lond. (A)*, **147**, 332-351, (1934).

64 R. J. Marttila, H. Lorentz, and U. K. Rinne. *J. Neurol. Sci.*, **86**, 321, (1988).

65 H. Saggu, J. Cooksey, D. Dexter, F. R. Wells, A. Lees, P. Jenner, and C. D. Marsden. *J. Neurochem.*, **53**, 69, (1989).

66 D. T. Dexter, C. J. Carter, F. R. Wells, et al. *J. Neurochem.*, **52**, 381, (1989).

67 M. B. H. Youdim, D. Ben-Shachar, and P. Riederer. *Acta Neurol. Scand.*, **126**, 47, (1989).

68 E. Sofic, K. W. Lange, K. Jellinger, and P. Riederer. *Neurosci. Lett.*, **142**, 128-130, (1992).

69 J. Sian, D. T. Dexter, A. J. Lees, et al. *Ann. Neurol.*, **36**, 348, (1994).

70 J. A. Imlay and S. Linn. *Science*, **240**, 1302-1309, (1988).

71 S. P. Wolff, A. Garner and R. T. Dean. *Trends Biol. Sci.*, **11**, 27-31, (1986).

72 G. Minotti and S. D. Aust. *Chem. Phys. Lipids*, **44**, 191-208, (1987).

73 M. P. Mattson and Y. Goodman. *Brain Res.*, **676**, 219-24, (1995).

74 C. Behl, J. B. Davis, R. Lesley, and S. Schubert. *Cell*, 77, 817-827, (1994).

75 C. Café, C. Torri, L. Bertorelli, N. Angeretti, E. Lucca, G. Forloni, and F. Marzatico. *Neurosci. Lett.*, **203**, 61-65, (1996).

76 J. S. Richardson, Y. Zhou, and U. Kumar. *Ann. N. Y. Acad. Sci.*, 777, 362-367, (1996).

77 M. B. H. Youdim. *Mt. Sinai J. Med.*, **55**, 97-101, (1988).

78 P. F. Good, D. P. Perl, L. M. Bierer, and J. Schmeideer. *Ann. Neurol.*, **31**, 286-292, (1992).

79 J. G. Greenfield and F. D. Boasanquet. *J. Neurol. Neurosurg. Psychiatry*, **16**, 213-226, (1957).

80 O. Hornykiewicz and S. J. Kish. *Adv. Neurol.*, **45**, 19-34, (1986).

81 P. Reiderer, E. Sofic, W. D. Rausch, B. Schmidt, G. Reynolds, K. Jellinger, and M. B. H. Youdim. *J. Neurochem.*, **52**, 515-520, (1989).

82 P. Jenner. *Acta Neurol. Scand.*, **87** (Suppl. 146), 6-13, (1993).

83 B. Fornstedt, A. Brun, E. Rosengren, and A. Carlsson. *J. Neural. Transm. Park. Dis. Dement. Sect.*, **1**, 279-295, (1989).

84 E. C. Hirsch, A. M. Graybiel, and Y. Agid. *Nature*, **334**, 345-348, (1988).

85 A. Kastner, E. C. Hirsch, O. Lejeune, F. Javoy-Agid, O. Rascol, and Y. Agid. *J. Neurochem.*, **59**, 1080-1089, (1992).

86 E. C. Hirsch. *Ann. Neurol.*, **32**, S88-S93, (1992).

87 D. M. A. Mann and P. O. Yates. *Mech. Ageing Dev.*, **21**, 193-203, (1983).

88 D. G. Graham. *Mol. Pharmacol.*, **14**, 633-643, (1978).

89 F. Zhang and G. Dryhurst. *J. Med. Chem.*, **37**, 1084-1098, (1994).

90 X.-M. Shen and G. Dryhurst. *Chem. Res. Toxicol.*, **9**, 751-763, (1996).

91 F. Zhang and G. Dryhurst. *J. Electroanal. Chem. Interfacial Electrochem.*, **398**, 117-128, (1995).

92 B. Scatton, F. Javoy-Agid, L. Rouquier, B. Dubois, and Y. Agid. *Brain Res.*, **275**, 321-328, (1983).

93 J. A. Hardy, D. M. A. Mann, P. Wester, and B. Winblad. *Neurobiol. Ageing*, **7**, 489-502, (1986).

94 P. Jenner, A. H. V. Schapira, and C. D. Marsden. *Neurology*, **42**, 2241-2250, (1992).

95 J. J. Liccione and M. D. Maines. *J. Pharmacol. Exp. Ther.*, **247**, 156-161, (1988).

96 R. T. Miller, S. S. Lau, and T. J. Monks. *Chem. Res. Toxicol.*, **8**, 634-641, (1995).

97 X.-M. Shen and G. Dryhurst. *J. Med. Chem.*, **39**, 2018-2029, (1996).

98 G. D. Christian and W. C. Purdy. *J. Electroanal. Chem. Interfacial Electrochem.*, **3**, 363, (1962).

99 F. Zhang, R. N. Goyal, C. L. Blank, and G. Dryhurst. *J. Med. Chem.*, **35**, 82-93, (1993).

100 D. C. S. Tse, R. L. McCreery, and R. N. Adams. *J. Med. Chem.*, **19**, 37-40, (1976).

101 C. D. Smith, J. M. Carney, P. E. Starke-Reed, C. N. Oliver, E. R. Stadman, R. A. Foyd, and W. R. Markesbery. *Proc. Nat. Acad. Sci. U.S.A.*, **88**, 10540-10543, (1991).

102 B. Halliwell. *Ann. Neurol.*, **32**, S10-S15, (1992).

103 J. M. C. Gutteridge. *FEBS Lett.*, **201**, 291-295, (1986).

104 S. V. Kala, B. B. Hasinoff, and J. S. Richardson. *Int. J. Neurosci.*, **86**, 263-269, (1996).

105 S. Udenfriend, C. T. Clark, J. Axelrod, and B. B. Brodie. *J. Biol. Chem.*, **208**, 731, (1954).

106 R. Chander, N. K. Kapoor, and B. N. Dhawan. *Biochem. Pharmacol.*, **44**, 180-183, (1992).

107 B. Halliwell, J. M. C. Gumeridge, in Methods in Enzymology, S. P. Colowick and N. O. Kaplan Eds., Vol. 105, pp 47-56, (1984).

108 A. H. V. Schapira, A. Hartley, M. W. J. Cleeter, and J. M. Cooper. *Biochem. Soc. Trans.*, **21**, 367, (1993).

109 M. Markert, P. C. Andrews, and B M. Babior. *Methods Enzymol.* **105**, 356-365,

(1984).

110 A. Boveris and B. Chance. *Biochem. J.*, **134**, 707-716, (1973).

111 S. C. Salaris, C. F. Babbs, and W. D. Voorhees III. *Biochem. Pharmacol.*, **42**, 499-506, (1991).

112 D. A. Parks and D. N. Granger. *Acta Physiol. Scand. [Suppl]*, **548**, 87-99, (1986).

113 I. Fridovich. *J. Biol. Chem.*, **245**, 4053-4057, (1970).

114 R. C. Bray, in The Enzymes, D. P. Boyer, Ed., Vol. XII, part B, pp. 300-419, Academic Press, New York, (1975).

115 R. Hille and V. Massey. *J. Biol. Chem.*, **256**, 9090-9095, (1981).

116 A. G. Porras, J. S. Olson, and G. Palmer. *J. Biol. Chem.*, **256**, 9096-9103, (1981).

117 H. J. Freisleben and L. Packer. *Biochem. Soc. Trans.*, **21**, 325, (1993).

118 T. P. A. Devasagayam, A. R. Sundquist, P. D. Mascio, S. Kaiser, and H. Sies. *J. Photochem. Photobiol. B: Biol.*, **9**, 105, (1991).

119 A. Meister. *J. Biol. Chem.*, **269**, 9397, (1994).

120 D. P. Perl and P. F. Good. *Ann. Neurol.*, **32** (Suppl.), S76-S81, (1992).

121 E. J. Corey, M. M. Mehrotra, and A. U. Khan. *Biochem. Biophys. Res. Commun.*, **145**, 842-846, (1987).

122 M. Athar, H. Mukhtar, C. A. Elmets, M. T. Zaim, J. R. Lloyd, and D. R. Bickers. *Biochem. Biophys. Res. Commun.*, **151**, 1054-1059, (1988).

123 T. M. McIntyre and N. P. Curthoys. *J. Biol. Chem.*, **257**, 11915-11921, (1982).

124 E. Kozak and S. S. Tate. *J. Biol Chem.*, **257**, 6322-6327, (1982).

125 X.-M. Shen, B. Xia, M. Z. Wrona, and G. Dryhurst. *Chem. Res. Toxicol.*, **9**, 1117-1126, (1996).

126 C. A. Hinchman and N. Ballatori. *J. Toxicol. Environ. Health*, **41**, 387-409, (1994).

127 P. Riederer, E. Sofic, W. D. Rausch, B. Schmidt, G. Reynolds, K. Jellinger, and M. B. H. Youdim. *J. Neurochem.*, **52**, 515-520, (1989).

128 E. Sofic, K. W. Lange, K. Jellinger, and P. Riederer. *Neurosci. Lett.*, **142**, 128-130, (1992).

129 J. Sian, D. T. Dexter, P. Jenner, and C. D. Marsden. *Br. J. Pharmacol. (Suppl.)*, **107**, 429P, (1992).

130 B. Marcyniuk, D. M. A. Mann, and P. O. Yates. *J. Neurol. Sci.*, **76**, 335-345, (1986).

Appendix A Synthesis and Cyclic Voltammetric Study of 5-*S*-(*N*-Acetylcysteinyl)norepinephrine (5-*S*-NAc-Cys-NE) and 5-*S*-Cysteinylglycinylnorepinephrine (5-*S*-Cys-Gly-NE)

A.1 Synthesis of 5-*S*-NAc-Cys-NE

5 mg NE•HCl (24 mmol) was dissolved in 25 mL of 0.1 M HCl. The resulting solution was electrolyzed at 1.0 V for 60 minutes. NE was converted into NE-*o*-quinone and the solution turned a dark brown in color. Upon addition of 20 mg *N*-acetylcysteine, the solution turned colorless. The reaction solution was injected directly into a preparative HPLC system. HPLC method IV was employed and 2-*S*-NAc-Cys-NE and 5-*S*-NAc-Cys-NE eluted at retention times of 22.9 and 26.2 min, respectively, with a ratio of 2:5. 5-*S*-NAc-Cys-NE was collected by repeating the same procedure several times and freeze-dried. The resulting solid was dissolved in a minimum amount of deionized water and was purified (desalting) by HPLC method VI. The purified eluent was collected and freeze-dried.

5-*S*-NAc-Cys-NE was a white solid compound and in PBS (pH = 7.4, μ = 1.0), it exhibited UV bands at λ_{max},nm (log $\varepsilon_{max}/M^{-1}cm^{-1}$): 256 (3.77) and 292 (3.57) (Figure B.23 in Appendix B). FAB-MS (thioglycerol/glycerol matrix) gave m/e = 331.0935 (MH^{+1}, 14.6%, $C_{13}H_{19}N_2O_6S$; calculated m/e = 331.09638) (Figure B.24 in Appendix B). ^1H NMR (D_2O)

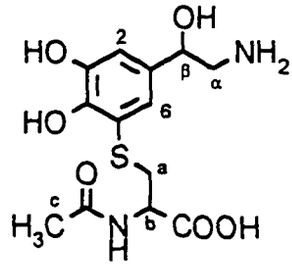

5-*S*-NAc-Cys-NE

gave δ: 6.84 (d, $J_{2,6}$ = 2.4 Hz, 1H, C(2)-H), 6.73 (d, $J_{2,6}$ = 2.4 Hz, 1H, C(6)-H), 4.69-4.65 (m, 1H, C(β)-H), 4.12-4.08 (m, 1H, C(b)-H), 3.26-3.20 (m, 1H, C(a)-H), 3.10-2.90 (m, 3H, C(a)-H, C(α)-H_2), 1.68 (s, 3H, C(c)-H_3) (Figure B.21 and B.22 in Appendix B).

A.2 Cyclic voltammetry of 5-*S*-NAc-Cys-NE

A cyclic voltammogram (v = 100 mVs^{-1}) of 5-*S*-NAc-Cys-NE at PBS (pH = 7.4, μ = 1.0) exhibited two oxidation peaks I_a (E_P = 126 mV) and II_a (E_P = 570 mV) on the initial anodic sweep. After scan reversal, reduction peak I_c (E_P = 94 mV) formed a reversible couple with oxidation peak I_a. At more negative potentials, reduction peak III_c (E_P = – 238 mV) formed a reversible couple with oxidation peak III_a (E_P = – 212 mV)

Scheme VIII

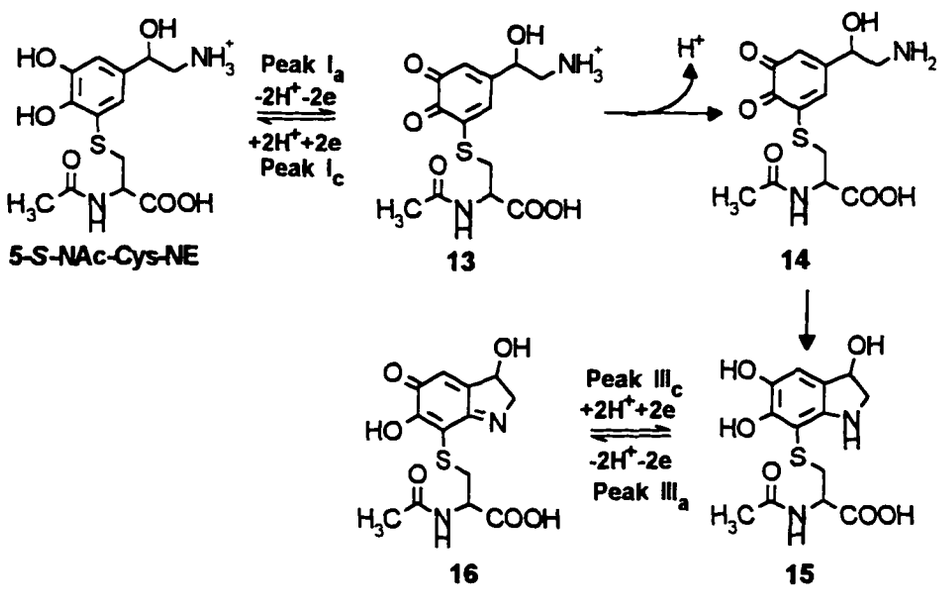

which appeared on the second anodic sweep (Figure 3.1 A). Peak I_a corresponds to the oxidation of 5-*S*-NAc-Cys-NE to 5-*S*-NAc-Cys-NE *o*-quinone (**13**) during the initial

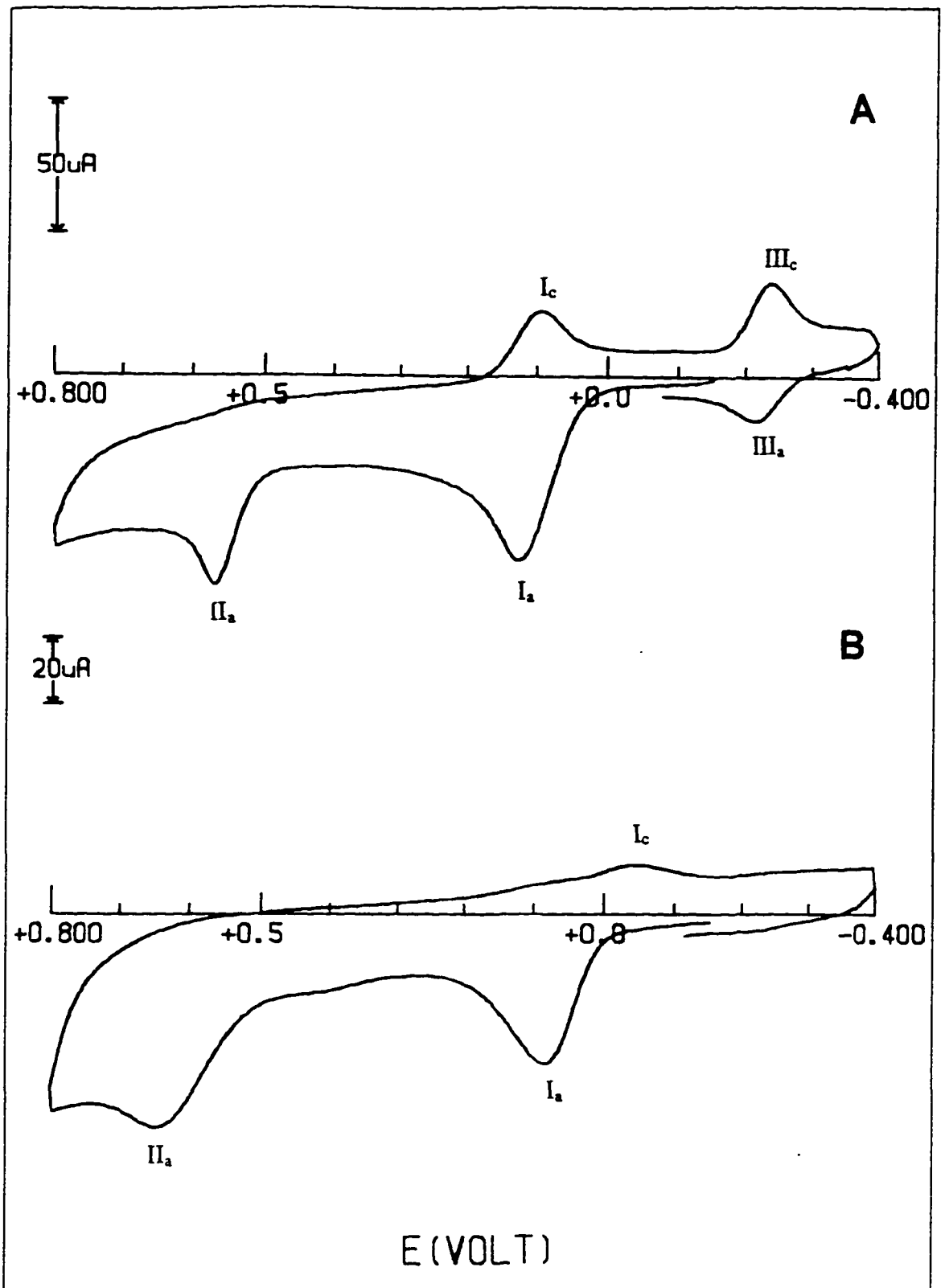

Figure A.1 Cyclic voltamograms of 0.5 mM A) 5-*S*-NAc-Cys-NE and B) 5-*S*-Cys-Gly-NE in PBS (pH = 7.4, μ = 1.0). Sweep rate = 100 mVs^{-1}.

anodic scan (Scheme V), while peak I_c corresponds to the **13**. Compound **13** deprotonates to compound **14**, which undergoes intramolecular cyclization to form indoline **15**. Further chemical oxidation of the indoline **15** by **13** may yield aminochrome **16**. The proximate products of **15/16** couple are responsible for the peak III_c/peak III_a (Scheme V). However, the oxidation reaction corresponding to peak II_a is unknown and remained to be further investigated[96,119].

A.3 Synthesis of 5-*S*-Cys-Gly-NE

5 mg NE•HCl (24 mmol) was dissolved in 25 mL of 0.1 M HCl. The resulting solution was electrolyzed at 1.0 V for 60 minutes. NE was converted into NE-*o*-quinone and the solution turned dark brown in color. Upon addition of 22 mg L-cysteinylglycine (124 mmol), the solution turned to colorless. The reaction solution was injected into preparative HPLC system, using HPLC method V. 2-*S*-Cys-Gly-NE and 5-*S*-Cys-Gly-NE were eluted at retention times of 20.9 and 24.3 minutes, respectively, with a peak area ratio of 1:4. 5-*S*-Cys-Gly-NE was collected by repeating the same procedure several times and freeze-dried. The resulting solid was dissolved in a minimum amount of deionized water and was purified using HPLC method VI. The purified eluent was collected and freeze-dried.

5-*S*-Cys-Gly-NE was a white solid and in PBS (pH = 7.4, μ = 1.0), it exhibited UV bands at λ_{max},nm (log $\varepsilon_{max}/M^{-1}cm^{-1}$): 252 sh (3.49), 296 (3.26) and 316 sh (2.89) (Figure B.27 in Appendix B). FAB-MS (thioglycerol/glycerol matrix) gave m/e = 346.1044 (MH^{+1}, 3.5%, $C_{13}H_{20}N_3O_6S$; calculated m/e = 346.1073) (Figure B.28 in

Appendix B). ^{1}H NMR (D_2O) gave δ: 7.02 (d, $J_{2,6}$ = 2.1 Hz, 1H, C(2)-H), 6.90 (d, $J_{2,6}$ = 2.1 Hz, 1H, C(6)-H), 4.83-4.81 (m, 1H, C(β)-H), 4.19-4.16 (m, 1H, C(b)-H), 3.60-3.54 (m, 1H, C(a)-H), 3.44-3.31 (m, 5H, C(a)-H, C(α)-H_2, C(c)-H_2) (Figure B.25 and B.26 in Appendix B).

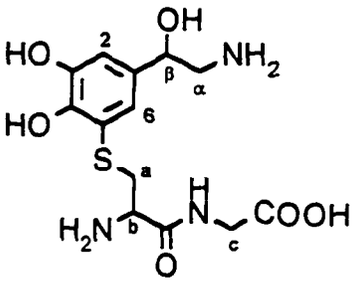

5-*S*-Cys-Gly-NE

A.4 Cyclic voltammetry of 5-*S*-Cys-Gly-NE

A cyclic voltammogram (v = 100 mVs^{-1}) of 5-*S*-Cys-Gly-NE at PBS (pH = 7.4, μ = 1.0) exhibited two oxidation peaks I_a (E_P = 90 mV) and II_a (E_P = 634 mV) on the initial anodic sweep. After scan reversal, reduction peak I_c (E_P = – 50 mV) formed a quasi-reversible couple with oxidation peak I_a. There was no more peaks at more negative potentials during the scan reversal and second anodic sweep (Figure 3.1 B). Peak I_a corresponds to the oxidation of 5-*S*-Cys-Gly-NE to its *o*-quinone intermediate **17** (Scheme VI) while peak I_c corresponds to the reduction **17** back to 5-*S*-Cys-Gly-NE. Compound **18** might have undergone intramolecular cyclization to *o*-quinone imine to **18**, which ultimately converted into dihydrobenzenethiazine **20**[96]. The difference of the cyclic voltammetric behaviors between 5-*S*-NAc-Cys-NE and 5-*S*-Cys-Gly-NE depends on the different ways of intramolecular cyclization. During the oxidation process, 5-*S*-Cys-Gly-NE utilizes the cysteine moiety for the intramolecular cylization. In contrast, 5-*S*-NAc-Cys-NE, with the amino group on the cysteine moiety protected by an acetyl group, utilizes the side chain on NE moiety for the intramolecular cyclization.

Scheme IX

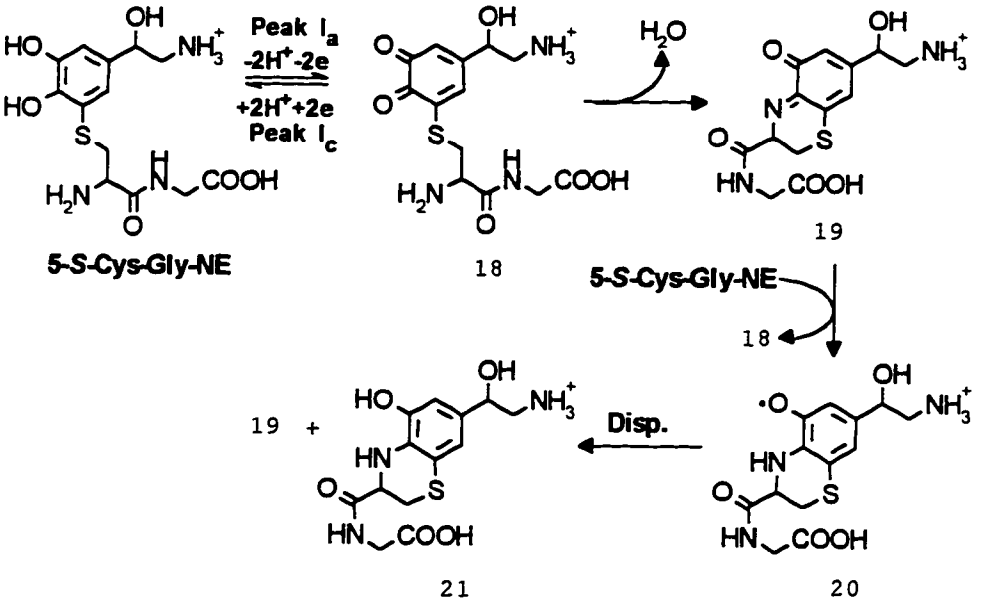
Peak I_a
$-2H^+-2e$
$+2H^++2e$
Peak I_c
5-S-Cys-Gly-NE
18
19
5-S-Cys-Gly-NE
18
Disp.
19 +
21
20

Appendix B NMR (^{1}H and COSY), UV-Vis and MS Spectra

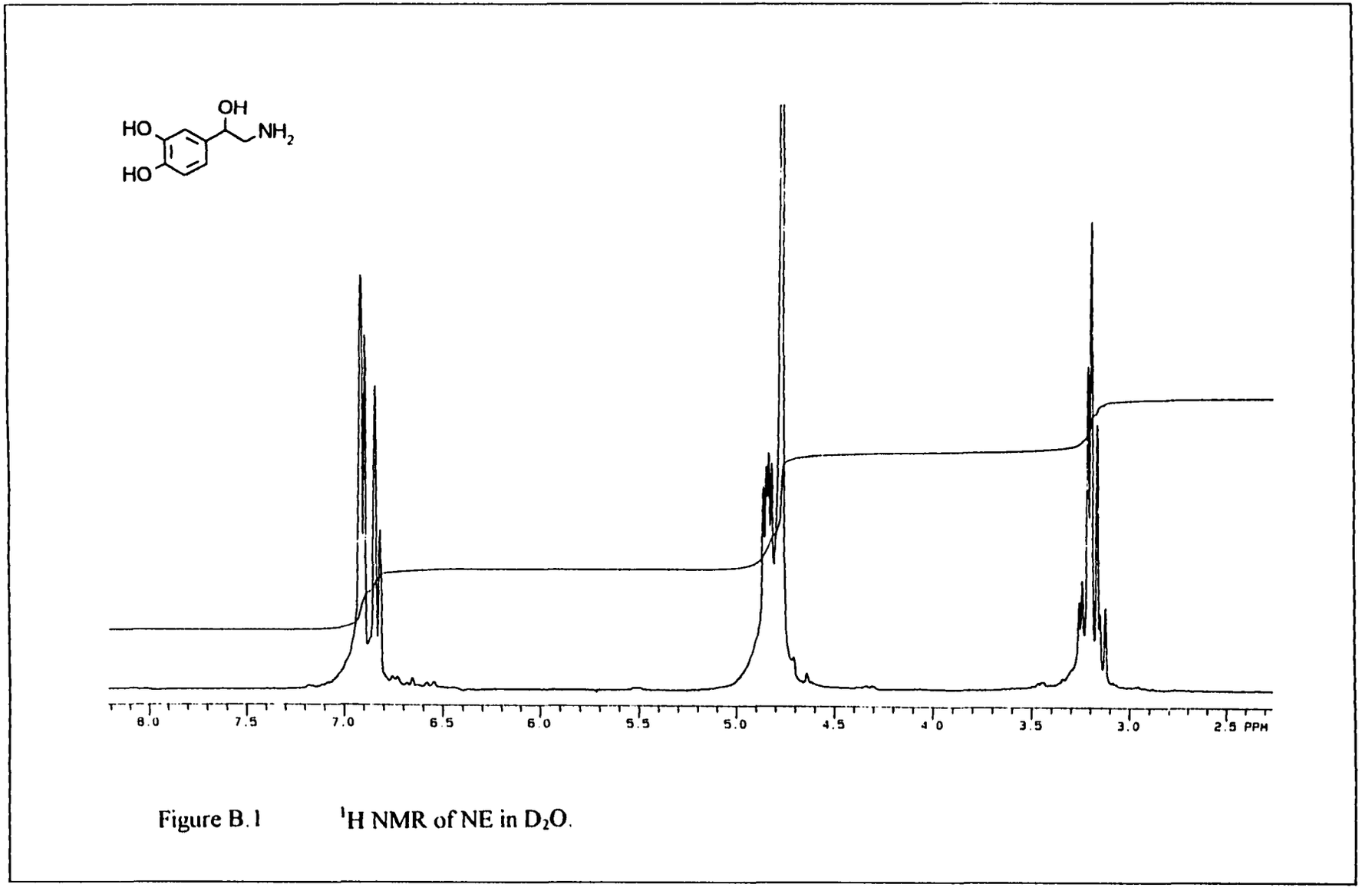

Figure B.1 ^{1}H NMR of NE in D_2O.

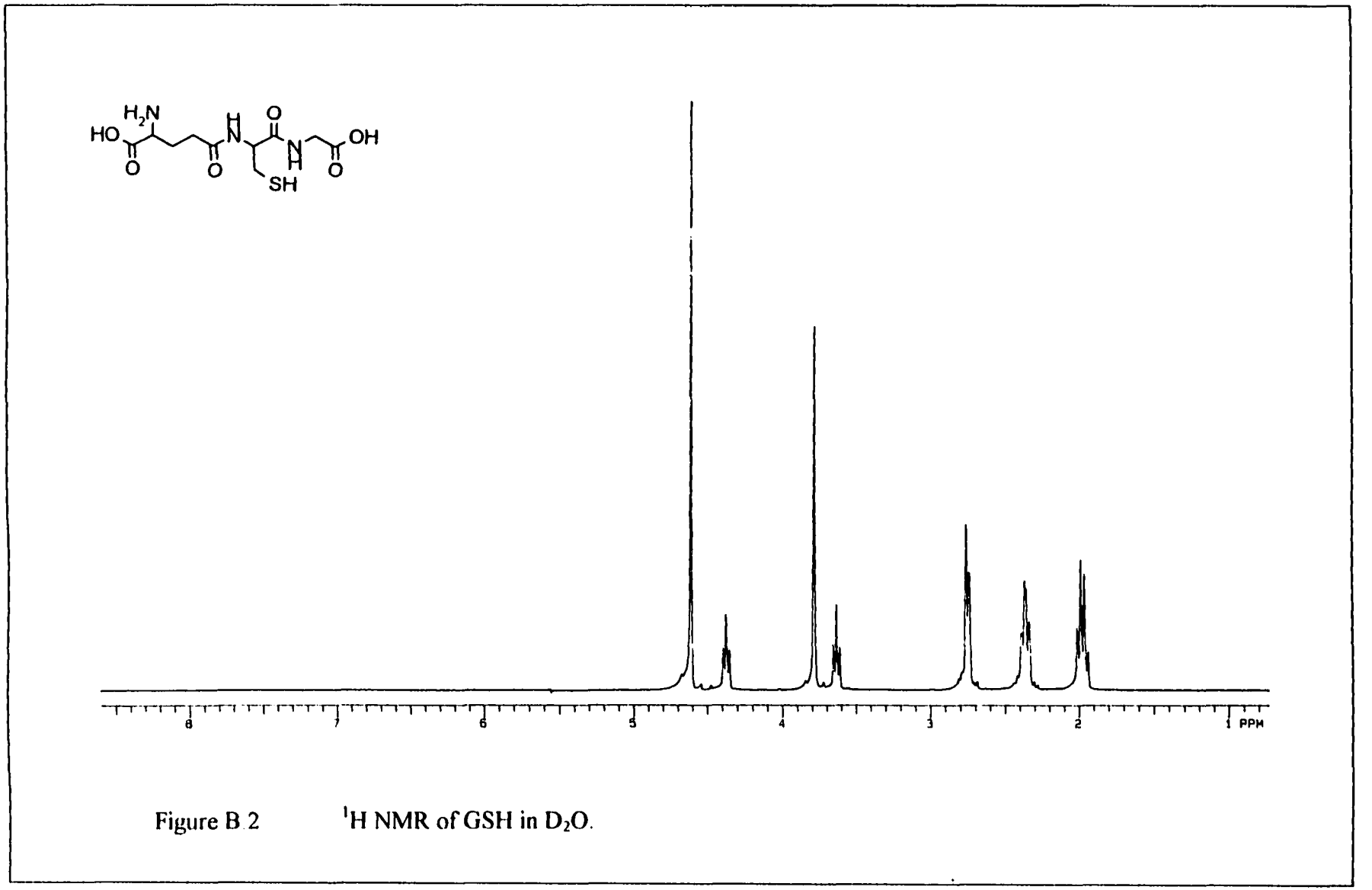

Figure B.2 ^{1}H NMR of GSH in D_2O.

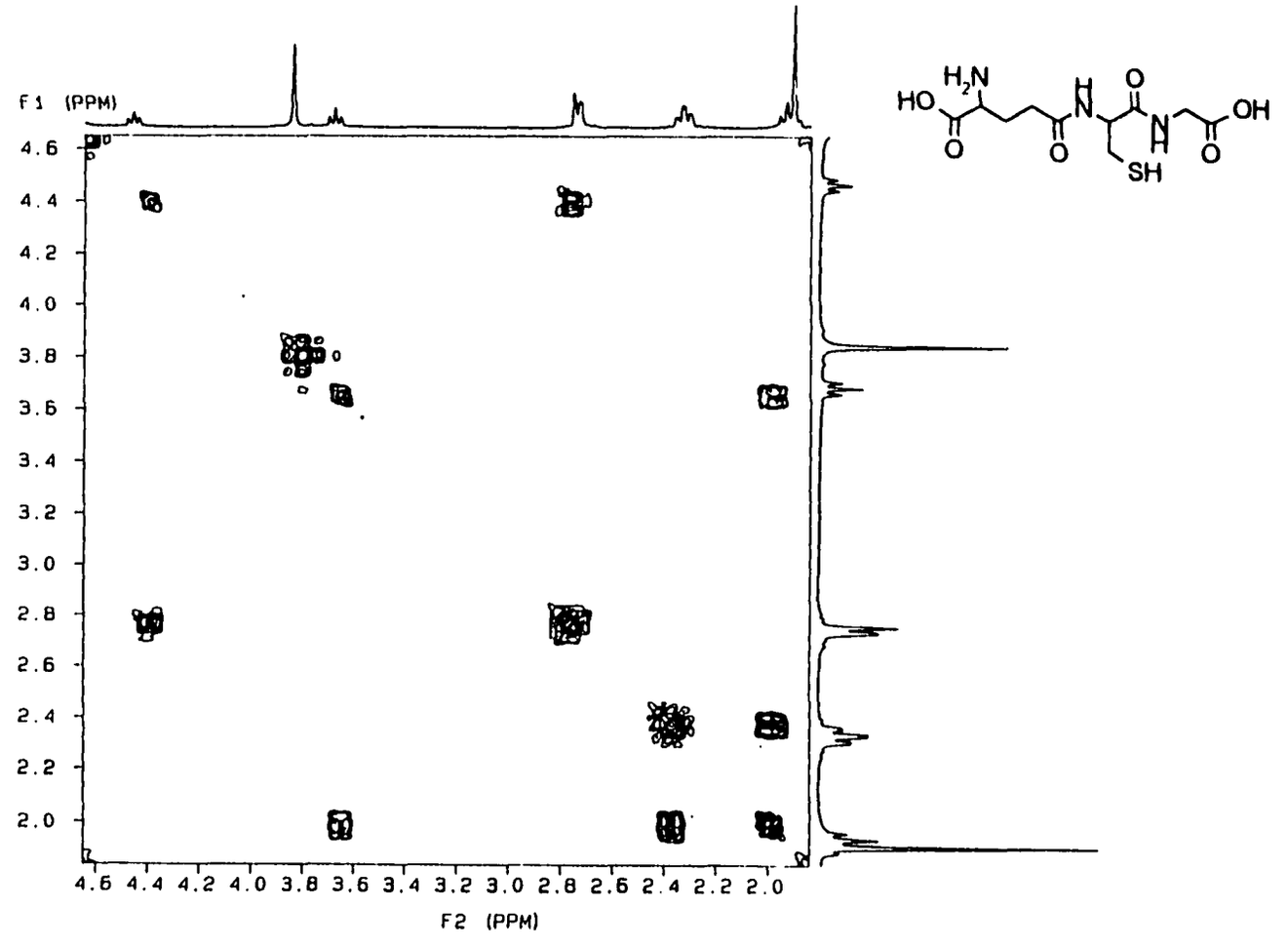

Figure B.3 Correlated spectroscopy (COSY) contour of GHS in D_2O.

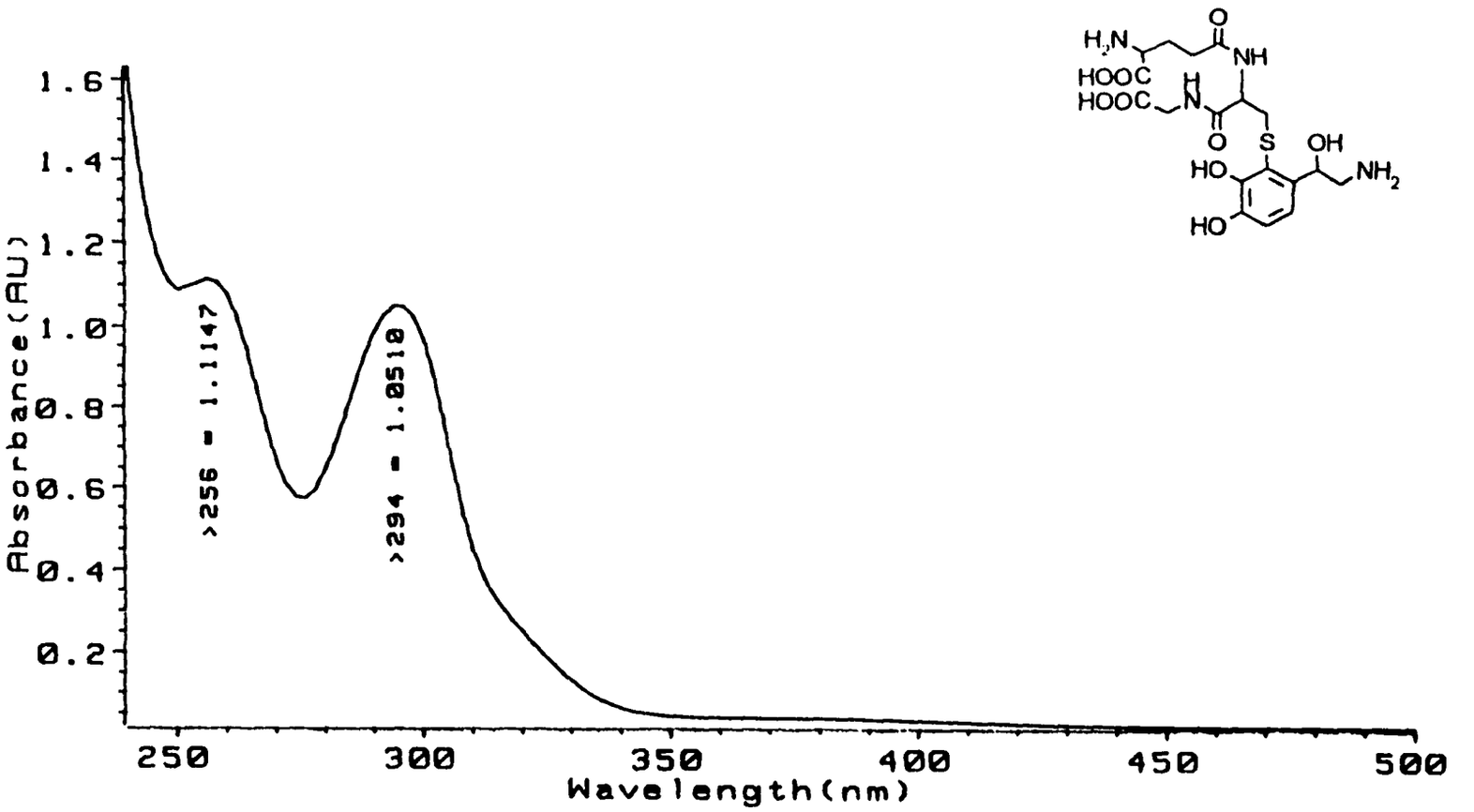

Figure B.4 UV-visible spectrum of 0.5 mM 2-*S*-Glu-NE in PBS (pH = 7.4, μ = 1.0).

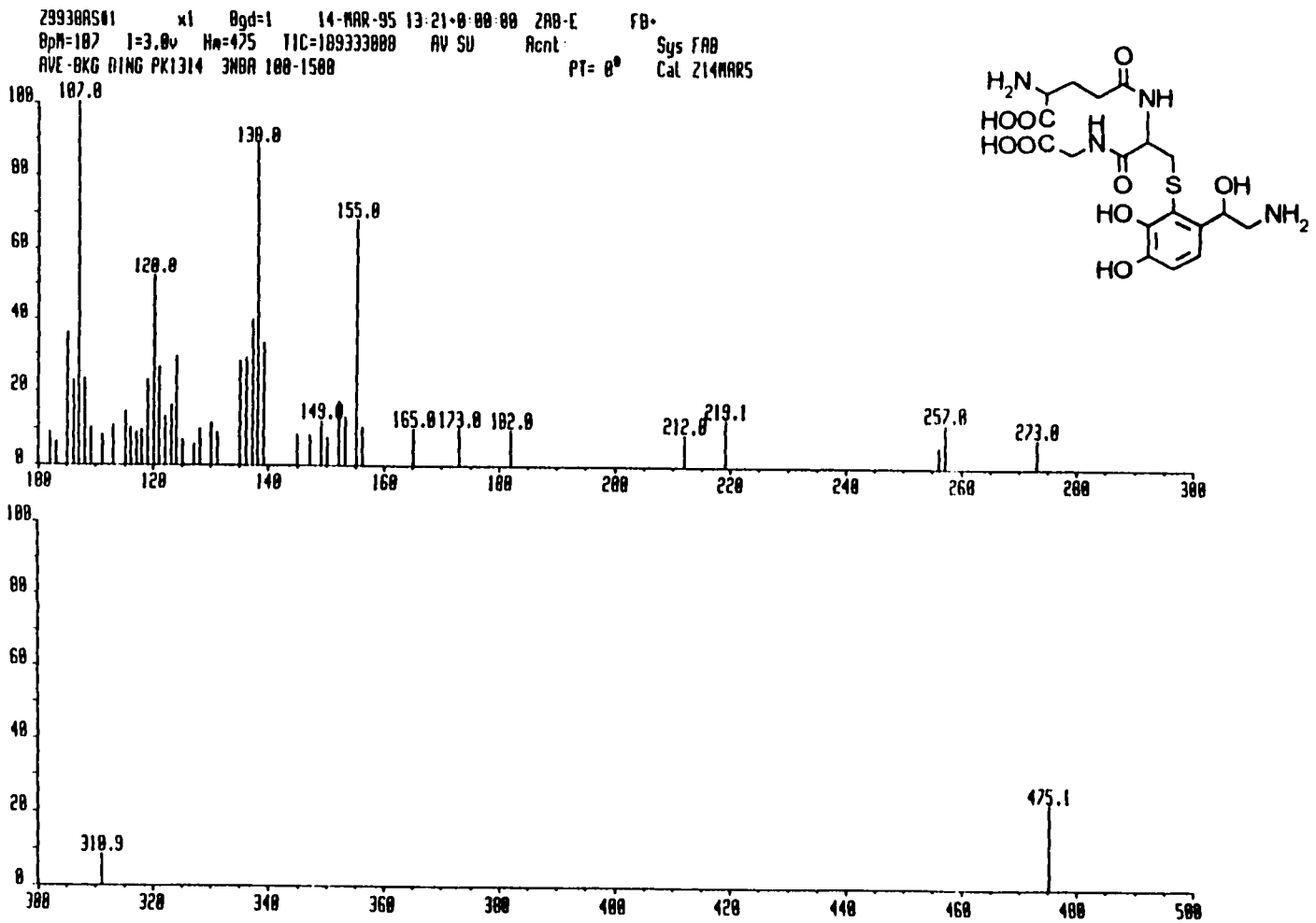

Figure B.5 Low resolution FAB-MS of 2-*S*-Glu-NE in 3-nitrobenzyl alcohol matrix.

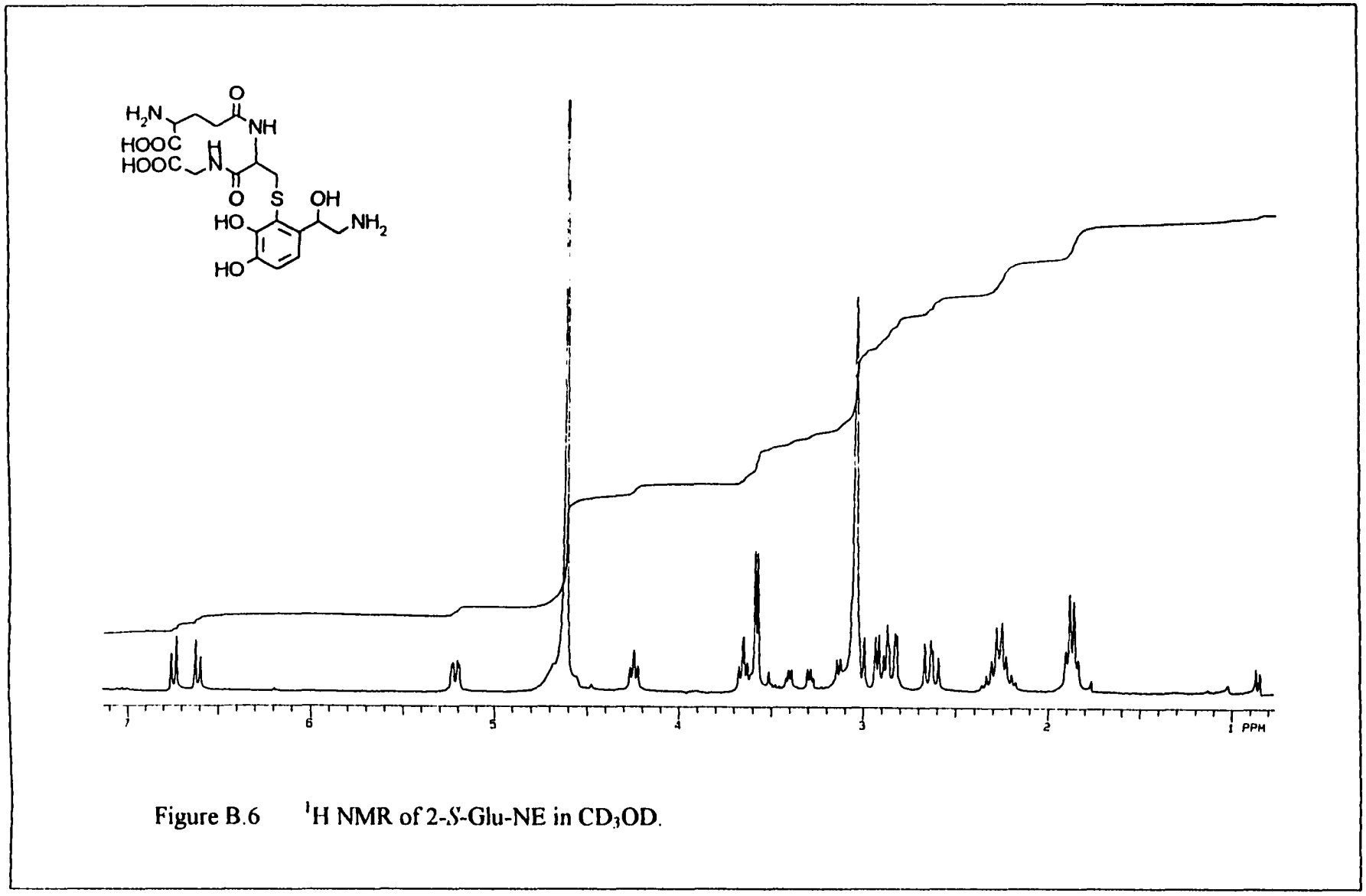

Figure B.6 ^{1}H NMR of 2-*S*-Glu-NE in CD_3OD.

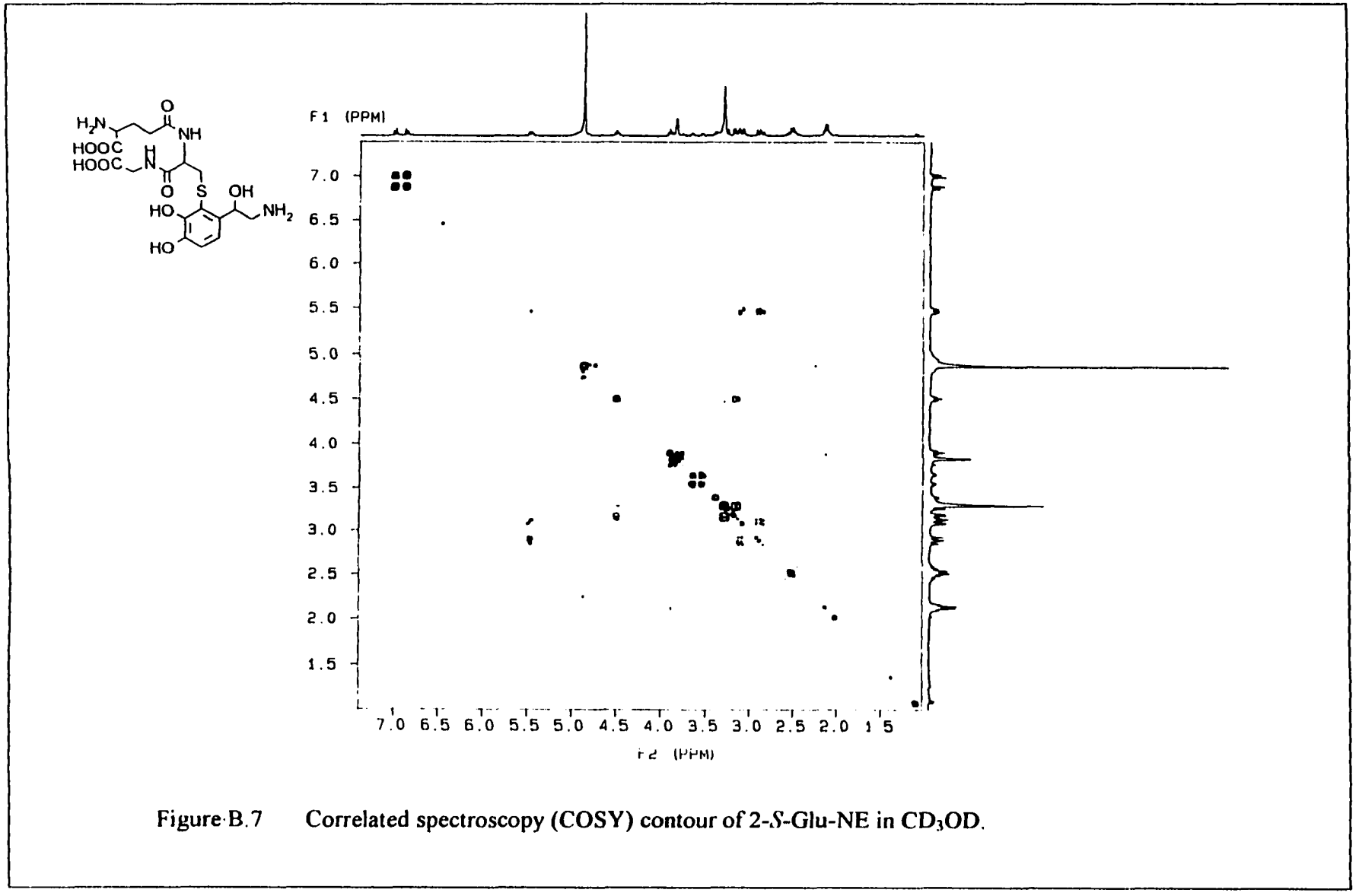

Figure B.7 Correlated spectroscopy (COSY) contour of 2-*S*-Glu-NE in CD_3OD.

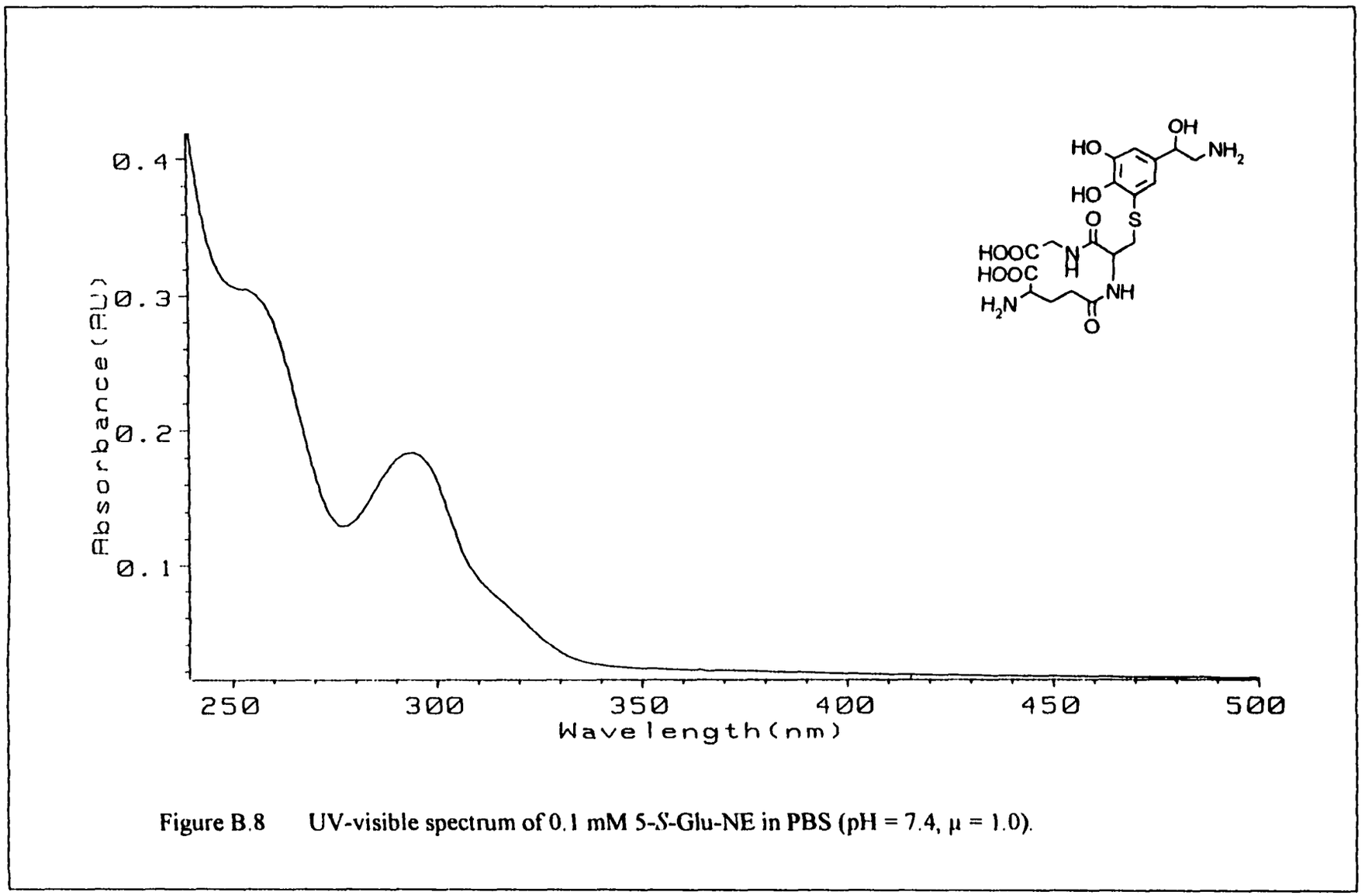

Figure B.8 UV-visible spectrum of 0.1 mM 5-*S*-Glu-NE in PBS (pH = 7.4, μ = 1.0).

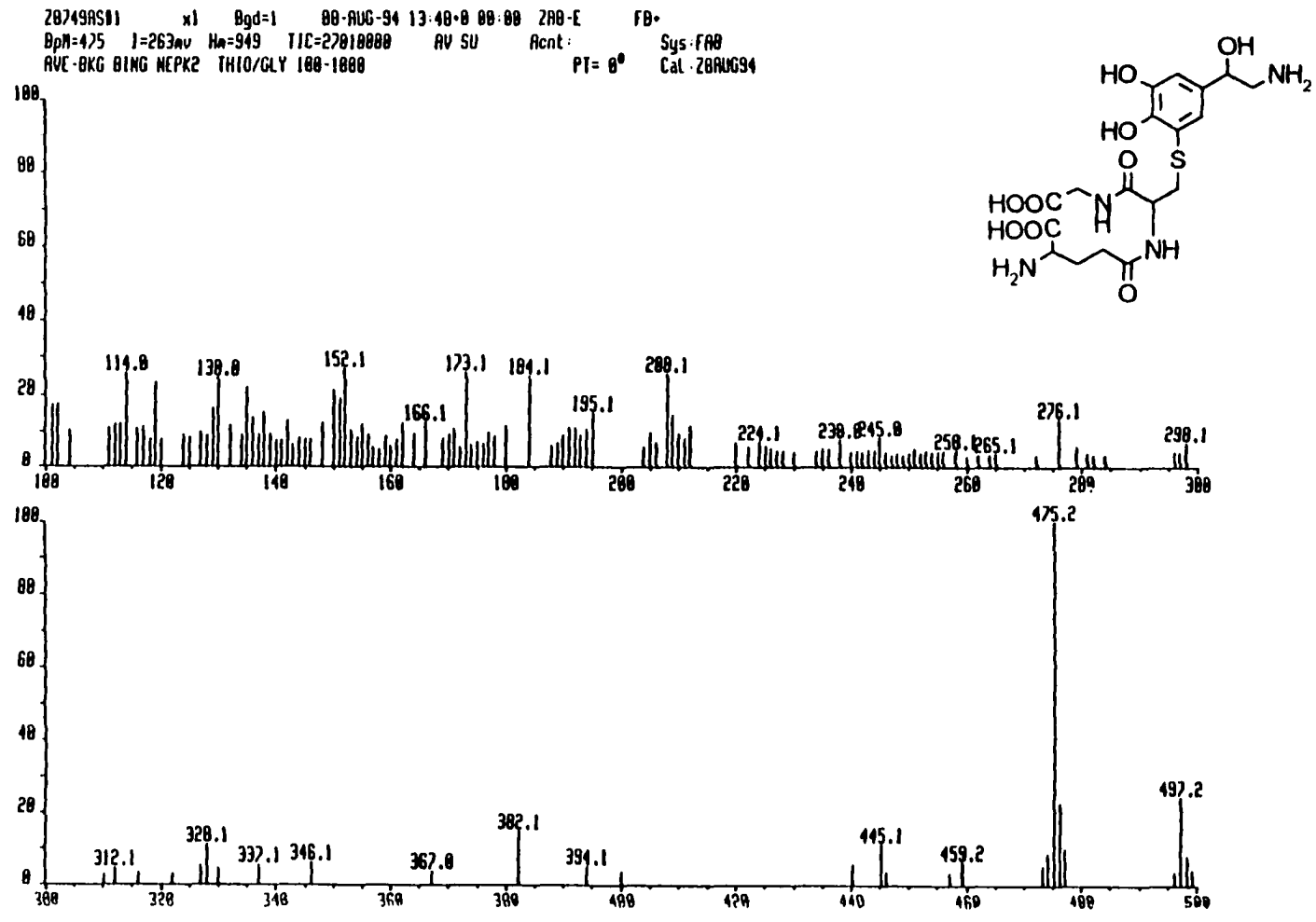

Figure B.9 Low resolution FAB-MS spectrum of 5-*S*-Glu-NE in thioglycerol/glycerol matrix.

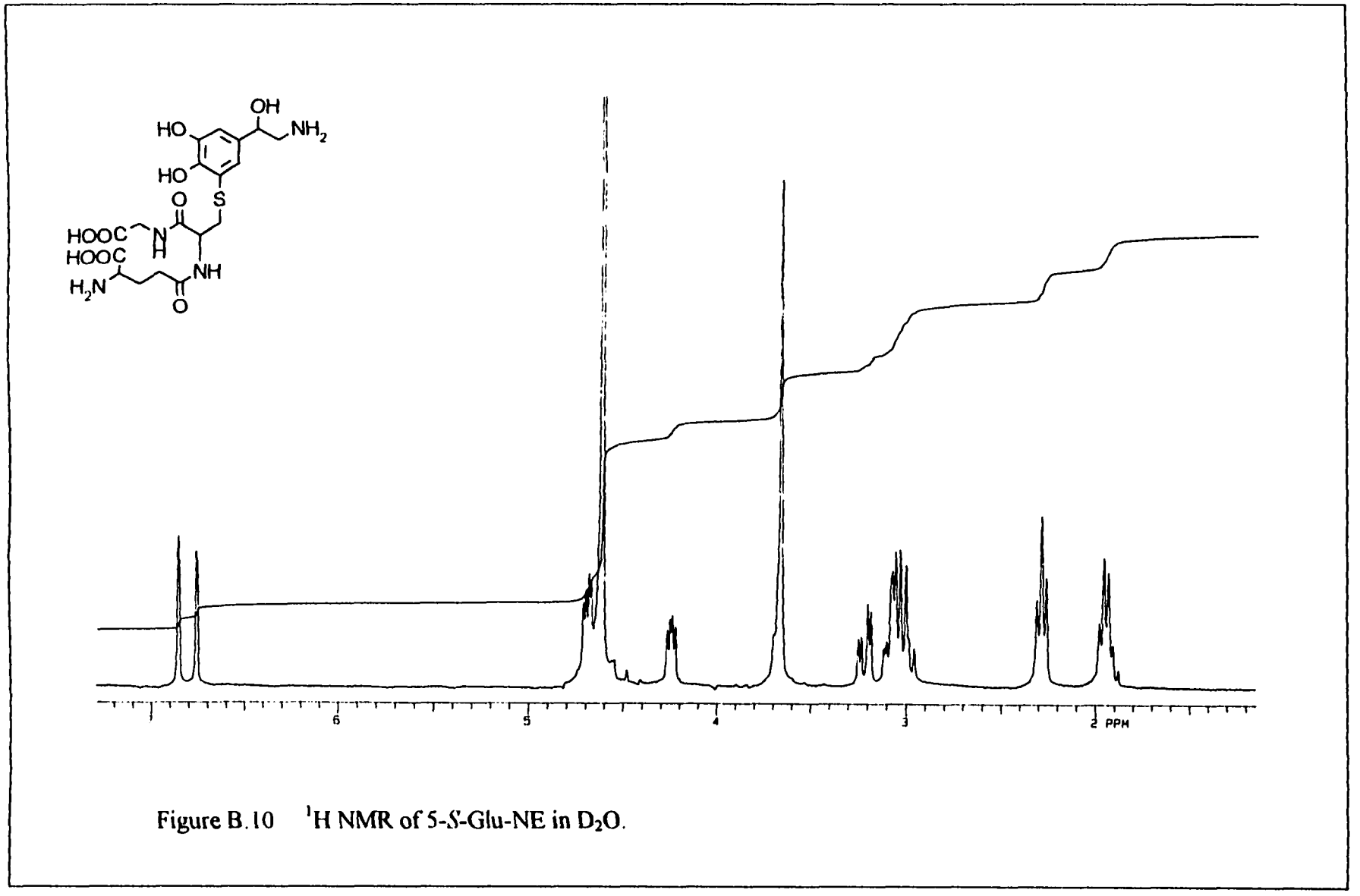

Figure B.10 ^{1}H NMR of 5-*S*-Glu-NE in D_2O.

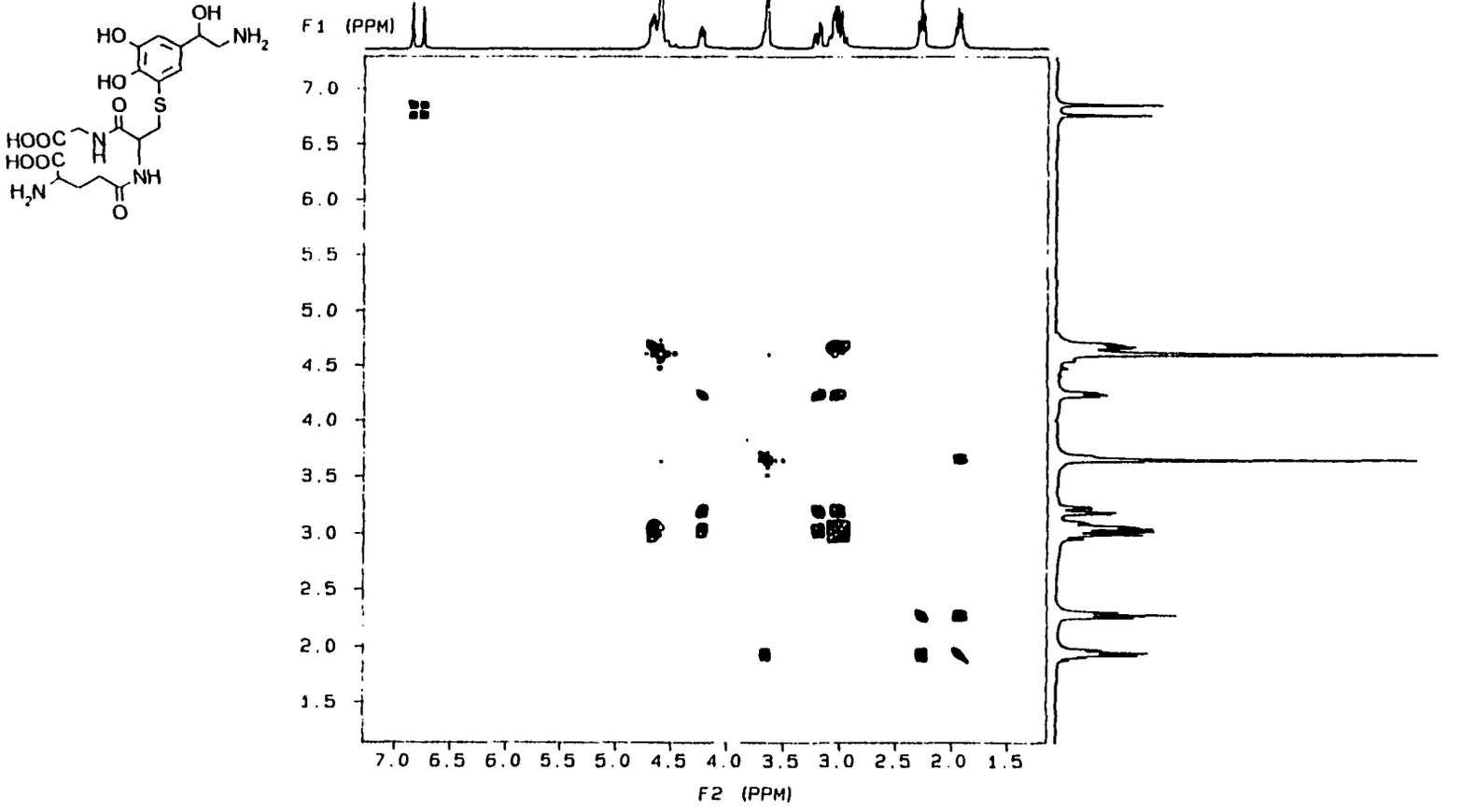

Figure B.11 Correlated spectroscopy (COSY) contour of 5-*S*-Glu-NE in D_2O.

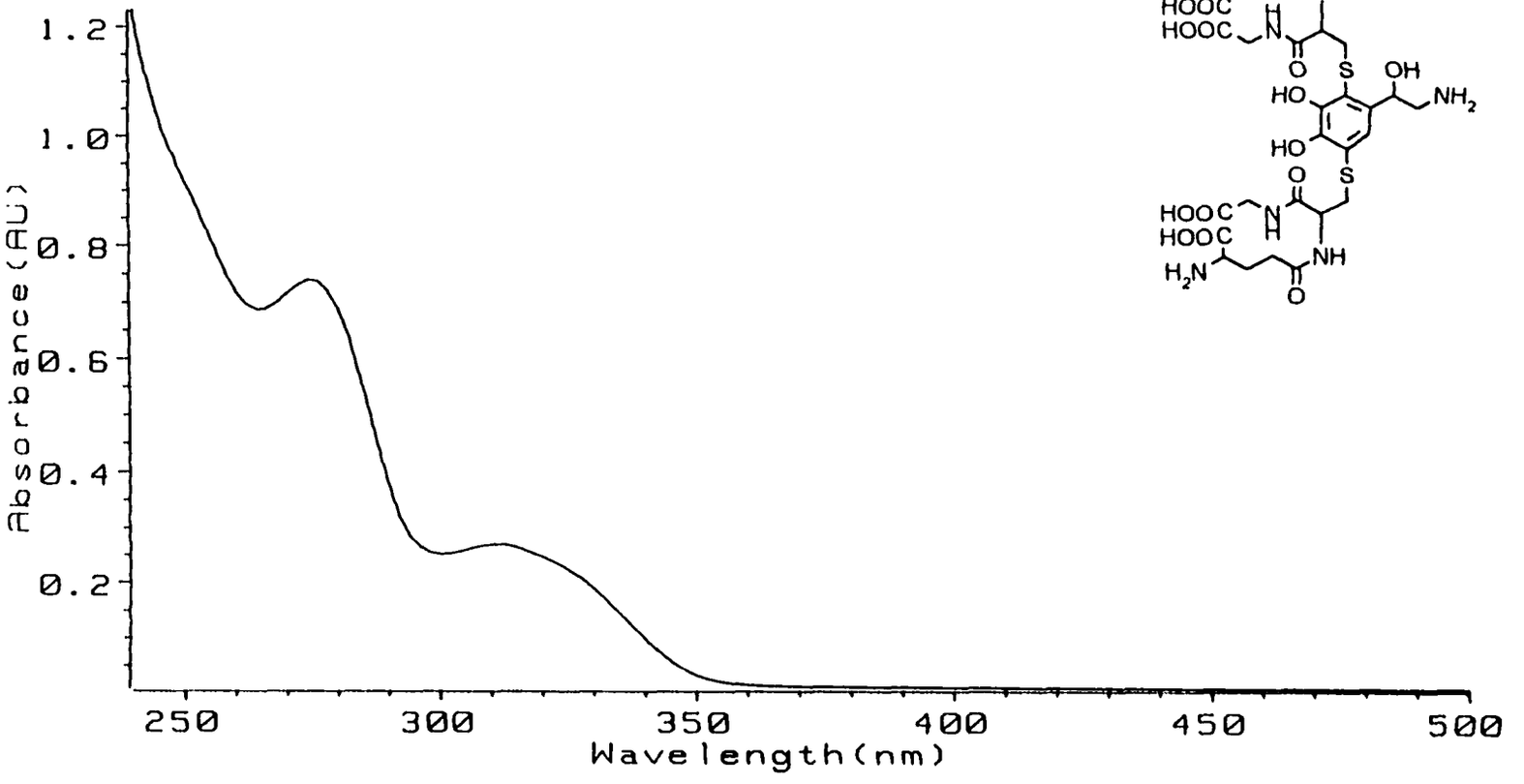

Figure B.12 UV-visible spectrum of 0.1 mM 2,5-bis-*S*-Glu-NE in PBS (pH = 7.4, μ = 1.0).

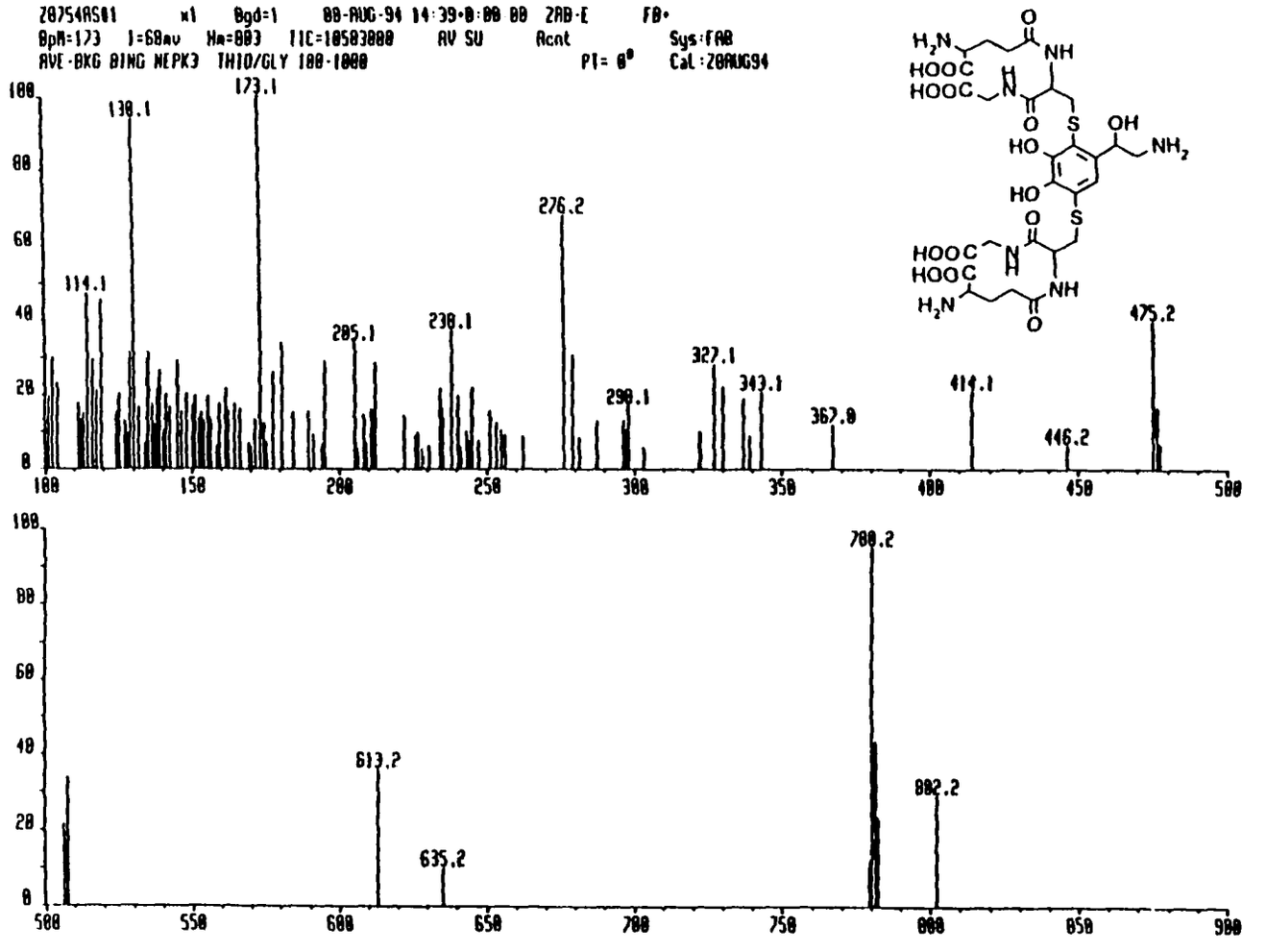

Figure B.13 Low resolution FAB-MS spectrum of 2,5-bis-*S*-Glu-NE in thioglycerol/glycerol matrix.

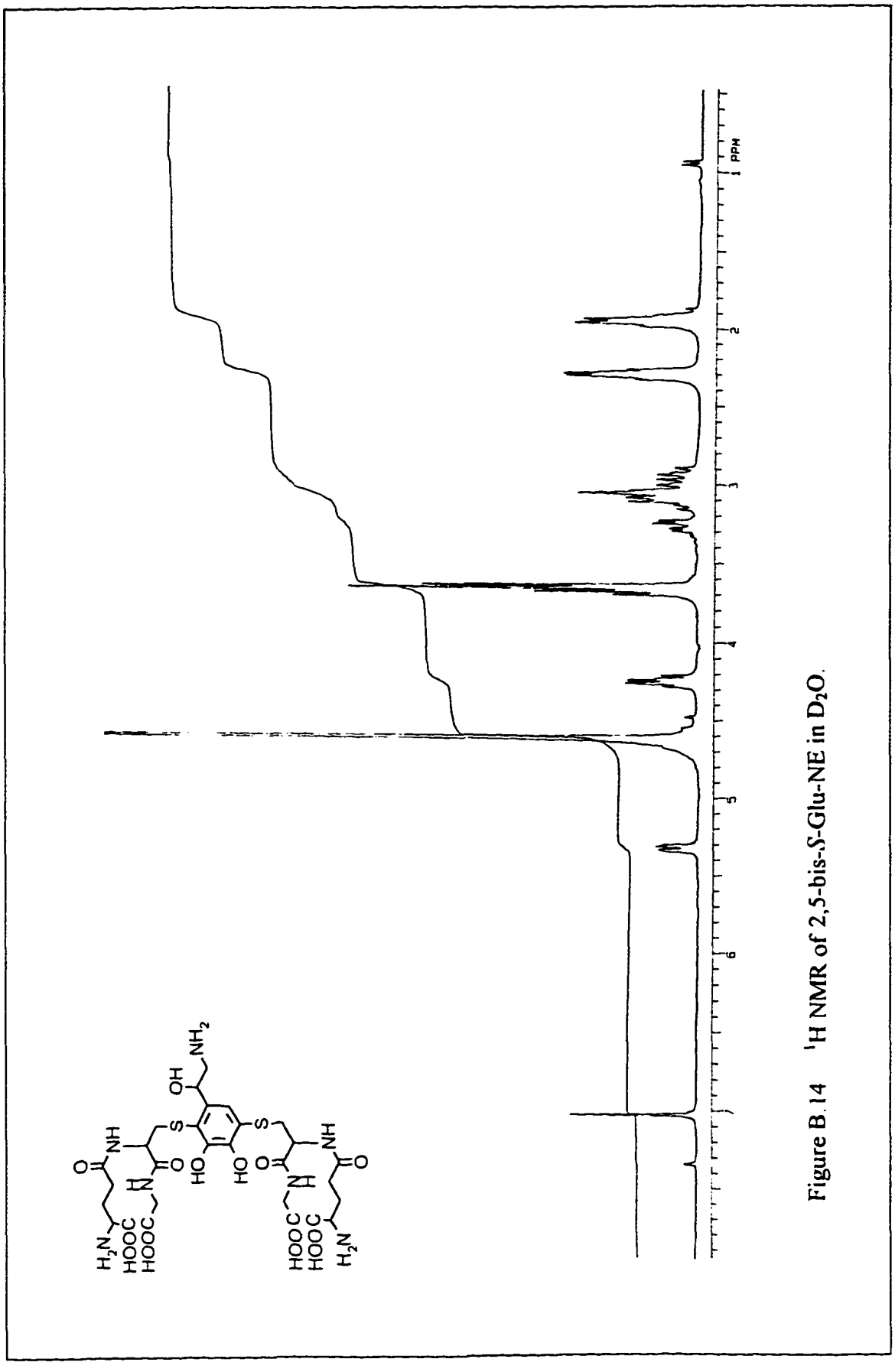

Figure B.14 ^{1}H NMR of 2,5-bis-*S*-Glu-NE in D_2O.

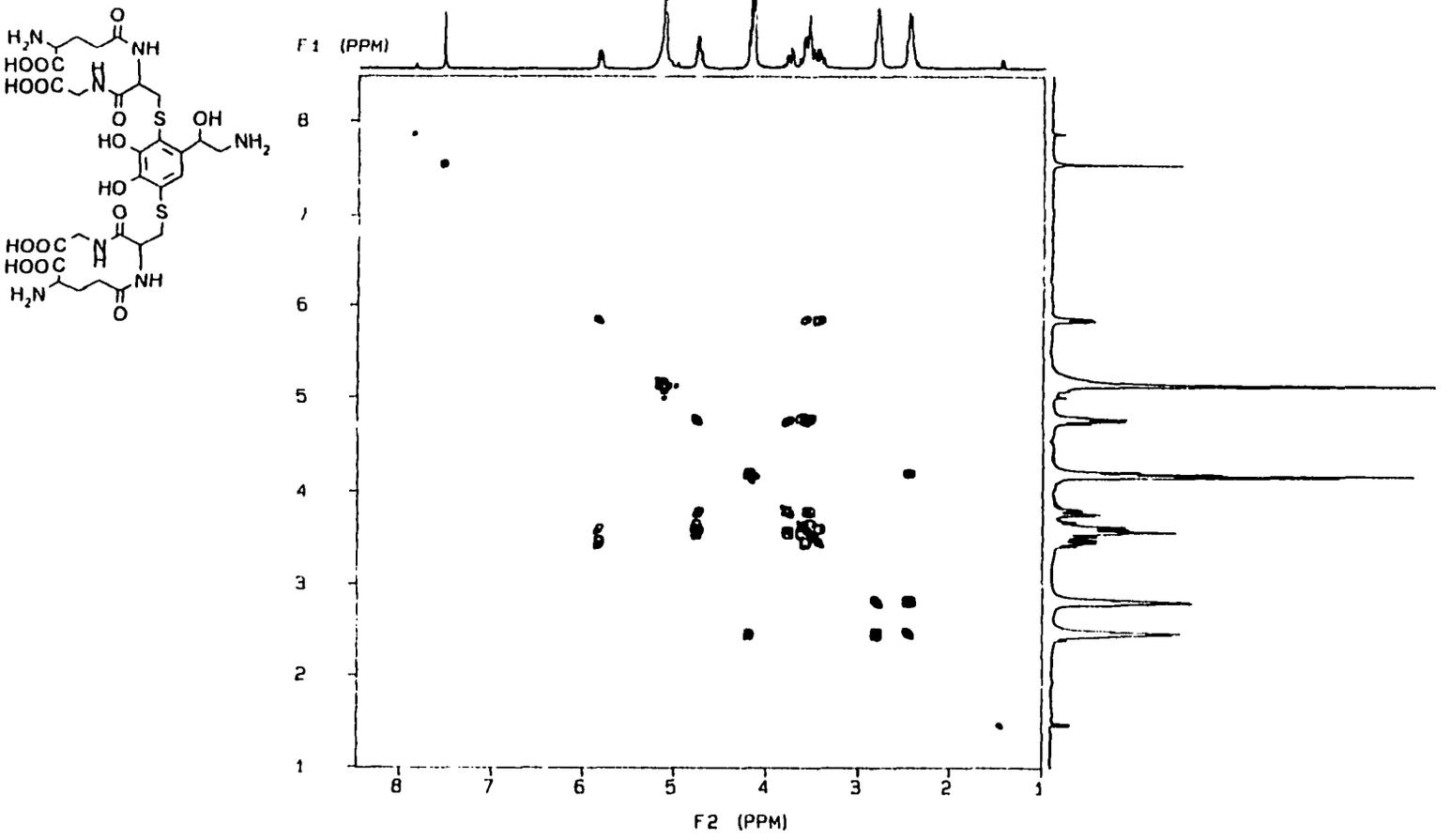

Figure B.15 Correlated spectroscopy (COSY) contour of 2,5-bis-*S*-Glu-NE in D_2O.

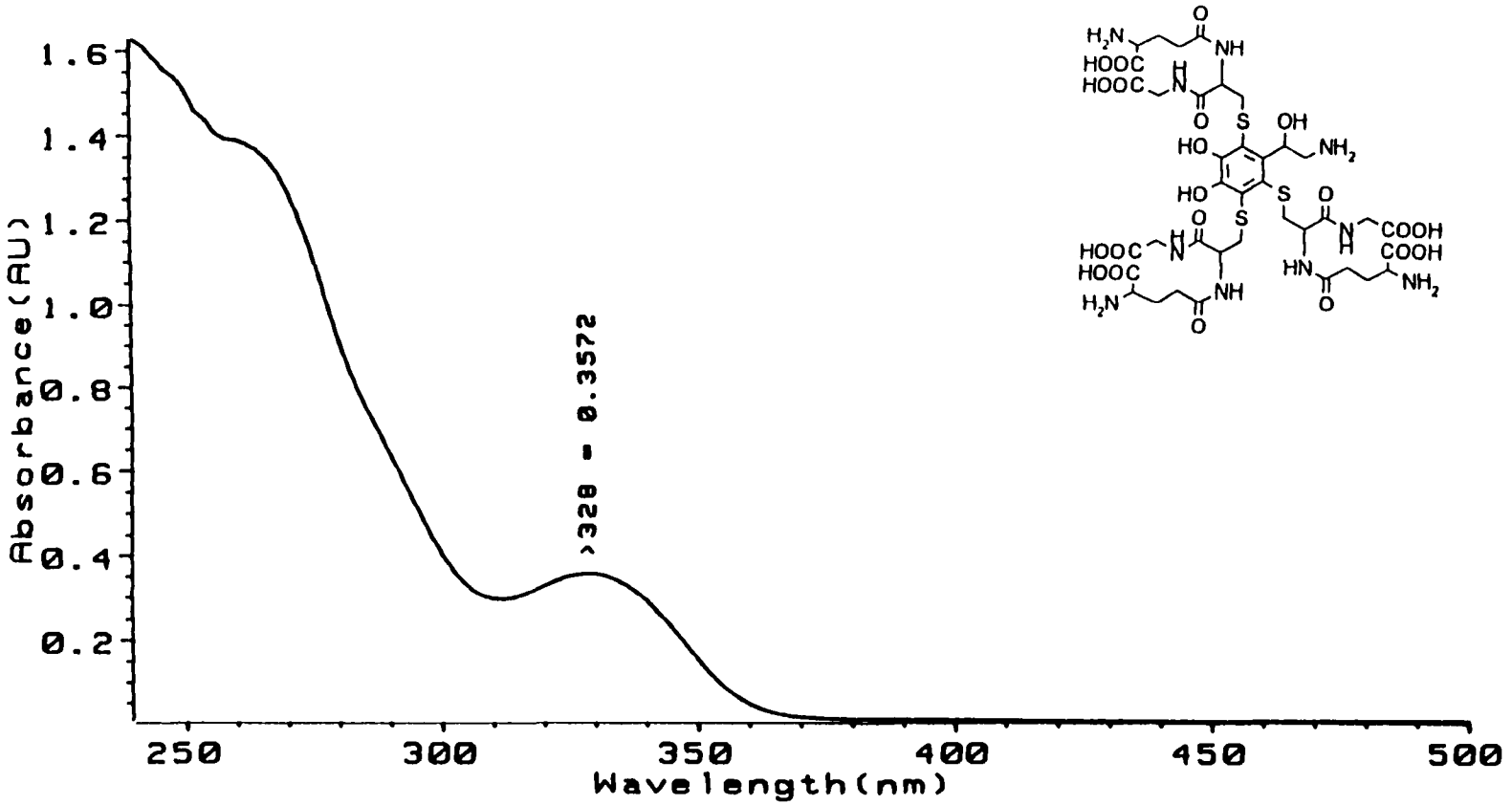

Figure B.16 UV-visible spectrum of 0.1 mM 2,5,6-tris-*S*-Glu-NE in PBS (pH = 7.4, μ = 1.0).

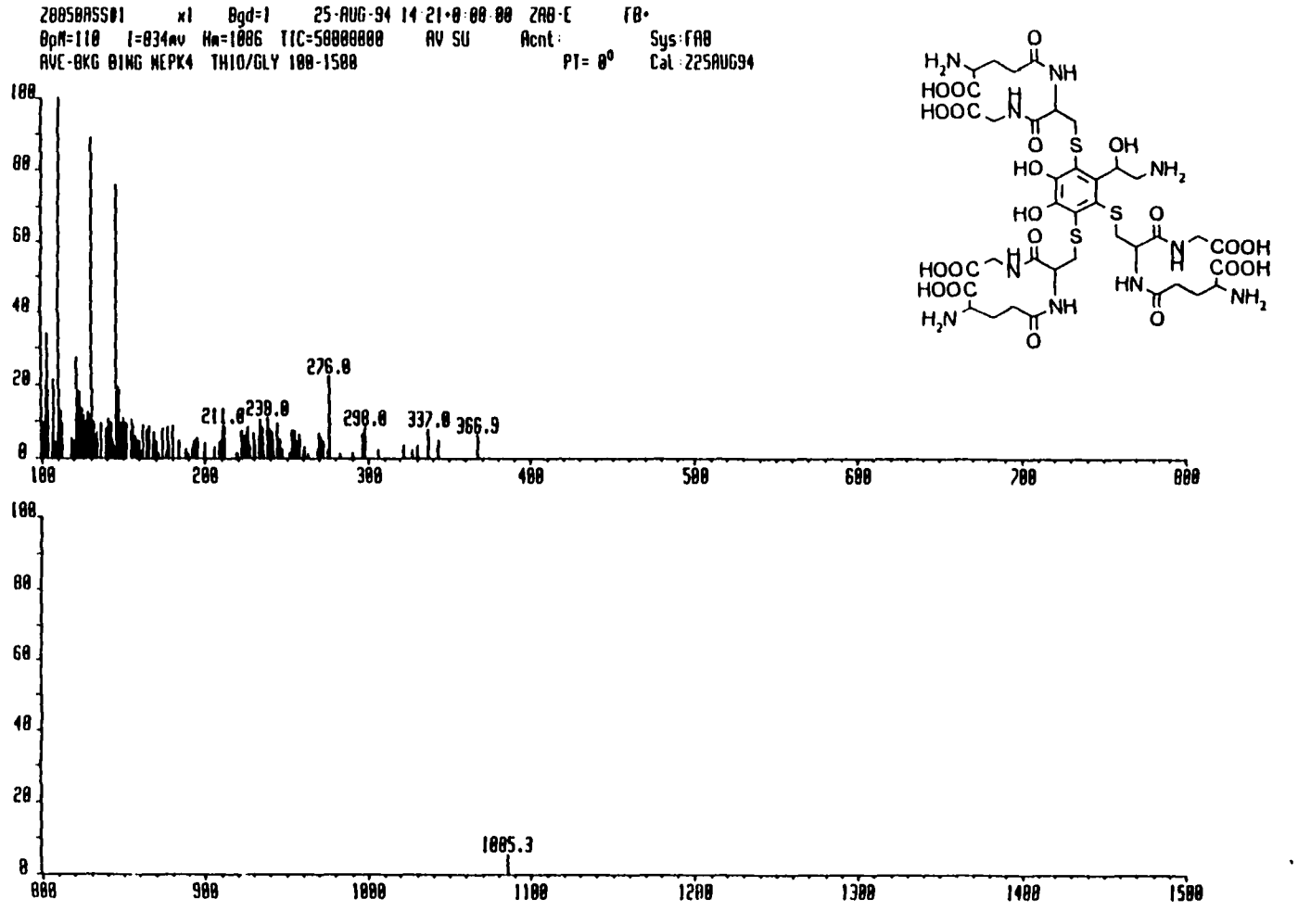

Figure B.17 Low resolution FAB-MS spectrum of 2,5,6-tris-*S*-Glu-NE in thioglycerol/glycerol matrix.

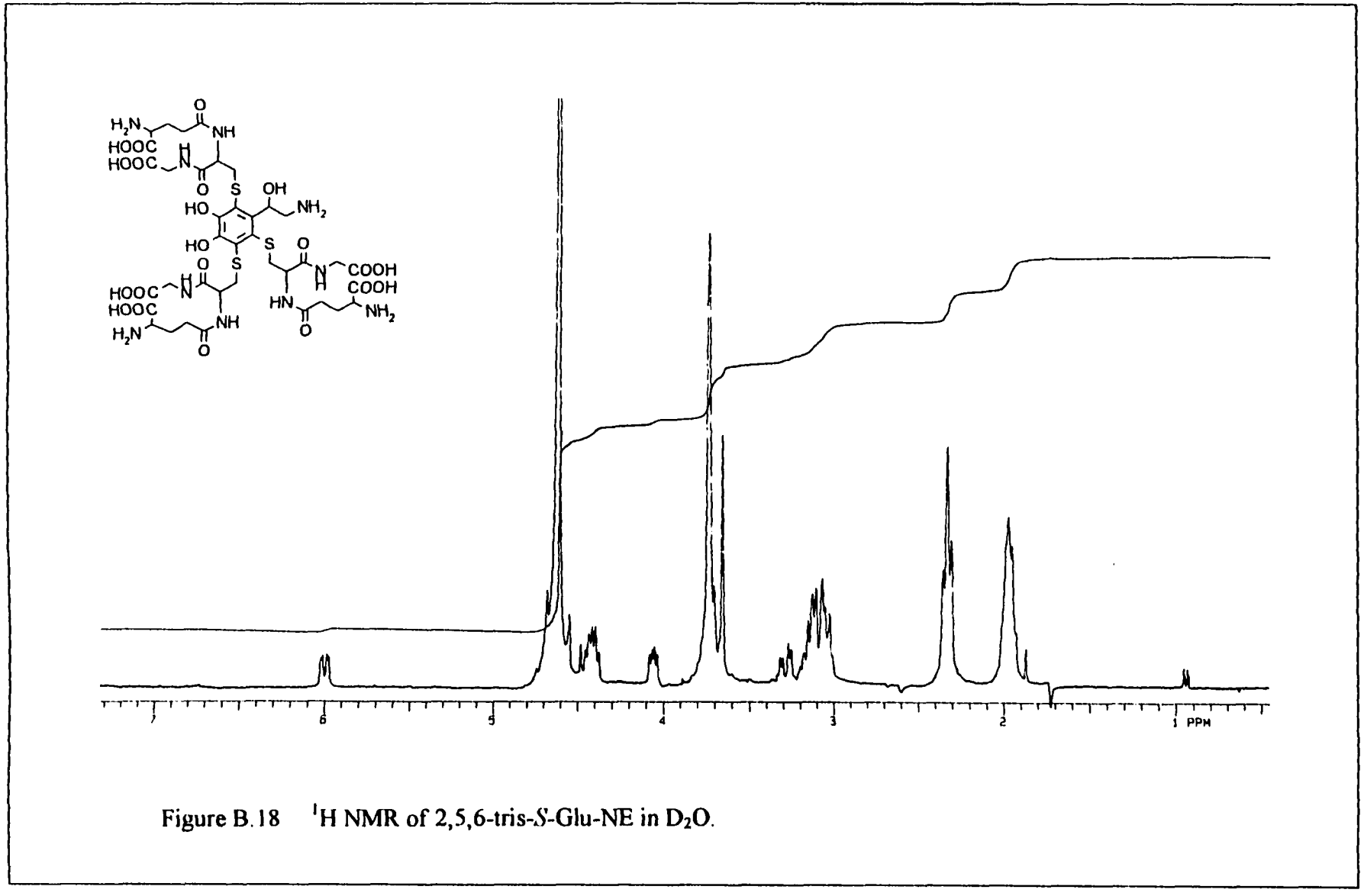

Figure B.18 ^{1}H NMR of 2,5,6-tris-*S*-Glu-NE in D_2O.

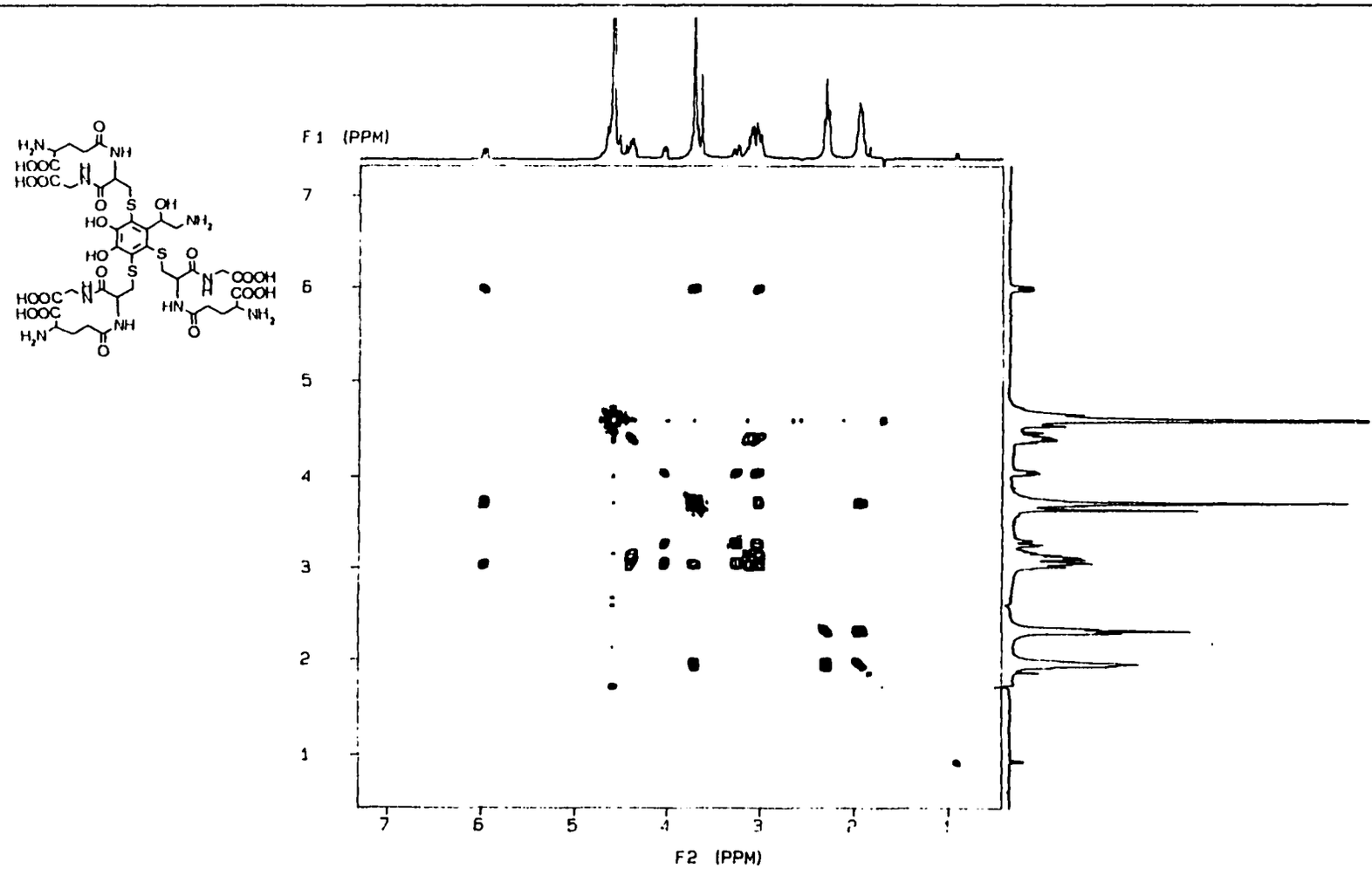

Figure B.19 Correlated spectroscopy (COSY) contour of 2,5,6-tris-*S*-Glu-NE in D_2O.

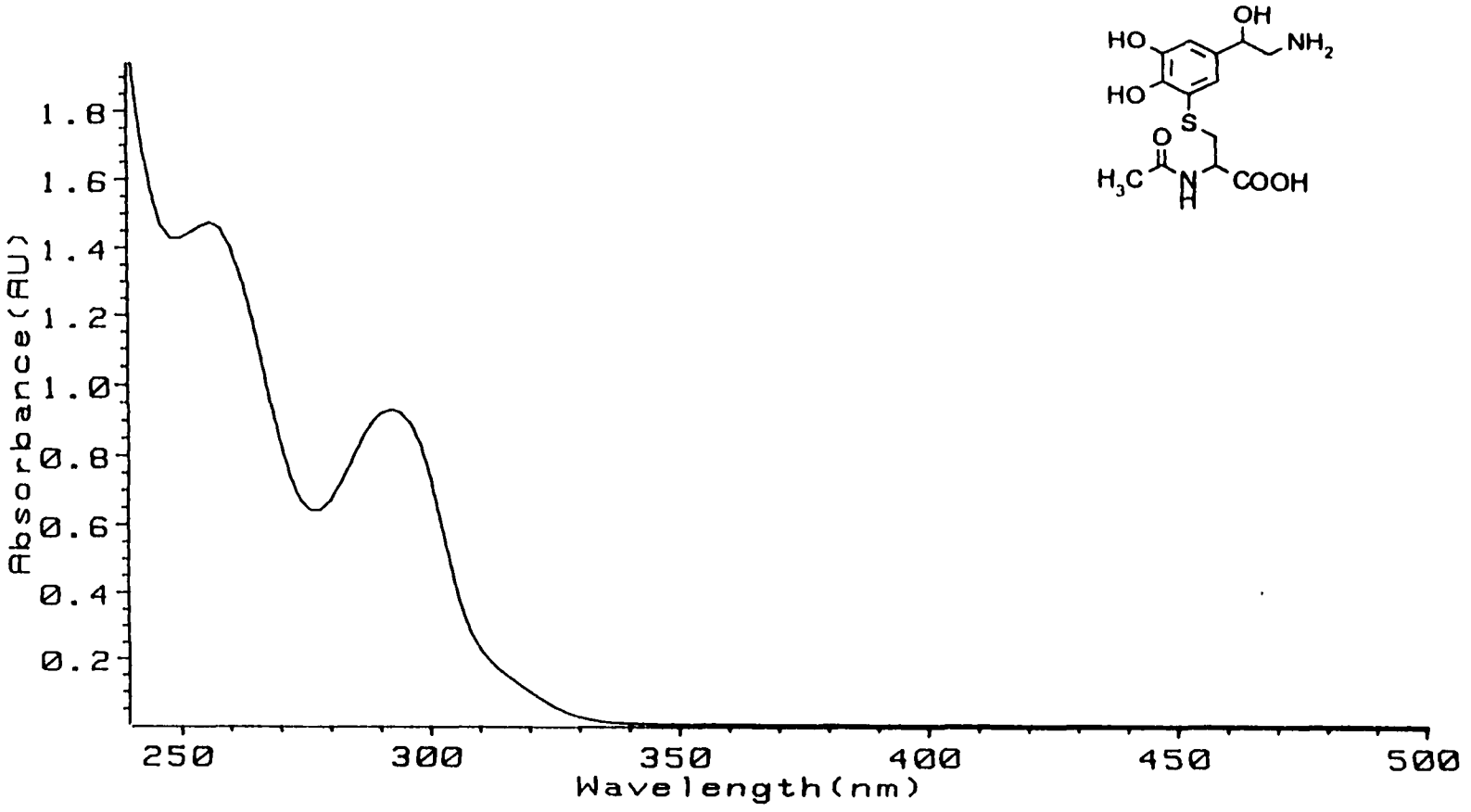

Figure B.20 UV-visible spectrum of 0.1 mM 5-*S*-NAc-Cys-NE in PBS (pH = 7.4, μ = 1.0).

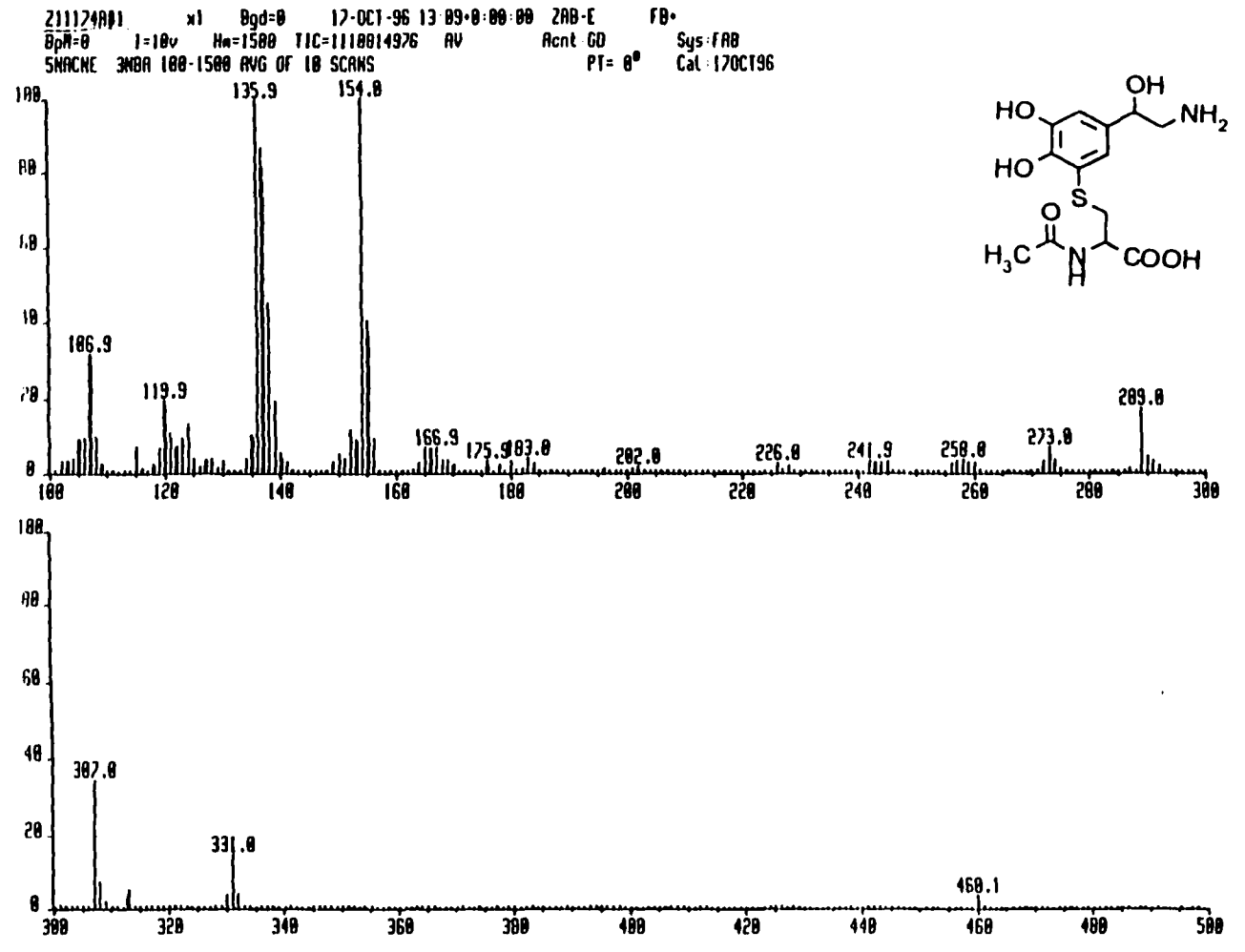

Figure B.21 Low resolution FAB-MS spectrum of 5-*S*-NAc-Cys-NE in 3-nitrobenzyl alcohol matrix.

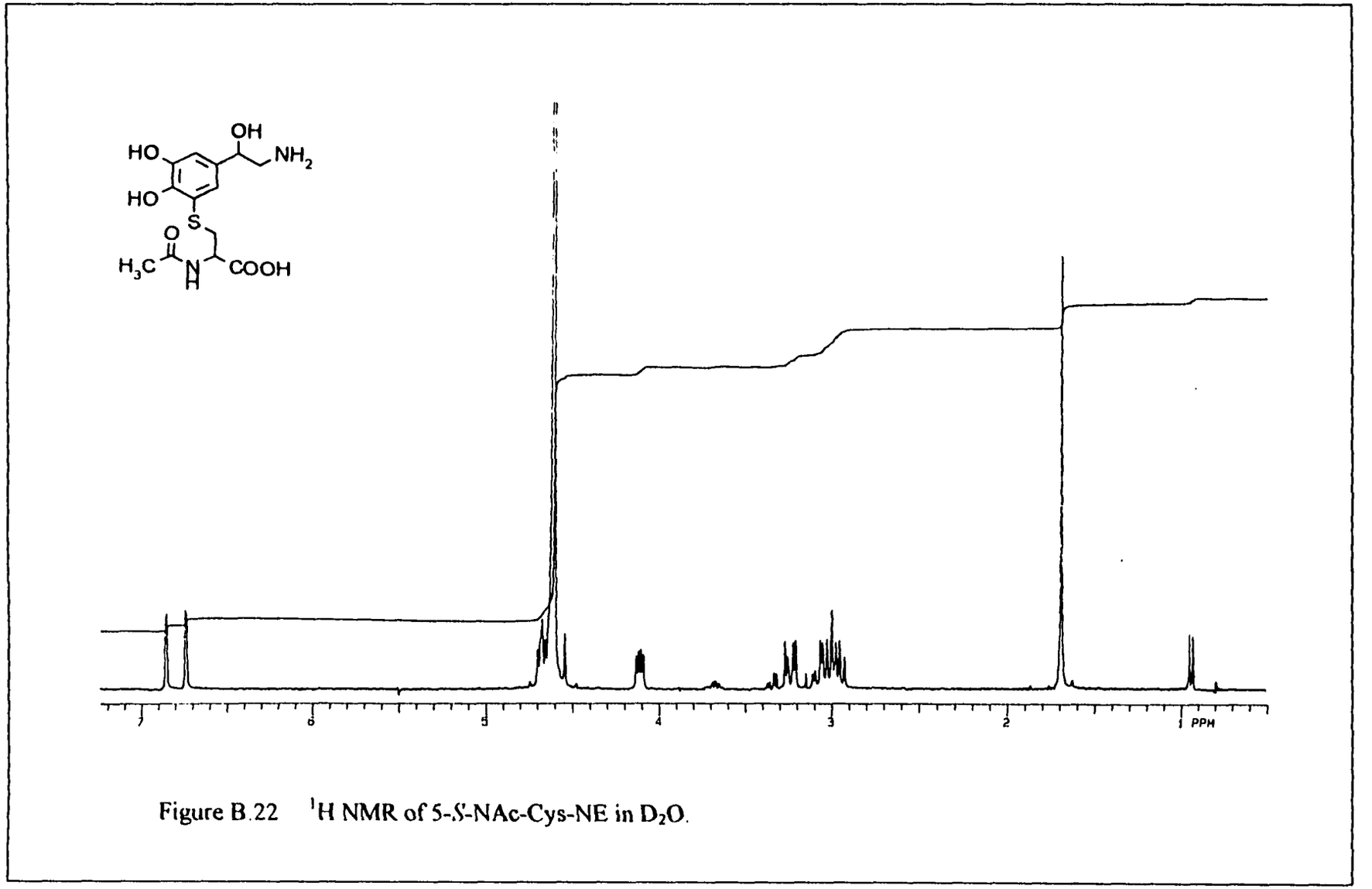

Figure B.22 ^{1}H NMR of 5-*S*-NAc-Cys-NE in D_2O.

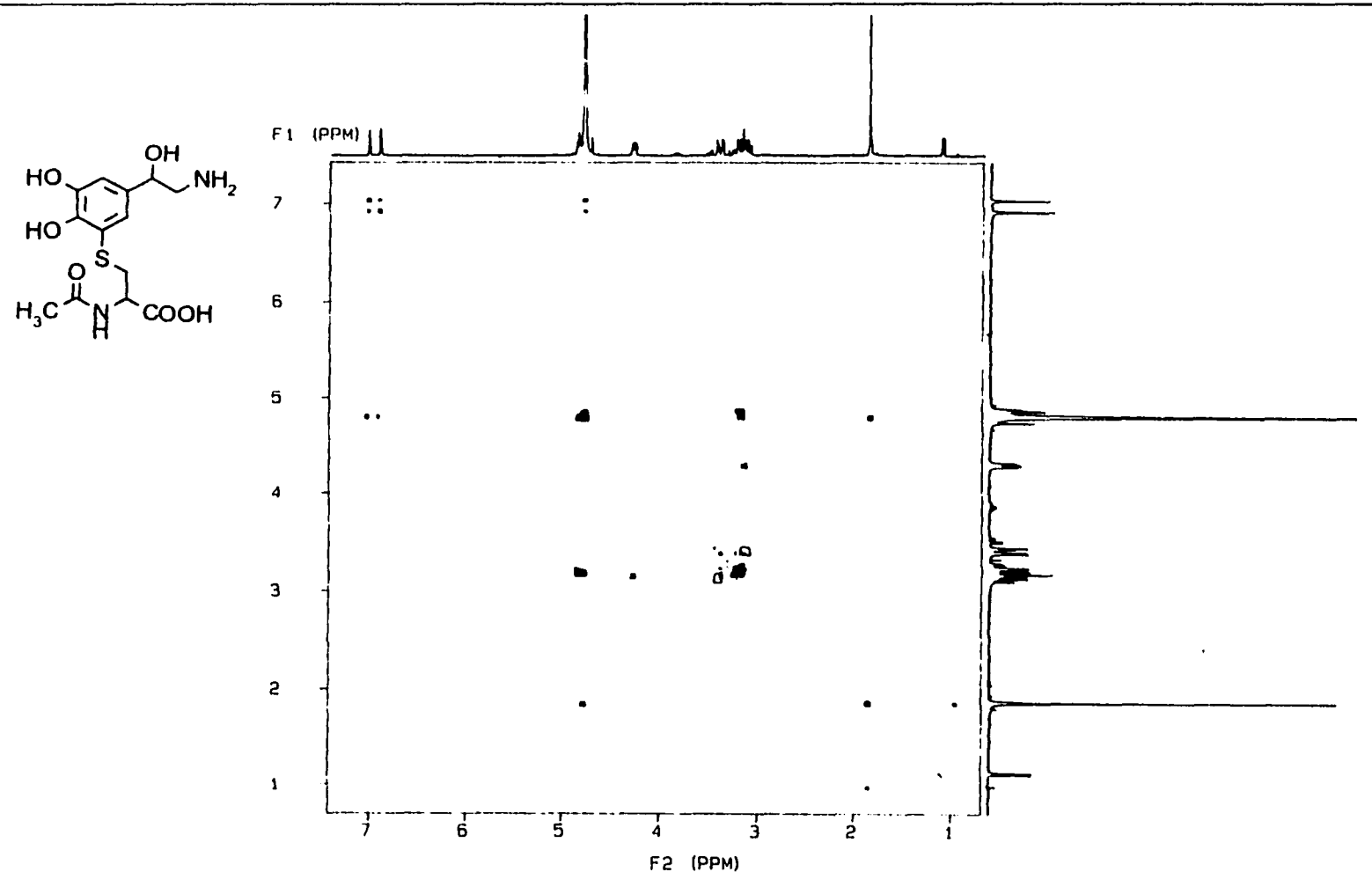

Figure B.23 Correlated spectroscopy (COSY) contour of 5-*S*-NAc-Cys-NE in D_2O.

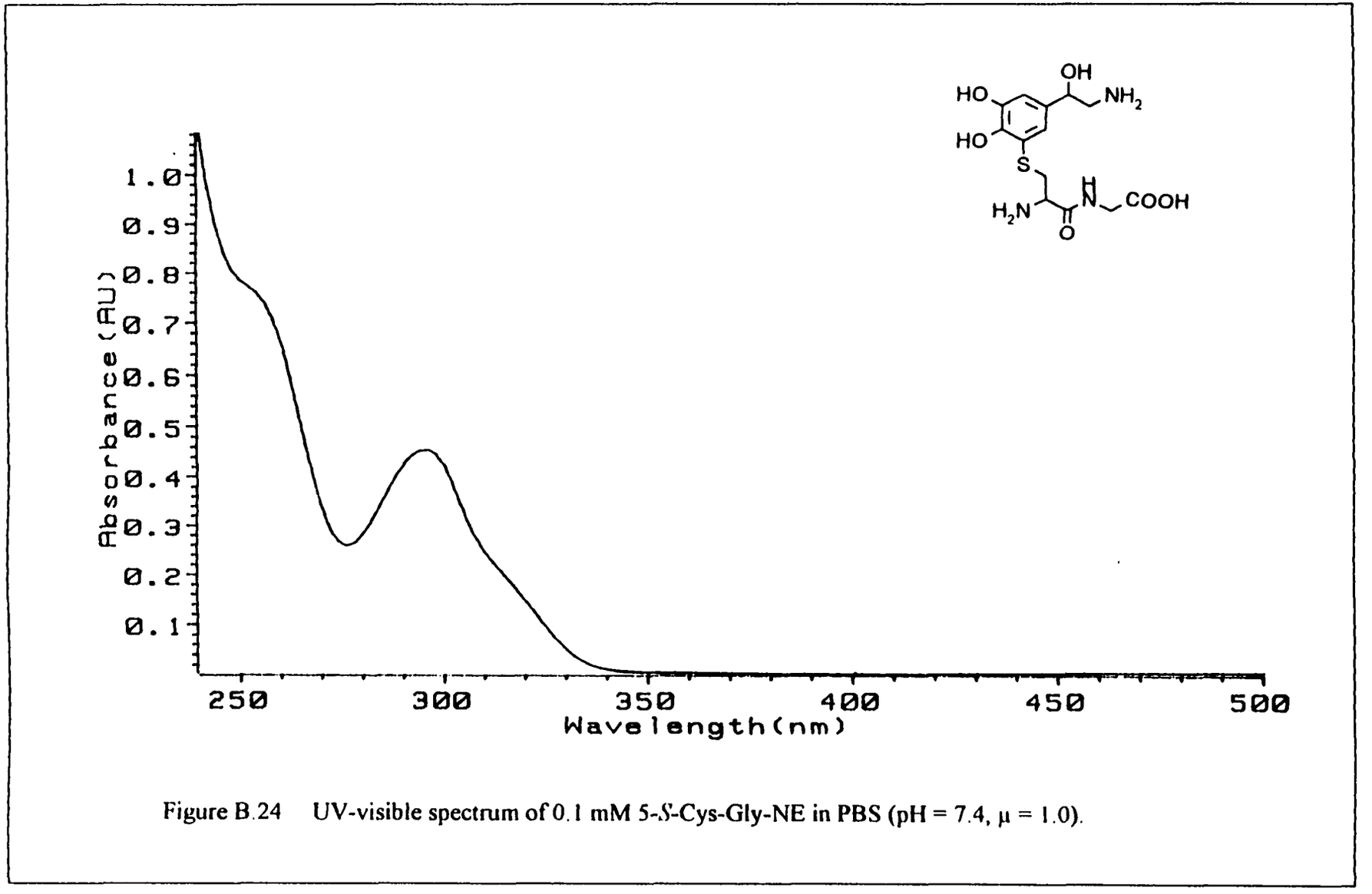

Figure B.24 UV-visible spectrum of 0.1 mM 5-*S*-Cys-Gly-NE in PBS (pH = 7.4, μ = 1.0).

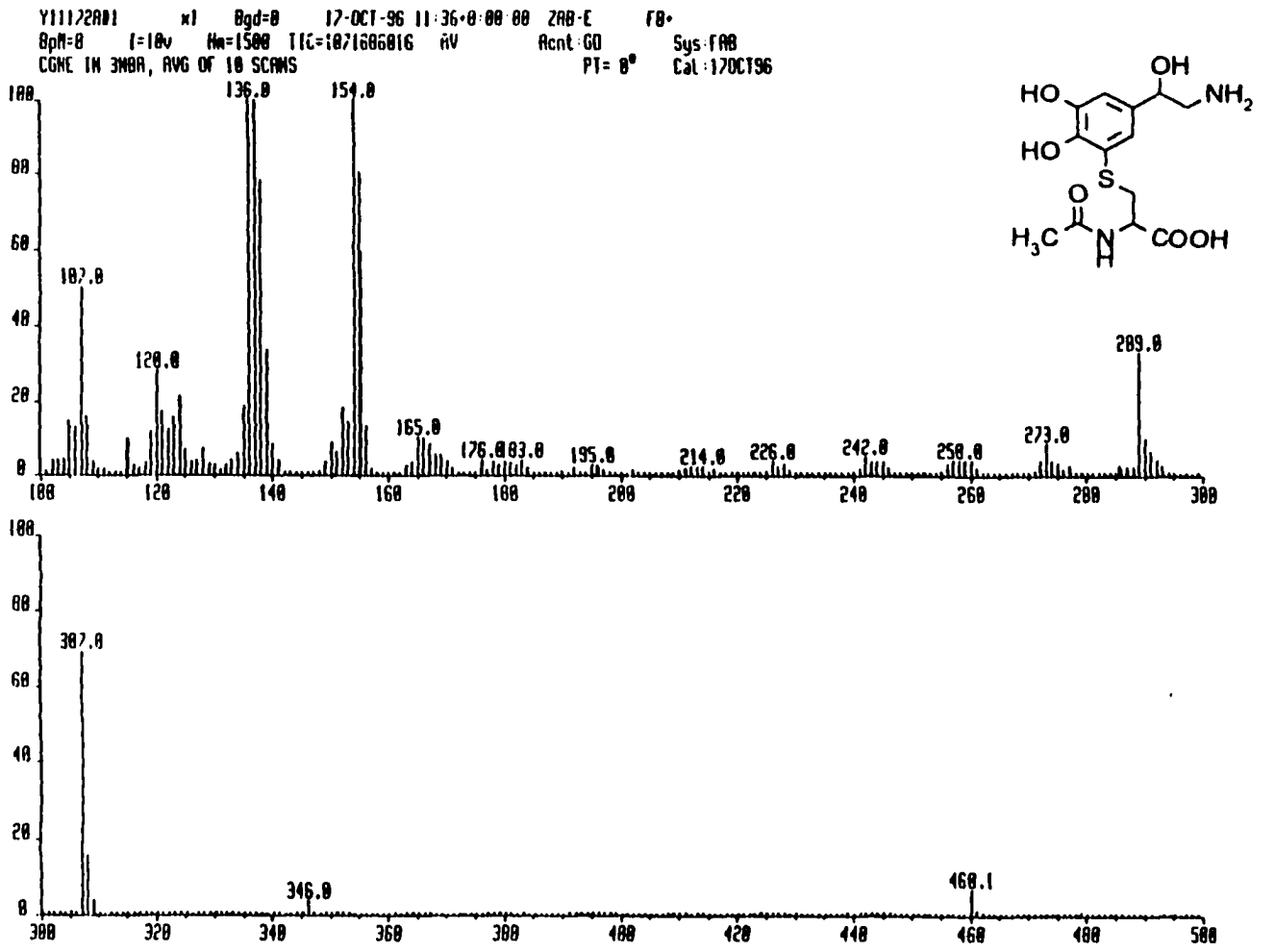

Figure B.25 Low resolution FAB-MS spectrum of 5-*S*-Cys-Gly-NE in 3-nitrobenzyl alcohol matrix.

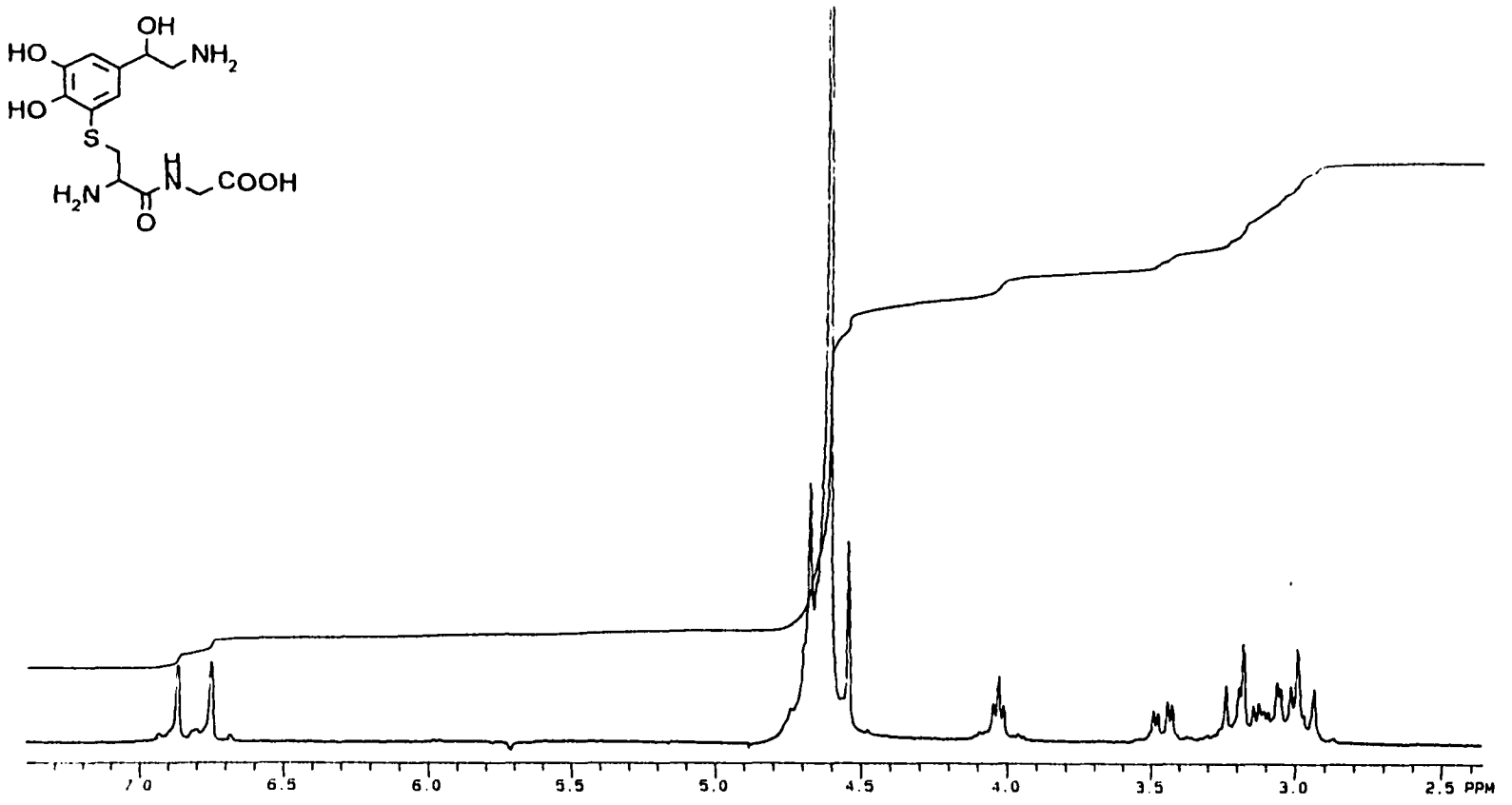

Figure B.26 ^{1}H NMR of 5-*S*-Cys-Gly-NE in D_2O.

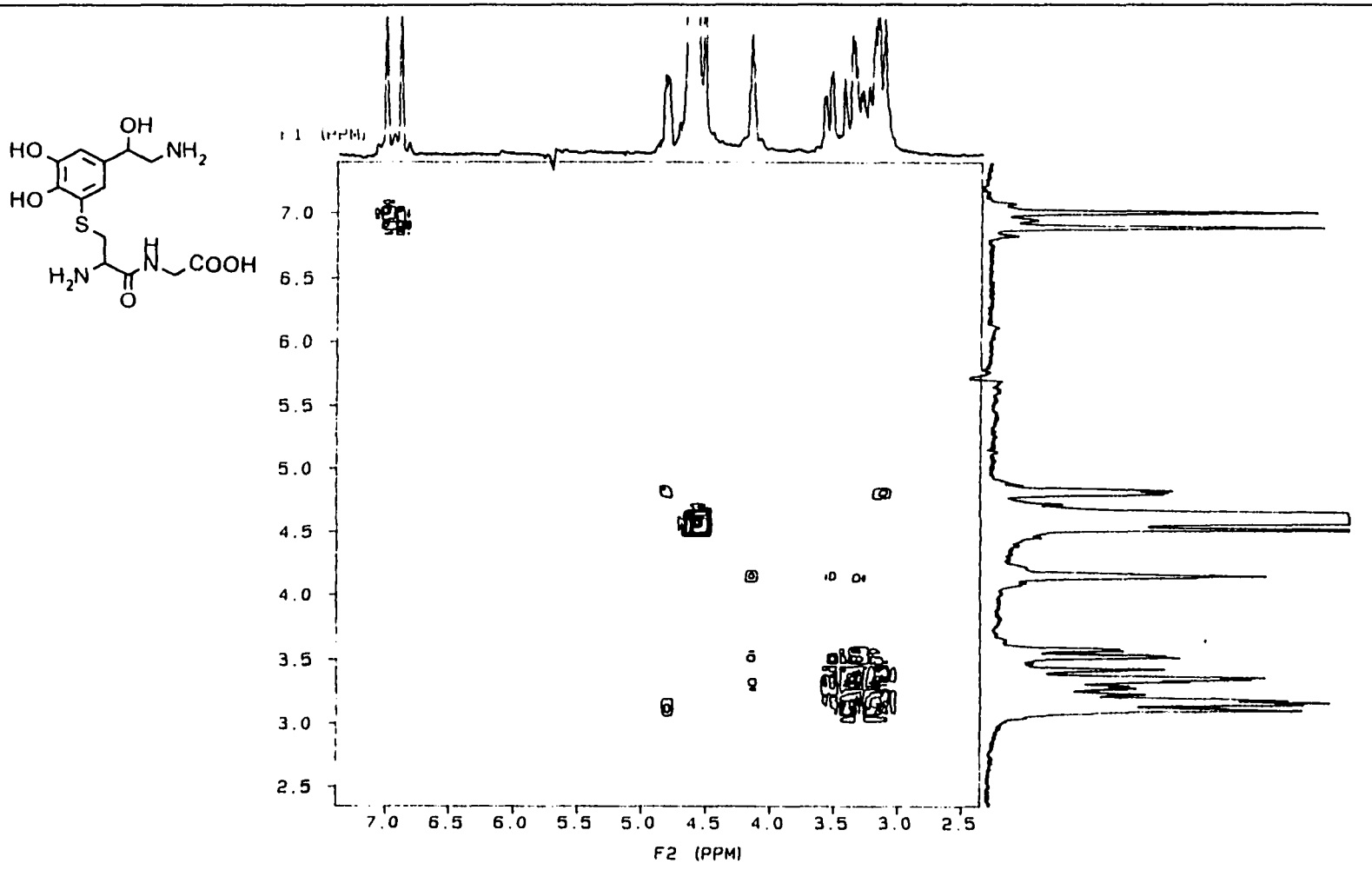

Figure B.27 Correlated spectroscopy (COSY) contour of 5-*S*-Cys-Gly-NE in D_2O.

Appendix C HPLC Methods

Table 1 HPLC Method I

Time/min	Flow/mL/min	%B
0.00	7.000	0.0
2.00		0.0
20.00		30.0
35.00		100.0
45.00		100.0
46.00		0.0
49.95	7.000	0.0
50.00	0.000	0.0

Pump: Two Gilson model 302 pumps
Detector: Gilson model 112 UV detector set at 254 nm
Column: J. T. Baker, Bakerbond C-18, 10 μm, 22.5 × 250 mm
Injector: Rheodyne model 7125 with 10.0 mL loop.
Solvent A: 30.0 mL concentrated ammonium hydroxide added to 4.0 L deionized water, pH adjusted to 3.0 by TFA.
Solvent B: 30.0 mL concentrated ammonium hydroxide added to 2.0 L methanol and 2.0 L deionized water, pH adjusted to 3.0 by TFA.

Table 2 HPLC Method II

Time/min	Flow/mL/min	%D
0.00	7.000	0.0
2.00		0.0
40.00		100.0
45.00		100.0
46.00		0.0
49.95	7.000	0.0
50.00	0.000	0.0

Pump: Two Gilson model 302 pumps
Detector: Gilson model 112 UV detector set at 254 nm
Column: J. T. Baker, Bakerbond C-18, 10 μm, 22.5 × 250 mm
Injector: Rheodyne model 7125 with 10.0 mL loop.
Solvent C: 4.0 L deionized water, pH adjusted to 3.0 by TFA.
Solvent D: 2.0 L acetonitrile and 2.0 L deionized water, pH adjusted to 3.0 by TFA.

Table 3 HPLC Method III

Isocratic at a constant flow rate of 0.6 mL/min

Pump:	Bio-Rad Model 1300
Detector:	BAS LC-4C electrochemical detector, full range set to 10 nA
Column:	BAS, Phase-II ODS, 3 μm, 100 × 3.2 mm
Injector:	Rhoedyne model 7125 injector with 5 μL loop
Solvent:	Add 3.4 mL diethylamine, 76 mg Na_2EDTA (anhydrite), 84 g citric acid, and 464 mg sodium octyl sulfate to 3630 ml deionized water, filter, add 370 mL acetonitrile, and degas. pH = 2.34.

Table 4 HPLC Method IV

Time/min	Flow/mL/min	%B
0.00	7.000	0.0
2.00		0.0
25.00		45.0
25.50		100.0
45.00		100.0
45.01		0.0
54.95	7.000	0.0
55.00	0.000	0.0

Pump:	Two Gilson model 302 pumps
Detector:	Gilson model 112 UV detector set at 254 nm
Column:	J. T. Baker, Bakerbond C-18, 10 μm, 22.5 × 250 mm
Injector:	Rheodyne model 7125 with 10.0 mL loop.
Solvent A:	30.0 mL concentrated ammonium hydroxide added to 4.0 L deionized water, pH adjusted to 3.0 by TFA.
Solvent B:	30.0 mL concentrated ammonium hydroxide added to 2.0 L methanol and 2.0 L deionized water, pH adjusted to 3.0 by TFA.

Table 5 HPLC Method V

Time/min	Flow/mL/min	%B
0.00	7.000	0.0
2.00		0.0
25.00		45.0
25.50		100.0
40.00		100.0
40.01		0.0
49.95	7.000	0.0
50.00	0.000	0.0

Pump: Two Gilson model 302 pumps
Detector: Gilson model 112 UV detector set at 254 nm
Column: J. T. Baker, Bakerbond C-18, 10 μm, 22.5 × 250 mm
Injector: Rheodyne model 7125 with 10.0 mL loop.
Solvent A: 30.0 mL concentrated ammonium hydroxide added to 4.0 L deionized water, pH adjusted to 3.0 by TFA.
Solvent B: 30.0 mL concentrated ammonium hydroxide added to 2.0 L methanol and 2.0 L deionized water, pH adjusted to 3.0 by TFA.

Table 6 HPLC Method VI

Time/min	Flow/mL/min	%F
0.00	7.000	0.0
5.00		0.0
45.00		40.0
45.01		0.0
54.90	7.000	0.0
55.00	0.000	0.0

Pump: Two Gilson model 302 pumps
Detector: Gilson model 112 UV detector set at 254 nm
Column: J. T. Baker, Bakerbond C-18, 10 μm, 22.5 × 250 mm
Injector: Rheodyne model 7125 with 10.0 mL loop.
Solvent E: Deionized water.
Solvent F: Acetonitrile.

Table 7 HPLC Method VII

Time/min	Flow/mL/min	%B
0.00	7.000	0.0
2.00		1.0
25.00		5.0
36.00		100.0
46.00		100.0
47.00		0.0
54.90	7.000	0.0
55.00	0.000	0.0

Pump: Two Gilson model 302 pumps
Detector: Gilson model 112 UV detector set at 254 nm
Column: J. T. Baker, Bakerbond C-18, 10 μm, 22.5 × 250 mm
Injector: Rheodyne model 7125 with 10.0 mL loop.
Solvent A: 30.0 mL concentrated ammonium hydroxide added to 4.0 L deionized water, pH adjusted to 3.0 by TFA.
Solvent B: 30.0 mL concentrated ammonium hydroxide added to 2.0 L methanol and 2.0 L deionized water, pH adjusted to 3.0 by TFA.

Table 8 HPLC Method VIII

Isocratic at a constant flow rate of 0.6 mL/min

Pump: Bio-Rad Model 1300
Detector: BAS LC-4C electrochemical detector, full range set to 10 nA
Column: BAS, Phase-II ODS, 3 μm, 100 × 3.2 mm
Injector: Rhoedyne model 7125 injector with 5 μL loop
Solvent: Add 3.4 mL diethylamine, 88 mg $Na_2EDTA{\cdot}2H_2O$, 20.8 g citric acid, and 436 mg sodium octyl sulfate to 3800 mL deionized water, filter, add 120 mL methanol, and degas. Final pH is adjusted to 2.30 by concentrated HCl.

Table 9 HPLC Method IX

Isocratic at a constant flow rate of 0.9 mL/min

Pump:	Bio-Rad Model 1300
Detector:	BAS LC-4C electrochemical detector, full range set to 10 nA
Column:	BAS, Phase-II ODS, 3 μm, 100 × 3.2 mm
Injector:	Rhoedyne model 7125 injector with 5 μL loop
Solvent:	Add 3.4 mL diethylamine, 88 mg $Na_2EDTA{\cdot}2H_2O$, 20.8 g citric acid, and 436 mg sodium octyl sulfate to 3800 mL deionized water, filter, add 120 mL methanol, and degas. Final pH is adjusted to 2.30 by concentrated HCl.

Table 10 HPLC Method X

Time/min	Flow/mL/min	%B
0.00	0.000	0.0
0.05	7.000	0.0
2.00		0.0
20.00		30.0
35.00		100.0
45.00		100.0
46.00		0.0
49.95	7.000	0.0
50.00	0.000	0.0

Pump:	Two Gilson model 302 pumps
Detector:	Gilson model 112 UV detector set at 254 nm
Column:	J. T. Baker, Bakerbond C-18, 10 μm, 22.5 × 250 mm
Injector:	Rheodyne model 7125 with 10.0 mL loop.
Solvent A:	30.0 mL concentrated ammonium hydroxide added to 4.0 L deionized water, pH adjusted to 3.0 by TFA.
Solvent B:	30.0 mL concentrated ammonium hydroxide added to 2.0 L methanol and 2.0 L deionized water, pH adjusted to 3.0 by TFA.

Table 11 HPLC Method XI

Time/min	Flow/mL/min	%B
0.00	7.000	0.0
2.00		0.0
25.00		28.0
25.50		100.0
35.00		100.0
35.01		0.0
44.95	7.000	0.0
45.00	0.000	0.0

Pump: Two Gilson model 302 pumps
Detector: Gilson model 112 UV detector set at 254 nm
Column: J. T. Baker, Bakerbond C-18, 10 μm, 22.5 × 250 mm
Injector: Rheodyne model 7125 with 10.0 mL loop.
Solvent A: 30.0 mL concentrated ammonium hydroxide added to 4.0 L deionized water, pH adjusted to 3.0 by TFA.
Solvent B: 30.0 mL concentrated ammonium hydroxide added to 2.0 L methanol and 2.0 L deionized water, pH adjusted to 3.0 by TFA.

Table 12 HPLC Method XII

Time/min	Flow/mL/min	%B
0.00	7.000	0.0
2.00		0.0
25.00		45.0
25.50		100.0
40.00		100.0
40.01		0.0
49.95	7.000	0.0
50.00	0.000	0.0

Pump: Two Gilson model 302 pumps
Detector: Gilson model 112 UV detector set at 254 nm
Column: J. T. Baker, Bakerbond C-18, 10 μm, 22.5 × 250 mm
Injector: Rheodyne model 7125 with 10.0 mL loop.
Solvent A: 30.0 mL concentrated ammonium hydroxide added to 4.0 L deionized water, pH adjusted to 3.0 by TFA.
Solvent B: 30.0 mL concentrated ammonium hydroxide added to 2.0 L methanol and 2.0 L deionized water, pH adjusted to 3.0 by TFA.

Table 13 HPLC Method XIII

Isocratic at a constant flow rate of 0.6 mL/min

Pump:	Bio-Rad Model 1300
Detector:	BAS LC-4C electrochemical detector, full range set to 10 nA
Column:	BAS, Phase-II ODS, 3 μm, 100 × 3.2 mm
Injector:	Rhoedyne model 7125 injector with 5 μL loop
Solvent:	Add 3.4 mL diethylamine, 83 mg $Na_2EDTA \cdot H_2O$, 84 g citric acid, and 436 mg sodium octyl sulfate to 3800 ml deionized water, filter, add 250 mL acetonitrile, and degas. pH is adjusted to 2.37 by concentrated HCl and/or NaOH.